UNIVERSITY OF NAPLES FEDERICO II

Department of Structures
for Engineering and Architecture

PH.D. PROGRAMME IN

MATERIALS ENGINEERING AND STRUCTURES

COORDINATOR PROF. GIUSEPPE MENSITIERI

XXVII CYCLE

MARCO GAETANI D'ARAGONA

PH.D. THESIS

POST-EARTHQUAKE ASSESSMENT OF DAMAGED NON-DUCTILE BUILDINGS: DETAILED EVALUATION FOR RATIONAL REPARABILITY DECISIONS

TUTORS: PROF. DR. MARIA POLESE
PROF. DR. ANDREA PROTA

2015

Ai miei straordinari genitori

"… when you have eliminated the impossible, whatever remains, however improbable, must be the truth"

Sir Arthur Conan Doyle

Acknowledgments

Table of Contents

List of figures

List of Tables

Chapter 1

INTRODUCTION

1.1   MOTIVATION AND SCOPE

After a seismic event, a number of possible alternatives for dealing with a building damaged by an earthquake, ranging from the acceptance of the damage up to the building replacement are available. For instance, for buildings complying with modern seismic codes, the upgrading is generally not required, but damage must be repaired to bring the building back to pre-earthquake conditions. On the other hand, existing buildings designed with older seismic codes, or gravity load designed ones, are required to be retrofitted or improved as well as repaired, to make the building more robust in future earthquakes. Recent studies by Liel et al. (2011) have pointed out that older RC structures, in terms of annualized risk, are approximately 40 times more susceptible to seismic collapse and more likely to incurr in significant repair costs than modern code-conforming RC buildings (Liel and Deierlein, 2008). Despite that, plan of action or policy road map to reduce earthquake risks in existing buildings, as well as effective guidelines for repair and rebuilding that will expedite recovery after an earthquake, usefully supporting the decision-making process towards reparability decisions for damaged buildings, have not been acknowledged by the most of modern codes. In fact, as pointed out by Holmes et al. (2014), nowadays there is still a lack of comprehensive and uniformly applicable post-earthquake repair regulations. These policies can make cities safer and more resilient to earthquakes over time by strengthening those buildings that have been shown by an earthquake to have inadequate seismic resistance. A possible strategy would be to encourage or require owners of more vulnerable structures to undertake risk assessment and mitigation; for instance, the city of San Diego released an ordinance (SDMC, 2004) requiring some mandatory strengthening of all unreinforced masonry buildings, URM, while several cities of California adopted loss reduction programs (mandatory or voluntary strengthening of URMs), see SSC 2006-04. However, these provision do not always meet the general consensus due to the high costs incurred by private owners, and consequently, incentives to encourage seismic upgrades and penalties for non-conformance within a predetermined period are often required to make

these provisions effective. Another effective strategy is to require seismic upgrading when major modification are realized to existing structures (e.g., NNT 2008) or when existing buildings suffered significant damage despite low intensity of the damaging earthquake, to improve resilience to more intense earthquakes.

Indeed, while buildings compliant with modern seismic codes, if damaged, only need to restore pre-earthquake capacity, for older buildings a good strategy is to establish damage "triggers" that require not only repair of damage, but also retrofit to improve seismic performance (e.g. SF, 2012). Thresholds triggering different post-earthquake actions are connected to basic safety levels and include a balance with sustainable costs; typically, they are established at a political level and take into consideration the failure probability with reference to performance objective and return period. However, while post-earthquake regulations are often issued in emergency phase, it would be highly valuable to have the possibility to perform a cost/benefit assessment in "peace-time", investigating on the effects of setting relevant policy thresholds. In other words, a rough evaluation of the costs (of re-construction) versus the benefits (public safety preservation and/or enhancement) of the envisioned application of a policy would significantly help the decision maker to establish if it is effective towards community resilience objectives. As evidenced above, effective earthquake repair policy and individual decisions require reliable estimates of future seismic performance. The most commonly used damage trigger is a threshold value for the loss of strength in the lateral-force-resisting system above which retrofit is required. In fact, the FEMA 308 (1998) introduced a Performance-Based Policy Framework (PBPF), see Fig. 1-1, that relies on performance index (IP) of the building in its intact and damaged state and on the relative performance loss PL as significant indicators for repair and/or upgrade decisions. However, while the general framework facilitating decisions on appropriate course of action for specific buildings was set, no specific guidance for the establishment of PL and IP thresholds governing damage acceptability were given.

Some proposals for IP and PL thresholds can be found in the San Francisco Building Code (CCSF, 2010), that has used for a long time a 20% loss of capacity as a damage trigger to establish if non-complying buildings are "sufficiently damaged" to enforce retrofit. Similarly, after the 2009 L'Aquila earthquake, the Italian government established that buildings having an initial seismic capacity lower than 60% of the one required for new buildings to be upgraded, and a fund to increase the seismic capacity up to 80% was granted (OPCM 3790, 2009). Acknowledging the need for a standard method for calculating the loss levels triggering repair/upgrade requirements, in ATC52-4 (ATC, 2010) a set of retrofit trigger values for selected building typologies was outlined. More recently, in (SF 2012) further specifications on PL thresholds and on their calculation based on FEMA 306 (1998) were given. However, the suggested PL thresholds are based on previous established values of percent loss triggers (e.g. CCSF 2010), without a clear quantitative justification for the proposed values. Therefore, there

is a clear need to further investigate on criteria and methods for establishing suitable PL and IP thresholds governing damage acceptability; to this end, building loss levels should be considered and clearly connected to the variation of building safety, but also an estimate of the costs to repair the building to its original state and, if necessary, of retrofit costs are key factors helping decisions.
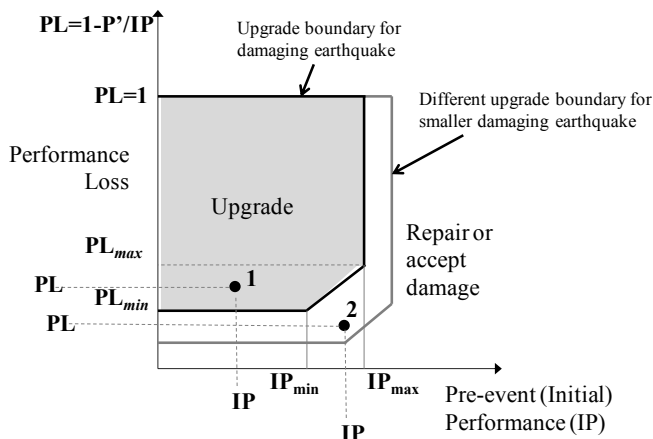
Fig. 1.1 The PBPF according to (FEMA 308,1998) (adapted figure)

 Quantification of these loss thresholds represent a key issue into the reconstruction policy framework, and requires further investigations through detailed cases. These cases should explicitly consider repair/upgrade cost, economic constraints as well as technical feasibility of the intervention; detailed analyses should take into account the permanent structural drift, coupled to the structural safety variation after an earthquake, conditioned on the hazard at the site.

Holmes (1994) summarized some technical difficulties that impair the development of effective standards for the evaluation and repair of earthquake damage; among other factors, one of the main impediments was the lack of formalized methods for analyzing the realistic effects of earthquake shaking and resulting damage on the performance of buildings and their components. The calculation of loss of strength has proven problematic in past earthquakes, creating disputes and causing delays in repairs, re-occupancy, and recovery. In response to this issue the ATC-43 project, sponsored by FEMA, addressed the investigation and evaluation of earthquake damage and discussed policy issues related to the repair and upgrade of earthquake damaged buildings. As a first result, in (FEMA 306, 1998) the available instruments and methods for seismic analyses of damaged buildings were analyzed and a pushover based procedure proposed where the behavior of damaged buildings could be simulated with suitable modification of plastic hinges for damaged elements. Starting from this first proposal, some efforts were made to implement assessment procedures allowing to explicitly consider

earthquake damage in the post-earthquake safety assessment both for steel (Bazzurro et al., 2004; Maffei et al., 2006) and RC buildings (Polese et al., 2013a,b; Di Ludovico et al., 2013; Polese et al., 2014). These tools are directed to develop practice oriented methods for the assessment of building safety variation and residual capacity, useful for practitioners and supporting informed decisions in the aftermath of damaging earthquakes or for pre-event studies. Coupled to this simplified type of analyses, expected economic losses due to scenario earthquakes can be assessed with regional based methods (e.g. HAZUS, Polese et al.,2015).

On the other hand, depending on the needs, the building's seismic performance and residual capacity can be evaluated on different levels of accuracy. If more accurate performance prediction is desired by decision-makers, then more detailed modeling for nonlinear time history analyses shall be adopted, site-specific information shall be incorporated in the structural analysis and this way the analyses can be closer to the real-life behavior of the structure. Also, expected repair costs can be determined based on effective damage amount and distribution on the building structural and non-structural system, allowing for accurate assessment towards reparability decisions.

The PEER approach (e.g., Porter 2003) allows the complete assessment of expected damage and costs within a fully probabilistic framework. However, although several applications exist (e.g., Deirlein 2004, Miranda et al. 2004, Aslani and Miranda 2005, Miranda and Taghavi 2005, Krawinkler and Miranda 2004, Aslani et al. 2004, Mitrani-Reiser and Beck 2007, Baker and Cornell 2008b, Ramirez and Miranda 2009), there is the clear need to further investigate on the applicability and limitations of the framework and of the single modules composing the framework. For instance, few applications adopted Multi-degree-of-freedom models properly accounting in an explicit way for both the potential brittle failures of structural members and the collapse mechanism that is likely to occur for existing non-ductile structures (i.e., gravity load collapse).

Different performance assessment can be carried out using PEER framework; a recent introduction is the Time-based assessment (ATC, 2012), that evaluate performance over time, considering all possible earthquakes and their probability of occurrence. This loss assessment can be linked to a Time-based assessment of seismic structural safety in order to obtain a full indication of future building's performances.

A key needed aspect for the evaluation of building reparability is the estimation of the building's residual capacity after damage; it is a vital part of the seismic performance evaluation of buildings with respect to multiple performance objectives. A proper evaluation of seismic performance before and after earthquakes is essential for decision making involved in managing the risk of buildings in seismically active areas, especially useful if coupled with a sound estimation of expected repair costs.

Concerning, the estimation of residual capacity with non-linear dynamic analyses, although several studies allowed its estimation after earthquake-induced damage (e.g., Luco et al. ; Bazzurro et al., 2004; Ryu et al., 2011; Uma et al., 2011, Réveillère et al., 2012), few authors adopted a Multi-degree-of-freedom model (e.g., Raghundandan et al., 2014) and just in one case analyses were carried out on structures susceptible to brittle failures (Jeon et al., 2015).

The main objective of this research is to explore and test different methods and tools for the assessment of buildings reparability taking into account both the residual capacity variation, that is connected to the variation of safety, and costs. The intent is to clarify, develop and promote state-of-the-art engineering resources and applications to suitably estimate building's residual capacity of existing Reinforced Concrete (RC) buildings. Existing RC frame structures represent a large portion of the existing building inventory all over the world and the lacking of important features of good seismic design, such as strong columns and ductile detailing of reinforcement, make these building potentially vulnerable to earthquake-induced damage or collapse even for moderate strong motions. These buildings, often referred as non-ductile detailed, may present a significant hazard to life and safety in future earthquakes as well as a significant source of economic losses during moderate to severe seismic ground motions.

In the thesis, two main level of analyses for the assessment of damaged buildings are investigated, namely detailed analysis based on non-linear time-histories, that is finalized to accurate estimation of expected safety variation for mainshocks corresponding to increasing return period and related repair costs, and pushover based ones, that allows simplified, practice oriented, assessment of variation of the residual capacity and performance loss due to assigned earthquakes.

Accordingly, the thesis is organized in two main parts, describing the models, analyses and results of the two different approaches.

The first part of the work focuses on the development of a clear framework for the assessment of building's residual capacity for non-ductile buildings through a dynamic approach. This framework is oriented towards a building-specific time-based assessment that can be useful to estimate likelihood variation of structural safety consequent to probable earthquakes that can strike the structure in the specific site (conditioned on the site hazard). The proposed framework will be demonstrated through a detailed evaluation of existing case-study buildings performances.

The behavior of these buildings is predicted using simulation models capable of capturing the critical aspects of strength and stiffness deterioration as well as typical non-ductile member failures (i.e., joint behavior, shear and axial failures); furthermore, a recent definition of system-level collapse typical for existing buildings has been

adopted. The so-called back-to-back Incremental Dynamic Analysis (e.g., Jeon et al., 2015), the most common emerging tool in seismic risk assessment, can be used to assess the variation of building's capacity due to earthquake damage. In order to carry out a multi-objective performance assessment earthquake-induced repair costs have to be accounted for. This framework may represent a useful tool to guide decision-makers through possible mitigation strategies in order to improve the resilience of existing buildings to future earthquakes.

However, the dynamic computation of residual capacity requires an intensive computational effort that although made possible by the availability of enhancement of computer performances it is not readily available to practitioners. Such efforts are not justified for all risk management problems. In most cases, a high-end solution is unnecessary and must be justified by the importance of the specific building.

Consequently, the second part of this study proposes a simplified pushover-based approach similar to the one proposed in FEMA 308 (1998). This approach relies on the execution of pushover analyses of the buildings in various damage states adopting a lumped plasticity model in which the plastic hinges may be suitably modified to account for the damage in the single elements.

However, there are not explicit indications for suitable modification factors to be applied to RC members of buildings in Mediterranean regions, where reinforcement detailing and confinement of columns are usually inadequate. The few indications that may be found for RC columns cannot be indiscriminately used for RC members typical of Mediterranean regions, because their mechanical properties, the type of reinforcement (smooth or deformed bars) and the relative percentage as well as type of detailing, may differ significantly from those of North America or Japan. Therefore, there is a need for proper calibration of damage–dependent modification factors for plastic hinges of damaged columns representative of existing elements with design characteristics non-conforming to present-day seismic provisions.

Finally, the usability of pushover analysis for the assessment of the behavior of damaged buildings has not been verified yet, and the study presented in this paper aims at contributing in the evaluation of this issue.

1.2   ORGANIZATION

The dissertation is organized into six chapters with the following contents:

Chapter 2 summarizes existing modeling strategies to simulate the brittle behavior of non-ductile buildings. Analytical models of flexure-shear critical columns, beam-column joints as well as existing collapse simulation techniques are extensively and critically reviewed.

Chapter 3 provides case-study building description and associated analytical frame models along with a detailed description of the adopted collapse simulation methodology. The deterministic response in terms of damage and capacity of the intact building is assessed through both nonlinear static and nonlinear dynamic analyses; then the framework for the assessment of earthquake-damaged buildings performance through the introduction of the TR-dependent aftershock fragility framework is laid out. The framework is composed of several phases: definition of a suitable analytical model, selection of Mainshock and Aftershock ground motion suites, definition damaging earthquake and formulation of probabilistic TR-dependent aftershock fragility curves. The framework is applied to two case-study buildings.

Chapter 4 presents the building-specific loss assessment for the computation of direct earthquake-induced economic losses for studied buildings. The PEER framework is adopted to produce the reliable estimate of repair costs for a time-based assessment of economic losses.

Chapter 5 introduces a pushover-based method for the assessment of residual capacity of damaged buildings. The method adopts suitable modification factors for plastic hinges to simulate damage due to earthquake. Modification factor are obtained for non-ductile columns failing in flexure or flexure-shear reinforced with smooth and deformed rebars. The effectiveness of the method is demonstrated by comparison with results from nonlinear time histories.

Chapter 6 presents the conclusions from the present research along with suggestion for future research.

Chapter 2

NONLINEAR MODELING OF EXISTING RC FRAMES

The structural engineering community is increasingly using nonlinear static or dynamic analysis to evaluate the response of a structure subjected to seismic events.

Nonlinear dynamic analysis is explicitly required during advanced rehabilitation processes of existing buildings. For instance, ASCE/SEI 31 (ASCE, 2003) and ASCE/SEI 41 (ASCE, 2007) require nonlinear dynamic analysis in the assessment and rehabilitation of a structure. Nonlinear response is usually limited to a reduced number of elements and the definition of their hysteretic response generally follows simple rules. Although a nonlinear dynamic analysis is an excellent way to evaluate the performance of structures subjected to strong ground motions, the modeling complexities involved in characterizing the number and type of material nonlinearities often discourage engineers from using this advanced option. The current chapter address existing modeling alternatives to explicitly simulate columns and beam-column joints brittle behavior. Further it describes the collapse simulation strategies that have been adopted in previous studies.

2.1   NON-CONFORMING COLUMNS

To accomplish the objective of predicting in a realistic way the damage generated all over a structure by a seismic event, the associated repair costs and retrofit/upgrade actions, as well as the variation in building seismic safety against collapse, advanced modeling and analysis techniques for RC elements have to be used. In fact, it is crucial that the numerical model contains reliable and robust component models that allow the simulation of the actual behavior of existing buildings from the elastic region to element failure. This chapter presents a literature review on reinforced concrete modeling techniques. The review covers the modeling of collapse-governing components such as beam-columns elements and beam-column joints, code-based modeling for the analysis platform OpenSees (McKenna, 2011) and past research on RC frame modeling.

2.1.1 ELEMENT MODELING

In order to simulate the response of older RC frames, with detailing that are representative of underdesigned frames in seismic zones, it is required to take into account the flexural response of beams and columns, shear behavior of columns, and possible joint failure. A review of element formulations used to simulate these response modes and studies using the formulations is presented in the following paragraphs.

2.1.1.1 NONLINEAR BEAM-COLUMN

The inelastic structural component models can be differentiated depending on how the plasticity is distributed through the member cross sections and along its length. According to NIST GCR 10-917-7 (2010), five idealized model types are possible, Fig. 2.1.
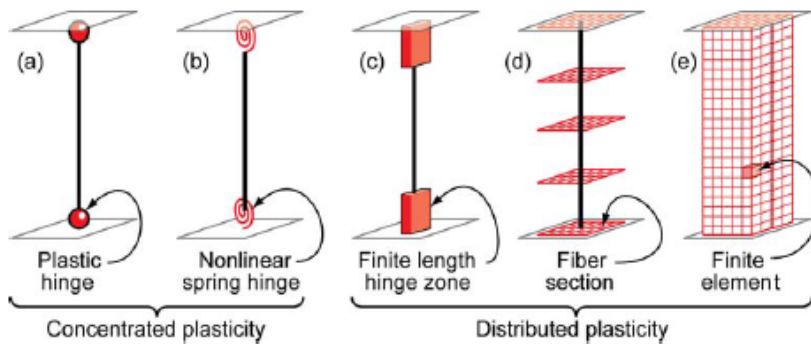
Fig. 2.1 Idealization of structural component (from NIST GCR 10-917-7, 2010)

These idealized nonlinear beam-column models can be divided in two main categories: 1) concentrated plasticity models and 2) distributed plasticity models. The simplest models concentrate the inelastic deformations at the ends of the element through a rigid-plastic (fig. Fig. 2.1(a)) or a nonlinear spring hinge with hysteretic properties (Fig. 2.1(b)). These models may capture relevant feature simulating the nonlinear degrading response of members when calibrated using member test data on phenomenological moment-rotations and hysteresis curves. On the other hand, the inelastic behavior can be captured using distributed plasticity models that simulates the inelastic response either in a finite length hinge model (Fig. 2.1(c)) or with a fiber formulation (Fig. 2.1(d)) where the plasticity is distributed by numerical integrations through the member cross sections and along the member length; finally, a Finite Element Model (FEM) can be used (Fig. 2.1(e)).The most complex FEM requires to discretize the continuum along the member length and through the cross sections into micro-finite elements with nonlinear hysteretic constitutive properties that have numerous input parameters. Distributed plasticity model variations can capture the

stress and strain through the section and along the member in more detail, while important local behaviors, such as strength degradation due to local buckling of steel reinforcing bars, or the nonlinear interaction of flexure and shear, are difficult to capture without sophisticated and numerically intensive models.

While more sophisticated formulations may seem to offer better capabilities for modeling certain aspects of behavior, simplified models may capture more effectively relevant features with the same or lower approximation if using well-calibrated models. For this reason, and for the computational effort related to the sophisticated model, lumped plasticity and fiber models are often preferred to simulate behavior of building behavior.

Simulation strategies for nonlinear beam-column in OpenSees

Three different beam-column element options are available in Opensees (McKenna, 2011) to simulate nonlinear material response. The first method consist into model the column using lumped plasticity in which the nonlinear behavior is concentrated at the ends of an elastic element. The other two modeling solutions allow the simulation of nonlinear response using a distributed plasticity formulation based on finite-element methods.

-Lumped plasticity Element

Lumped plasticity can be introduced in the model using two different possible strategies: The strategy 1) consists in the use of an elastic beam-column element with two zero-length elements at both the element extremities. The zero-length elements are associated to a rotational hinge model with hysteretic rules able to capture the flexural behavior of the elements. The behavior of rotational hinge is associated to a uniaxial material that express the plastic hinge behavior in terms of moment-rotation relationship. Particular attention must be paid to the stiffness of the macro-element obtained connecting in series two hinges and an elastic beam-column. The element global deformability in the plastic zone will result equal to the sum of deformability of elements connected in series. This issue will be addressed further in Chapter 5.

In the option 2) all members are modeled using a force-based element formulation in which nonlinear behavior is concentrated in plastic hinge regions at the ends of the element. A fiber section is utilized to define the inelastic moment-curvature response of the plastic hinge regions. One-dimensional concrete and steel material models are also used to develop element cross section response. To simulate this second option, OpenSees implements the beam with hinges element by dividing the element into three pieces: two inelastic hinges at the ends and an elastic center region. The beam with hinges element localizes the integration points in the hinge. The inelastic hinges are defined by assigning a fiber section and the user must define its length; the elastic

section is assigned using the dimensions of the member cross section and concrete modulus of elasticity.

-Nonlinear Force-Based Element
When adopting this option, beams and columns are modeled using a force-based beam-column element formulation in which nonlinear behavior is allowed to spread along the length of the element. A fiber section is utilized to define the inelastic moment-curvature response of the element. A linear moment distribution is assumed over the length of the elements. The deformation is defined by the curvatures developing at integration points along the length of the element. An integration scheme is applied to represent the distributed plasticity in the elements. OpenSees implements the force-based beam-column element by assigning a fiber section to the element and defining the number of integration points along the length of the element. The Gauss-Lobatto integration is the most common approach for evaluating the response of force-based elements because it places an integration point at each end of the element (Neuenhofer and Filippou 1997). Multiple numerical integration options are however available for this element.

-Nonlinear Displacement-Based Element
Similarly to the force-based formulation, members are modeled using a displacement-based beam-column element formulation in which nonlinear behavior is allowed to spread along the length of the element. To approximate nonlinear element response, constant axial deformation and linear curvature distribution are enforced along the element length. The Gauss-Lobatto quadrature rule is the default integration scheme for displacement-based elements. A fiber section is utilized to define the inelastic moment-curvature response of the element. OpenSees implements the displacement-based beam-column element by assigning a fiber section to the element and defining the number of integration points along the length of the element.

2.1.1.2 SHEAR FAILURE
Reinforced concrete columns designed or constructed prior to the introduction of modern seismic codes are typically lacking in reinforcement detailing and may exhibit brittle behavior. .In North America, pre 1970 RC buildings do not comply to modern standards, while in other parts of the world modern seismic codes were enforced later, with a time delay that can reach 20 years or more in European Mediterranean regions.

Due to their inadequate reinforcement details, non-conforming columns may be dominated by shear mechanisms, exhibiting dramatic strength and stiffness degradation until failing shear or due to axial load. These columns may gradually lose their shear capacity either if shear failure is triggered before or after flexural yielding.

While most current modeling approaches allow a reasonably accurate prediction of flexural and longitudinal bar slip response, the modeling of shear behavior is still under development. Next, existing column's shear failure models are presented.

First attempts to consider the shear failure in columns can be found in Otani and Sozen (1972), Spacone et al. (1996). In these works, to capture the occurrence of shear failure, they modified nonlinear flexure elements (lumped or fiber elements) through a post-processing without explicitly accounting for shear behavior. Although the post-processing can capture the detection of column's shear failure, it cannot estimate appropriate inelastic shear deformations and degrading behavior.

Nowadays, a very common technique to account for shear failure, used in several studies (e.g. Pincheira and Jirsa, 1992, Paspuleti, 2002, Theiss, 2005), is to use a shear strength prediction model. In this model, when the column shear demand exceed shear strength, it is assumed that column fails in a brittle manner losing instantly its lateral load-carrying capacity. The use of this approach assumes that columns have no lateral stiffness after reaching their shear capacity; therefore, it may significantly underestimate the effective structural behavior in the post-peak.

The most popular technique for modeling the shear response of RC columns is the use of nonlinear springs. Pincheira et al. (1999), Lee and Elnashai (2001), Sezen and Chowdhury (2009), used column elements incorporating nonlinear shear springs in series with flexural elements. In their works, the backbone curve for shear spring is obtained thought the Modified Compression Field Theory MCFT (Vecchio and Collins 1986).

(a) Pincheira et al. (1999)   (b) Lee and Elnashai et al. (2001)   (c) Sezen and Chowdury (2009)
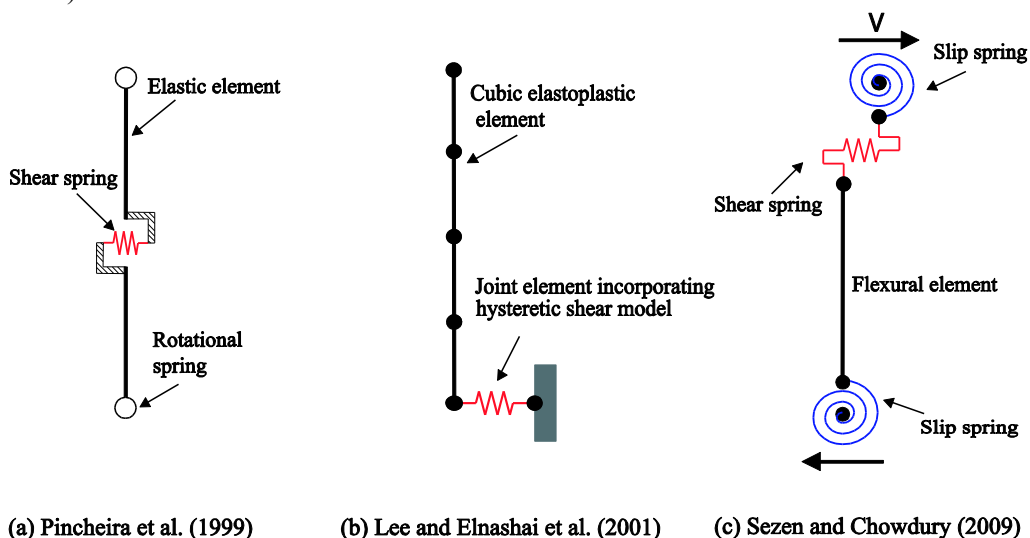
Fig. 2.2 Shear models

Pincheira et al. (1999) developed a column element that incorporate a zero-length shear spring, that can account for the strength and stiffness degradation with increasing

deformation amplitude, and rotational springs in series (Fig. 2.2(a)). Although their model yielded satisfactory results and properly includes the effects of strength decay, they introduced a small fictitious positive stiffness on the descending branch of the backbone to elude the convergence issue within the existing solution algorithm, resulting in a force unbalance at each increment whenever strength degradation occurs. Additionally, the procedure may be very computationally intensive and may not predict the dynamic characteristics of a softening structure. Lee and Elnashai (2001) also utilized the MCFT to establish the backbone curve of a spring and developed hysteretic rules including the variation of column axial loads (Fig. 2.2(b)). Although their shear model can capture the hysteretic response of columns with a relatively flat yield plateau, it did not address the post-peak degrading slope of the backbone curve. Barin and Pincheira (2002) defined a shear force versus shear strain relationship. The shear data used in the study was implemented in a Drain-2D model. This model did not fail in a very brittle manner and retained some residual shear strength after reaching a user defined shear spring deformation. Sezen and Chowdhury (2009) developed a hysteretic model (Fig. 2.2(c)) including the flexure-shear-axial interaction based on the backbone curve obtained from the MCFT, and employed the bond-slip model developed by Sezen and Moehle (2003). Although their model provided reasonable strength degrading behavior, the overall response was not predicted well in many cycles mainly because the sum of experimental component displacements did not match the total experimental displacement. Furthermore, the MCFT only predicts the backbone curve of shear model up to the point of maximum strength, and therefore requires additional assumptions for defining the shear strength degradation.

The shear spring models discussed above concentrate the flexural deformations in the beam-column element and the shear deformations are modeled with the introduction of a shear spring. When the shear strength is lower than the flexural yield strength of the column the models are able to capture the degrading shear behavior. Instead, if the shear strength is larger than the flexural yield strength, then the models fail to capture shear degradation. Consequently, this response is not realistic for columns yielding in flexure close to their shear strengths.

A few shear strength models are useful for estimating the column shear strength as a function of deformations (Watanabe and Ichinose 1992, Aschheim and Moehle 1992, Sezen 2002). Despite that, these models do not provide a reliable estimate of the drift capacity at shear failure (Elwood and Moehle 2004). Drift capacity models are essential in displacement-based framework for existing structures (ATC 1996 and ASCE 2000); however, only a limited number of drift capacity models were proposed for columns experiencing flexural yielding prior to shear failure. Pujol et al. (1999) proposed a drift capacity model for shear-dominated columns, which established a conservative estimate of the maximum drift ratio through the statistical evaluation of an experimental database

of 92 columns with both circular and rectangular cross sections. However, the database includes columns with transverse reinforcement ratios exceeding 0.01, which are typical for ductile frames.

To provide a better estimate of drift capacity at shear failure, Elwood and Moehle (2005) proposed an empirical drift capacity model by using a database of 50 flexure-shear-critical RC columns with configurations representative of those used in pre-1970s building construction. The model identifies a shear failure based on both the column shear demand and deformation of the column. The total deformation is captured coupling the shear spring and beam-column element.

Using the drift capacity model of Elwood and Moehle (2005), Elwood (2004) developed a new material model, called limit state material that can identify a shear failure associated with column shear and column's total deformation.

The model for shear and axial failure tracks the flexural response of the associated beam-column element, detecting axial and shear failure when the response reaches predefined shear and axial limit surfaces and changes the backbone of the material model to include strength degradation. These limit surfaces are determined based on the properties of the columns. In the case of shear failure, the limit surface is defined in the small displacement range, for brittle shear failure, by the shear strength model proposed by Sezen and Moehle (2003); in the larger displacement range, for a column that yields in flexure then fails in shear, the limit surface is defined by the force-displacement relationship proposed by Elwood (2004). The axial force-displacement limit surface is defined by Elwood (2004).

Fig. 2.3 illustrates the model proposed by Elwood (2004) in which both a shear and an axial spring are placed in series with a nonlinear beam-column element. These springs are provided only at the top of each element, because they represent the shear and axial response over the height of the column in an average sense. Flexural deformation is concentrated in the beam-column element, and shear deformation are accounted by the shear spring. To define the constitutive relationship for the shear spring, the hysteretic uniaxial material, available in OpenSees (McKenna, 2011), with strength degradation (called limit state material) was utilized. The limit state material has a predefined trilinear backbone curve and five parameters to define pinching and stiffness degradation. It traces the beam-column element response and changes the backbone of the material model to include strength degradation once the response of the beam-column element exceeds a predefined limit state surface (limit curve). After the shear limit curve is reached on the total response backbone, the response changes to represent a shear failure. The same procedure can be used to incorporate an axial spring into the column model. The axial capacity model assumes that shear failure has already occurred using a limit state material for shear response.

The model by Elwood (2004) was used by Elwood and Moehle (2008) to capture the response of a three-column, shake-table RCF specimen for which the middle column incurred shear failure. The analysis provided satisfactory estimates of the response of the specimen until the occurrence of shear failure; after this point, the lateral displacements of the structure were underestimated.

Owing to the significant change in the response of the structure once a limit curve is reached, the limit state failure model is particularly sensitive to any variability in the limit curves. An additional difficulty is the accurate modeling of the limit curve, due to the limited number of comparison studies with experimental results. A possible approach to identify the variability associated with this type of modeling for different RC columns in building frames is to employ probabilistic models for the limit curves.
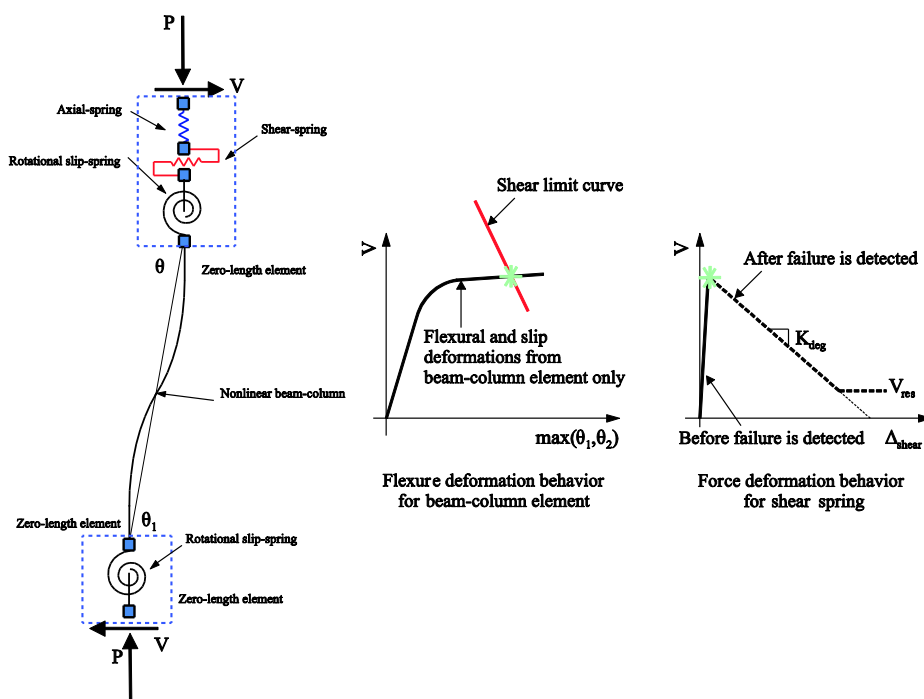
Fig. 2.3 Limit state material used to model shear failure (Elwood, 2004)

The model proposed by Elwood (2004) was further developed in Baradaran Shoraka and Elwood (2013). The authors proposed a column mechanical model able to capture pre-peak shear behavior, the point of shear failure and post-peak shear behavior. The two types of shear failure, diagonal tension and compression failure are numerically accounted in the mechanical model and used to detect shear failure. Shear failure is determined following the MCFT while the post peak response is evaluated based on shear-friction concepts. The use of a mechanical model allows applying the model to a

16

broader range of columns compared with similar empirical based models (e.g., Elwood, 2004). The comparison of the analytical model with experimental test data indicated that the numerical model adequately captures the pre-peak response and point of shear failure. However, the authors highlight that additional research is required to improve the post-peak behavior for columns that experience diagonal tension failure while a more reasonable estimation is provided for columns experiencing diagonal compression failure.

LeBorgne (2012) extended the model of Elwood (2004) to estimate the lateral strength degrading behavior of RC columns prone to shear failure. The model triggers shear failure when either a shear capacity or plastic hinge rotation capacity is reached. This model monitors the difference in rotation between user defined nodes and triggers degrading behavior in a shear spring. LeBorgne developed a rotation-based shear failure model while Elwood (2004) proposed a drift-based shear failure model. Fig. 2.4 shows the analytical model of flexure-shear-critical columns developed by LeBorgne (2012). The shear model can account for cyclic shear damage up to complete loss of lateral strength and stiffness. The constitutive properties were determined through linear regressions for pinching parameters extracted from experimental data. The author compared analytical predictions and experimental results for shear-dominated columns. Once shear failure is detected, a zero-length shear spring with a trilinear backbone curve linked in series with beam-column elements modifies its constitutive properties to consider pinching and strength and stiffness degradation.

Leborgne and Ghannoum (2014) have shown that their model can capture the results of various quasi-static experimental tests on shear-dominated columns; however, despite the establishment of algorithms to calibrate the model from experimental data, manual adjustments may still be required to achieve the best possible agreement with experimental results (Leborgne, 2012). Additionally, due to the experimental based calibration and model adjustment, the physical meaning of several parameters in the model, affecting the hysteretic behavior and strength degradation with repeated loading, is not clearly inferable because it cannot be directly related to the mechanical behavior. The same applies for the model formulated by Elwood (2004).

The applicability of the different kind of models to full frames has not been addressed for dynamic analysis, and dynamic instability remains an open question. A review of previous research on the shear behavior of older columns indicates that a reliable column shear failure model should be accurate, computationally efficient and compatible with existing software programs in order to conduct numerous nonlinear dynamic analyses. However, none of the column shear models reviewed above meets all three of those requirements. Due to its computational efficiency and compatibility with OpenSees (McKenna, 2011), the column shear model, developed by Elwood

(2004), will be used in this research. A more detailed discussion of the modeling techniques used for this shear spring formulation will be found in §3.2.2.1.

Despite, not explicitly accounting for the shear failure in columns, one of the most used model to simulate the behavior of existing columns is the model proposed by Haselton et al. (2008). This approach involves the use of a lumped plasticity model in which the plasticity is concentrated in two rotational hinges connected by an elastic beam-column element. The lumped plasticity element model used to simulate plastic hinges in beam-column elements requires the use of a nonlinear spring model developed by Ibarra, Medina, and Krawinkler (2005), and implemented in OpenSees by Altoontash (2004).
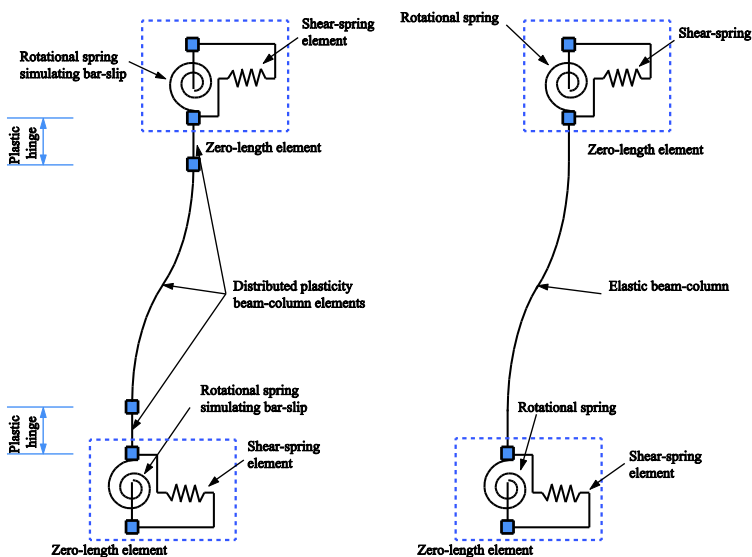
Fig. 2.4 Analytical model developed by LeBorgne (2012)

The model is capable of capturing the important modes of deterioration that precipitate sidesway collapse of RC frames, and account for four aspects of cyclic deterioration: strength deterioration of the inelastic strain hardening branch, strength deterioration of the post-peak strain softening branch, accelerated reloading stiffness deterioration, and unloading stiffness deterioration. In-cycle and cyclic degradation are also accounted in the definition of hysteretic parameters.

The detailed hysteretic nonlinear model representing the rotational springs is based on regression-based equations to estimate both linear and nonlinear parameters as a function of column properties (Fig. 2.5).

The parameters of the Ibarra material model are calibrated to data from rectangular columns included in the PEER Structural Performance Database (Berry et al. 2004). The database includes RC columns with both ductile and non-ductile detailing, and varying levels of axial load and geometries and, for each, reports force-displacement

history and other relevant data. However, approximately 35 of the 255 column tests have non-ductile detailing and failed in flexure-shear, as expected for the older RC columns of interest in this study. Although the model is calibrated to a larger dataset compared with previous models, it shows several limitations:1) Lumped plasticity model cannot take into account axial load variation in their response due to axial load redistribution during earthquakes. 2) The parameters are calibrated to a dataset that includes very few non-ductile detailed columns. 3) Model parameters are based on the initial conditions (gravity load conditions), and this model is not capable of adapting to varying boundary conditions during the simulation. 4) Finally, the parameters do not cover the wide spectrum of column properties observed in existing concrete frames.
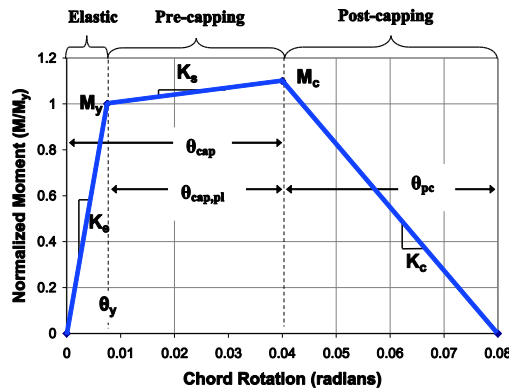
Fig. 2.5 Monotonic behavior of rotational hinge by Haselton et al. (2008)
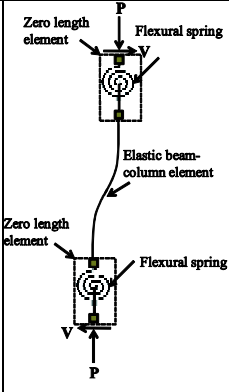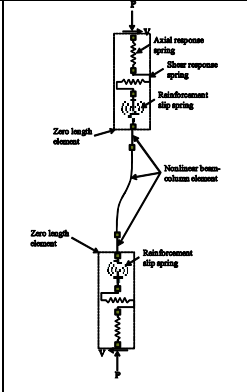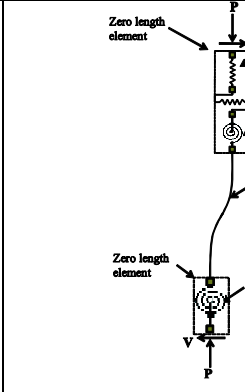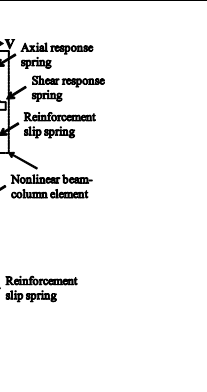
	Haselton et al. (2008)	Leborgne and Ghannoum (2009)	Elwood (2004)	Baradaran Shoraka and Elwood (2013)
Analytical model	Zero length element, Flexural spring, Elastic beam-column element, Zero length element, Flexural spring	Axial response spring, Shear response spring, Reinforcement slip spring, Zero length element, Nonlinear beam-column element, Zero length element, Reinforcement slip spring	Zero length element, Axial response spring, Shear response spring, Reinforcement slip spring, Nonlinear beam-column element, Zero length element, Reinforcement slip spring	
Failure	Flexure, flexure–shear	Shear, flexure–shear	Shear, flexure–shear	Shear, flexure–shear
Column model	Elastic beam–column element + zero-length flexural spring	3 nonlinear elements + zero-length shear springs	Nonlinear element + zero-length springs	Nonlinear element + zero-length springs
Model features	The model provides regression-based equations that are used to estimate linear and nonlinear parameters of flexural springs based on column properties and loading conditions. Calibrated on 255 column tests.	The shear spring model has the ability during analyses to monitor the deformations between two nodes bracketing the plastic hinge region and forces in the adjacent column element. The model compares the shear force in the column with a limiting shear force and the rotation of the plastic hinge region with a limiting rotation. Calibrated on 32 column tests.	This model detects shear or flexure– shear failure based on global column drift. The model detect the onset of shear failure based on an empirical drift model; however, it does not currently capture flexural failures. Calibrated on 50 column tests.	This model detects shear or flexure– shear failure based on shear strains in the plastic hinge zone of the column element. The model can detect when shear capacity is sufficient and flexural deformations govern response. Calibrated on 20 column tests.
Cyclic behavior	Calibrated for the full cyclic behaviour, including in-cycle and cyclic degradation	The model can simulate the full degrading behaviour, including incycle and cyclic degradation	The model can simulate the full degrading behaviour, including in-cycle and cyclic degradation; however, cyclic parameters are not calibrated.	The model can simulate the full degrading behaviour, including in-cycle and cyclic degradation; however, cyclic parameters are not calibrated.
Input vs. adaptive model	All model parameters are fixed by user input at the model building phase. Thus, the model does not adjust behaviour to varying boundary conditions during analysis.	The user can either input fixed values for rotation and shear-force limits or use the calibrated version of the model that automatically evaluates limits during analysis; this model uses the ASCE 41 shear strength Eqn. and a regression-based plastic rotation Eqn.	During analysis the model monitors column forces and deformation demands between integration points and adjusts the limit state that triggers strength degradation	During analysis the model monitors column forces and deformation demands between integration points and adjusts the limit state that triggers strength degradation
OpenSees material	Pinching4 using hysteretic model by Ibarra and Krawinkler (2005)	PinchingLimitState Material described in Leborgne (2012)	LimitState Material (Elwood, 2004)	LimitState Material (Elwood, 2004) with modifications

Table 2-1 Summary of shear models (adapted from Baradaran Shoraka, 2013)

2.2   NON-CONFORMING JOINTS MODELING

Beam-column joints in RC buildings are key components to ensure structural integrity of building performance under seismic loading. Experimental investigations (Walker 2001, Alire 2002, and Lowes and Moehle 1999) and post-earthquake reconnaissance (EERI 1994) have documented that under earthquake loading substantial damage (strength and stiffness loss) can result in under-designed RC beam-column joints. This degradation can have serious implications on the response of structures that rely on RC frames for their seismic resistance.

In typical existing buildings, constructed prior to developing details for ductility in modern seismic codes, seismic collapse safety might be significantly affected by the non-linear behavior of the joints that are involved in the failure mechanisms because of poor structural detailing, as the lack of an adequate transverse reinforcement in the joint panel or deficiencies in the anchorage due to the absence of any capacity design principle. Such unreinforced joints are vulnerable to brittle shear failure under seismic action due to insufficient shear reinforcement in the joint region, especially for exterior joints. In some cases, in fact, failure of older-type corner joints have caused partial or total structural collapses during past earthquakes.

The behavior of beam-column joints is a critical issue in the assessment of seismic performance of existing RC moment resisting frames; therefore, within the context of Performance-Based Earthquake Engineering, a growing attention is being addressed to the modeling of RC beam-column connections and the influence of failure of joints on the seismic performance of RC buildings.

While a wide literature concerning the performance of joints with ductile details exist, tools to predict older joints behavior is relatively limited.

Little or no shear reinforcement in beam-column joints and insufficient bars anchorage are two main problematic reinforcement details in underdesigned RC frames. Due to this poor detailing, the beam-column joint behavior is often governed by shear and bond-slip phenomena in existing frames. The presence of only little or no shear reinforcement in beam-column joints can lead to substantial shear deformations in the panel zone. This kind of detailing also can limit flexural capacities of connected beams and columns both exterior and interior joints can be affected by this problem.

On the other hand, the absence of hooks at the end of longitudinal bars, coupled with the inadequate anchorage length, make the bottom reinforcement susceptible to pullout during seismic excitation. Insufficient beam bottom bar anchorage precludes the formation of bond stresses necessary to develop yield stress in bottom reinforcement. The latter detailing only regards exterior joints and do not allow the whole development of beam moment capacity.

Although several modeling approaches have been proposed in past years, in literature there is not yet a commonly accepted approach for the determination of the

shear strength and for nonlinear modeling of RC beam-column joints in moment resisting RC frames. Many nonlinear joint models are available, however most of them may be unsuitable for modeling all sources of nonlinearity for the assessment of older concrete buildings, either because they were developed and calibrated for confined joints or they are complicated to implement. Moreover, the very poor dataset from experimental tests on unconfined joints makes it difficult to calibrate a comprehensive and simple nonlinear model.

The results of previous research indicate that joint stiffness and strength loss can have a significant impact on frame response (Mosier 2000) and failure of the beam-column joints may contribute to partial or total building collapse (e.g. Moehle and Mahin 1991, Hassan et al. 2010).

As shown in Fig. 2.6, the contribution of joint shear deformations to the overall deformation response can be significant, especially in the inelastic range. This can lead to underestimation of global displacements if a simple rigid joint is assumed. Many other experimental studies reported substantial contribution of joint shear deformations to total story drifts (Engindeniz 2008, Walker 2001, among others). Furthermore, recent tests on the behavior of exterior joints (Hassan 2011) showed that joint flexibility contributed significantly, up to 40%, to overall drift, especially in the nonlinear range.
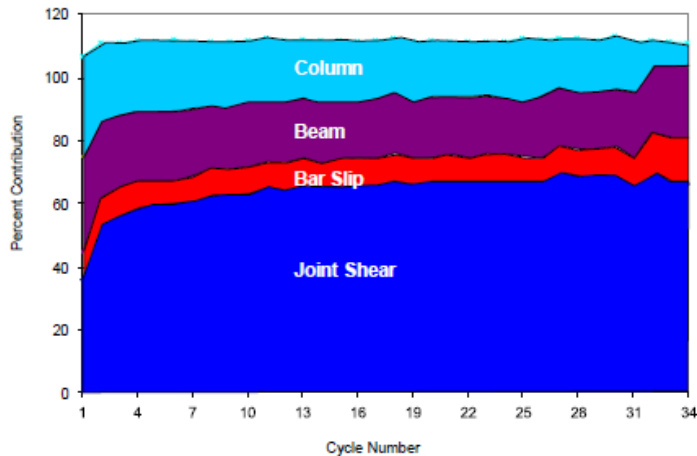
Fig. 2.6 Contribution of different components of deformation to overall story drifts (Walker , 2001)

Basically, there are two main contributions to the overall deformability related to beam-column joints that cannot be neglected: 1) Shear deformation of the joint panel zone and 2) the contribution of bars longitudinal slip anchored into the joint (e.g., Cosenza et al, 2006). For joints, two main different modes of failure can be identified: 1) J-failure, namely joint failure occurs prior to yielding of beam longitudinal reinforcement; 2) BJ-failure, namely joint failure occurs after yielding of beam longitudinal reinforcement. Other frequent failure modes are CJ-failure, namely joint

failure occurs after yielding of column longitudinal reinforcement, or failure modes that not entail joint failure, such as pullout failure of the beam bottom reinforcement (S-failure), beam (B-failure) or column (C-failure) yielding without joint shear failure (e.g., Hassan, 2011)

2.3 JOINT MODELS

The beam-column joint behavior of RC frames is complex and depends on a number of design parameters. Simulating the strength, stiffness, drift-capacity, and failure of joints requires a model complex enough to account for multiple response mechanisms, despite that, it has to be simple enough to guarantee computational efficiency.

In the following, the existing monotonic or hysteretic joint models that have been proposed to model existing joint shear behavior are reviewed.

Some authors only proposed shear strength models, others tried to capture the actual joint behavior through more complex models that also account for cracking, yielding and post-failure behavior.

2.3.1 SHEAR STRENGTH MODELS

Several authors have proposed both analytical or empirical models to predict joint shear strength. Consequently, in literature, different possible approaches to evaluate such strength are possible. These approaches can be separated into analytical, empirical and semi-empirical models.

2.3.1.1 ANALYTICAL MODELS

Hwang and Lee (1999, 2000) predicted RC joint shear strength for both interior and exterior beam-column joints developing a softened strut-and-tie model. The softened strut-and-tie model is based on the strut-and-tie concept and derived to satisfy equilibrium, compatibility, and constitutive relationship for cracked reinforced concrete. Although the authors demonstrated that their analytical model was able to predict joint shear strength by comparison with 63 exterior and interior beam-column joints experimental tests, the proposed approach became more complicated by introducing these principles of mechanics in contrast to the simplicity of the strut-tie-model. The database used to validate the model includes specimens with governing failure modes of beam flexural failures, joint shear failures with and without beam yielding and regardless of joint transverse reinforcement

Attaalla (2004) proposed an analytical equation to estimate joint shear strength for interior and exterior beam-column joints. The equation accounts for most significant parameters that influence the joint panel behavior (i.e. axial forces in the beam and

column, joint reinforcement ratios and geometry), and it accounts for the compression-softening phenomenon associated with cracked reinforced concrete. The model was validated using 69 exterior and 61 interior beam-column joints. All specimens experienced joint shear failures with or without beam yielding.

Shiohara (2004) proposed a mathematical model to determine the joint shear strength of interior, exterior, and knee beam-column joints. The joint shear failure of beam-column connections is defined as the failure of quadruple flexural resistance. Failure criteria for concrete, steel, bond and anchorage are combined with the equilibrium conditions of the members framing into the joint evaluated on the diagonal sections of the joint panel. The model validation based on experimental results was not provided.

Others strut-and-tie models were developed by Wong (2005) and Parker and Bullma (1997). Finally, Pantelides et al. (2002) and Vollum and Newman (1999) proposed strut-and-tie models based on beam-column test databases (i.e. semi-empirical models). Most of the "strut-and-tie-based" models have a conceptual limitation, because the average equilibrium and compatibility equations they are based on are not suitable to reproduce the real behavior of unreinforced beam-column joints – for which the joint shear failure is generally localized. Moreover, the accuracy of the strut-and-tie approach highly depends on the estimation of the diagonal strut area that strictly affects the joint shear strength.

2.3.1.2 EMPIRICAL MODELS

Kim and LaFave (2009) proposed an empirical joint shear strength model by using a Bayesian method based on 136 and 18 experimental beam-column ductile and non-ductile sub-assemblages experiencing joint shear failures, respectively. Their model directly provides a definition of the failure mode (J or BJ failure mode). For ductile joints, they constructed the joint shear strength model by performing a step-wise removal process to extract key parameters among ten parameters (spacing ratio, ratio of recommended to provided amount of joint transverse reinforcement, ratios of beam depth to column depth and beam width to column width, joint transverse reinforcement index, beam reinforcement index, joint eccentricity, in-plane and out-of-plane geometry, concrete compressive strength). For non-ductile joints, lacking of joint transverse reinforcement, a probabilistic joint strength model was established by modifying that for ductile joints because none of the included parameters in the proposed equation for ductile cases should be taken as zero. The ductile joint shear strength model provides reliable estimates while the non-ductile joint shear strength model should be improved because of the limited dimension of non-ductile joint database.

Hassan (2010) proposed an empirical strength model for unconfined exterior and corner joints showing J-failure mode based in 12 experimental tests (Hassan and Mohele, 2012). In addition, an empirical equation to estimate both bond failure in joints (S-failure) and axial collapse of nodes is presented. The strength model equation includes axial load, beam bar diameter, cover to bar diameter, cover to bar diameter ratio, and the presence of transverse beams to improve existing bond strength models. Using the proposed equation and equilibrium, the author compared the equivalent joint shear strength associated with bond failure with 52 experimental results for J-failure mode. The model verification for J-failure empirical model showed a mean and a coefficient of variation of the ratio of experimental and calculated joint shear strength equal to 0.99 and 0.13 respectively. Instead, the mean and a coefficient of variation of the ratio of experimental and calculated joint shear strength equal to 0.94 and 0.14, respectively, for S-failure proposed model. The validation of model was conducted considering 25 experimental tests performed on joints experiencing S-failure. The proposed equation is only applicable for the case of pullout failure before rebar yielding. In addition, two different distinct modes of joint axial failure were identified and an empirical model was proposed. Finally, the author, based on the current and previous tests with and without axial failure, identified an "axial failure safe zone" because joint axial failure was not observed for drift ratio demand below 2.5%-3%.

Starting from results by Hassan (2012), Hassan and Mohele (2012), present analytical tools for nonlinear modeling of exterior and corner joints in existing concrete buildings. A new nonlinear macro model was developed to model cyclic performance. The model incorporates new expressions for joint shear strength and axial capacity for J-failure and BJ-failure mode. The empirical equation has been calibrated on 12 experimental tests, and validated on 3 joint sub-assemblages.

Other empirical models were developed by Bakir and Boduroglu (1985) and Sarsam and Phipps (2002). These two last models were calibrated basing on monotonic tests, and cannot be used to predict the actual behavior of existing beam-column joints subjected to cyclic loadings during earthquake shaking.

However, it is worthy to note, that most of the empirical models proposed in literature were developed based on statistical regression analysis with large scatter or small size of experimental data sets.

2.3.2 JOINT SHEAR BEHAVIOR

Although joint shear strength is very important to model joint shear behavior, to realistically reproducing existing building behavior, the entire moment-rotation relationship has to be used to model joint behavior. Under cyclic loadings, the

deterioration of the shear strength of beam-column joints under cyclic displacement was experimentally observed. The diagonal tension cracking of the joint core in alternative directions during seismic loading causes the reduction of the diagonal compressive strength of the concrete; therefore, the joint shear strength may degrade with the increase in ductility demand in the adjacent members during cyclic loading. Previous experimental research on the seismic performance of the beam-column joints that have no transverse reinforcement in the panel zone (e.g., Walker, 2001; Alire, 2002; and Pantelides et al., 2002) has revealed that the joint shear stress-strain response typically has a degrading envelope and a highly pinched hysteresis. Some models in literature attempted to capture this effect. For instance, Park (1997) and Hakuto et al. (2000) proposed nominal shear strength degradation models for exterior and interior non-ductile beam-column joints as a function of imposed curvature ductility factor. Priestley (1997) presented a model for principal tension strength degradation as function of drift ratio. Finally, Pampanin et al. (2002) developed a strength degradation curve for exterior substandard joints, with smooth beam reinforcement having a small hook within the joint and no transverse reinforcement. This model expresses joint strength in terms of principal tension stress rather than shear strength, indirectly including the effect of axial load. In these studies, the relationship between the reduction of joint shear strength and the ductility factor is empirically proposed, but they cannot be accurately generalized because the ductility factor is uncertain and it takes also into account the deformation of the members adjacent to the joint.

Several analytical models have been proposed in the past to describe the behavior of reinforced concrete beam-to-column joints. The main distinction between proposed models can be based upon its derivation.

Simplified models are either empirical (i.e., based on experimental results and observations), or mechanics-based, (i.e., based on the salient response mechanisms). Empirical models are relatively simple models that rely on calibrated springs to represent behavior, essentially applying curve fitting to overall joint behavior. These models can present good agreement with the tests on which they are based, however, the models are barely extendable to other cases. Mechanism-based models are instead more appealing because of their potential to be used in a wide array of settings. These models attempt to capture the individual mechanisms that describe behavior rather than being calibrated based on a curved fit to the overall joint behavior. However, these models usually employ simplifying assumptions that can make these models simpler to apply while reducing their accuracy.

2.3.2.1 EMPIRICAL JOINT MODELS

Alath and Kunnath (1995) developed a simple empirical model. The joint shear deformations are modeled using a single rotational spring with degrading hysteresis. The finite dimension of the joint panel is reproduced by introducing four rigid links in

the immediate vicinity of the intersection of beam and column centerlines, as illustrated in Fig. 2.8(a). An empirical tri-linear shear-strain backbone curve, is used to define the nonlinear behavior, while the cyclic response was captured using a hysteretic model calibrated by experimental cyclic response. The model do not explicitly account for the effects of reinforcement, bond-slip, confinement or concrete behavior. The model was validated through the comparison of experimental and analytical response of a nonductile interior beam-column joint subassemblage.

Biddah and Ghobarah (1999) proposed to separate shear deformations and bond-slip by using different spring elements, Fig. 2.8(b). For the simulation of an interior joint, two bond-slip springs and one shear spring are required; while for an exterior joint, one bond-slip spring and one shear spring represent behavior. An idealized tri-linear constitutive model was described based on a softening truss model for monotonic behavior, while cyclic behavior is defined through a multi-linear hysteretic model that neglected pinching due to concrete cracking and crushing of concrete immediately surrounding reinforcement. These constitutive models are not deemed sufficient to describe material behavior.

Pampanin et al. (2003) proposed a single-spring model similar to scissor model by Alath and Kunnath (1995), but including pinching due to bond-slip and shear cracks in the joint in the hysteretic behavior. The model also includes lumped plasticity at beam's ends. The joint shear backbone is expressed in terms of moment-rotation relationship and is based on bilinear shear deformation-principal tensile stress relationship.

Anderson et al. (2008) developed a monotonic and cyclic shear stress-strain model based on joints without transverse reinforcement tested by Walker (2001) and Alire (2002) at the University of Washington. A tri-linear backbone representing 3 distinct levels of stiffness was combined with a multi-linear cyclic model, which had the ability to include degradation of stiffness and strength. The model can provide accurately the hysteretic response of the joint for various displacement histories, joint shear stress demands, and concrete compressive strength.

Park and Mosalam (2009) calibrated a semi-empirical moment-curvature relationship that is applied to a scissor model based on a single diagonal compression strut to resist joint shear for exterior and knee joints. Joint shear strength calculation accounts for joint aspect ratio and longitudinal beam reinforcement, while neglecting column axial load. Joint aspect ratio is the only parameter affecting maximum and minimum joint shear strength, but between these values the shear strength is linearly proportional to the beam reinforcement index.

Birely et al. (2011) proposed to model the joint as a rigid element using rigid offsets, at the end of which two springs are connected in series to the beams on either side of the joint, see Fig. 2.8(h). The model incorporates a lumped-plasticity beam-column element with the two springs representing the moment-rotation response of the joint and the moment-rotation response of the beam. No consideration is made for nonlinearity in the column. The model was calibrated considering 45 beam-column joint specimens. Specimens were all used normal weight, non-high-strength concrete in interior joints.

2.3.2.2 MECHANISM-BASED JOINT MODELS

Filippou et al. (1983) proposed an analytical joint model, see Fig. 2.7. The joint panel is divided into several layers, each representing either steel reinforcement or concrete. Each material is represented by a different constitutive nonlinear model. While Giuffrè-Menegotto-Pinto is used for steel, Filippou proposed a new concrete model. This concrete model bases crack closure on the crack width in a given layer, but does not account for any tensile strength in the concrete. A bond stress-slip model developed by Ciampi et al. (1981) is used to account for the incompatibility of steel and concrete strains. The model accounts for either bond-slip and concrete flexural cracking, while it do not account for any of the effects of shear within the joint.
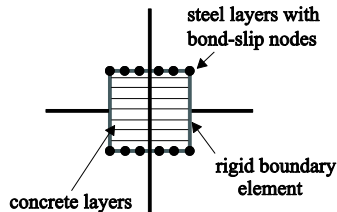
Filippou et al. (1983)

Fig. 2.7 Joint model developed by Filippou et al. (1983)

Youssef and Ghobarah (2001) proposed to model the joint element with two diagonal translational springs linking the opposite corners of the panel zone simulate the joint shear deformation, see Fig. 2.8(c). The backbone curve of the joint was defined using the MCFT. To account for the effect of bar-slip within the joint and concrete crushing at the joint perimeter, three translational springs at each joint face were used. The analytical model was validated using the experimental results of ductile and non-ductile exterior beam-column joints. The model requires a large number of translational springs and a separate constitutive relationship for each spring, which may not be available and restrict its applicability.

Lowes and Altoontash (2003) proposed a beam-column joint model capable of simulating inelastic connection behavior resulting from reinforcement bond slip and

joint shear deformation for joints with moderate to high volume of transverse reinforcement. The new element consisted in a four-node 12-DOF joint element that consists of eight zero-length bar slip springs, four interface shear springs, and a panel that deforms only in shear, as illustrated in Fig. 2.8(d).

The authors used the modified compression field theory MCFT by Vecchio and Collins (1986) to define the envelope of the joint shear stress versus joint shear strain history as a function of material properties, joint geometry, and joint reinforcement layout. The model was validated using 4 beam-column connection subassemblies, concluding that the model can well represent the fundamental response characteristics for beam-column joints subjected to moderate shear demands. The use of MCFT assumes at least a moderate amount of transverse reinforcement within the joint

Altoontash (2004) proposed a simplification of Lowes and Altoontash (2003) model by introducing a model composed by four zero-length bar-slip rotational springs located at beam and column-joint interfaces and a zero-length joint rotational spring at an internal node, as depicted in Fig. 2.8(e). The constitutive relationship of the shear panel follows the model of Lowes and Altoontash (2003), while Altoontash (2004) modified the beam or column fiber sections to represent the bar pull-out mechanisms based on the assumption that the development length is adequate to prevent complete pullout. The validation was performed for interior beam-column joint subassemblages tested by Walker (2001) and a scale two-story RC frame tested by Tsai et al. (2000).

Shin and LaFave (2004) , Fig. 2.8(f), suggested a joint model consisting of four rigid elements located along the edges of the panel zone connected via hinges and three nonlinear rotational springs embedded in one of the four hinges. These rotational springs are used to simulate the inelastic behavior of joint core under shear loading. Supplementary rotational springs are placed between the beam ends and the joint to describe bar-slip and the plastic hinge in the beams The three shear springs are combined to create a multi-linear envelope based on MCFT and hysteretic behavior calibrated from experimental data. The analytical predictions were compared with the experimental results of ductile RC interior beam-column joint subassemblages.

Mitra and Lowes (2007) modified the Lowes and Altoontash (2003) model to better simulate the unreinforced joint panel behavior. The experimental data used for the model validation, in fact, included interior specimens with at least a minimal amount of joint transverse reinforcement. Therefore, the model may not capture the hysteretic response for joints with little or no joint transverse reinforcement. The new model proposed by Mitra and Lowes (2007) assumed a diagonal compression-strut mechanism for load transfer within the joints rather than the uniform stress field suggested by the MCFT (Vecchio and Collins 1986). Furthermore, a new bond-slip model is proposed

and the placement of bond-slip springs was slightly altered to better represent true specimen geometry. The concrete strut within the joint carries the entire shear load. The contribution of steel reinforcement is only considered in relation to confinement of the core; the only relation of steel to the model is the resultant force orthogonal to the compression strut. No consideration is made for axial deformations or buckling of the reinforcement. The constitutive model for the springs was altered so that convergence issues in computation could be avoided. In the Lowes and Altoontash model, the loss of strength due to reaching the slip limit would result in a negative slope. In this model, however, the loss of strength is handled by the hysteretic model. As the model is cycled to increasing slip, the stiffness is decreased so that a higher amount of slip results in lower bond forces. The model was validated using an experimental database consisting of 57 subassemblies.

Celik and Ellingwood (2008), proposed to evaluate the maximum joint shear strength as the joint stress as a function of adjoining beam and column capacities. The moment transferred by beams is reduced to account for bottom rebars bond slip by an empirical factor. Finally, the panel node strength, to account for possible shear failure occurring before beams or columns reach their capacities, is limited so as not to exceed a maximum joint shear strength statistically defined through a dataset of experimental results in a range of values with a uniform distribution. The model was calibrated through a database of experimental sub-assembly tests with no transverse reinforcement in the joints. The database consisted of 10 experimental tests performed on exterior and 33 tests performed on interior joints. The tests included joints with well-anchored beam reinforcement (Walker, 2001) as well as beam reinforcement with short embedment length (Pantelides et al.2002). For beams with poorly anchored bottom reinforcement, the joint M-θ envelope was reduced to account for the decreased beam negative moment. However, additional rotation due to reinforcement slip was ignored. The beam-column joint model was validated using the results from two full-scale experimental RC beam-column joint test series.

Sharma et al. (2011) proposed a joint model based primarily on the principal tensile stress proposed by Priestley (1997). This model, Fig. 2.8(g), combines 3 hinges with a centerline model to describe behavior of non-ductile exterior joints with different reinforcement details. The beam and columns were modeled as lumped plasticity elements. The model validation was performed for non-ductile exterior beam-column joint assemblages with different types of beam bottom reinforcement. However, their model can only be applied to exterior beam-column joints Bond-slip in the model is not directly modeled. It also does not allow for the evaluation of the causative effects of individual components to failure.

Park and Mosalam (2012a) proposed a mechanical approach based on the strut-and-tie model to predict the joint shear strength of exterior beam-column joints without transverse reinforcement. The predict shear resistance for joints, which experienced joint shear failures with and without beam yielding. The proposed joint shear strength model accounted for joint aspect ratio and beam reinforcement ratio. In a previous work Park and Mosalam (2012b) conducted experimental tests on exterior unreinforced beam-column connections aimed at the definition of the main parameters having the greatest influence on joint shear strength. In this paper, the authors investigated the effects of three main parameters, namely (i) joint aspect ratio, (ii) beam longitudinal reinforcement ratio, and (iii) column axial load, and confirmed that joint aspect ratio and beam longitudinal tension reinforcement ratio and its strength mainly influence joint shear strength. Although their model can predict the joint shear strength for non-ductile exterior and corner joints well, their proposed formulation cannot be applied to interior or roof joints. In order to overcome the limitation of the applicability to other joint types, Park and Mosalam (2013) modified the joint shear strength model proposed by Park and Mosalam (2012a) by multiplying the formulation for exterior joints by the shear strength ratio, which is the ratio of joint shear strength coefficient for other three types of joints (interior, roof, and knee joints) to the exterior joint shear strength coefficient. Further, a multilinear backbone curve to represent the moment rotation relationship of joints is proposed. The backbone curve is developed empirically based on the joint responses measured and visual observation. The backbone curve has been calibrated to sole four corner specimens. Although analytical predictions provide reasonable results through the comparison of those and experiments, actual joint strength coefficient ratio based experimental observation is different.

Jeon et al.(2015) partially modified the backbone curve proposed by Anderson et al. (2008) in order to suggest a unified joint shear model that can be simply applied to both internal and external non-ductile joints. The author considered two possible failure modes (joint shear and bond failure) validating the model on 28 exterior and 35 interior beam-column subassemblages from experimental works available in literature.

Some of the aforementioned joint models (Youssef and Ghobarah 2001, Lowes and Altoontash 2003, Mitra and Lowes 2007, Altoontash 2004, Shin and LaFave 2004) were developed employing the MCFT by Vecchio and Collins (1986) to define the backbone curve of a joint panel. LaFave and Shin (2005) demonstrated that the MCFT may underestimate the joint shear strength for joints non-ductile joints with insufficient joint transverse reinforcement. Therefore, the MCFT can provide the reasonable estimate of joint shear strength for ductile joints while the application of the MCFT to non-ductile joints requires additional modifications
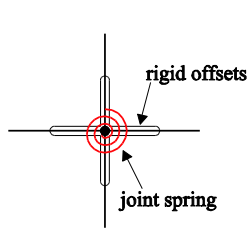
(a) Alath and Kunnath (1995)
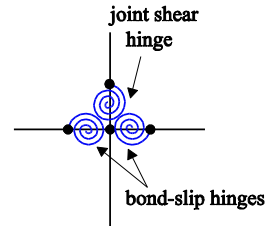
(b) Biddah and Ghobarah (1999)
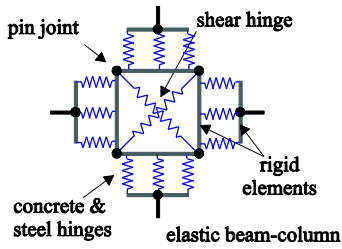
(c) Youssef and Ghobarah (2001)
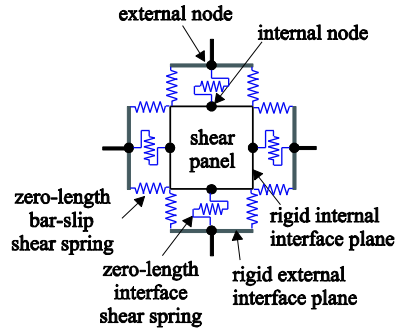
(d) Lowes and Altoontash (2003)
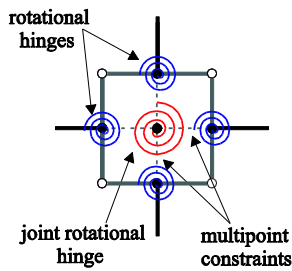
(e) Altoontash (2004)
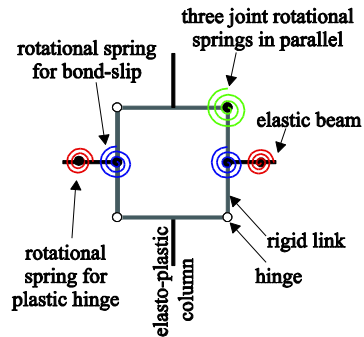
(f) Shin and LaFave (2004)
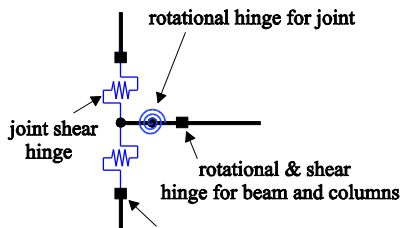
(g) Sharma et al. (2011)
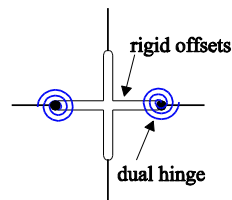
(h) Birely et al. (2011)

Fig. 2.8 Kinematic of joint models (adapted from Celik and Ellingwood, 2008)

32

2.4   COLLAPSE DEFINITION

In order to effectively prevent earthquake induced structural collapse, the collapse process and the failure modes of structures should be properly predicted.

For ductile buildings, it is typically assumed that sidesway collapse is the governing mechanism (ATC, 2009). In these buildings, the primary expected failure mode is flexural hinging leading to sidesway collapse, which the modeling approach can simulate by properly capturing post-peak degrading response under both monotonic and cyclic loading, and collapse prediction is based on lateral dynamic instability, or excessive lateral displacements. The modeling approach should then be able to properly simulate structural response up to collapse by simulating all expected modes of damage that could lead to collapse, such as strength and stiffness deterioration due to flexure and flexure-shear.

On the other hand, non-ductile concrete buildings may experience gravity-load collapse due to loss of vertical-load-carrying capacity prior to development of a side-sway collapse mode. For this reason nonlinear models should incorporate elements capable to simulate the onset of column shear failure and subsequent rapid deterioration and loss of gravity-load bearing capacity (Elwood, 2004), which may occur because reinforced concrete ordinary moment frame columns have light transverse reinforcement and are not subject to capacity design requirements. In addition, P-Delta effects should properly accounted for in the modeling.

In particular, the inability of the structural system to redistribute its loads following the failure of one or more structural components to carry gravity loads usually leads to a phenomenon usually named "Progressive Collapse". Especially for RC structures built according to older building code provisions (i.e. lacking of ductile reinforcement details), the loss of gravity load carrying capacity in columns has been observed to trigger a chain of collapse events leading to the collapse of the entire building or a large part of it.

Progressive Collapse

In last years, the engineering community has paid greater attention to the vulnerability of multistory buildings to disproportionate collapse, which could pose a substantial hazard to human life. In particular, "Progressive collapse" is defined as a "disproportionately large structural failure resulting from a relatively local event such as the failure of a gravity load-carrying structural member and the subsequent inability of the structural system to redistribute the resulting overload through a path that can maintain overall stability and integrity".

The progressive collapse of building structures occurs when one or more vertical load carrying members (typically columns) is removed. Once a column is removed, the

gravity load transfers to remaining structural elements. If these columns are not properly designed to resist and redistribute the additional gravity load, this failure usually occurs in a domino effect that leads to a progressive collapse failure in the structure

The risk of progressive collapse due to gravity load-carrying capacity loss during seismic events is particularly concerning for older structures, designed and detailed prior of current knowledge about structural response to seismic excitation and the requirements of ductile design.

Two possible options can be followed to model gravity load collapse. The first, usually referred as "Simulated Collapse", requires to explicitly model the sequential failure of frame members, and involves element removal until the structure is no more capable to carry gravity loads. In this case, the "Progressive Collapse" is explicitly simulated and the structural collapse is caused by collapse modes that are directly represented in the analytical model. The second alternative identify collapse with post-processing of the simulation results. This way the structural collapse is caused by collapse modes that are not represented in the analytical model and it is often referred as "Non-Simulated Collapse". Non-simulated collapse occurs when a component limit state is exceeded.

2.4.1 COLLAPSE SIMULATION

Progressive collapse of buildings is a field of research that has been receiving increasing attention in last decades. Nowadays, the availability of advanced computational resources and the several studies about the actual behavior of building members allow much detailed analyses that were no possible in the past.

Usually, Simulated Collapse involves elements removal of RC members that have collapsed during an ongoing FE simulation. Several studies have been carried out involving the collapse of structural elements and element removal during progressive collapse simulation.

According to the US Department of Defense (DoD) and US General Services Administration (GSA) guidelines, progressive collapse can be analyzed using linear static, linear dynamic, nonlinear static and nonlinear dynamic procedures with an increasing level of sophistication for the analysis. In these guidelines, a simplified analysis technique for investigating the potential of progressive collapse in the design of buildings, the so called "Alternate Load Path Method" was recommended as a simplified analysis tool. In this analysis, information about static load redistribution is obtained while dynamic effects are not directly taken into account. Instead, an amplification factor of 2 is suggested to indirectly account for dynamic effects. Despite that, these documents do not provide enough information to carry out progressive collapse studies of buildings (Bao and Kunnath, 2011)

Although several researchers presented the importance of considering inertial effects for progressive collapse analysis, dynamic load redistribution in the progressive collapse analysis of frame structures is hardly considered in practicing engineering because most of commercial softwares do not support progressive collapse analysis with dynamic effects. Even though the nonlinear dynamic analysis is computationally complex and time-consuming, its results are more accurate compared to other methods.

Progressive collapse assessment using nonlinear time-history is recently achieving popularity compared to traditional methods based on alternate-path analysis and redundancy-detailing.

A recent study by Kaewkulchai and Williamson (2004) defines a macro-level damage index based on maximum deformations and cumulated plastic energy to predict collapse of yielding beam-column elements. When the damage index reaches a threshold value (e.g., one), the collapsed element is removed from the structural system. External nodal forces are then applied at the end-nodes to represent the effect of the redistributed internal forces from the collapsed element. This approach is valid for simulating quasi-static behavior but is sensitive to the choice of time step (i.e., time step size) during a dynamic simulation and may not be accurately representative of the stored energy imparted into the damaged structure due to the release of internal forces from the collapsed element. The procedure also account for the downward motion of the collapsed element. In a more recent publication, Kaewkulchai and Williamson (2006) included a simplified approach to account for impact on the structure by a collapsed element.

Another analytical study reported in Grierson et al. (2005a,b) describes an analytical approach to use post-yield strength and stiffness degradation in order to conduct a quasi-static progressive failure analysis including a collision between elements due to partial collapses.

Kim (2006) studied the progressive collapse of RC structures with structural deficiency and limited ductility and later, Kim et al. (2009) developed an integrated system for progressive collapse analysis by using OpenSees to automatically evaluate the damage level of every member at each analysis step and to construct the modified structural model for next analysis step. Two alternative approaches to model failed members were adopted, the first considers nonlinear hinges to the ends of beam members, when the damage index becomes equal to one, the moment-resisting capacity of the hinge automatically drops to zero while axial and shear force-resisting capacities still remain, this way the behavior of the failed member cannot be modeled accurately. The second alternative requires to generate an additional node at the end of failed members to separate the failed member from the node. They showed that the collapse mechanism strongly depends on the modeling technique adopted for failed members.

Sasani and Kropelnicki (2007) studied the approach of load-bearing element removal to evaluate progressive collapse in RC structures.

Bazan (2008) used nonlinear dynamic analysis to examine the response of reinforced concrete elements and structures after removing load-bearing elements.

Talaat and Mosalam (2009) employed direct removal of element to model progressive collapse of reinforced concrete structures implementing a logical algorithm in Opensees. This algorithm is based on dynamic equilibrium and the resulting transient change in system kinematics, and involves the application of imposed accelerations instead of external forces at a node where an element was once connected. It simulates the dynamic redistribution of forces in addition to a simplified modeling of impact and recently developed criteria for element removal that involves updating in nodal masses, removing of floating nodes, and removing of all associated element and nodal forces after each element reaches the failure state. This method is very effective into the simulation of actual behavior of RC frames while its limitations are mainly related to the computationally intensive process required to update the structure after each element is removed, and convergence problems associated to sudden changes in the structural model after each element removal.

2.4.1.1 SIMULATED COLLAPSE MODES

As far as possible, frame models should directly simulate all significant deterioration modes that contribute to collapse behavior. Typically, this goal is achieved through structural components able to capture strength, stiffness degradation and inelastic deformation under large deformations.

Once the backbone curve is defined, the hysteretic response of elements that leads to the reduction of strength and stiffness with respect to boundaries defined by the monotonic backbone curve should be included given the degrading influence on the collapse response in nonlinear dynamic analyses. Several degrading hysteretic models are available in literature, of varying degrees of sophistication using phenomenological or physics-based approaches. Characterization of component backbone curves and hysteretic responses should represent the median response properties of structural components.

Critical response will vary for each specific component and configuration. Consequently, the adopted analytical model is case specific, and no single model is universally applicable. For instance, in ductile reinforced concrete components, nonlinear response is typically associated with moment-rotation in the hinge regions where degradation occurs at large deformations through a combination of concrete crushing, confinement tie yielding/rupture, and longitudinal bar buckling. In non-ductile reinforced concrete components, nonlinear response may include shear failures and axial failure following shear failure. Where the seismic-force-resisting system carries significant gravity load, characteristic force and deformation quantities may need to represent vertical deformation effects as well as horizontal response effects.

2.4.1.2 NON-SIMULATED COLLAPSE MODES

The term "non-simulated" is used to describe potential modes of collapse failure that are not directly simulated in the analytical model, but that is evaluated by alternative methods of analysis and included in the evaluation of collapse performance. When it is not possible, or practical, to explicitly simulate any deterioration modes contributing to collapse behavior, collapse mode can be evaluated using alternative state checks on structural response measured in the analyses. Usually, shear failure and subsequent axial failure in RC columns are often treated as non-simulated collapse modes by code provisions. Non-simulated collapse modes are usually associated with component failure modes (i.e. the first occurrence of this failure mode corresponds to the collapse of the entire structure), the so called component-based assessment procedures. Collapse of an entire structure predicated on the failure of a single component can, in many cases, be overly conservative.

Consequently, compared to directly simulated collapse modes, non-simulated limits state checks will generally results in lower estimates of median collapse (ATC, 2009)

Although non-simulated collapse modes is a practical approach, it ignores the ability of a structural system to redistribute loads as damage accumulates and will tend to lead to conservative assessments of collapse vulnerability. Seismic evaluation documents based on checklist assessments (e.g. ASCE/SEI 31, 2003, and ASCE/SEI 41, 2007) are generally conservative to ensure dangerous buildings are not misdiagnosed. Local failure modes should be explicitly simulated to account for forces redistribution to other components after a limit state has been reached.

Chapter 3

EVALUATION OF BUILDING SEISMIC PERFORMANCES IN INTACT AND DAMAGED STATES

The current chapter present a detailed description of case-study buildings' structural system, the modeling technique and the members analytical models adopted in this study to simulate brittle member behavior and a recently introduced system-level collapse definition. The performances of intact building are assessed through nonlinear static and dynamic analyses and the damage pattern is highlighted. A novel framework for the assessment of performance to collapse of existing structures is introduced with a detailed description of component modules (record selection, simulation of damaging earthquakes, post-earthquake fragility computation). The above-mentioned framework is applied to two case studies in order to estimate the variation of building's seismic performances.

3.1   BUILDING DESCRIPTION

American case-study building
The building selected for the study to be representative of a non-ductile American building is the Van-Nuys Holiday Inn building in Los Angeles City, California (north frame elevation is shown in Fig. 3.1). This building was designed in 1965 according to LA City Building Code 1964 (ACI 318-63) showing inadequate details for seismic zones by today's standards (e.g. no transverse steel in the beam-column joints). The building is located at 34.221°N, 118.471°W, in the San Fernando Valley, just northwest of downtown Los Angeles. The building experienced three different earthquakes (San Fernando, 1971, Whittier Narrows, 1987, and Northridge, 1994) and damage resulting from these earthquakes was extensively documented (Trifunac et al., 1999).

The case-study building has been studied by a number of authors. Notable examples include Jennings (1971), Scholl et al. (1982), Islam (1996a, 1996b), Islam et al (1998), Li and Jirsa (1998), and Trifunac et al. (1999); in Trifunac et al. (1999) a thorough description of the damage suffered by the building in the 1994 Northridge Earthquake is provided. It has also been used as a testbed for studies of performance-based

earthquake engineering (e.g. PEER funded project number 3272002, see www.peer.berkeley.edu).
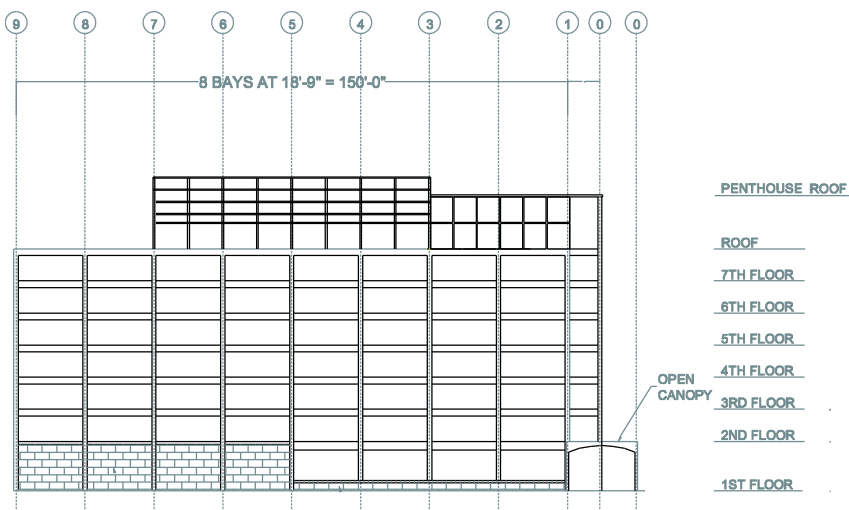
Fig. 3.1 North perimeter view (Reissman, 1965)

Italian case-study building
The building selected for the study to be representative of a non-ductile Italian building is an existing building in Benevento, Campania, Italia. The building was designed in 1958 according to first Italian seismic provisions (Regio Decreto n.2105 22/11/1937) showing inadequate details for seismic zones by today's standards. The building is located at 41.1277° N, 14.7742° E.

3.1.1 STRUCTURAL SYSTEM

American case-study building
The Van Nuys Holiday Inn building is a 66000 sf (6200 m^2), seven story hotel building with a highly regular framing plan with eight bays in the East-West (longitudinal) direction and three in the North-South (transverse) direction. The plan of the structure is regular and symmetric with the exceptions of an exterior canopy on the east side of the first floor, and an external stair tower on the east side at the northern corner. Four bays of the first floor framing on the east side of the North face are infilled with lightly reinforced brick walls. Expansion joints separate the sides of the brick wall from the surrounding columns and overhead spandrel beam.

For this study, the perimeter longitudinal frame has been extracted. All geometric features were taken from the original structural drawings by Rissman and Rissman Associates.

The first level of the building has a floor-to-floor height equal to 4.11 m (13.5 ft), of 2.64 m (8.67 ft) for the top story, and 2.65 m (8.7 ft) for all other levels for a total building height of 20 m (65 ft). The plan dimension of the longitudinal frame is 46 m (150 feet) with a constant beam length of 5.2 m (18.75 ft). The building was retrofitted following the 1994 Northridge earthquake, but this study considers the building in its pre-Northridge earthquake condition. The structural system is a cast-in-place reinforced-concrete moment-frame building with non-ductile column detailing. Perimeter moment frames provide the primary lateral force resistance, although the interior columns and slabs also contribute to lateral stiffness. The gravity system comprises 2-way reinforced-concrete flat slabs supported by rectangular columns of the perimeter frame. The original design included both the exterior beam-column frames and the interior slab-column frames as part of the lateral force-resisting system. The exterior columns are 36 x 51 cm (14 x 20 in.) at all levels, with the 51 cm dimension along the north-south direction. Beams are 36 x 76 cm (14 x 30 in.) at level one, 36 x 57 cm (14 x 22.5 in.) at levels two through six, and 36 x 56 cm (14 x 22 in.) at the roof level. Column reinforcement steel is A432-62T (Grade 60) for billet bars. Beam and slab reinforcement is ASTM A15-62T and A305-56T (Grade 40) for intermediate grade, deformed billet bars. Column reinforcement arrangement is shown in Fig. 3.3.

Scheme for column and beam element for the south frame is reported in Fig. 3.2. From Table 3-1 to Table 3-4, column and beam section and reinforcement schedules are summarized.
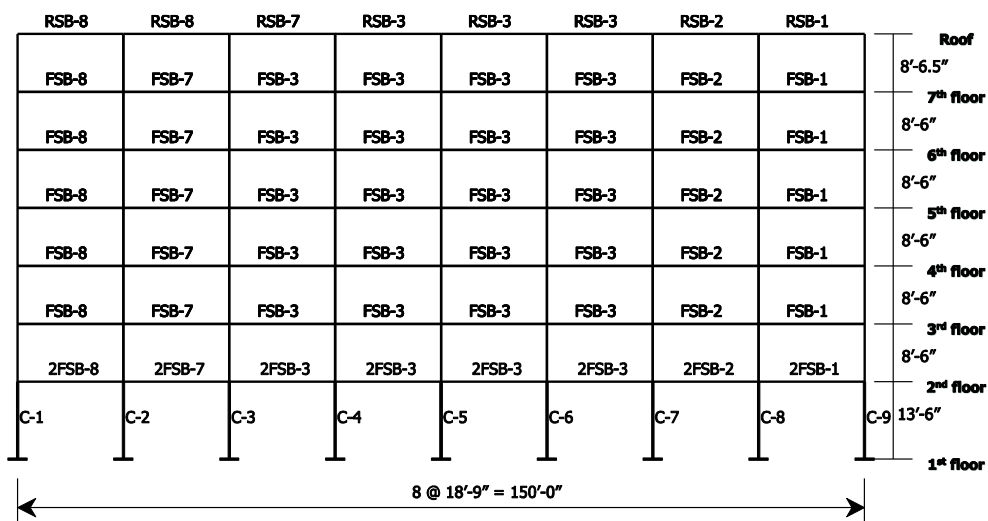
Fig. 3.2 Column-beam scheme for longitudinal Van Nuys frame

41

Column concrete has nominal strength of $f_c = 5$ ksi (34.34 MPa) for the first story, 4 ksi (27.58 MPa) for the second story, and 3 ksi (20.68 MPa) from the third story to the seventh. Beam and slab concrete strength is nominally $f'_c = 4$ ksi at the second floor and 3 ksi from the third floor to the roof.

| 6 BARS | 8 BARS | 10 BARS |
| 2TIE / SET | 2 TIE / SET | 3 TIE / SET |
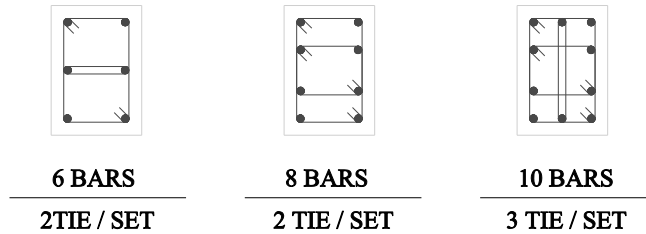
Fig. 3.3 Arrangement of column steel (Rissman and Rissman Associates, 1965)

COLUMN MARK			C-1, C-9			C-2, C-3, C-8			C-4 to C-7		
LEVEL	CONCRETE STRENGTH (psi)	COL SIZE	14"	x	20"	14"	x	20"	14"	x	20"
7th	3000	VERT. BARS	6	-	#7	6	-	#7	6	-	#7
		TIES	#2	@	12"	#2	@	12"	#2	@	12"
6th	3000	VERT. BARS	6	-	#7	6	-	#7	6	-	#7
		TIES	#2	@	12"	#2	@	12"	#2	@	12"
5th	3000	VERT. BARS	6	-	#7	6	-	#7	6	-	#7
		TIES	#2	@	12"	#2	@	12"	#2	@	12"
4th	3000	VERT. BARS	6	-	#7	6	-	#7	6	-	#9
		TIES	#2	@	12"	#2	@	12"	#2	@	12"
3rd	3000	VERT. BARS	6	-	#7	8	-	#9	6	-	#9
		TIES	#2	@	12"	#3	@	12"	#3	@	12"
2nd	4000	VERT. BARS	6	-	#7	8	-	#9	6	-	#9
		TIES	#2	@	12"	#3	@	12"	#3	@	12"
1st	5000	VERT. BARS	8	-	#9	10	-	#9	10	-	#9
		TIES	#3	@	12"	#3	@	12"	#3	@	12"

Table 3-1 Column schedule for American building

Soil conditions at the site are found in Tinsley and Fumal (1985), who mapped superficial soil deposits in the Los Angeles region using a variety of sources. They describe the site soil as Holocene fine-gained sediment (silt and clay) with a mean shear-wave velocity of 218 m/sec, corresponding to site class D according to NEHRP classification.

BEAM MARK	SIZE		REINFORCING		
	Width (in.)	Height (in.)	Top Bars	Bottom Bars	Ties
2FSB-1	16	30	@1 & 9 2 #9	2 #8	4 @6",2 @8", ea end, rest @13
			@2 & 8 3 #8		
2FSB-2	16	30	@2 & 8 3 #8	2 #6	same
			@3 & 7 2 #9		
2FSB-3	16	30	2 #9	2 #6	same
			2 #9		
2FSB-7	16	30	@3 2 #9	2 #7	same
			@2 2 #9		
2FSB-8	16	30	@2 2 #9	2 #8	same
			@1 2 #9		

Table 3-2 Second floor spandrel beam schedule for the American building

BEAM MARK	SIZE		REINFORCING TOP BARS					BOTTOM BARS	#3 Ties
	Width (in.)	Height (in.)	7th Floor	6th Floor	5th Floor	4th Floor	3rd Floor		
FSB-1	16	22.5	@1 & 9 '2 #9'	2 #9	2 #9	3 #8	3 #8	2 #7	@ 1 & 9 3@5", 5@6", rest @10", 3F- 5F
			@2 & 8 '2 #9'	same	same	same	same		@ 2 & 8 6@4", 5@6", 3F-5F
FSB-2	16	22.5	@2 & 8 '2 #9'	3 #8	3 #8	3 #8	3 #9	2 #6	8@5", 5@6" ea end
			@3 & 9 2 #8	same	same	same	same		Rest @ 10" 3F-5F
FSB-3	16	22.5	2 #8	2 #9	3 #8	3 #8	3 #9	2 #6	3@5", 5@6" ea end
			2 #8	same	same	same	same		Rest @ 10" 3F-5F
FSB-7	16	22.5	@3 2 #8	same	same	same	same	2 #7	3@5", 5@6" ea end
			@2 2 #8	same	same	same	same		Rest @ 10" 3F-5F
FSB-8	16	22.5	@2 2 #8	2 #9	2 #9	3 #8	3 #8	2 #7	@1 & 3@5", 5@6", rest@10" 3F-5F
			@1 2 #7	2 #8	2 #9	2 #9	3 #8		@2 6@4", 5@6" 3F-5F

Table 3-3 3rd through 7th floor spandrel beam schedule for the American building

Beam Mark	Size		Reinforcing		
	Width (in.)	Height (in.)	Top bars	Bottom bars	Ties
RSB1	16	22	@1 & 9 2 #6	2 #7	#3 @10"
			@2 & 8 2 #8		
RSB2	16	22	@2 & 8 2 #6	2 #6	same
			@3 & 7 2 #8		
RSB3	16	22	2#8	2 #6	same
RSB7	16	22	@4 2 #8	2 #6	same
			@3 2 #9		
RSB8	16	22	@3 2 #9	2 #9	same
			@2 3 #9		

Table 3-4 Roof spandrel beams schedule for the American building

Italian case-study building

The Italian building is a 2500 sf (232 m²), six story residential building with a highly regular framing plan with four bays in the longitudinal direction and two in the transverse direction. The plan of the structure is regular and symmetric with the exceptions of an internal concrete stair at the middle of the longitudinal frame.

For this study, the perimeter transversal frame, the only designed to resist to seismic actions, has been extracted. All geometric features were taken from the original structural drawings. Floor map and structural system for transversal frame is reported in Fig. 3.4 (a) and (b), respectively.

The first level of the building has a floor-to-floor height equal to 3.0 m (9.84 ft) for the first story and of 3.35 m (11.0 ft) for all other levels, for a total building height of 19.75 m (64.8 ft). The plan dimension of the transversal frame is 9.7 m (31.8 feet) with a constant beam length of 4.6 m (15.1 ft). The structural system is a cast-in-place reinforced-concrete moment-frame building with non-ductile detailing.

All the columns at the same story have constant section dimensions that decrease along the building's height, from 40 x 60 cm (16 x 23.6 in.) at the first story to 30 x 40 cm (12 x 15.7 in.) for the upper story. Any column has rectangular section with weak axis parallel to the longitudinal direction. Two different types of beams define the structural layout: spandrel and flat beams. Flat beams are disposed in the sole exterior parallel frame close to the stairwell, and their dimension is the same for each floor and equal to 25 x 145 cm (9.8 x 57 in.). Remaining two longitudinal frames have 60 x 30 cm (23.6 x 11.8 in) spandrel beams of constant section for any floor. Spandrel beam of transverse frames have a section dimension that reduces along the height of the building starting form 60 x 30 cm (23.6 x 11.8 in.) up to 40 x 30 cm (15.7 x 11.8 in.) for the roof

floor. Both beam and column's reinforcement steel is Aq 42 (f_y = 325.4 MPa) and concrete type is 680 (28.2 MPa). Column reinforcement arrangement is shown in Fig. 3.5. In Table 3-5 and Table 3-6, column and beam sections and reinforcement schedules are summarized.
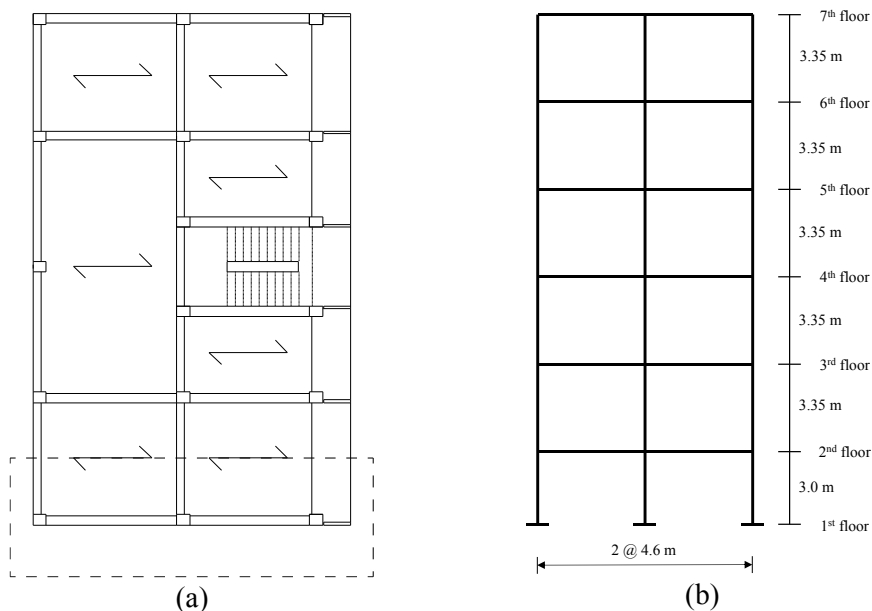
Fig. 3.4 Floor plant (a) and sketch of the Italian building transversal frame (b).

COLUMN SCHEDULE			
LEVEL	*COL SIZE*	*REINFORCEMENT*	
6th	30 x 40 cm	VERT. BARS	6ϕ16
		TIES	ϕ8/26 cm
5th	35 x 40 cm	VERT. BARS	4ϕ18+2ϕ16
		TIES	ϕ8/24 cm
4th	40 x 40 cm	VERT. BARS	10ϕ20
		TIES	ϕ8/22 cm
3rd	40 x 45 cm	VERT. BARS	8ϕ22+2ϕ20
		TIES	ϕ8/20 cm
2nd	40 x 50 cm	VERT. BARS	8ϕ24+2ϕ16
		TIES	ϕ8/18 cm
1st	40 x 60 cm	VERT. BARS	8ϕ26+2ϕ20
		TIES	ϕ8/15 cm

Table 3-5 Column schedule for Italian building

FLOOR	BEAM SIZE		REINFORCING		
	Width (cm)	Height (cm)	Top Bars	Bottom Bars	Ties
roof	30	40	2ϕ10+4ϕ12	2ϕ10	ϕ8/30 cm
6th	35	45	2ϕ10+4ϕ14	4ϕ10	same
5th	35	45	2ϕ10+2ϕ14+2ϕ16	2ϕ14+2ϕ16	same
4th	35	50	2ϕ12+2ϕ16+2ϕ20	2ϕ16+2ϕ20	same
3rd	35	55	2ϕ12+4ϕ20	2ϕ16+2ϕ20	same
2nd	40	60	5ϕ16+2ϕ20	2ϕ16+3ϕ20	same

Table 3-6 Column schedule for Italian building

Soil conditions at the site are found to be corresponding to B soil class according to Eurocode 8 (CEN 2004) classification (Santucci de Magistris et al., 2014). For this site a shear wave velocity ($V_{s,30}$) of 500 m/s^2 was assumed.

First Floor to sixth floor Columns units cm for dimensions mm for rebar diameter
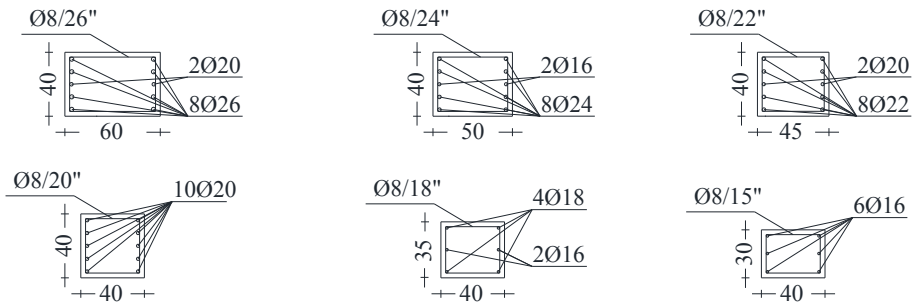
First Floor to sixth floor Beams
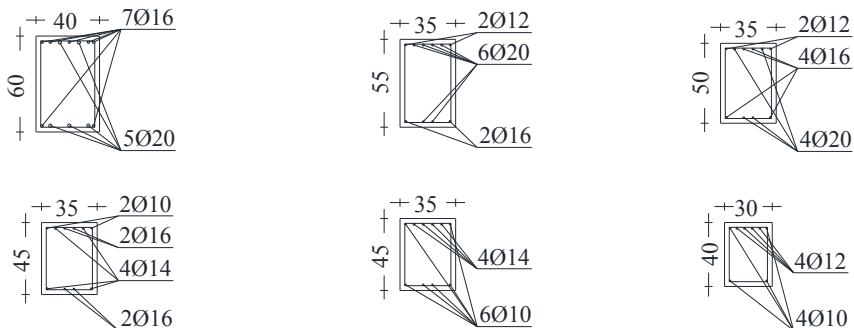
Fig. 3.5 Section and arrangement of columns and beams reinforcing bars for Italian building

3.2 ANALYTICAL MODEL

Assessment of structure's seismic performance, including estimation of seismic pre and post-earthquake seismic safety as well as repair cost analysis, requires development of a nonlinear model of the structure, which is then subjected to dynamic analysis to evaluate structural response. The structural model should be able to accurately capture building's behavior for both relatively low seismic intensity levels, frequent ground motions (mostly contributing to damage and economic loss) and high ones, rare ground motions (mostly contributing to collapse risk). While for low intensity levels, cracking and tension stiffening phenomena are important to capture the response of RC structures, for high or very high intensity levels, deterioration at large deformations leading to collapse is important.

3.2.1 OVERALL MODELING TECHNIQUE

As outlined in Chapter 2, several element models have been proposed to simulate the actual behavior of structures, from vary complex FEM models to more simple lumped plasticity models, however available element models generally do not accurately represent the full range of behavior.

Therefore, in the modeling of two case studies, a hybrid fiber-lumped model has been generated using OpenSees (McKenna, 2011) to simulate the building behavior from elastic to largely inelastic range. The fiber model is able to capture building behavior for low demand levels (where cracking and initial yielding behavior governs) while lumped hinge model can capture strength and stiffness deterioration as well as brittle failures and collapse.

Beams and columns are modelled using the force-based nonlinear beam–column element (deSouza, 2000). Due to non-ductile details that characterize both of the structures, is expected that the joints may influence the failure mechanism, consequently the joints are modeled using rotational spring elements, the so called "scissor model" by Alath and Kunnath (1995), including a pinching hysteric behavior to account for the nonlinear shear deformation of the joint. Similarly, shear and axial failure are expected to occur in non-ductile detailed columns, and consequently shear and axial failure in the columns are modeled using the Limit State material (Elwood, 2004). Bond-slip rotations for beams have been included modifying joint backbone as proposed in Celik and Ellingwood (2008), while column-base bond-slip at first floor has been explicitly modeled by means of elastic springs. The model includes 5% Rayleigh damping anchored to the first and third modal periods. P-Δ effects were included in the model because they can significantly increase displacements and internal member forces in the post-yield response of the structures. For simplicity, only the lateral resisting system is modeled, neglecting the contributions of elements designed primarily for gravity loads

or nonstructural elements. The effect of slip at bottom of fist floor columns is incorporated using elastic rotational springs at the base of each column. A sketch of the model adopted in this study for both case studies is depicted in Fig. 3.6.
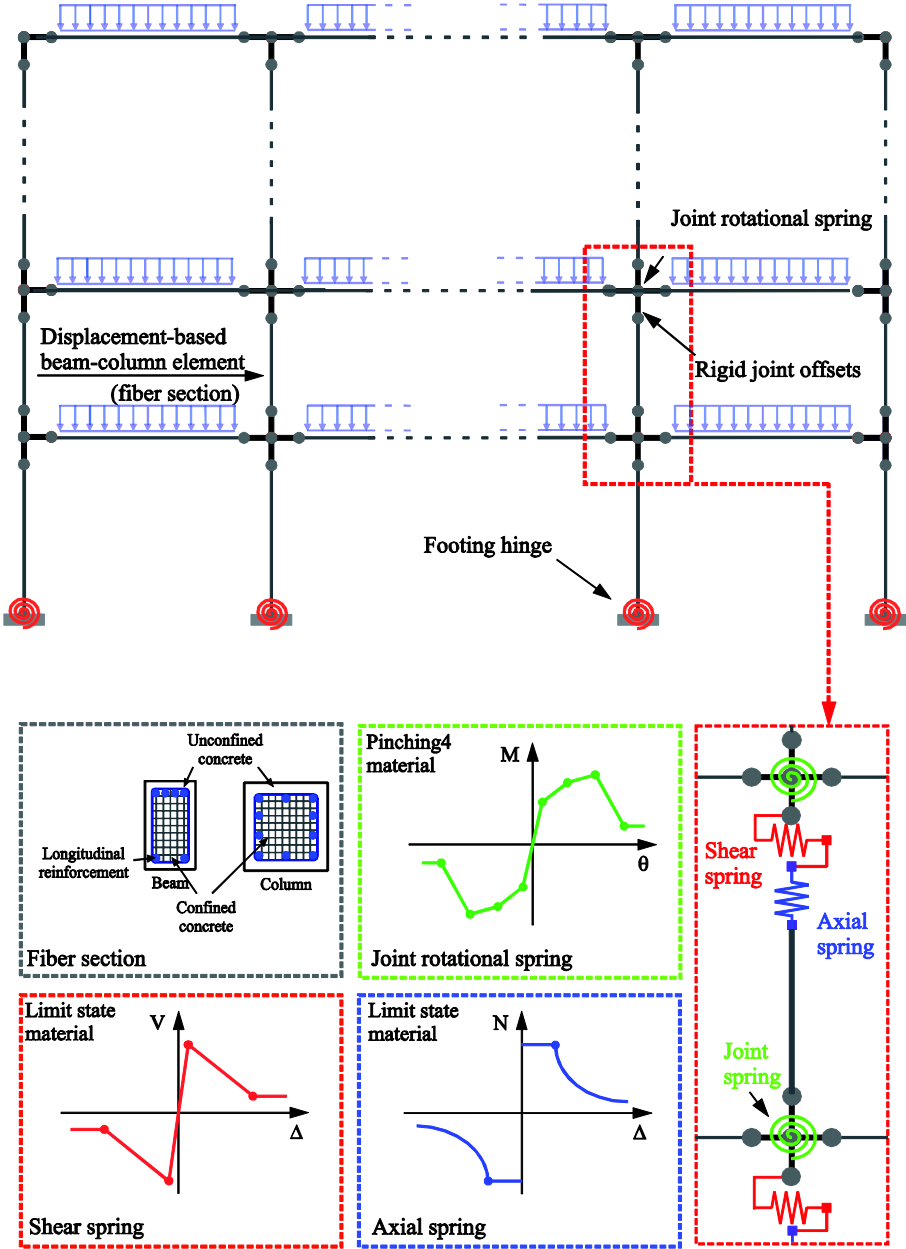
Fig. 3.6 Model adopted in this study

3.2.1.1 MODEL LIMITATIONS

The inelastic analytical models represent an idealization of real structures including their geometry, material properties and reinforcing details with some simplification assumptions:

- Floor diaphragms are assumed to be infinitely rigid in their plane;
- Soil-structure interaction has been neglected (i.e., fixed base model);
- Lap-splices effect has been not accounted for;
- Bond-slip effects at column extremities has been neglected assuming that column longitudinal reinforcement is adequately embedded in well-compacted concrete so that the yield strength can be reliably developed without associated deformations such as slip or pull-out. However, bond-slip effect at the first floor column footing is accounted because experimental evidence suggests it is not negligible.
- Infills contribution to seismic behavior has been neglected. This contribution should be explicitly included in the model when nonstructural components significantly contribute to the strength or stiffness of the building. However, in this study it has been assumed that infills are not well connected to the surrounding frame.

3.2.2 COLUMN BRITTLE FAILURE MODEL

Experimental tests and post-earthquake surveys, conducted by several researchers in the past decades, have shown that non-ductile reinforced concrete columns are particularly vulnerable to shear failure. Furthermore, deficiencies such as small amounts of transverse reinforcement, typically with 90° hook, and small concrete cover can make these the columns susceptible to the axial failure after they experienced shear failure due to the lack of confinement and poor protection against spalling and rebar buckling.

Several authors, as highlighted in §2.1.1.2, have developed models to simulate behavior of shear and flexure-shear critical columns. Among these, the most comprehensive model that accounts for both shear and axial failure was developed by Elwood (2004). This model has been recently updated by Baradaran Shoraka, but this study uses the formulation proposed by Elwood (2004).

3.2.2.1 LIMIT STATE MATERIAL

The complete simulation of brittle behavior of non-ductile column to collapse can be suitable simulated through the adoption of the Limit State material model developed by Elwood (2004) and implemented in OpenSees (McKenna, 2011). The model proposed

by Elwood (2004) accounts for columns failing in shear after flexural yielding and subsequent axial failure for excessive deformation.

The onset of shear failure is empirically determined by a drift capacity model that relates the shear demand to the drift at shear failure, while the onset of subsequent axial failure by a shear-friction-based model. The point of shear or axial failure in the model is determined by intersection of a shear (or axial) drift curve and the limit surface defined by the drift capacity models, see Fig. 3.7. These expressions are included below for completeness:

$$\frac{\Delta_s}{L} = \frac{3}{100} + 4\rho'' - \frac{v}{40\sqrt{f_c}} - \frac{P}{40 A_g f'_c} \geq \frac{1}{100}$$ Eq. 3-1

$$\frac{\Delta_a}{L} = \frac{4}{100} \frac{1+\tan^2\theta}{\tan\theta + \left(s/A_{st} f_{st} d_c \tan\theta\right)}$$ Eq. 3-2

where Δ_s and Δ_a are drift at shear and axial failure, respectively, L is the length of the column, v and P are the applied shear stress and axial load, respectively; ρ'' is the transverse reinforcement ratio A_{st}/bs where b is the cross-section width, s, A_{st}, f_{st} and d_c are the spacing, cross-sectional area, yield stress and core depth form centerline to centerline of transverse reinforcement, respectively, and θ is the critical crack angle (assumed to be equal to 65°).

The shear and axial failure models can be employed by adding zero-length springs in series with a beam-column element that reproduces the nonlinear flexural behavior, as illustrated in Fig. 3.7. The column is modeled with a force-based beam-column element with fiber sections.

The limit state material model traces the total response of the beam-column element (e.g. column drift). Prior to shear failure, the shear spring is linear-elastic with stiffness corresponding to the equivalent elastic shear stiffness of the column. Once the column's total response exceeds the shear failure surface (limit shear curve defined by Eq. 3-1), its shear response follows the constitutive law of the limit shear curve to include pinching and strength and stiffness degradation. Similar to shear limit curve, the zero-length axial spring has a "rigid" backbone prior to reaching the axial load-drift limit curve. After axial failure occurs, the backbone will be redefined to include a degrading slope and a residual strength. Since the shear-friction model describes only compression failure, the backbone is only redefined for compressive axial loads.

Since the shear spring is in series with the components of columns, updating the stiffness of the shear spring updates the stiffness of the whole column response. This stiffness update aims to simulate stiffness degradation occurs in a concrete column after shear failure occurs. However, for both shear and axial failure, behavior after the onset of failure is not well understood and, as indicated in Elwood (2002) further studies are

required to address this issue. A more detailed description of the Limit State model can be found in Elwood (2004).
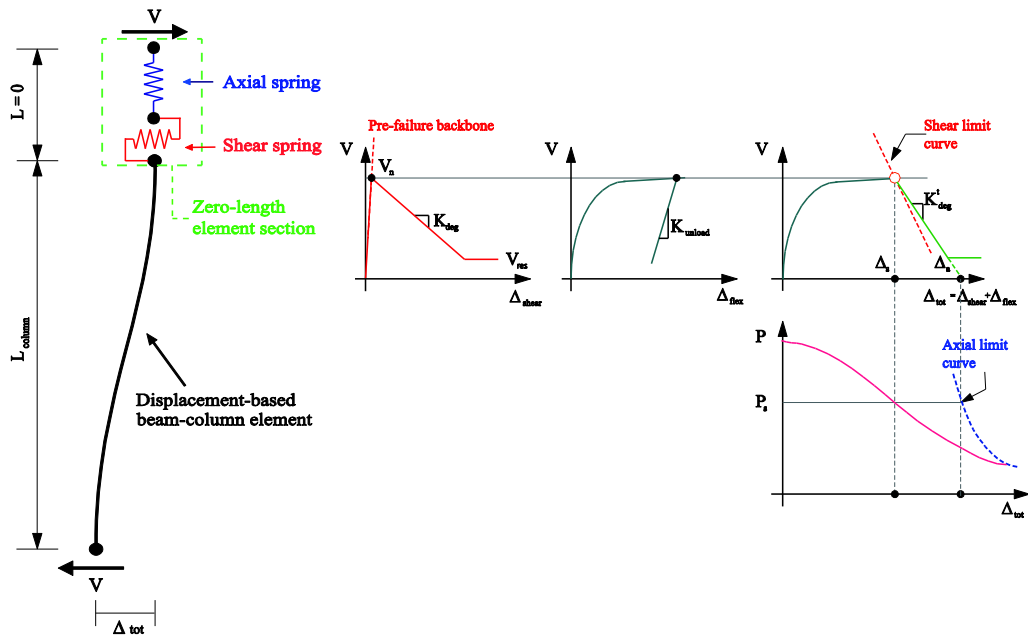
Fig. 3.7 Limit state material used to model shear and axial failure (Elwood, 2004)

3.2.3 JOINT MODEL

3.2.3.1 SCISSOR MODEL

A practical and computationally efficient model is so called "*scissors model"*, which is a relatively simple model composed of a rotational spring with rigid links that span the joint dimensions. The model is a simplification of a model developed by Krawinkler (2005) for steel panel zones. This model was first suggested by Alath and Kunnath (1995). The scissors model was also tested by Theiss (2005), Celik and Ellingwood (2008), and Favvata et al. (2008), for interior and exterior unconfined beam-column joints under the effect of cyclic and dynamic loading, and by Burak (2010) for confined beam-column joints under cyclic loading. Their analyses yielded promising results.

Due to its simplicity and practicality, joint panel zone model proposed by Alath Kunnath (1995) has been selected for modeling the unconfined joints in the current study. Although the model may not capture the actual behavior of the joints,the scissors model has some drawbacks, e.g. the inability to model the true kinematics of the joint; however, it is widely used due to its computational efficiency and its ease implementation.

OpenSees Model –Joint panel zone

In scissor model, Fig. 3.8, joint shear deformation is simulated by a rotational spring model with degrading hysteresis. The element is implemented in OpenSees (McKenna, 2011) through defining duplicate nodes, node i (master) and node j (slave), with the same coordinates at the center of the joint (intersection of beam and column centerlines).
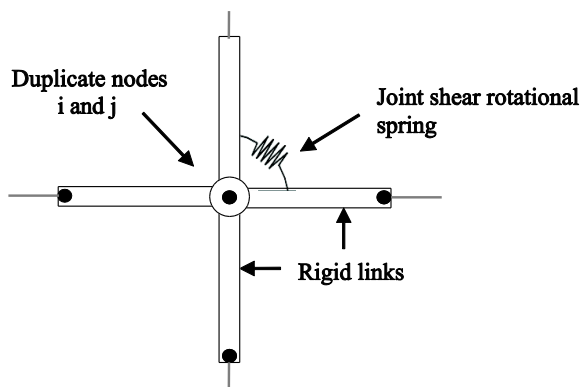
Fig. 3.8 Scissor model kinematic (Alath and Kunnath, 1995)

After defining the two nodes, the element connectivity is set such that node i is connected to the column rigid link and node j is connected to the beam rigid link. Next, a zero length rotational spring is used to connect the two nodes so that the column rigid link is connected to one end of the spring while the beam rigid link is connected to the other. The degrees of freedom at the two central nodes are defined to permit only relative rotation between the two nodes through the constitutive model of the rotational spring, which incorporates shear deformation of the joint. The rotational spring transforms the shear deformation into an equivalent rotation as following described. The moment-rotation relationship for the joint panel zone is obtained starting from the join shear stress-strain allowable relationships. The joint shear stress-strain is determined empirically, and the cyclic response is captured through a hysteretic model calibrated to experimental cyclic response (Lowes and Altoontash, 2003), Fig. 3.8.

3.2.3.2 JOINT MODEL FOR AMERICAN BUILDING

There are several techniques to represent bond-slip rotation in an analytical model of a beam-column joint. The most direct approach is to introduce a slip spring whose properties are either calibrated directly from tests or are calculated using a bond-slip model. An alternative approach is to scale the moment-shear strain (rotation) backbone to account for higher rotation resulting from slip; this method was used successfully by Celik and Ellingwood (2008). Yet, another approach is to reduce the effective stiffness of beams and columns to account for slip deformation as recommended by ASCE/SEI 41 supplement (ASCE, 2007). In the present study, the first approach is used with the

slip spring properties calculated based on the bond-slip model by Elwood and Eberhard (2008).
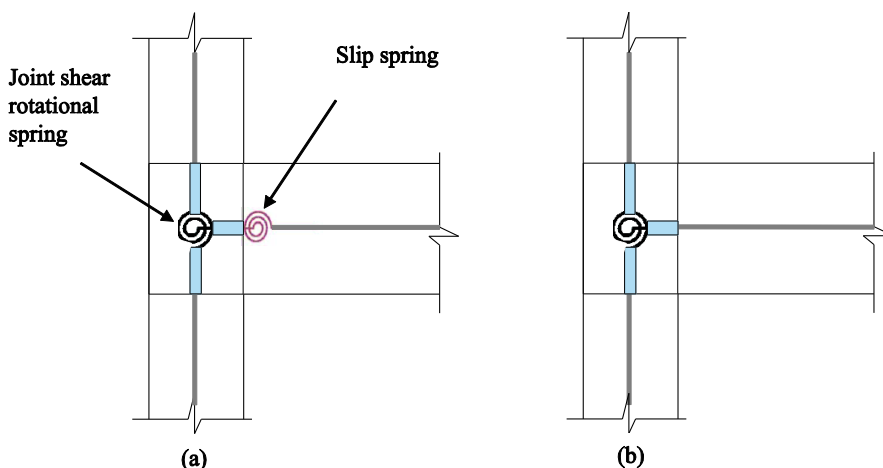
Fig. 3.9 Modeling of slip in beams: (a) Explicit slip modeling, (b) Implicit slip modeling (from Hassan, 2011)

Shear stress-strain backbone curve
The backbone curve proposed by Hassan (2011) is a quad-linear curve that resembles the experimental joint shear stress-strain envelopes for unconfined joints. As demonstrated by Celik (2007), the moment transferred through the rotational spring M_j is related to the joint shear stress τ_j through:

$$M_j = \tau_j A_j \frac{L}{\frac{L - h_c/2}{jd_b} - \frac{L}{H}}$$

Eq. 3-3

where L is the length from beam inflection point to the column centerline, which can be approximated as half beam centerline span. The parameter j is the effective beam lever arm ratio, which can be approximated as 0.875 for J-Failure joints and 0.9 for BJ-Failure joints. The column height H is measured between column inflection points, which can be approximated by story height.

The rotation of the spring can be defined in two ways. One way is to consider the joint panel rotation as solely the joint shear strain, which can be expressed as:

$$\theta_j = \gamma_s$$

Eq. 3-4

In this case, the joint rotation resulting from beam bar slip is explicitly defined by a separate zero length rotational slip spring element attached between the beam-joint interface section and the end of the beam rigid link. The other assumption is to include

the joint rotation due to beam bar slip in Eq. 3-4 for joint rotation by adding it to the joint shear strain as:

$$\theta_j = \gamma_s + \theta_{slip} \qquad\qquad \text{Eq. 3-5}$$

In this case there will be no need for a separate slip spring for the beam. The author showed that the use of two different alternatives do not produces significant changes in the joint panel response.

Hysteretic model for joint rotational spring

The Pinching4 model has been widely used to simulate the joint shear spring in the model of Alath and Kunnath (1995). The one dimensional material model used to implement the proposed backbone curve for the joint constitutive model and to describe the hysteresis, pinching, energy dissipation, and cyclic degradation of the response is the Pinching4 material model in OpenSees (Fig. 3.10), developed by Lowes et al. (2003). This model is particularly useful to represent the pinched hysteretic behavior of shear critical elements like unconfined-beam column joints

The model has eight positive and negative envelope parameters. Further, it has different parameters to define pinching behavior (rDispP to uForceN), parameters to define unloading stiffness degradation (K_1 to K_{Lim}), parameters to define reloading stiffness degradation (D_1 to D_{Lim}), parameters to define strength degradation (F_1 to F_{Lim}), and finally a parameter gE to define energy dissipation rule. Based on experimental tests, various authors proposed different values for the 22 required parameters describing the response, ad resumed in Table 3-7. These parameters can produce good agreement with the tests on which they are based, however, the models are barely extendable to other cases.
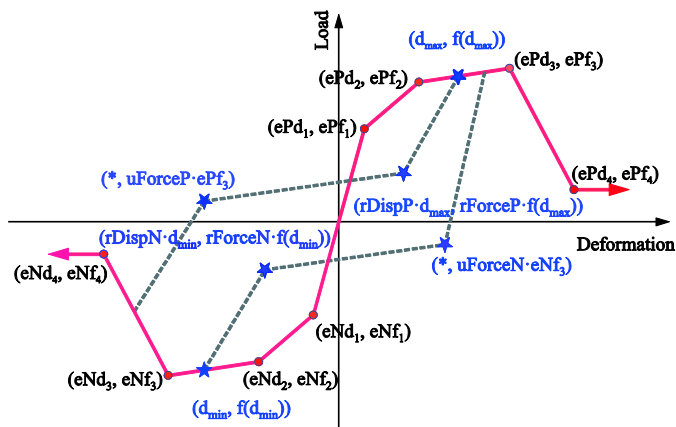
Fig. 3.10 Pinching4 Material (Lowes et al., 2003)

54

	Parameter ID	Stevens (1991)	Theiss (2005)	Celik (2008)	Walker (2011)	Jeon (2013)			
						mean°	COV°	mean°°	COV°°
Pinching parameters	rDispP	0.250	0.107	0.100	0.150	0.19	0.18	0.21	0.29
	rForceP	0.150	0.254	0.150	0.350	0.19	0.19	0.19	0.25
	uForceP	0	0	0	-0.100	-0.06	1.37	0	0
	rDispN	-0.250	-0.107	0.100	0.150	0.19	0.2	0.21	0.29
	rForceN	-0.150	-0.254	0.150	0.150	0.18	0.26	0.19	0.26
	uForceN	0	0	0	-0.400	-0.06	1.4	0	0
Unloading Stiffness Degradation Parameters	gK1	1.299	0.415		0.500	0.94	0.19	0.99	0.1
	gK2	0	0.351		0.200	0	‡	0	‡
	gK3	0.235	0.197	*	0.100	0.1	‡	0.1	‡
	gK4	0.000	0.028		-0.400	0	‡	0	‡
	gKLim	0.894	0.999		0.990	0.95	‡	0.95	‡
Reloading Stiffness Degradation Parameters	gD1	0.120	0.046		0.100	0.38	0.49	0.33	0.47
	gD2	0	0.005		0.400	0	‡	0	‡
	gD3	0.230	1.385	*	1.000	0.15	‡	0.15	‡
	gD4	0	0		0.500	0	‡	0	‡
	gDLim	0.950	0.999		0.990	0.95	‡	0.95	‡
Strength degradation Parameters	gF1	1.110	1.000		0.050	0.06	1.63	0.18	1.57
	gF2	0	0		0.020	0	‡	0	‡
	gF3	0.319	2.000	*	1.000	0.32	‡	0.32	‡
	gF4	0	0		0.050	0.1	‡	0.1	‡
	gFLim	0.125	0.990		0.990	0.25	‡	0.25	‡
Energy Dissipation	gE	10	2	†	10				
	dmgType	energy	energy		energy	cycle		cycle	

*cyclic strength and stiffness degradation were not considered
°exterior non-ductile joints   °°interior non-ductile joints   Table 3-7 Pinching4 parameters for joint modeling
†not provided in the paper
‡parameter assumed constant for all specimens

To model joint shear behavior, the model proposed by Hassan (2011) was adopted. The model was developed to simulate exterior unconfined joint behavior failing in shear with or without beam or column yielding, however in this study it has been adopted in a simplified way for both interior and exterior joints. Although the model cannot properly simulate interior joint behavior, it has been developed also accounting for 4 full-scale corner beam-column subassembly extracted from the VanNuys Holiday Inn building, and, for this reason it has been considered particularly representative of model joint behavior.

3.2.3.3 JOINT MODEL FOR ITALIAN BUILDING

To simulate shear behavior of typical Italian beam-columns joints, this research employs the analytical model developed by Alath and Kunnath (1995). In the so called "scissor model ", the kinematic of joint is reproduced by four rigid offset, representative of the finite size of the joint, connected by a zero-length rotational spring. To model the joint shear stress-strain relationship for both interior and exterior joints the backbone proposed by Jeon et al. (2015) has been employed. The present model has been chosen due to its simplicity and applicability, furthermore it has been proposed to model both interior and exterior non-conforming joints.

The model was calibrated to an experimental dataset chosen to be representative of "non-conforming" joint according to ASCE/SEI41 (2007). The specimens in the dataset exhibited joint failure either prior to or following beam or column yielding in flexure. The model was validated on 23 exterior and 35 interior joints exhibiting joint shear failure and 5 exterior joints exhibiting bond failure. In addition, parameters to model hysteretic behavior have been provided.

The backbone curve of the joint, as depicted in Fig. 3.11, is represented by a quad-linear curve consisting of four key points: concrete cracking, an intermediate point, ultimate, and residual conditions.

Following the model by Jeon et al. (2015), the first point and the abscissa of the second point are fixed while the ordinate of the second point and third and fourth point can be determined from experimental joint shear tests. Residual joint stress ($\tau_{j,4}$) is defined as 20% of joint shear strength ($\tau_{j,3}$) in order to alleviate convergence issues.

Once the joint shear stress-strain backbone curve is determined, the equivalent moment-rotation relationship can be computed from equilibrium and compatibility from the joint shear-stress relationship using the formulation proposed by Celik and Ellinghwood (2008):

$$M_j = \frac{\tau_j A_j}{\left(1 - h_c/L_b\right)/jd_b - \eta/L_c} \; ; \; \theta_j = \gamma_j \qquad \text{Eq. 3-6}$$

where M_j=joint rotational moment, τ_j=joint shear stress; h_c=depth of the column; A_j=joint area ($h_c \cdot b_j$); b_j=effective width of the joint panel calculated from ACI 352R-02 (2002); L_b=total length of the left and the right beams; L_c=total length of the top and bottom columns; j=internal lever arm factor (assumed equal to 0.872); d_b=effective depth of the beam; h=2 and 1 for the top floor joints and others, respectively; θ_j=joint rotation; and γ_j=joint shear strain.
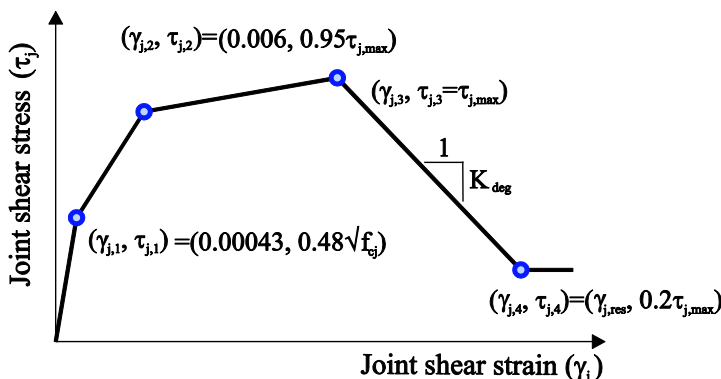
Fig. 3.11 Envelope of joint stress-strain relationship (Jeon et al., 2014)

The backbone curve requires the definition of the maximum joint shear resistance. The joint shear strength ($\tau_{j,3}$) depends on the failure mechanism of the beam-joint subassemblage. When the beam longitudinal reinforcement terminates in the joint with a sufficient embedment length (i.e. internal nodes), the shear strength depends on the panel node behavior, while when the embedment length is not enough to allow the reaching of the yielding tension in the bottom reinforcement, the shear strength is limited by the bond failure of bottom reinforcement.

Shear strength for joints exhibiting shear failure
According to Jeon et al. (2015), for internal "non conforming" beam-column joints, and for external joints provided of sufficient embedment length, the maximum joint shear strength can be computed as follows:

$$\tau_{max} = -0.586 \ (TB)^{0.774}(BI)^{0.495}(JP)^{1.25}(f_c)^{0.941} \qquad \text{Eq. 3-7}$$

where τ_{max} = maximum joint shear stress in MPa; BI = beam reinforcement index, which is defined as the product of the beam longitudinal reinforcement ratio and the beam longitudinal reinforcement yield stress divided by the beam concrete compressive strength (averaging quantities for top and bottom reinforcement); JP = parameter for describing in-plane geometry (1 for interior and 0.75 for exterior joints); TB = joint

confinement factor (1.0 for subassemblages with 0 or 1 transverse beam and 1.2 for subassemblages with 2 transverse beams), and f_c = joint concrete compressive strength in MPa. The proposed model has a mean and a COV of the predicted-to-experimental shear strength ratio of 1.011 and 0.148, respectively. Fig. 3.12 shows joint shear strength computed using Eq. 3-18 compare with experimental joint shear strengths.
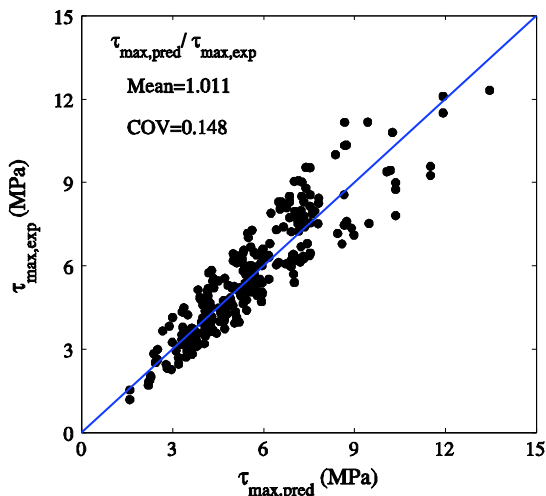
Fig. 3.12 Comparison of computed vs experimental joint shear strength (from Jeon et al., 2015)

Shear strength for joints exhibiting anchorage failure

Exterior beam-column joints in which beam longitudinal reinforcement terminates in the joint with a short embedment length may undergo to unpredictable brittle failure under more severe earthquakes due to premature bond pullout failure strongly reducing joint stress strength when bottom reinforcement is in tension (Fig. 3.13).
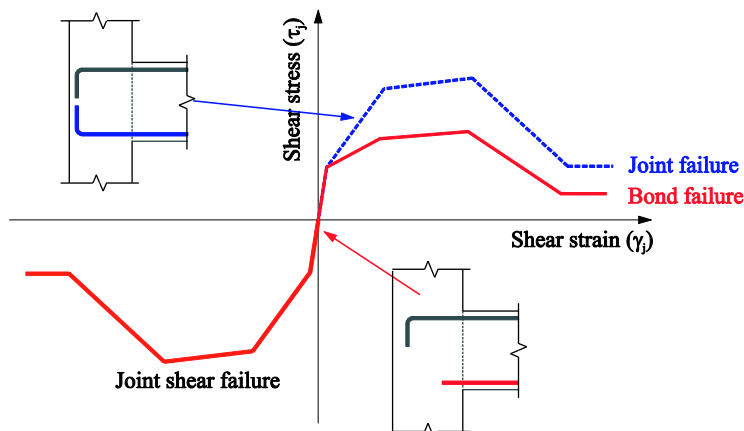
Fig. 3.13 Backbone accounting for shear and bond failure (from Jeon, 2015)

In order to account for the reduced shear strength associated with the insufficient embedment length, this research utilizes the empirical bond strength model of Hassan (2011), which was developed through the experimental observations of 21 specimens with no beam yielding showing a mean and a COV of the predicted-to-experimental shear strength ratio of 1.099 and 0.161, respectively, as depicted in Fig. 3.12. The bond strength model includes influential parameters such as column axial load (P), beam reinforcement diameter (ϕ_b), ratio of cover to reinforcement diameter (c/ϕ_b), presence of transverse beams, as expressed in the following equation:

$$\tau_{bond} = 1.1\left(\frac{P}{f_c A_g}\right)^{1/4}\sqrt{f_c}\,\Psi_s\,\Omega\,\frac{c}{\phi_b} \qquad \text{Eq. 3-8}$$

where τ_{bond} = concrete average bond stress capacity of discontinuous beam bottom reinforcement; Ψ_s = reinforcement factor ($\Psi_s = 1$ for $\phi_b \geq 19$ mm and $\Psi_s = 1.25$ for $\phi_b \leq 19$ mm), and Ω = transverse beam confinement factor ($\Omega = 1, 1.12, 1.20$ for exterior joints with no, one or two transverse beam, respectively). c/ϕ_b = minimum of bottom and side concrete cover-to-rebar diameter ratio measuring cover to rebar centroid, which is less than 2.5. Ag is the column area.

The equivalent shear strength associated with a bottom beam rebar insufficient embedment length can be calculated, using the equilibrium for the subassemblage, with the equation:

$$\tau_{max} = \frac{T_s}{A_j}\left[1 - \frac{\left(1 + 0.5h_c/l_b\right)jd_b}{L_c}\right] \qquad \text{Eq. 3-9}$$

That derives from the equilibrium of the sub-assemblage. In the above equation T_s = tension force in beam longitudinal reinforcement corresponding to pullout failure can be calculated as:

$$T_s = n_b l_{sp}\pi\phi_b\tau_{bond} \qquad \text{Eq. 3-10}$$

with n_b = number of beam longitudinal reinforcement, l_{bsp} = embedment length within a joint, ϕ_b = diameter of the reinforcement, and l_b = beam length measured from the face of column to the face of column to the end of beam for subassemblages or the mid-span of beam for frames.
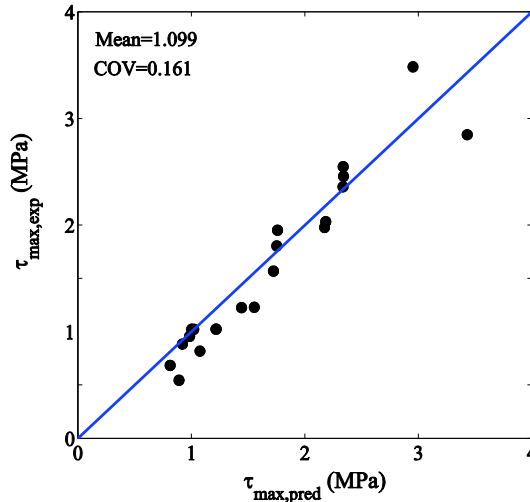
Fig. 3.14 Comparison of computed vs experimental joint shear strength (adapted from Hassan, 2011)

Modeling of bar slip in columns and beams

Experimental test evidenced that additional rotation at the end of beams may caused by bond deterioration and failure for continuous beam rebars anchored within the (Hassan, 2011, Kaku and Asakusa, 1991). However, Leon (1989) interpreted that the larger amount of slip measured in laboratory tests can be largely associated with the lack of horizontal restraint, i.e., the ends of beams are restrained only vertically.

This effect is not likely to occur in continuous frames where the single beam is restrained by two connected beam-column nodes, unless all the joints at a particular story experienced significant bond deterioration simultaneously. Similarly, Hoffman et al. (1992) concluded that for frames, bar slip at the beam–joint interface is typically small and difficult to detect visually during testing. For these reasons rotation at the beam–joint interface due to slip of beam reinforcement within the joint is not explicitly modeled for joints either with or without sufficient anchorage length, but the additional rotation due to bar-slip effect is only considered at the columns.

3.2.4 SYSTEM-LEVEL COLLAPSE DEFINITION

Existing Reinforced Concrete Moment Frames are vulnerable to a wider range of possible collapse modes (Aycardi et al. 1994; Kurama et al. 1994; Kunnath et al. 1995; El-Attar et al. 1997). These structures have a demonstrated tendency to fail in soft story, column-hinging mechanisms or gravity load collapse.

In order to effectively predict earthquake induced structural collapse, the collapse process and the failure modes of structures should be properly predicted. Concrete structures built prior to the entering into force of modern seismic codes introducing basics concepts of capacity design, are particularly susceptible to shear-axial column

failure as well as joint shear failure. Current codes and standards (e.g. ASCE/SEI 41, 2007, Eurocode 8, 2005, NNT2008, 2008, ATC 2009) assume that a single element reaching collapse entail the collapse of the entire structure. However, the failure of a single column or even multiple columns does not necessarily entail structural collapse, but does have a significant effect on the load path of both lateral inertial seismic loads and gravity loads within the frame system. Particular focus must be given to columns surrounding the damaged area, as well as the changes in demand and capacity experienced by the portions of the structure directly above and below the failures.

As highlighted in ATC (2009) capturing the collapse modes by means of non-simulated limit state checks, during a post-processing phase, will generally result in lower estimate of the median collapse capacity. In fact, non-simulated collapse modes are usually associated with a component-based assessment procedure in which the occurrence of the first failure corresponds to the global collapse of the entire structure. It ignores the ability of a structural system to redistribute loads as damage accumulates and will tend to lead to conservative assessments of collapse vulnerability. Therefore, in order to better reflect the impact on the structural performance at the near-collapse limit state, it is preferable to explicitly simulate failure mode in the model.

Even if the sidesway collapse is typically assumed as the governing collapse mechanism (e.g. ATC, 2009, and FEMA 440A, 2007), for non-ductile RC buildings, it is expected that structural components, may lose the capacity to carrying gravity loads prior to the development of the flexural mechanism necessary to the activation of a sidesway collapse. Gravity load collapse may be precipitated by axial failure in columns, punching shear failure of slab-column connections, failure of slab-diaphragm connections, or axial-load failure of beam-column joints.

Non-ductile behavior originating from column shear and subsequent axial failure plays an important role in these structures, and analytical model must have the ability to capture such behavior. Baradaran Shoraka (2013) introduced a detailed and robust procedure to define a system-level collapse definition that explicitly accounts for both ductile and brittle failure modes of single members and focusing on how non-ductile RC frame structures behave after shear-axial column failures occur. Two possible collapse modes are introduced: Sidesway collapse and Gravity load collapse.

3.2.4.1 SIDESWAY COLLAPSE

As stated in recent documents (e.g. ATC, 2009, and FEMA 440A, 2007), the sidesway collapse is typically assumed as the governing global collapse mechanism. This assumption can be considered realistic for most of ductile RC buildings and very limited existing frames. Sidesway collapse is defined as a "Structural collapse due to excessive story drift associated with loss of lateral strength and stiffness due to material and geometric nonlinearities" in ATC (2009).
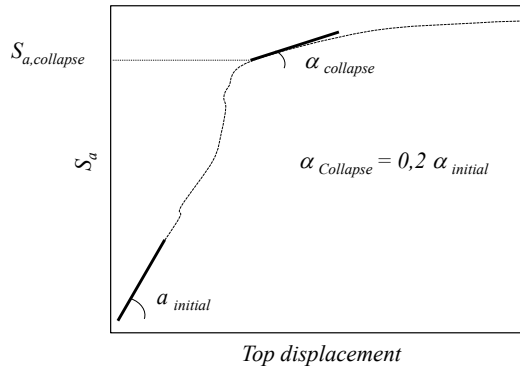
Fig. 3.15 Definition of sideway collapse using Incremental dynamic analysis

Generally, sideway collapse is considered to occur when a small increase in ground-shaking intensity causes a large increase in response or when the interstorey drift ratio exceed a given threshold (e.g. Haselton, 2006, and ATC, 2009). Considering sideway collapse when the interstorey drift ratio rapidly increases for small increasing of spectral acceleration, the state of incipient collapse is subjective, and the collapse probability could vary slightly based on the selection of this state. In DeBock et al. (2013), to overcome this issue, the collapse is defined as the point (IDR$_{collapse}$, S$_{a,collapse}$) on the IDA curve at which the slope decreases to less than 20% of its initial value, Fig. 3.15. The difficulty in the implementantion of this procedure is that it is possible to capture a conventional sideway collapse only by performing incremental dynamic analyses while no information can be obtained from the single nonlinear time history. In Baradaran Shoraka (2013), to overcome such issues, an objective definition of collapse similar to the definition for gravity load collapse is given, considering that sideway collapse consist in the loss of lateral strength. Whenever the lateral resistance (defined by the story strength corresponding to a interstorey drift ratio peak) decreases below a pre-established residual value, the structure is considered to sustain a sideway collapse.

In this study, a subroutine implemented in Opensees by Baradaran Shoraka (2013) has been implemented. The procedure used to identify sideway collapse is illustrated in Fig. 3.16. The 2 bays-2story building, subjected to a ground motion record, exhibits a first-floor response that is represented in the right corner figure. When on a peak interstorey drift the capacity of all columns at a specific floor reaches it residual strength capacity (bottom part of Fig. 3.15), the sideway collapse is detected in that floor (red dot).
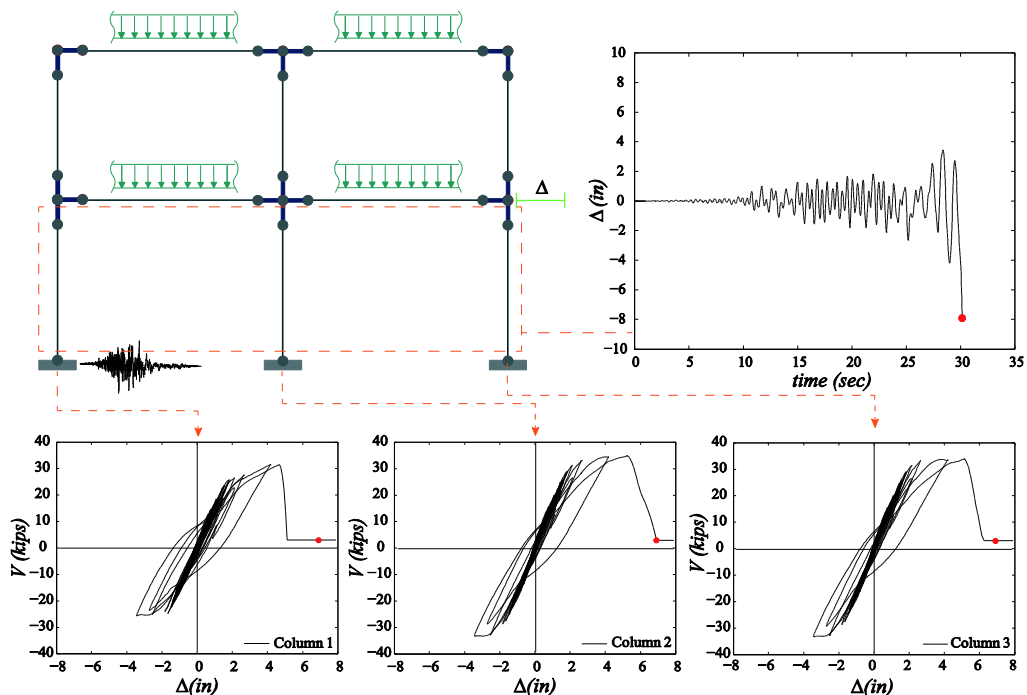
Fig. 3.16 Definition of sidesway collapse in the single NTH according to Baradaran Shoraka, 2013: The structural model subjected to the ground motion; the first floor response during NTH; first-floor column responses during NTH. Red dot indicates the point at which sidesway collapse occurs.

The expected failure mode is flexural hinging leading to sidesway collapse, which the modeling approach can simulate reasonably well by capturing post-peak degrading response under both monotonic and cyclic loading

3.2.4.2 GRAVITY LOAD COLLAPSE

In existing non-ductile frames it is expected that components with poor detailing may lose them capacity to support gravity loads prior to the development of a complete flexural mechanism leading to sidesway collapse. In FEMA P440A (2007) is stated that behavior of real structures can include loss of vertical-load-carrying capacity at lateral displacements that are significantly smaller than those associated with sidesway collapse. Inelastic deformation of structural components can result in shear and flexural-shear failures in members, and failures in joints and connections, which can lead to an inability to support vertical loads (vertical collapse) long before sidesway collapse can be reached.

The same observation is reported in Baradaran Shoraka (2013) where an example building subjected to several ground motions, always exhibiting the gravity load collapse prior the sidesway collapse.
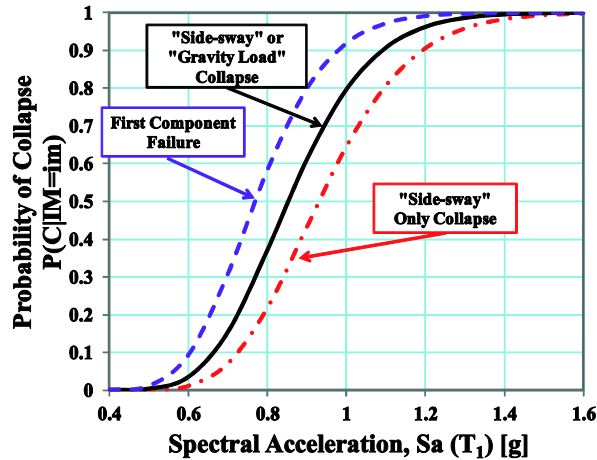
Fig. 3.17 Effect of collapse simulations in the definition of Collapse fragility (after Baradaran Shoraka, 2013)

As can be deduced from Fig. 3.17, the capacity of the building, when considering both sidesway and gravity load collapse, is very different with respect to that obtained only considering sidesway collapse.

When a non-ductile RC frame is subjected to excessive lateral deformations local axial failure is likely to occur in vertical members after shear failure. As a consequence of the local collapse of one or more columns, the gravity load that was carried by failed elements must be transferred to neighboring elements. During a seismic event, the successive failing of gravity load carrying member can generate the global collapse of the structure, when the gravity load capacity is smaller than the demand in a specific floor. In this sense gravity load collapse can be interpreted as a progressive collapse in which the axial failure of the first column rapidly triggers the failing of neighbor elemenst, leading to global collapse.

The damage progression can be followed through the numerical analysis by comparing at each time step the floor gravity load demand and capacity.

In this study, the Limit State material (Elwood, 2004) has been implemented in the model to simulate shear and subsequent axial failure of columns. In this case, gravity load capacity in each vertical element is automatically updated at each time step accounting for shear and subsequent axial failure of members. Gravity load demand in each floor is the sum of gravity load in each column of that floor and it will be assumed constant during the analysis and equal to the load deriving from the sole gravity load analysis performed on the intact frame. Gravity load capacity of a floor is given by the sum of axial load capacities for all columns in that floor. As the interstorey drift increases, both internal and exterior columns capacities will decrease affecting the total floor vertical load capacity. In Fig. 3.18, the comparison between 1st floor Axial Load

64

Capacity and Demand is depicted for the same structure reported in Fig. 3.16 when subjected to an earthquake ground motion. The floor Demand is assumed to be constant during the analysis and equal to the initial load, while the floor capacity is given by the sum of column capacities at the same floor. As can be deduced from Fig. 3.18, the floor capacity is limited by the intact floor capacity while it varies as a function of drift demand; despite contradictory, the model assumes that the original capacity can also be restored when drift demand decreases.
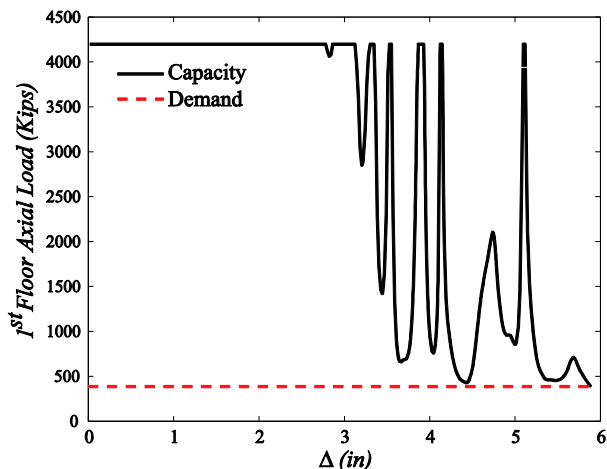
Fig. 3.18 Comparison 1st floor Axial Load Demand-Capacity

In this study, the subroutine developed by Baradaran Shoraka (2013) for OpenSees has been implemented to detect the first point at which floor level vertical load demand exceed the total vertical load capacity at that floor.

The axial capacity for each column is based on the Eq. 3-2 in which the drift at the onset of axial failure is a function of member details and axial load demand. Rearranging the Eq. 3-2 equation, the axial load can be interpreted as axial load capacity decreasing as a function of increasing drift demand in the column:

3.3   DAMAGE ANALYSIS

It is well known that storey level engineering demand parameters (EDPs), such as the maximum interstorey drift ratio, are representative of both structural and nonstructural damage. However, to allow considerations about the damage distribution and the necessary repair interventions, a more detailed estimate of damage is necessary.

To describe the spreading and the intensity of the damage it has been monitored in all the elements of the structural system. In particular, for both beams and columns, modeled by means of nonlinear beam column (deSouza, 2002), the yielding in reinforcement bars as the onset of nonlinear behavior up to the ductile failure of the

element (when the concrete strain reaches the value of 4‰, i.e., concrete crush) has been considered. For columns, two additional potential failures were considered: shear and axial failures. These brittle failures have been considered thanks to the Limit State material (Elwood, 2004). Finally, the potential brittle failure of joints was considered by means of a scissor model (Alath and Kunnath, 1995).

To check the attainment of first yielding in the single member, an internal algorithm monitors the strain in fibers corresponding to top and bottom longitudinal steel bars. The yield in section is attained when the maximum absolute value between top and bottom bar strain overcome the yielding strain given by f_y/E_s. For both columns and beams, the strain in steel rebars is checked at both extremities, the first section corresponds to a hypothetic hinge positioned in node I, while the last corresponds to the hinge positioned in node J of the nonlinear beam-column. The number of sections for the nonlinear beam column elements corresponds to the number of Gauss-Lobatto integration points, so that the monitored sections are the 1st one and the section corresponding to the maximum number of integration points. The same procedure has been implemented to check the attainment of concrete crushing in the extreme fibers of the member sections.

To control the activation of a brittle failure in columns the *CstateFlag* is monitored. *CstateFlag* is an integer number that indicates if the limit curve has been exceeded, and specifies the current state of the material. Possible values for *CstateFlag* and corresponding state of materials are indicated in Table 3-8 for both shear and axial Limit State materials.

0	*Prior to failure*
1	Limit curve reached for the first time
2	On limit curve
3	Off limit curve
4	At residual capacity

Table 3-8 CstateFlag values for limit state material

For joints, different limit states were defined based on specific limit rotations, corresponding to significant points on the joint backbone curve. In this case, the behavior is checked by monitoring the rotation of the two rigid links connected by the rotational hinge Note that the axial failure of joints has not been considered in this study.

3.4   NONLINEAR STATIC ANALYSIS

Static pushover analyses were performed to investigate the general load-deflection relationship for the case-study buildings and most likely collapse modes evidencing relative contribution to the collapse modes of brittle members.

Pushover analysis consists into applying the distributed gravity load to the structure and then applying and increasing lateral loads, with a preset shape, to the structure until the reaching of collapse.

Displacement-controlled pushover analyses were conducted through the OpenSees model of the case study building.

3.4.1 LATERAL LOAD PATTERNS

Pushover analyses are a very common approach for performance evaluation of a structure. Different load patterns, adaptive or invariant, can be applied to the structure in order to represent and bound the distribution of inertia forces in a "design" earthquake, however there is no common agreement on the choice of load pattern shape. Obviously, different load patterns can result in different failure mechanisms. When applying an invariant load pattern, since no single pattern can capture the variability in the local demands expected in a design earthquake, the use of at least two load patterns that are expected to bound inertia force distributions is recommended (Krawinkler and Seneviratna, 1998). One should be a "uniform" load pattern, in order to emphasize the demand in lower stories compared to that of upper stories and magnifying the relative importance of story shear forces compared to overturning moment. The other could be the design pattern usually suggested in codes (e.g, ASCE, 2000) or a load pattern that also account for higher modes contribution. In this study two load distributions were considered, a uniform distribution (Fig. 3.19a) and a linear load distribution (Fig. 3.19b)
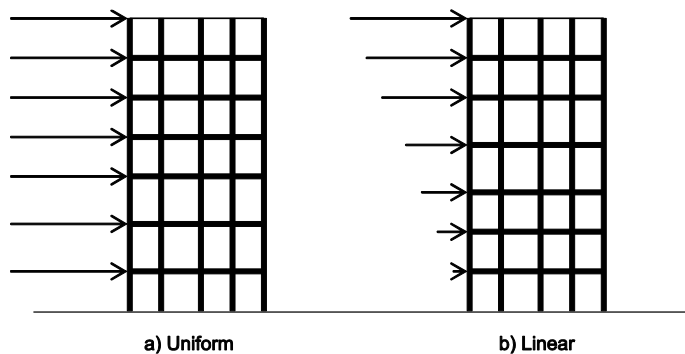
Fig. 3.19 Load pattern for Pushover Analysis

3.4.2 PUSHOVER ANALYSIS RESULTS

American Case-study

The base shear vs the roof displacement is depicted in Fig. 3.20 and Fig. 3.21 for linear and uniform load pattern, respectively. In the same figures, different markers have been

used to indicate the displacement corresponding to the attainment of a given limit state the first time it has been reached, as outlined in §3.3.
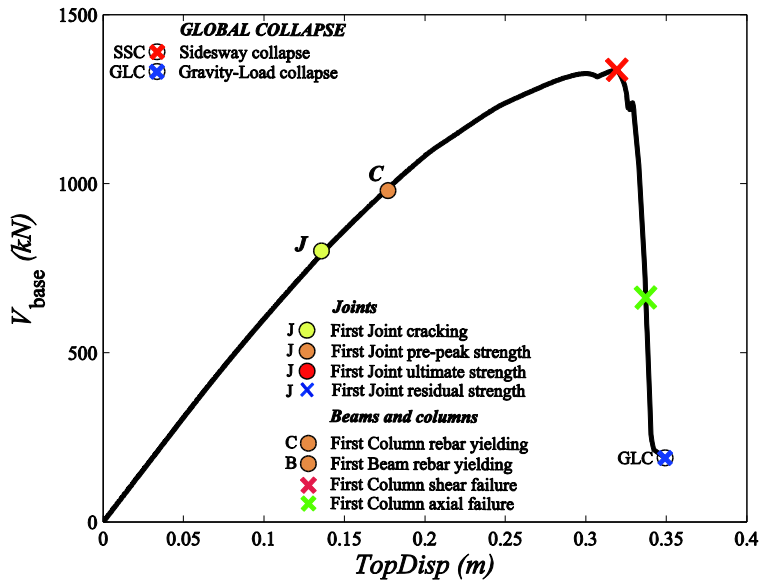
Fig. 3.20 Pushover curve for American building assuming a linear load pattern
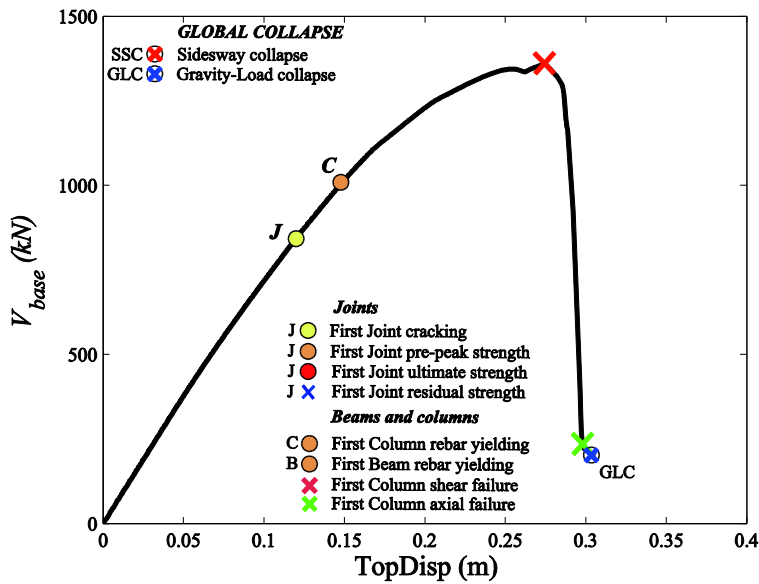
Fig. 3.21 Pushover curve for American building assuming a uniform load pattern

Two pushover curves are quite similar, main differences result in the different initial slope of the pushover and the displacement corresponding to the attainment of single limit states and the global collapse. The two different load pattern shapes adopted for the analysis caused these differences. However, even if the global collapse is attained at about 0.35m for the linear load patterns and 0.30 for the uniform, the maximum base shear and the curve shape is about the same because the collapse mode is independent from the load pattern and consists in the Gravity load collapse of the first floor for both load patterns. The first limit state reached on the pushover curve corresponds to the joint cracking, however, this is the only limit state reached for joints due to their high resistance. Further, can be noted that yielding is never reached in beams suggesting that the collapse mode only involves columns and joints leading to a soft-storey collapse mode.

Italian Case-study

Global pushover curves for Italian building are shown in Fig. 3.22 and Fig. 3.23 for linear and uniform load pattern, respectively.
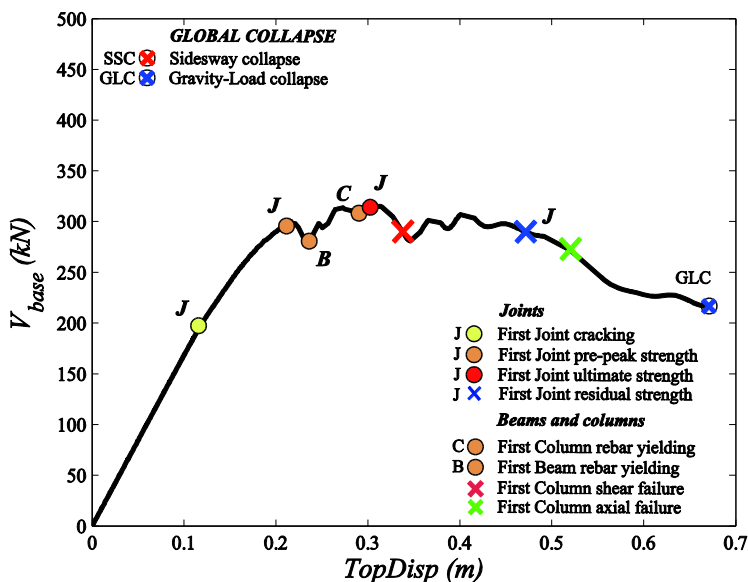
Fig. 3.22 Pushover curve for Italian building assuming a linear load pattern

Similarly to the American building, joint cracking firstly occurs, however, the damage pattern is more spread for both load pattern involving several elements. For the linear pattern the displacement capacity prior to global collapse (0.67m) is greater than the corresponding for uniform pattern (0.43m), this is related to the involvement of more elements in the collapse mode as will be shown in the following paragraph.

69
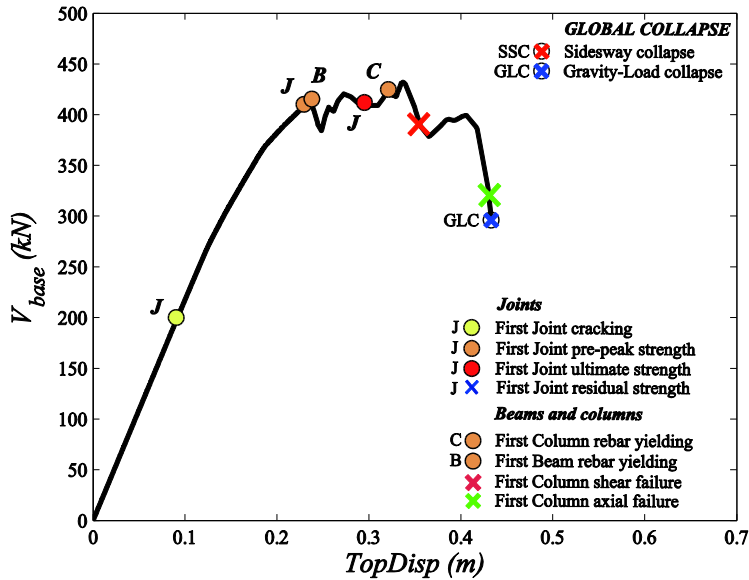
Fig. 3.23 Pushover curve for Italian building assuming a uniform load pattern

3.4.2.1 NONLINEAR STATIC COLLAPSE MECHANISM

As outlined in §3.3, to describe the spreading and the intensity of the damage in the structural elements of the frame, the damage in any single element has been monitored through implementation of an internal algorithm.
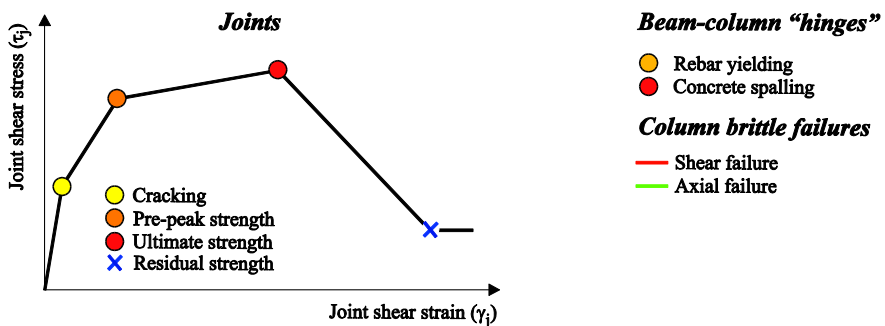
Fig. 3.24 Markers adopted for the definition of component-level limit states

Different limit states have been considered for the three structural members used in this analysis: columns, beams and joints, see Fig. 3.24. For both beams and columns, markers plotted at both extremities can be representative of rebar yielding (orange) or concrete crushing (red). For the sole columns, shear and axial failures have been considered: red column corresponds to the attainment of the shear failure, while green

to the attainment of axial failure. Finally, for the joints four different control points have been considered: cracking, pre-peak strength, ultimate strength and residual strength. Fig. 3.25 shows the damage spread through the frame of the American building for linear and uniform load pattern at collapse. For this building, load pattern does not influence damage at collapse, but only the damage pattern, as can be inferred by comparison of Fig. 3.20 and Fig. 3.21. The collapse mechanism only involves first floor columns leading to a soft-storey mechanism, while other floor are almost not damaged except for joint cracking.
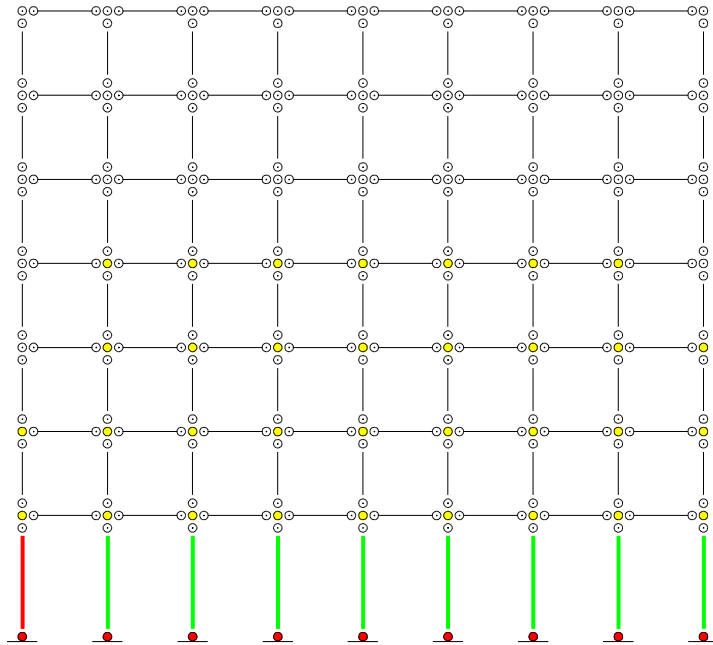
Fig. 3.25 Diagram showing the structural damage at collapse for linear and uniform load pattern

Differently from the American building, the Italian one exhibits a completely different damage distribution through the structure. For the linear load pattern, Fig. 3.26a, the damage is spread through 3th and 5th floor involving columns and joints in the collapse mechanism, while the collapse (gravity load collapse) occurs in the 4th floor. In these floors each column has experienced shear failure, and damage state greater than yielding is detected in all the joint . Three joints have also reached their residual capacity, while yielding is only observable in one beam and several columns have experienced concrete crushing.

(a) Linear Load Pattern   (b) Uniform Load Pattern
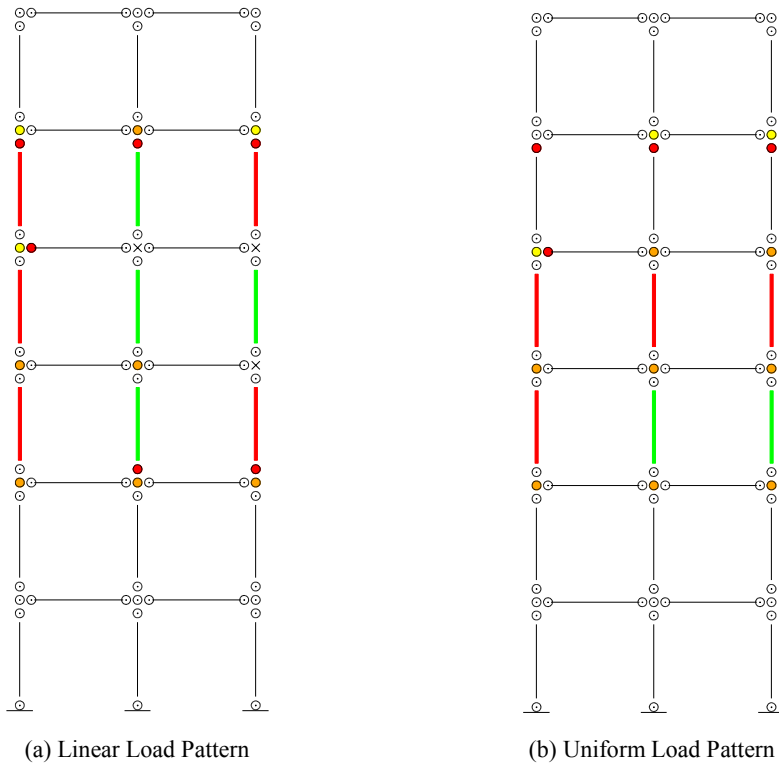
Fig. 3.26 Diagram showing the structural damage at collapse for linear and uniform load pattern

For the uniform load pattern, the damage is extended to same floors but shows to be lighter, showing shear failure only for 4th and 5th floor columns. Furthermore, no joints overcame pre-peak strength.

3.5 QUANTIFICATION OF SEISMIC HAZARD

This paragraph describes the selection of ground motion record sets for collapse assessment of building structures using nonlinear dynamic analysis methods. The methodology here adopted requires a set of ground motion records that are appropriate for incremental dynamic analysis

One of the main issues in assessing the seismic response of structures through nonlinear dynamic analysis is the selection of an appropriate seismic input. The seismic input should allow for an accurate estimation of the seismic hazard at the site where the structure is located (Shome et al., 1998).

When performing nonlinear dynamic analyses, seismic codes basically require a certain number of natural (or synthetic) records to be selected consistently with the

design earthquake and the *code spectrum* in a broad range of period. Consequently they have to be chosen in order have a mean response spectrum that approximate a reference elastic design response spectrum at the site (Iervolino et al. 2010). This is because spectral compatibility is the main criterion required for seismic input by international codes. For example, Eurocode 8 (2008), states that: "In the range of periods between $0.2T_1$ and $2T_1$, where T_1 is the fundamental period of the structure in the direction where the accelerogram will be applied, no value of the mean 5% damping elastic spectrum, calculated from all time histories, should be less than 90% of the corresponding value of the 5% damping elastic response spectrum".

If the probabilistic risk assessment of structures is concerned, to properly select the seismic input, the first step consists in the probabilistic seismic hazard analysis (PSHA) at the site, often used to define the target spectrum (e.g. Uniform Hazard Spectrum, UHS, and Conditional Mean Spectrum, CMS). When the hazard at the site is known, the disaggregation of seismic hazard (e.g. Bazzurro and Cornell, 1999), for the chosen intensity measure, provides the relative contributions from different sources and earthquake events.

3.5.1 PROBABILISTIC SEISMIC HAZARD ANALYSIS

Probabilistic seismic hazard analysis (PSHA) is commonly used to compute the ground motion hazard for which geotechnical and structural systems are analyzed and designed. PSHA considers all possible earthquake scenarios on contributing faults near a site to compute exceedance probabilities of spectral quantities. In practice, this is typically computed using the tools such as OpenSHA (http://opensha.org/) or proprietary software. A fortunate case in this respect are the U.S., where hazard data may be downloaded by the U.S. Geological Survey (USGS) website (http://geohazards.usgs.gov/deaggint/2008/). Italy also has a similar service due to the work of the Istituto Nazionale di Geofisica e Vulcanologia (INGV). The results of the project include hazard curves on rock, based on 9 return periods, for 11 oscillation periods of engineering interest and disaggregation for the whole Italian territory (Meletti and Montaldo, 2007; Montaldo and Meletti, 2007). This study has been acknowledged by the new Italian seismic code (CS. LL. PP., 2008) which now allows to design considering response spectra derived from seismic hazard (technically coincident with the UHSs) and to select time histories with respect the characteristics of the dominating earthquake.

3.5.2 DEAGGREGATION OF SEISMIC HAZARD

As a key step in defining the seismic load input to dynamic analysis, ground motion selection often involves specification of a target spectrum, (e.g., the Conditional Mean

Spectrum). Computation of such a target spectrum requires deaggregation to identify the causal ground motion parameters.

The deaggregation of seismic hazard (McGuire, 1995; Bazzurro and Cornell, 1999) is an extension of the PSHA procedure that allows to evaluate the contributions of different seismic sources to the hazard of a site. Deaggregation identify magnitude (M), distance (R) and standard deviation (ε) as predicted by a ground motion prediction relationship (GMPE) that contribute the most to that hazard.

Magnitude, distance, and epsilon are currently the ground motion parameters that are of most interest, and deaggregation results for these parameters can be easily obtained from standard PSHA software

The computation of a target spectrum, e.g. the CMS, requires deaggregation to identify the causal parameters, along with the choice of a GMPE.

IMPORTANCE OF SPECTRAL SHAPE

For records with the same $S_a(T_1)$ value, spectral shape will affect the response of multi-degree-of-freedom and non-linear structures, because spectral values at other periods affect response of higher modes of the structure as well as non-linear response when the structure's effective period has lengthened. It is also recognized that magnitude and distance can affect the spectral shape of records. In Baker and Cornell (2005), the ground motion parameter ε has been identified as an indicator of spectral shape and it is highlighted that its effect is at least as great as that of magnitude or distance.

Thus, rather than trying to match target M, R and ε values when selecting records, one might use M, R and ε to determine a target spectral shape.

Epsilon is defined as the number of standard deviations by which an observed logarithmic spectral acceleration differs from the mean logarithmic spectral acceleration of a ground-motion prediction (attenuation) equation. In other words, it specifies the number of logarithmic standard deviations away from the median ground motion model. The equation corresponding to this definition is:

$$\varepsilon(T) = \frac{\ln S_a(T) - \mu_{\ln S_a}(M, R, T)}{\sigma_{\ln S_a}(T)} \qquad \text{Eq. 3-11}$$

where $\ln S_a(T)$ is the natural logarithm of the spectral acceleration at a specified period T and $\mu_{\ln Sa}(M,R,T)$ and $\sigma_{\ln Sa}(M,R,T)$ are, respectively, the mean and the standard deviation as predicted by a ground motion prediction relationship (GMPE). It should be noted that epsilon is defined with respect to the unscaled record and will not change in value when the record is scaled. The Fig. 3.27 shows the value of ε at three different periods. It can be argued that ε depends on the GMPE used and the period of calculation. Note that the +/- σ bands are not symmetric around the median because they are +/- σ values of $\ln S_a$, rather than (non-log) S_a.
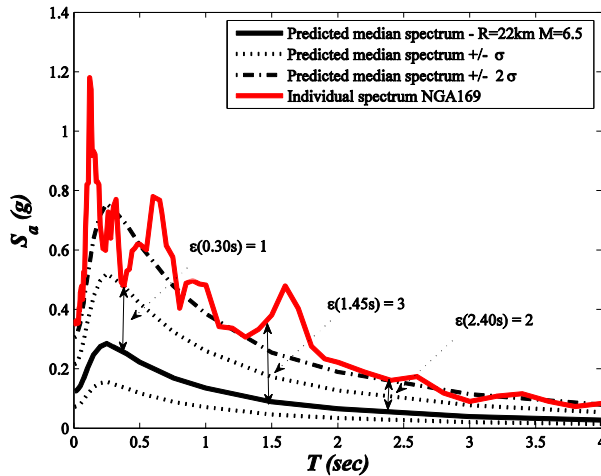
Fig. 3.27 Response spectrum from the ground motion NGA169, and Bore and Atkinson's GMPE for the same earthquake, used to illustrate calculation of ε values at three different periods.

The physical meaning of why epsilon is important is its capability to indicate "peaks" and "valleys" in the response spectrum for a given value of the period. A positive ε indicates a local peak of the spectrum with respect to the GMPE, a negative, a valley. Consequently, ε is an indicator of spectral shape, and this shape is very important when selecting accelerograms because it can affect the nonlinear response of MDOF systems acting on higher vibration modes.

The importance of accounting for ε in accelerograms selection has been highlighted by several authors. For instance, Haselton and Baker (2006), Liel (2008), Zareian and Krawinkler (2006), have found that varying the target spectral shape from one associated with $\varepsilon(T_1)=0$ to one associated with $\varepsilon(T_1)=2$ resulted in a 40% to 80% increase in median collapse, depending upon the structure considered. Goulet et al. (2007) found that, neglecting ε, the median predicted collapse capacities is reduced by 20–40%.When dealing with non-collapse responses, Baker and Cornell (2006b), Goulet et al. (2008), Haselton et al. (2008) observed that, under similar conditions, neglecting this ε effect often results in an overestimation of mean structural response by 30% to 60%.

3.5.3 TARGET SPECTRA

In the majority of cases, the records are selected to have response spectra that approximate the Uniform Hazard Spectrum or other "design" spectrum (e.g. Iervolino et al., 2010). However, the code-based spectra (e.g., Eurocode 8 – CEN, 2003) may be very weakly related to the hazard and therefore may be quite different from the UHSs. Nonlinear multi-degree of freedom systems may be sensitive to excitation at a wide

range of periods and thus will be sensitive to the target response spectrum used for selecting ground motions. For this reasons the target spectrum should carefully selected considering the analyses purposes.

3.5.3.1 UNIFORM HAZARD SPECTRUM

A widely used procedure for the selection and scaling of ground motions is based on the spectral matching of ground motions to a Uniform Hazard Spectrum (UHS). In fact, an increasing number of building codes worldwide acknowledges the uniform hazard spectra as the reference ground motion to determine seismic actions on structures and to select input signals for seismic structural analysis.

The UHS is defined with the purpose that all its spectral ordinates have the same probability of exceedance in a time interval depending on the limit-state of interest (e.g. 2% in 50 years). The target UHS spectrum is derived from the Probabilistic Seismic Hazard (Bazzurro and Cornell, 1994, 1999) considering the envelope of spectral amplitudes at all periods which exceed a specific probability in a specific time frame. Probabilistic seismic hazard analysis (PSHA) is currently the soundest basis for the evaluation of the hazard for site-specific engineering both design and assessment purposes.

If the return period of seismic action for assessment purposes is defined *a priori*, and the IM is the elastic spectral acceleration at different structural periods, it is possible to build the UHS. For example, the response spectrum with a constant exceedance probability for all ordinates (e.g., 10% in 50 year or 475 year return period in the case of design for life-safety structural performance, Reiter, 1990). The Italian seismic code (CS.LL.PP, DM 14 gennaio 2008) is based on the work of the Instituto Nazionale di Geofisica e Vulcanologia (INGV), which computed uniform hazard spectra over a grid of more than 10,000 points for 9 return periods (T_r) from 30 to 2475 years, and 10 spectral ordinates from 0.1 to 2 s (http://esse1.mi.ingv.it/). Therefore, at each site, Italian design spectra are a close approximation of the UHS. An example of UHS computation is depicted in Fig. 3.28. Once performed the PSHA at the specific site, Fig. 3.28(a) for two different oscillation periods, the S_a values corresponding to a given probability of exceedance in 50 years can be reported on a T-S_a plane, Fig. 3.28(b). Repeating this procedure for several periods, the UHS can be simply calculated.

Once the UHS has been defined, for the level of spectral acceleration given by the UHS at the first oscillation period of the structure, the ground motion selection requires the disaggregation of seismic hazard (e.g., McGuire, 1995). Starting from the PSHA results, disaggregation is a procedure that allows identification of the hazard contribution of each magnitude (M), distance (R), and ε vector. Disaggregation is based on the computation of the relative contributions of the elements used to compute seismic hazard, e.g., seismogenic zones, recurrence relationships, and focal mechanisms (Convertito and Herrero, 2004). The deaggregation allows to identify the values of some

earthquake characteristics that provide the largest contributions to the hazard in terms of exceeding a specified spectral ordinate threshold. These events may be referred to as the earthquakes dominating the seismic hazard in a probabilistic sense, and may be used as Design Earthquakes, as conceptually introduced by McGuire (2004).

(a) Seismic Hazard Curves for T=0.2 and 2.0 sec

(b) Uniform Hazard Spectrum
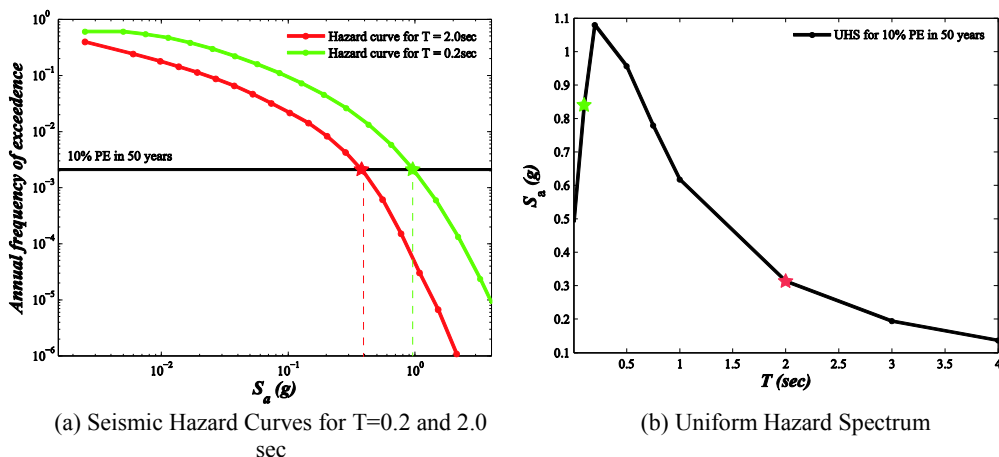
Fig. 3.28 Example of UHS calculation for Van Nuys site (soil D according to NEHRP) for 10% in 50 years

Given the dominant M, R, and ε values, time histories can be chosen to match within tolerable limits the mean or modal value of these parameters, i.e., the expected value or most likely value of these characteristics. The records may also be selected considering other earthquake-specific characteristics, such as directivity, faulting style and duration, soil type. Often, the sole last parameter is accounted for in the selection because of its importance in the frequency content of the earthquake.

After the design earthquake is identified, a database is accessed and a number of time histories is selected to match, within tolerable limits, the values of these parameters believed to be important for a correct estimation of the structural response.

Finally, the selected records are usually scaled to match in some average way the UHS, as it is often recommended, precisely to the UHS level at a period near that of the first period, T_1, of the structure when the structure is known (Shome et al. 1998).

Time histories obtained in this way are used as the input for a set of nonlinear dynamic analyses to evaluate the behavior of the structure in the case of the ground motion represented by the UHS (Cornell, 2004).

The Uniform Hazard Spectrum (UHS) has been used as the target spectrum in design practice for the past two decades. However, UHS is not the only possible PSHA-based design spectrum (Baker, 2011), although it is considered the basis for the definition of design seismic actions on structures in the most advanced seismic codes. It is worthy to note that the UHS is a conservative target spectrum for seismic analysis of buildings,

77

especially for very rare levels of ground motion (e.g., Bommer et al., 2000; Naeim and Lew, 1995; Reiter, 1990), where it is most unlikely that high amplitude spectral values are observed at all periods in a single ground motion set. The probability level associated with a UHS is the probability of exceeding any single spectral value; however, the probability of simultaneously exceeding all spectral values from a UHS is much smaller.

3.5.3.2 CONDITIONAL MEAN SPECTRUM

The shape of a UHS has been criticized to be unrealistic for a site where the spectral ordinates of the UHS at different periods govern by different scenarios (Baker and Cornell, 2006a). Furthermore, the spectral ordinates of the UHS for long-return period are associated with high values of ε across a wide range of period (Harmsen, 2001), i.e. it conservatively implies that large-amplitude spectral values will occur at all periods within a single ground motion. Given that the uniform hazard spectrum is thus not representative of the spectra from any individual ground motion, it will make an unsatisfactory ground motion selection target in many cases (Baker, 2011).

To address the above issues, Baker and Cornell (2005, 2006a) introduced the *Conditional Mean Spectrum* (*CMS-ε*), which consider the correlation of spectral demands (represented by ε) at different periods. The parameter ε, as stated above, specifies the number of logarithmic standard deviations away from the median ground motion model.

The CMS conditions the entire spectrum on spectral acceleration at a single user-specified period and then computes the mean values of spectral acceleration at all other periods. This conditional calculation ensures that ground motions are modified to match the spectrum have properties of recorded ground motions. The CMS calculation requires hazard disaggregation information, making it site-specific. The appropriate conditioning period may not be immediately obvious and the CMS changes with conditioning period, unlike the UHS. Further, the spectrum changes shape as the peak spectral value is changed, even when the site and period are not changed. Multiple conditioning periods could be used to generate a family of CMS for either design or performance assessment (Somerville and Thio, 2011)

The *CMS* estimates the median geometric mean spectral acceleration response of a pair of ground motions given a magnitude M and distance R and a target spectral ordinate $S_a(T_1)$, with T_1 corresponding to the fundamental period of vibration, and where the parameter $\varepsilon(T_1)$ is back-calculated using an appropriate attenuation relationship. Conditional Mean Spectrum maintains the probabilistic rigor of PSHA, so that consistency is achieved between the PSHA and the ground motion selection.

The CMS supplies the mean spectral shape associated with the $S_a(T^*)$ target, so ground motions that match that target spectral shape can be treated as representative of ground motions that naturally have the target $S_a(T^*)$ value. In other words, the main

advantage in the use of CMS as a target spectrum, relies in the fact that the analyses results are comparable to those that can be obtained by using unscaled records.

Because the CMS effect is more pronounced for rare ground motions, it is important to consider when predicting the safety of buildings against collapse (which is typically caused by very high amplitude ground motions). The ATC-63 project found that accounting for the effect of the CMS increased the median spectral acceleration that a building could withstand prior to collapsing by up to 60%, relative to analyses with ground motions having response spectra similar in shape to the UHS (Applied Technology Council 2008).

As anticipated, the UHS can be significantly conservative because the probability level associated with a UHS is the probability of exceeding any single spectral value, while the CMS is conditioned to a single period usually corresponding to the structure fundamental period. The conservativism of the UHS compared to CM spectrum can be deduced from Fig. GH, where CMS and UHS for a southern California site is plotted. The CMS is conditioned to T*=1sec for a Return period of 475 years and has been calculated by using Abrahamson and Silva (1997) Ground Motion Prediction Equation. It can be seen that two spectra perfectly match when T=T* while for all other periods the CMS always relies under the UHS.
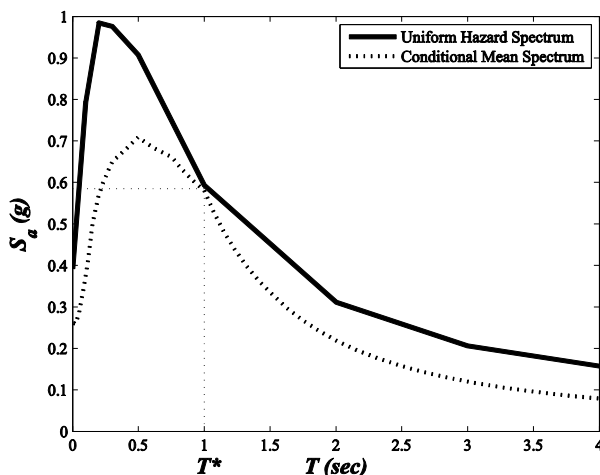
Fig. 3.29 Comparison between UHS and CMS computed for Californian site, with reference to a Return Period of 475 years. The CMS is conditioned to S_a(T*=1 sec).

Development of CMS-epsilon

The CMS-ε target spectrum, called *conditional mean spectrum considering ε,* was originally developed for analysis of nuclear facilities (Nuclear Regulatory Commission, 1997), however Baker and Cornell (2006a) incorporate also the effect of ε in the procedure, developing the *conditional mean spectrum considering ε (CMS-ε)* that accounts for the relationship between ε and spectral shape. To develop a *CMS-ε*, PSHA

is used to find the $S_a(T_1)$ value corresponding to the target probability of exceedance at the site of interest.

Using the hazard curve and disaggregation information for a particular conditioning period, the Conditional Spectrum calculation is used to compute the mean and standard deviation of logarithmic response spectral values at all other periods, conditioned on an amplitude of $S_a(T^*)$. The mean and standard deviation of $\ln S_a$ are given by the following equations (Baker and Cornell, 2005).

$$\mu_{\ln S_a(T_i)|\ln S_a(T^*)} = \mu_{\ln S_a}(M,R,T_i) + \rho(T_i,T^*)\varepsilon(T^*)\sigma_{\ln S_a}(T_i) \qquad \text{Eq. 3-12}$$

$$\sigma_{\ln S_a(T_i)|\ln S_a(T^*)} = \sigma_{\ln S_a}(T_i)\sqrt{1-\rho^2(T_i,T^*)} \qquad \text{Eq. 3-13}$$

where $\mu_{\ln S_a}(M,R,T_i)$ and $\sigma_{\ln S_a}(T_i)$ are the predicted mean and standard deviation from a ground motion prediction equation, $\rho(T_i,T^*)$nis the correlation between the spectral values at the period T_i and the conditioning period T*, and M, R and ε(T*) come are the mean values from the disaggregation distribution. For further information about the definition of Conditional mean spectrum refers to Baker and Cornell (2011).

3.5.4 SELECTION AND SCALING

In the past, irrespective of the procedure used to obtain a target response spectrum, a wide variety of techniques have been developed for ground motion selection and scaling for performing nonlinear analysis of structures in terms of inelastic seismic response (e.g., Haselton et al. 2009; Katsanos 2010). A comprehensive study performed by Haselton et al. (2009) as a part of the *PEER Ground Motion Selection and Modification Program* has identified 40 different methods.

One approach is to select individual ground motions (scaled or unscaled) that deviate the least from the target response spectrum. The deviation can be measured using the sum of squared differences between the response spectrum of the record and the target response spectrum (e.g., Youngs et al. 2007). Alternately, the ground motion set can be selected by minimizing the mean spectrum of the selected records from the target response spectrum, rather than select one record at a time. This more complicated procedure requires special algorithms to accelerate selection process such as genetic algorithm (Naeim et al. 2004). Other approaches only requires that selected ground motions to be representative of a scenario earthquake having specified magnitude, distance, epsilon (e.g., Jayaram and Baker 2010). However, Jayaram et al. (2011) developed a computationally fast and theoretically consistent ground-motion selection algorithm to match the Conditional Mean Spectrum mean and variance. The algorithm make use of the Montecarlo simulation and a greedy optimization technique to minimize the sum of squared errors between the selected set and the CMS. Jayaram et al. (2011)

also developed a useful tool, here adopted, to simplify accelerograms selection using CMS as target spectrum.

3.6 SELECTION OF ACCELEROGRAMS FOR AMERICAN AND ITALIAN BUILDING

In this study the CMS-ε has been adopted as target spectrum to select input ground motions due to several advantages: 1) Nonlinear multi-degree of freedom systems may be sensitive to excitation at a wide range of periods and thus will be sensitive to the target response spectrum used for selecting ground motions. It has been empirically confirmed that ductile and higher-mode-sensitive structures are more sensitive to consideration of the CMS (ATC 2009; Haselton and Dierlein 2008). Given that the UHS is not representative of the spectra from any individual ground motionit will make an unsatisfactory ground motion selection target in many cases (Baker, 2011). 2) The conservative nature of the UHS with respect to the CMS, as well as its conservative nature, in fact, the ATC-63 project, found that accounting for the effect of the CMS in ductile structures, increased the median spectral acceleration that a building could withstand prior to collapsing by up to 60%, relative to analyses with ground motions having response spectra similar in shape to the UHS (ATC, 2009). 3) Several studies have demonstrated that the use of CMS as target spectrum into the accelerogram selections allows obtaining results similar to those obtained by using unscaled records (Baker, 2011). 4) It perfectly meets the needs of the selection of a large bin of earthquakes (31 natural records), because it widens the range of acceptable records for analysis because the selected records do not necessarily have appropriate magnitude, distance and ε values, but rather the records need only have a spectral shape that matches the mean spectrum from the causal event (Baker and Cornell, 2006a).

The compatibility with this target spectrum has been checked in the period range of 0.2T to 1.5T, where T is the fundamental translational period of the structure, to account for an increase in period due to inelastic action (increasing the fundamental period to an effective value of 1.5T) and the second mode translational period, which often falls between one-quarter and one-third of the fundamental period if the building framing is regular according to ASCE 7-05. It is worth to note, however, that statistical studies suggest that nonlinear buildings are often sensitive to response spectra at periods longer than 1.5T1 (Baker and Cornell 2008a; Cordova et al. 2001; Haselton and Baker 2006; Vamvatsikos and Cornell 2005). The ground motion hazard characterization involves two aspects: quantification of the earthquake IM and selection of ground motions consistent with the hazard.

3.6.1 RECORD SELECTION FOR AMERICAN CASE-STUDY

The selected site for the American case-study building, shown in, is the Van Nuys district, Los Angeles, California (latitude: 34.2054 N, longitude: 118.3729 W).
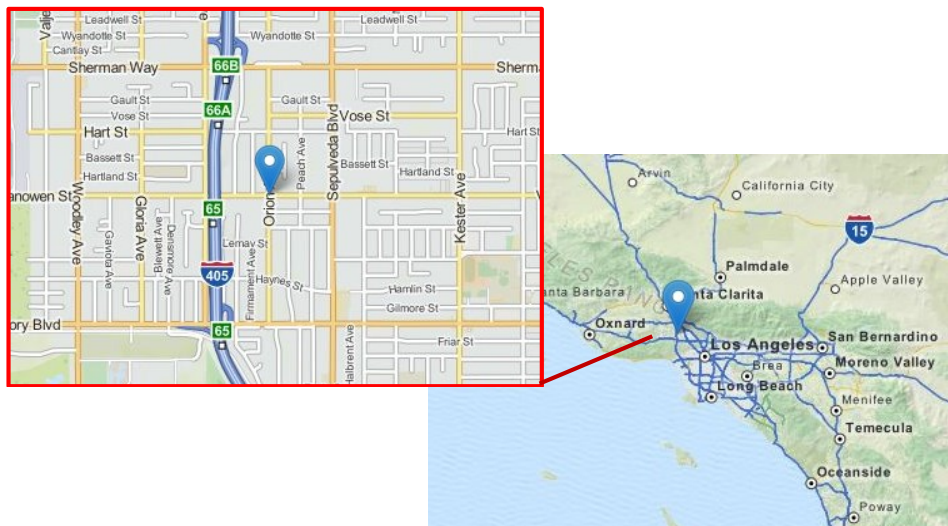
Fig. 3.30 Van Nuys site

For the study area, the magnitude, distance and epsilon values were computed from disaggregation of seismic hazard, specifically calculated, for $S_a(T_1)$. Uniform Hazard Spectra, M, R and ε from deaggregation of the seismic hazard for any site in the United States can be derived from the USGS probabilistic ground motion maps available online in http://geohazards.usgs.gov/deaggint/2008/.

Based on the OpenSees model, the first three modes of the structure exhibit the following periods of vibration: 1.0, 0.45 and 0.18 seconds.

Uniform hazard spectrum and fundamental parameters from deaggregation for Van Nuys site were derived in Baradaran Shoraka (2013). UHS was derived for 2%, 5%, 10%, 20% and 50% probability of exceedance in 50 years, while parameters from deaggregation were referred to a period T corresponding to the fundamental oscillation period of the specific structure and a specific Return Period. For this deaggregation, a shear wave velocity ($V_{s,30}$) of 218 m/s^2, corresponding to D soil class according to NEHRP classification and a first-mode period of 1.0 seconds were assumed. Uniform hazard spectra, used to derive the $S_a(T_1)$ to which scale the damaging earthquake, are illustrated in Fig. 3.31.
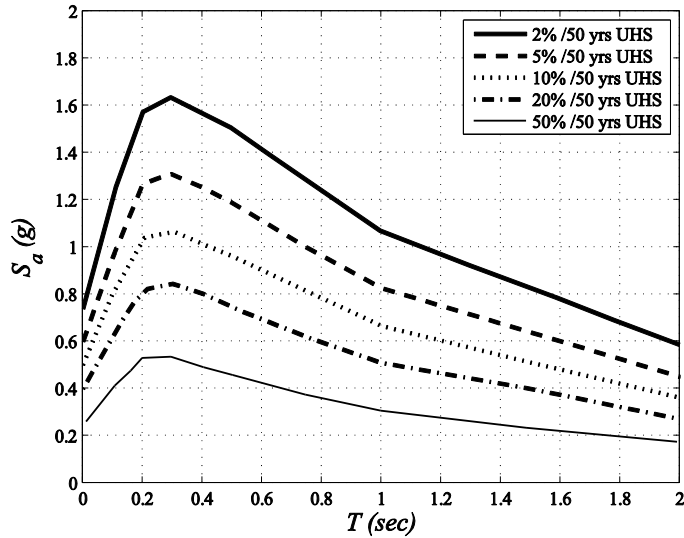
Fig. 3.31 Probabilistic Uniform Hazard Spectra for the site in Van Nuys, CA, for five levels of annual exceedance probabilities.

The selected hazard level for accelerograms selection corresponds to 10% of probability of exceedance in 50 years, which is a reference return period for the life-safety limit state of ordinary constructions. Mean R, M and ε values of the deaggregation distribution provided by USGS for a Return Period of 475 years are 23.2, 6.97 and 1.18, respectively. Based on the results of the seismic hazard deaggregation, 31 ground motions are selected from the PEER Next Generation Attenuation (NGA) database (Chiou et al., 2008) to match the Conditional Mean Spectrum (Baker, 2011). To reflect differences in the spectral shape at different shaking intensities, ground motions have been selected with ε values similar to the target ε. The ground motion set presented in Table 3-9 has a mean ε = 1.15 while hazard deaggregation for this site provides a target epsilon of 1.18 for a 475 years return period, using Abrahamson and Silva 1997 attenuation model (Abrahamson and Silva, 1997).

For the studied site $S_a(T_1)$ values for 2%, 5%, 10%, 20% and 50% probability of exceedance in 50 years, corresponding to 72, 224, 475, 975 and 2475 years Return Periods, respectively, are summarized in Table 2-1. These values will be used in the following chapters as a reference value to perform cost analyses and to scale damaging ground motions in the assessment of Residual building capacities.

Earthquake	Mw	Station	Record	Dist. (km)	PGA (g)	$\varepsilon(T_1)$
Chi-Chi,Taiwan 20/09/1999	7.6	TCU042	TCU042-N	23.34	0.199	0.9
Chi-Chi,Taiwan 20/09/1999	7.6	CHY035	CHY035-N	18.12	0.246	1.1
Chi-Chi,Taiwan 20/09/1999	7.6	TCU123	TCU123-W	15.12	0.164	1.7
Chi-Chi,Taiwan 20/09/1999	7.6	CHY006	CHY006-E	14.93	0.364	1.2
Duzce, Turkey 12/11/1999	7.1	Bolu	BOL090	17.6	0.822	1.6
Imperial Valley 15/10/1979	6.5	6617 Cucapah	H-QKP085	23.6	0.309	1.3
Imperial Valley 15/10/1979	6.5	5059 El Centro Array #13	H-E13230	21.9	0.139	0.9
Imperial Valley 15/10/1979	6.5	6621 Chiuaua	H-CHI012	17.7	0.27	1.2
Imperial Valley 15/10/1979	6.5	5115 El Centro Array #2	H-E02140	10.4	0.315	1.1
Landers 28/06/1992	7.3	22074 Yermo Fire Station	YER270	24.9	0.245	1.4
Loma Prieta 18/10/1989	6.9	57425 Gilroy Array #7	GMR090	24.2	0.323	0.6
Loma Prieta 18/10/1989	6.9	57382 Gilroy Array #4	G04000	16.1	0.417	0.8
Loma Prieta 18/10/1989	6.9	47125 Capotola	CAP000	14.5	0.529	1.4
N.Palm Springs 08/07/1986	6	12025 Palm Springs Airport	PSA090	16.6	0.187	1.1
Northridge 17/01/1994	6.7	90054 LA - Centinela St	CEN155	30.9	0.465	1.4
Northridge 17/01/1994	6.7	90091 LA - Saturn St	STN020	30	0.474	1
Northridge 17/01/1994	6.7	24303 - LA - Holliwood Store FF	HOL360	25.5	0.358	1
Northridge 17/01/1994	6.7	90063 Glendale - Las Palmas	GLP177	25.4	0.357	1.4
Northridge 17/01/1994	6.7	90053 Canoga Park	CNP196	15.8	0.42	0.6
Northridge 17/01/1994	6.7	90003 Northridge - 17654 Sat. St	STC180	13.3	0.477	0.7
Northridge 17/01/1994	6.7	90057 Canyon C.- W Lost Cany	LOS270	13	0.482	1
Northridge 17/01/1994	6.7	24279 Newhall -Fire Station	NWH360	7.1	0.59	0.9
San Fernando 09/02/1971	6.6	94 Gormon - Oso Pump Plant	OPP270	48.1	0.105	1.4
San Fernando 09/02/1972	6.6	135 LA - Holliwood Store Lot	PEL090	21.2	0.21	0.9
Whittier Narrows 01/10/1987	6	24303 LA - Holliwood Store FF	A-HOL000	25.2	0.221	1.6
Whittier Narrows 01/10/1987	6	90012 Burbank - N Buena Vista	A-BUE250	23.7	0.233	1
Whittier Narrows 01/10/1987	6	90084 Lakewood - Del Amo Blvd	A-DEL000	20.9	0.277	1.1
Whittier Narrows 01/10/1987	6	90063 Glendale - Las Palmas	A-GLP177	19	0.296	1.7
Whittier Narrows 01/10/1987	6	14368 Downey - Co Maint Bldg	A-DWN180	18.3	0.221	1.6
Whittier Narrows 01/10/1987	6	90078 Compton - Castelgate St	A-CAS270	16.9	0.333	1
Whittier Narrows 01/10/1987	6	90077 Santa Fe Springs - E Joslin	A-EJS318	10.8	0.443	1.1

Table 3-9 Ground motions selected for case study (after Baradaran Shoraka, 2013)

Return Period (yrs)	72	224	475	975	2475
$S_a(1.00\ sec)$ (g)	0.29	0.49	0.65	0.82	1.06

Table 3-10 $S_a(T_1)$ for different hazard levels for the American case study

3.6.2 RECORD SELECTION FOR ITALIAN CASE-STUDY

The selected site for the Italian case-study building, shown in Fig. 3.32, is the Rione Libertà, Benevento, Italy (latitude: 41.1277 N, longitude: 14.7742 E).
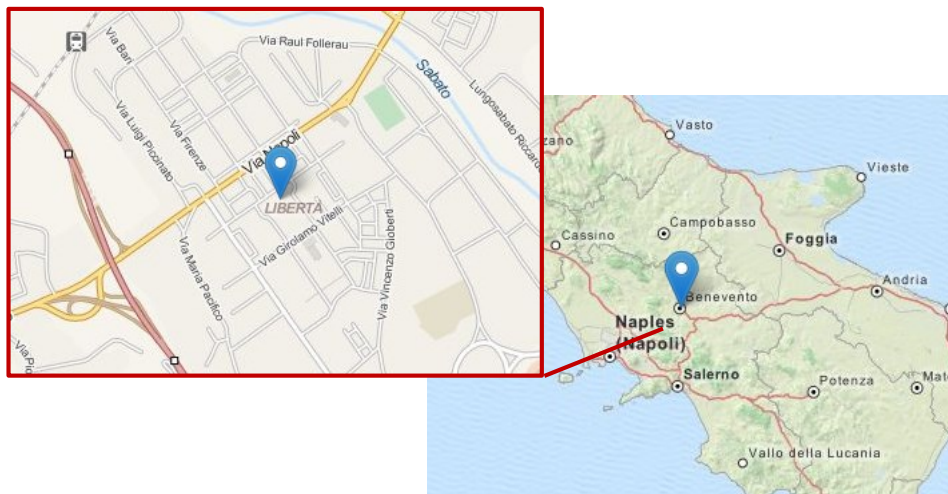
Fig. 3.32 Rione Libertà site

For the study area, the magnitude, distance and epsilon values were computed from disaggregation of seismic hazard, specifically calculated, for $S_a(T_1)$. Uniform Hazard Spectra for any site in Italy and for different probabilities of exceedance in 50 years can derived from the INGV seismic hazard interactive maps site available online in http://esse1-gis.mi.ingv.it/.

Uniform hazard spectrum for Rione Libertà site in Benevento was derived for 2%, 5%, 10%, 20% and 50% probability of exceedance in 50 years. Uniform hazard spectra were used to derive the $S_a(T_1)$ to which scale the damaging earthquake and are illustrated inFig. 3.33.

Because the INGV only provides parameters from deaggregation associated with Peak Ground Acceleration (PGA), the parameters (magnitude, distance and epsilon) necessary to the computation of the CMS were extracted from the program REXEL (Iervolino et al. 2010) for a period T corresponding to the fundamental oscillation period of the specific structure and a Return Period corresponding to life-safety limit state. For this spectral period, the rate of exceeding that amplitude and a disaggregation distribution providing the causal magnitudes, distances and ε values associated with spectral accelerations were obtained.

For this deaggregation, a shear wave velocity ($V_{s,30}$) of 500 m/s^2, corresponding to B soil class according to Eurocode 8 (CEN 2004) classification (see Santucci de Magistris

et al., 2014) and a first-mode period of 1.05 second were assumed. Based on the OpenSees model (presented in following chapters), the first three modes of the structure exhibit the following periods of vibration: 1.05, 0.35 and 0.20 seconds.
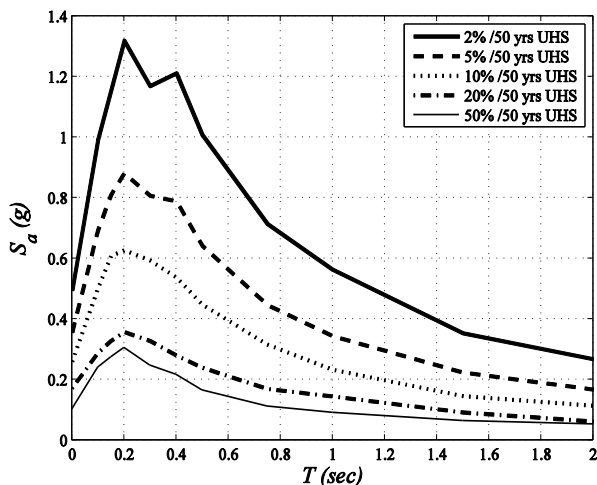
Fig. 3.33 Uniform Hazard Spectrum for Rione Libertà site (Benevento) for different exceedance probabilities

The selected hazard level for accelerograms selection corresponds to 10% of probability of exceedance in 50 years, which, as above reported, is a reference return period for the life-safety limit state of ordinary constructions. Under these hypotheses, mean R, M and ε values of the deaggregation distribution for a Return Period of 475 years are 6.04, 8.51 and 0.736, respectively.

Using the hazard curve and disaggregation information for a particular conditioning period, the Conditional Spectrum calculation is used to compute the mean and standard deviation of logarithmic response spectral values at all other periods, conditioned on an amplitude of $S_a(T^*)$. Once the CMS is computed, it has been used as target spectrum to select and scale ground motions for use in nonlinear analyses. Conditional Mean Spectrum and its deviation, conditioned on $S_a(1.05sec)$ for a probability of exceedance of the 10% in 50 years is depicted in Fig. 3.34(a). Along with the CMS the Ground motion prediction equation for the same couple M,R is reported.

Based on the results of the seismic hazard deaggregation and hazard curve, 31 ground motions were selected from the PEER Next Generation Attenuation (NGA) database (Chiou et al., 2008) to match the Conditional Mean Spectrum (Baker, 2011) using the tool provided by Jayaram et al. (2011). More details regarding the ground motion selection algorithm and its implications are provided by Jayaram et al. (2011). No further constraints were placed on the ground motion selection (e.g., magnitudes and distances) other than limiting scale factors to less than four, with the primary selection

focus being on the match of the ground motion spectra to the target Conditional Mean Spectrum. This was done because the structural response parameter of interest in this case is thought to be most closely related to spectral values. Also, earthquake magnitude and distance affect this structural response primarily as they relate to spectral values (which are accounted for carefully) rather than other ground motion parameters such as duration.

It is important to mention that the seismic hazard disaggregation at each grid point of the Italian probabilistic seismic hazard map (Spallarossa and Barani, 2007) is done using Ambraseys (1985) attenuation relationship. Even if the ε value depends on the GMPE adopted, according to Baker, it is not essential to use the same GMPE when selecting accelerograms using CMS as target spectrum. In this case, the Campbell-Bozognia (2008) attenuation relationship has been used.

The accelerograms set composed of 31 earthquakes, resulting from the selection process is reported in Fig. 3.34(b) along with the CMS target spectrum and 2.5 and 97.5 percentiles. Selected accelerograms
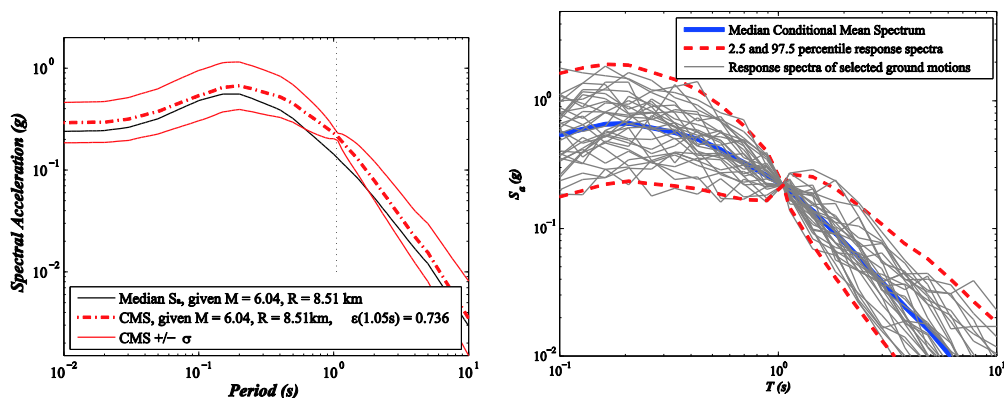
Fig. 3.34 Conditional Mean Spectrum (a) and selected ground motion spectra (b) for Rione Libertà site (Benevento)

The ground motion set selected for the Rione Libertà site is presented in Table 3-11. For the studied site $S_a(T_1)$ values for 2%, 5%, 10%, 20% and 50% probability of exceedance in 50 years, corresponding to 72, 224, 475, 975 and 2475 years Return Periods, respectively, are summarized in Table 3-12. These values will be used in the following chapters as a reference value to perform cost analyses and to scale damaging ground motions in the assessment of Residual building capacities.

Earthquake	Mw	Station	Record	Distance (km)	PGA (g)
Borrego Mtn 1968-04-09	6.63	USGS El Centro Array #9	A-ELC180	70.75	0.0876
Landers 1992-06-28	7.3	90094 Bell Gard. - Jaboneria	JAB220	153.9	0.036
Victoria, Mexico 1980-06-09	6.33	Cerro Prieto	CPE045	35.48	0.5722
Whittier Narrows-01 1987-10-01	5.99	Pasadena - Old House Rd	A-OLD090	13.21	0.2622
Coalinga-02 1983-05-09	5.09	Skunk Hollow	D-SKH360	12.44	0.1402
Morgan Hill 1984-04-24	6.19	Coyote Lake Dam (SW Abut)	CYC195	24.55	0.9652
Northridge-01 1994-01-17	6.69	Elizabeth Lake	ELI180	53.04	0.1331
Chi-Chi, Taiwan 1999-09-20	7.62	HWA059	HWA059-N	69.29	0.128
Chi-Chi, Taiwan-02 1999-09-20	5.9	CHY088	CHY088-E	88.71	0.0287
DUZCE 1999-12-11	7.14	LAMONT 1062	1062-N	29.27	0.2101
Chi-Chi, Taiwan-02 1999-09-20	5.9	TCU067	TCU067-E	33.94	0.1235
Northridge-01 1994-01-17	6.69	Seal Beach - Office Bldg	SEA090	66.13	0.0755
Coalinga-05 1983-07-22	5.77	Oil Fields Fire Station - Pad	D-OLP360	83.55	0.2083
Imperial Valley-06 1979-10-15	6.53	Calexico Fire Station	H-CXO225	33.73	0.2329
N. Palm Springs 1986-07-08	6.06	Desert Hot Springs	DSP090	10.38	0.3432
Imperial Valley-06 1979-10-15	6.53	Delta	H-DLT352	35.17	0.2849
Northridge-01 1994-01-17	6.69	Tarzana - Cedar Hill	TAR090	5.41	1.6615
Denali, Alaska 2002-11-03	7.9	ANSS/UA R109 R109 (temp)	5596-090	61.85	0.083
Coalinga-04 1983-07-09 07:40	5.18	Transmitter Hill	C-TSM270	8.55	0.2083
Chi-Chi, Taiwan 1999-09-20	7.62	TCU-123	TCU129-E	14.16	0.788
Chi-Chi, Taiwan-02 1999-09-20	5.9	KAU050	KAU050-N	90.28	0.0076
Westmorland 1981-04-26	5.9	Brawley Airport	BRA225	15.71	0.1571
Chi-Chi, Taiwan 1999-09-20	7.62	CHY028	CHY028-N	32.67	0.794
Whittier Narrows-01 1987-10-01	5.99	N Hollywood - Coldwater Can	CWC270	34.48	0.1709
Northridge-01 1994-01-17	6.69	Baldwin Park - N Holly	NHO270	54.68	0.1079
Morgan Hill 1984-04-24	6.19	Gilroy Array #2	G02000	38.1	0.1867
Whittier Narrows-01 1987-10-01	5.99	Compton - Castlegate St	CAS000	19.81	0.3306
Morgan Hill 1984-04-24	6.19	Gilroy Array #2	G02090	38.1	0.1867
Norcia, Italy 1979-09-19	5.9	Cascia	F-CSC-NS	4.29	0.1856
Chi-Chi, Taiwan 1999-09-20	7.62	TCU145	TCU145-W	51.24	0.0699
Coalinga-02 1983-05-09	5.09	Skunk Hollow	A-SUB090	8.09	0.1599

Table 3-11 Ground motions selected for the Italian case study

Return Period (yrs)	72	224	475	975	2475
$S_a(1.05\ sec)$ (g)	0.09	0.14	0.23	0.34	0.56

Table 3-12 $S_a(T_1)$ for different hazard levels for the American case study

3.7 NONLINEAR DYNAMIC ANALYSIS AT DIFFERENT MAINSHOCK INTENSITIES

The assessment of building's seismic response under several earthquake intensities is a fundamental step in order to have a realistic estimation of potential seismic losses. As explained in FEMA P-58 (ATC 2011), the time-based loss assessment is one of the most complete performance assessment procedures; it requires the knowledge of significant engineering demand parameters (EDPs that have a direct link to damage) and their probability distribution considering all possible earthquake scenarios and the annual occurrence frequency of each scenario.

In order to apply a detailed time-based assessment , this work has considered five different ground motion intensity levels, associated to exceedance probability of 2, 5, 10, 20, 50% -in-50-years (i.e. 2475, 975, 465, 224, 72 years return period). Seismic intensities adopted for these analyses come from PSHA, and have been indicated in §3.6.1 and §3.6.2.

The NTH with the nonlinear models described in previous sections was performed for the entire suits of selected ground motions (see selection procedure §3.6) scaled to the intensity levels of the 5 mentioned TR (see Table 3-10 and Table 3-12)

Results of NTH are summarized in terms of maximum transient and residual drifts as well as drift profiles. In particular, Fig. 3.35 shows the probabilistic representation of maximum interstorey drift profiles for each return period considered in this study for the American building. For each return period and input ground motion, the maximum interstorey drift through the whole structure was monitored along with interstorey drift profile associated with that maximum drift. Fig. 3.35 only considers profile corresponding to the maximum interstorey drift recorded through the analysis. As expected, maximum interstorey drift increases with increasing ground motion intensities, while the dispersion, represented by the 16th and 84th percentiles, does not vary significantly. Interstorey drift demand is manly concentrated in first two storeys. For the return period of 2475 years, for which collapse did not occur only for 4 ground motions, the interstorey drift demand is concentrated in first storey.

The same representation of interstorey drift profile is reported in Fig. 3.47 for the Italian building. Interstorey drift increases with increasing ground motion intensities, but in this case, also dispersion increases. Due to smaller seismic intensities the Italian building has been subjected during analyses, maximum interstorey drifts are about one-half than that shown in the American case study.

Demand to capacity ratio for the Italian building is less demanding compared to the case of American building; in fact, even considering the return period of 2475 years (with maximum Sa=0.56g) the seismic demand on the building represent a condition far from collapse. In fact, median collapse spectral acceleration is 0.825g, as it will be explained in the next paragraph. on the other hand, a change in nonlinear mechanism is

observed,; in fact for smaller intensities interstorey drifts are concentrated between 2nd and 5th storeys with maximum deformation demand between 3rd and 5th story, but for the maximum intensity considered the drift profile changes and maximum demand displaces to upper storeys.
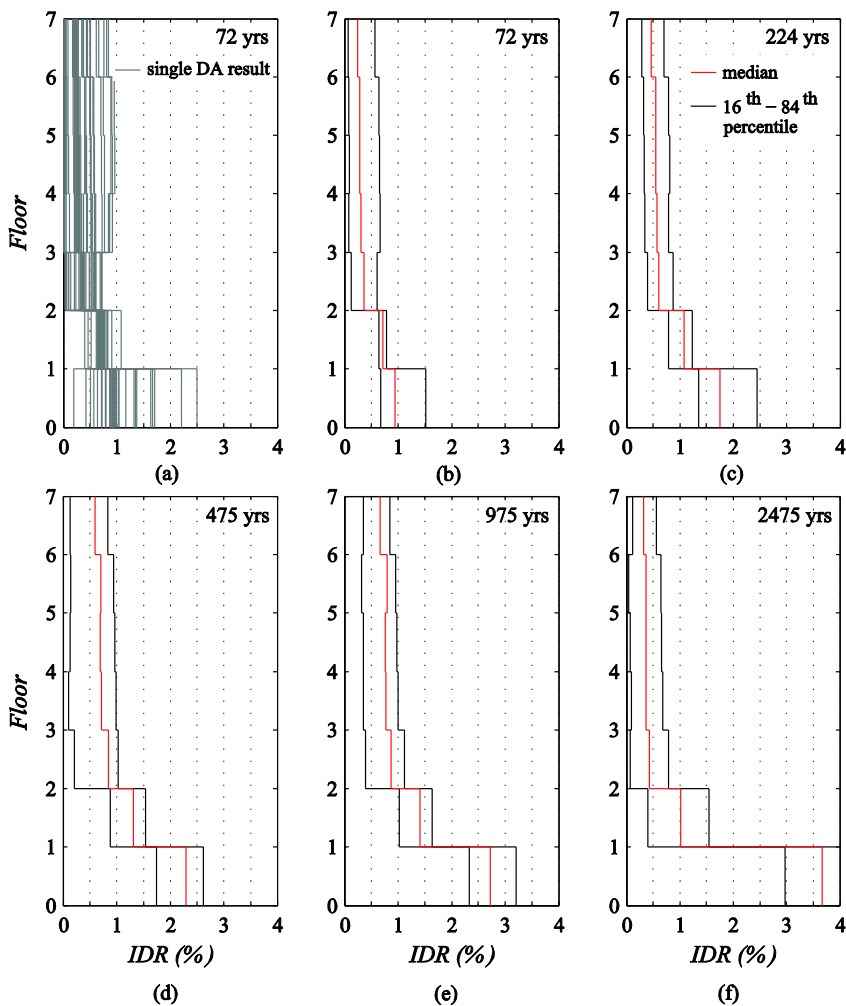
Fig. 3.35 (a) Maximum transient interstorey drift ratio profile for 31 earthquakes adopted in this study and a return period of 72 years; maximum interstorey drift ratio median and 16th and 84th percentiles for different return periods: (b) 72 years, (c) 224 years, (d) 475 years, (e) 975 years, (f) 2475 years (American case-study).

Fig. 3.37 (a) shows maximum transient interstorey drift ratio (IDR_{max}) obtained from NTH analysis for several input ground motions and for different return periods. Maximum IDRs increase with the increasing of seismic demand in a less than linear way, while dispersion of data is almost constant.
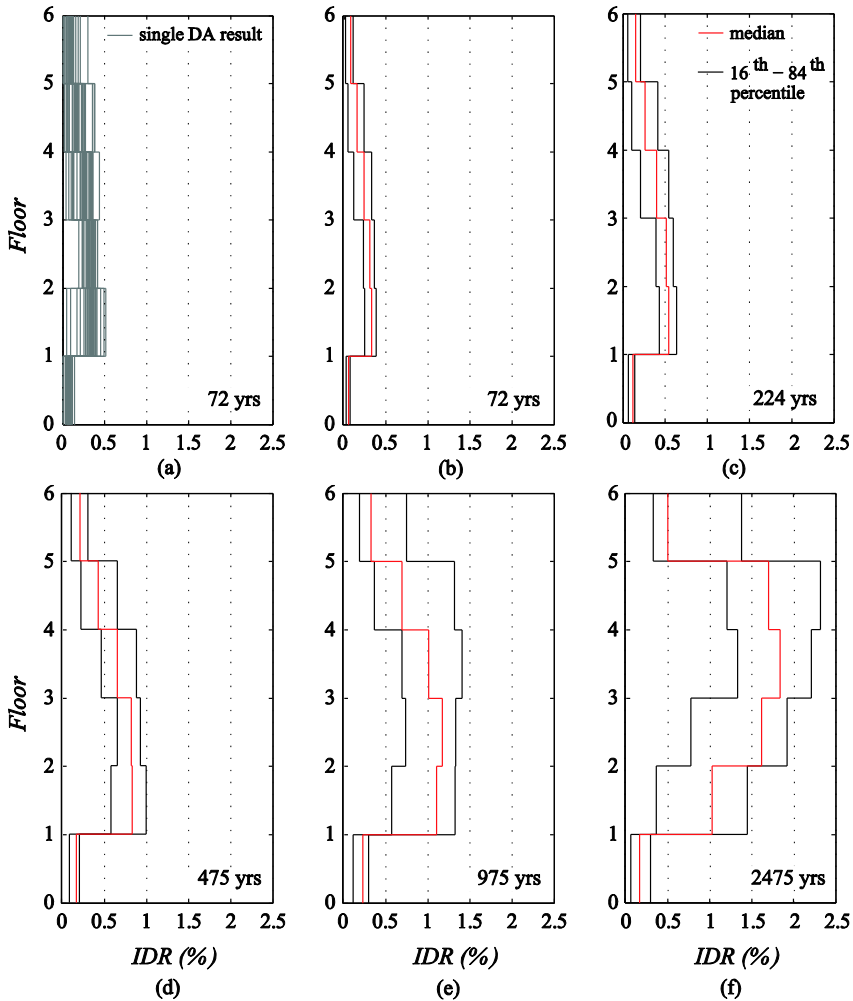
Fig. 3.36 (a) Maximum transient interstorey drift ratio profile for 31 earthquakes adopted in this study and a return period of 72 years; maximum interstorey drift ratio median and 16th and 84th percentiles for different return periods: (b) 72 years, (c) 224 years, (d) 475 years, (e) 975 years, (f) 2475 years (Italian case-study).

Note that the sample used decreases with the increasing of seismic action, for instance for the 2475 years return period only four ground motions did not lead to collapse as can be noted in Fig. 3.37 (a). Fig. 3.37 (b) shows statistical representation of maximum transient interstorey drift ratios through the adoption of fragility curves that give the likelihood that the structure will reach or exceed a specific level of maximum transient IDR conditioned on a given return period. Fragility curves are reported only up to a return period of 975 years because for T_R=2475 years the statistical sample is composed by only four analyses. Fig. 3.38(a) shows maximum residual interstorey drift ratio (IDR_{res}) obtained for several input ground motions and for different return periods considered in this study. Note that for representation purposes, two results are excluded

from the figure corresponding to IDR_{res} of 0.92% and 2.61% and for 224 and 2475 years, respectively. In this case, residual IDRs show a higher dispersion for smaller return period, and a clear trend is not apparent.
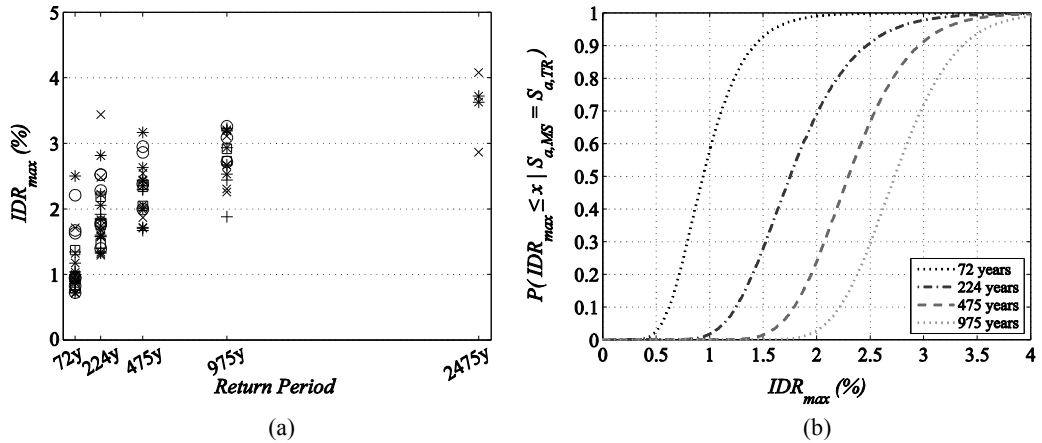
Fig. 3.37 Maximum transient interstorey drift ratios (IDR_{max}) for different return periods: (a) analytical results, (b) fragility curve (American case-study).
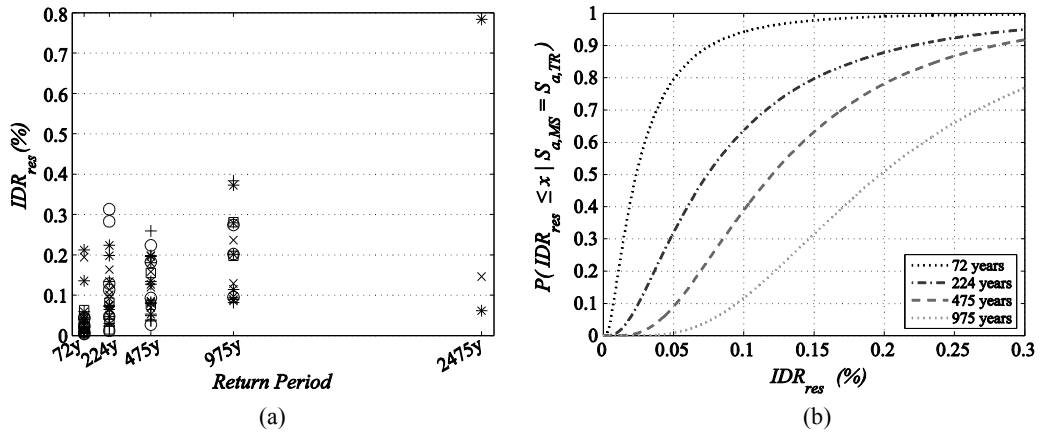
Fig. 3.38 Maximum residual interstorey drift ratios (IDR_{max}) for different return periods: (a) analytical results, (b) fragility curve (American case-study).

The fragilities obtained for IDR_{res}, Fig. 3.38(b), show this great dispersion for 72 and 224 years return periods, while a smaller dispersion occurs for 475 and 975 year return periods. Statistical parameters from lognormal fitting of fragility curves are reported in Table 3-13 for both IDR_{max} and IDR_{res}. Parameters from fragility curves conditioned on 2475 years return period are also included in the Table even if lacking of effectiveness due to the small size of the sample.

Return Period (yrs)		72	224	475	975	2475
IDR_{max}	median (%)	0.94	1.75	2.30	2.73	3.67
	β	0.36	0.30	0.20	0.16	0.15
IDR_{res}	median (%)	0.02	0.07	0.12	0.20	0.46
	β	0.99	0.91	0.68	0.57	1.73

Table 3-13 Median and logarithmic standard deviation (β) of IDR_{max} and IDR_{res} fragilities for different return periods (American case study)

Fig. 3.39(a) shows IDR_{max} recorded during the NTH analysis for the Italian building. In this case a clear trend is visible such in for the American case-study. By comparing IDR_{max} for two case study buildings, Fig. 3.37(a) and Fig. 3.39(a), it is clear that for the same return period, building's response for the Italian building is almost one-half than that obtained for the American building. This is mainly due to the hazard at the site that is quite different for two cases (e.g. for 2475 years S_a is equal to 1.06g for the American site while it is only 0.56g for the Italian site). The differences in the hazard at site reflects on the building's response in terms of EDPs and in particular in terms of number of collapses cases detected for each return period. In fact, for any return period up to 975 years, in the Italian building global collapse was not detected, while for 2475 years return period only two ground motions led to collapse. For the American building, instead, 3, 8, 16 and 27 ground motion records over the 31 record set led to collapse for 224, 475, 975, 2475 year return period, respectively.

Fig. 3.40(b) shows IDR_{max} fragilities for the five return period level considered in this study for the Italian building. From the figure and Table 3-14, where median and logarithmic dispersion for lognormal fragility fitting are reported, it is clear that for increasing seismic demands, also response of the building increases along with the dispersion in results.

(a)   (b)
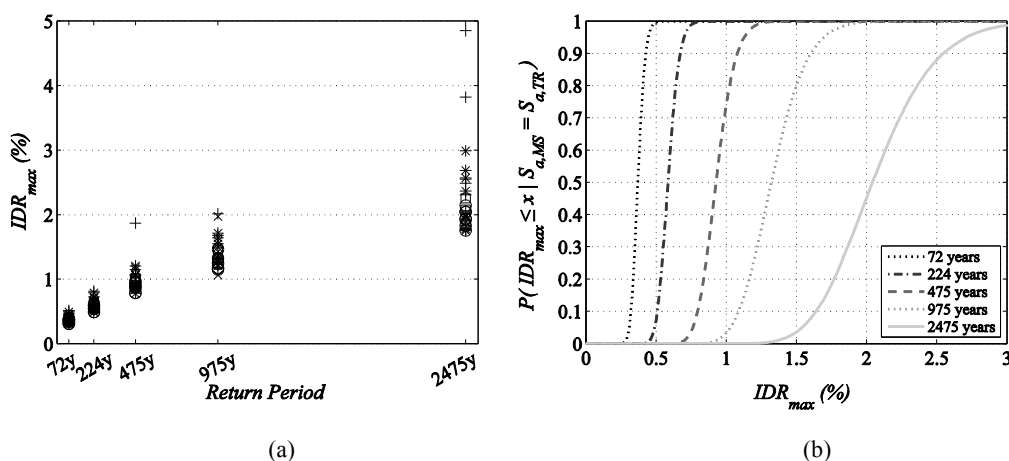
Fig. 3.39 Maximum transient interstorey drift ratios (IDR_{max}) for different return periods: (a) analytical results, (b) fragility curve (Italian case-study).

Fig. 3.40(a) depicts IDR_{res} results from simulation for five return period ground motion levels, note that for 2475 years return period one value corresponding to 3.4% have been excluded for representation purposes.

(a)   (b)
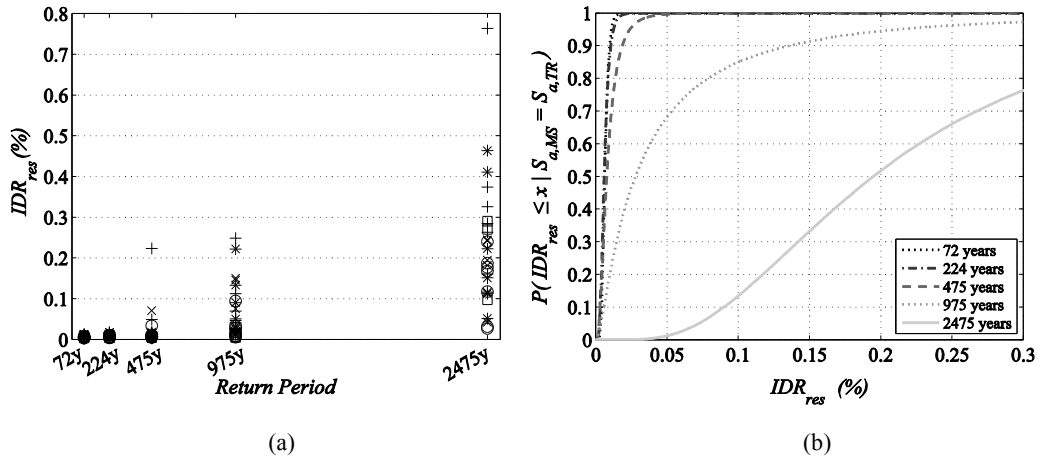
Fig. 3.40 Maximum residual interstorey drift ratios (IDR_{res}) for different return periods: (a) analytical results, (b) fragility curve (Italian case-study).

Differently from Fig. 3.38(a), where results for the correspondent American building are reported, dispersion in results is very small for return periods lower than 475 years (see Table 3-14). This result is obvious when considering the different intensities of ground motions for two different hazards at the site that are significant lower for the Italian site. For instance, for the 72 years return period level, the Italian structure is almost into the elastic range while the American one already shows significant nonlinear response. Fig. 3.40(a) depicts fragility curves for IDR_{res} response of the Italian building. From the figure it can be observed that for 72 and 224 years return period level, and also for 475 years, the residual IDR, that can be interpreted as a measure of structural damage, or inelastic demand, is very small while it significantly increases for higher return periods whenever significantly smaller than that for the American case-study building.

Return Period (yrs)		72	224	475	975	2475
IDR_{max}	median (%)	0.37	0.59	0.93	1.32	2.04
	β	0.12	0.12	0.12	0.15	0.17
IDR_{res}	median (%)	0.01	0.01	0.01	0.03	0.19
	β	0.38	0.46	0.69	1.24	0.60

Table 3-14 Median and logarithmic standard deviation (β) of IDR_{max} and IDR_{res} fragilities for different return periods (Italian case study)

Other remarkable observation concern the variation in the fundamental vibration period (T_1), which is strictly related to the global damage (Di Pasquale et al., 1990). The median variation of the fundamental vibration period with respect to the one for intact

building varies with the return period of damaging earthquake as can be seen in Fig. 3.41 for two case studies where dots represent single results from NTH and cruciform markers connected by a black line the median value for the specific return period.

For the American case-study periods vary in a less than linear way, from a minimum of 0.5% for 72 years return period up to 21.1% for the 2475 years return period, while for the Italian building this variation is almost linear and vary from a minimum of 1.0% for 72 years return period up to 16.3% for 2475 years. Although the intensities of seismic action are quite different for the same return period, for higher return period lead to similar variation of the fundamental vibration period.
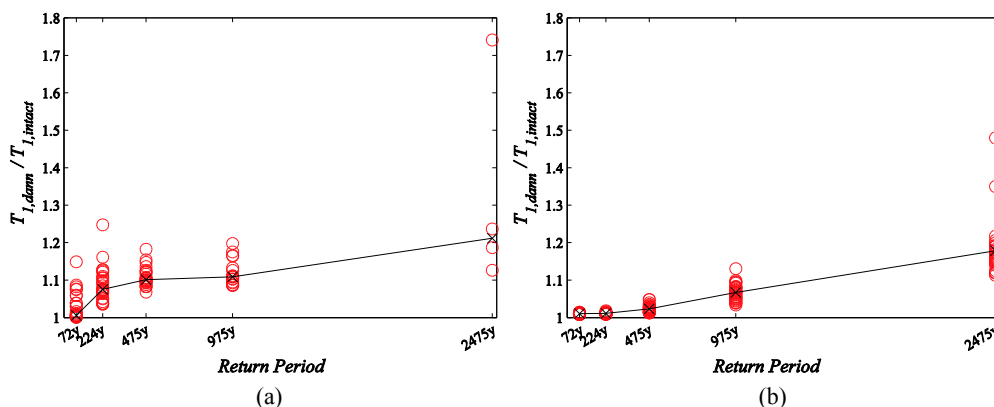
Fig. 3.41 Variation of fundamental vibration period as a function of return period of the damaging earthquake: for (a) the American and (b) the Italian building

3.7.1 EFFECT OF THE JOINT MODEL FOR THE ITALIAN CASE-STUDY

The Italian building model is the same adopted for the American one, except for the joint model. In fact, for the Italian building the Joint model from Jeon et al. (2015) was considered, as explained in §3.2.3.3, while the joints in the American building are modeled with Hassan (2011), see §3.2.3.2. This choice mainly depends on the essential differences existing in the construction technologies between two countries. However, results in building response of the Italian case study are not significantly affected by the model of joints adopted as can be deduced from interstorey drift ratios depicted in Fig. 3.42, independently from the intensity of the seismic action on the structure. When the model by Hassan (2011) is assumed to reproduce joint behavior, the first model period increases up to 1.12 seconds, while second and third vibration periods are 0.36 sec and 0.21sec, respectively. Fig. 3.42(a) shows IDR_{max} fragilities for Italian case study with two different joint models. The maximum response is very similar when two joint models are adopted. Greater differences can be observed in terms of residual response, as evidenced in Fig. 3.42(b), showing the IDR_{res} fragilities.
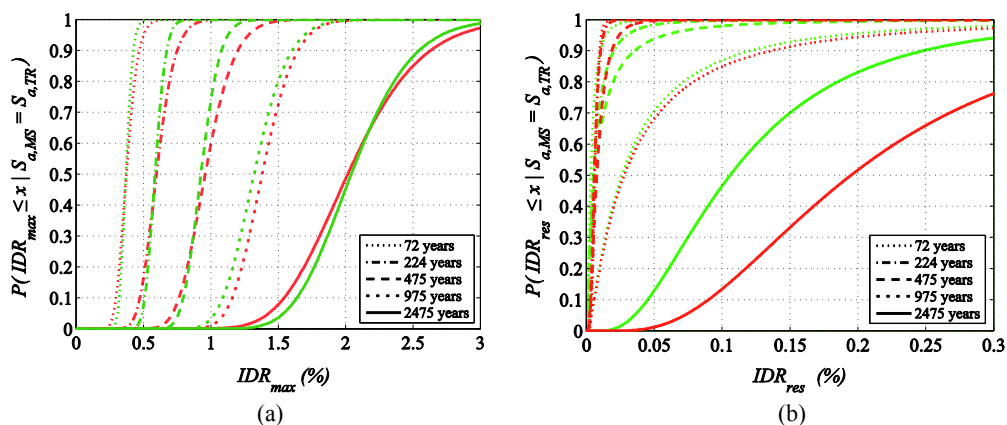
Fig. 3.42 Fragility curves for Italian building with joint model by Hassan (2011), red curves, and by Jeon (2015), green curves, for (a) maximum transient drift ratio (IDR_{max}) and (b) residual drift ratio (IDR_{res})

While for lower intensities, the response is very similar, for the intensity corresponding to 2475 years return period the residual deformations are quite different. In particular, for this specific return period, the model by Hassan leads to greater residual IDRs although for the same earthquake joint damage is greater for the model by Jeon. This peculiarity is due to the damage mechanism in the structure, in fact, the concentration of damage in joints when using Jeon model prevents the development of brittle mechanism in columns and excessive plastic demand in beams that mostly contribute to the global residual IDR.

The effect of different modeling choices in beam-column joints can also be showed through the differences in pushover response. Fig. 3.44 shows pushover curve for different load patterns and different beam-column joint models including the case in which joints are considered to be rigid. Adopting different joint model for the Italian building, results from pushover analysis show that the model by Jeon et al. (2015) leads to an increased initial stiffness when compared to that when the structure adopts stress-strain relationship by Hassan (2011).

The adoption of the analytical model by Jeon et al.(2015), instead, significantly increases the drift demand for the linear load pattern and for both linear and uniform load patterns it also reduces the maximum shear force due to the spread of the damage into joints. The analytical frame model that account for joints and column brittle behavior is the most vulnerable with respect to model that does not consider joint contribution, because it has a sudden drop of lateral load resistance in pushover analysis. However, it is observed that concentrated inelastic action in joints delays the inelastic shear response in columns when compared to the model that account for the sole column brittle failure.
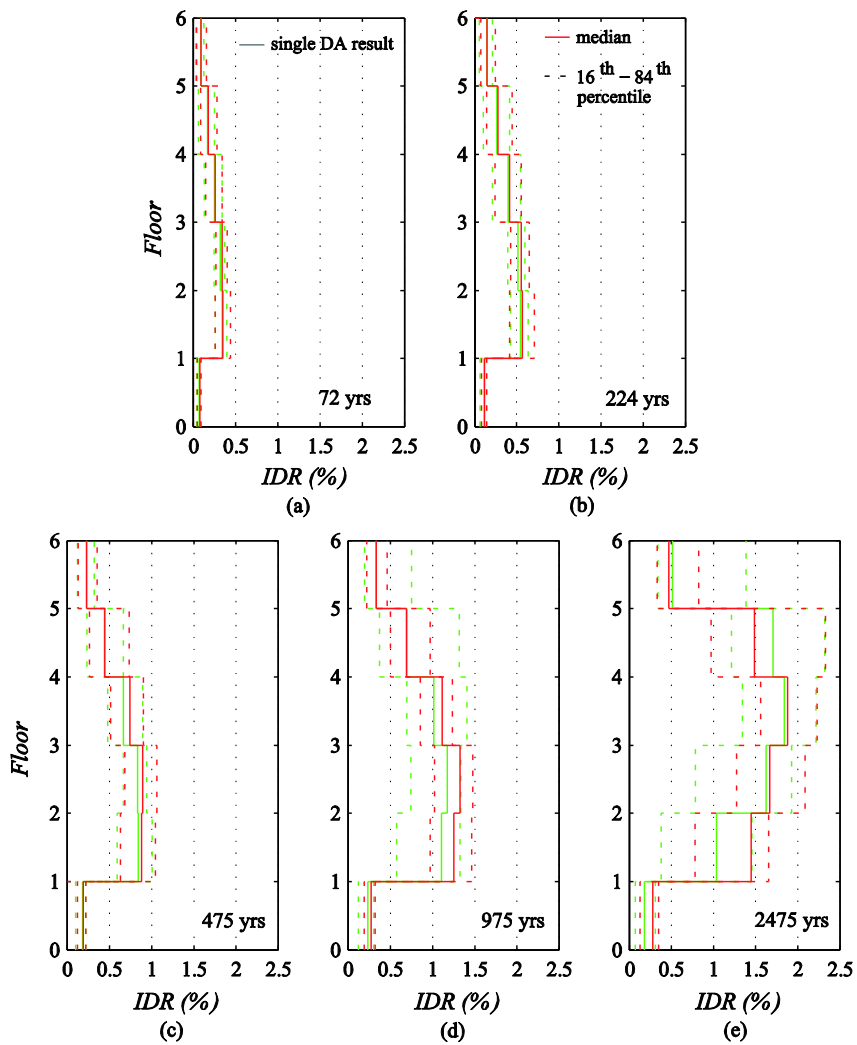
Fig. 3.43 Maximum transient drift ratio (IDR_{max}) for Italian building with joint model by Hassan (2011), red curves, and by Jeon et al. (2015), green curves, for (a) 72, (b) 224, (c) 475, (d) 975, (e) 2475 years return period
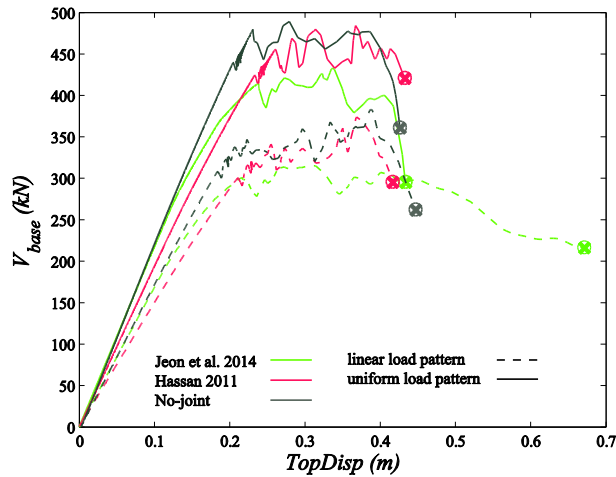
Fig. 3.44 Pushover curve, continuous line for uniform and dotted for linear load pattern, for the Italian building adopting different beam-column joint models: red for Jeon et al. (2015), green for Hassan (2011) and gray for rigid nodes.

3.8 BUILDING'S SEISMIC CAPACITY ASSESSMENT

In the Performance-Based Earthquake Engineering (PBEE) an accurate estimation of the seismic performance of structures (e.g., the mean annual frequency of exceeding a specified structural demand or a certain limit-state capacity) takes on a great interest. To accomplish this task, several important methods have emerged. One of these is the Incremental Dynamic Analysis (IDA), Vamvatsikos and Cornell (2002), a computer-intensive procedure that offers thorough prediction capability and involves performing nonlinear time history analyses (NTH) of the structural model under a suite of ground motion records, each scaled to several intensity levels up to the reaching of structural collapse. In particular, a recorded ground motion is selected, applied to the nonlinear analysis model of the structure, and structural time-history response is computed. Once this analysis is completed, the ground motion record is multiplied by a scale factor, and the simulation model is analyzed again. The ground motion is then scaled to increasing intensity, repeating the dynamic analysis until the structural collapse. Here the Global Collapse defined in §3.2.4 has been adopted. Due to differences in frequency content, duration and other characteristics, different ground motion records do not give the same response, even when they are scaled to the same intensity. Therefore, the collapse prediction must be repeated for a suite of ground motion records, in order to capture record-to-record variability in the response. The outcome of this assessment is a prediction of the probability the structure collapses, as a function of ground motion intensity.

Once the structural model has been built and the ground motion records have been selected, an efficient algorithm is necessary to fast and automatically perform NTH required for the IDA. This entails appropriately scaling each record to cover the entire range of structural response, from elasticity, to yielding, and finally global collapse. In this study, a bisection algorithm has been chosen to trace the IDA curves of the studied building. Although there do exist better algorithms to identify the collapse IM-level, like the hunt & fill (Vamvatsikos and Cornell 2004), the used algorithm has to be found efficient and easy to implement for the specific study.

Various scalar intensity measures have been proposed in the past, one of the most used IMs is PGA, although PGA is generally perceived to be a poor predictor of the structural response of mid-to-high-rise moment-resisting frames. Another widely used IM is the spectral acceleration at the fundamental period (T_1) of the structure, referred to a specific critical damping ratio, $S_a(T_1,5\%)$. S_a also takes into account the ground motion frequency content around the structure's first-mode period and Shome et al. (1998) demonstrated that S_a is a good predictor of the structural response for moment-resisting frames of low to moderate fundamental period. In this work, the IM chosen to be representative of the earthquake intensity is the $S_a(T_1,5\%)$. Hence, in $S_a(T_1,5\%)$ terms, the algorithm was configured to use an initial step of 0.2g while a maximum of 20 runs was allowed for each record. A default resolution of 0.025 g on the global collapse capacity, has been selected.

3.9   SEISMIC PERFORMANCE: INTACT BUILDINGS

In this paragraph, the model of structure proposed in §3.2 is analyzed in its intact state in order to estimate its original performance in terms of capacity. The IDA procedure has been here adopted to compute the structure capacity to withstand to future earthquakes. The capacity here corresponds to the capacity leading to collapse, as defined in §3.2.4, and it has been estimated in terms of $S_a(T_1)$ with a precision of ±0.05g.

Collapse fragility

The correct assessment of structural safety, along with a realistic estimation of repair costs, is one of the main concerning topics of modern structural engineering in terms of seismic performance. The knowledge of building's initial performance and its variation due to earthquake damage has been extensively used to set building tagging criteria and in this work, it is used as a complement to seismic losses to lead through reparability decisions. Consequently, it is necessary to define the probability of incurring structural collapse as a function of ground motion intensity. This is represented in the form of collapse fragility function, which is a relationship that defines the probability of incurring structural collapse as a function of ground motion intensity.

Fragility function definition:

Fragility functions are statistical distributions used to specify the probability of collapse, or some other limit state of interest, of a system as a function of some ground motion intensity measure, IM. Typically, fagility functions can be represented as lognormal cumulative distribution functions, having a median value, θ, and logarithmic standard deviation, or dispersion, β. The mathematical form for such a fragility function is:

$$P(C \mid IM \le x) = \Phi\left(\frac{\ln(x/\theta)}{\beta}\right)$$ Eq. 3-14

where P(C | IM ≤ x) is the probability that a ground motion with IM ≤ x will cause the structure to collapse, $\Phi( )$ is the standard normal cumulative distribution function (CDF), θ is the median of the fragility function and β is the standard deviation of ln(IM). Equation Eq. 3-14 implies that the IM values of ground motions causing collapse of a given structure are log-normally distributed; this common assumption has been confirmed as reasonable in a number of cases (e.g., Ibarra and Krawinkler 2005; Eads et al. 2013).

Fragility functions can be derived using a variety of approaches such as field observations of damage, static structural analyses, or judgment (e.g., Calvi et al. 2006, Porter et al. 2007). Analytical fragility functions developed from dynamic structural analysis due to a deepened knowledge of material an structural behavior, improved modeling features for both structural components and systems, and thanks to the development of more reliable analysis tools and the enhanced power of new generation of personal computers, the analytical fragility curves represent a sustainable and often preferable alternative to empirical ones (Polese et al., 2008) .

There are a number of procedures for performing nonlinear dynamic structural analyses to collect the data for estimating a fragility function (Baker, 2014), e.g., Incremental Dynamic Analysis, Multiple Stripe Analysis (Jalayer and Cornell, 2009). In this chapter, the IDA procedure for establishing building-specific collapse fragility functions has been adopted.

Incremental dynamic analysis involves scaling each ground motion in a suite until it causes collapse of the structure (Vamvatsikos and Cornell, 2002). This process produces a set of IM values associated with the onset of collapse for each ground motion, as illustrated in Fig. 3.45. The probability of collapse for IM = x can be estimated as the fraction of records for which collapse occurs at a level lower than x.
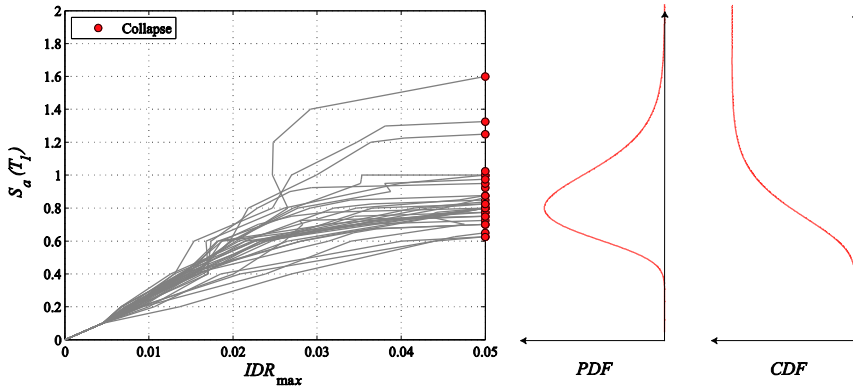
Fig. 3.45 a) Incremental dynamic analyses results for Italian building, used to identify IM values associated with collapse for each ground motion. b) Probability and c) Cumulative Distribution Functions of collapse as a function of $IM=S_a(T_1)$.

3.9.1 BUILDING INTACT CAPACITY

Fig. 3.45 and Fig. 3.46 show outcomes from incremental dynamic analyses (IDAs) for both the American and the Italian building, respectively. Here the IM adopted to estimate collapse capacity corresponds to the spectral acceleration at the fundamental period of undamaged building (T_1) for a 5% damped system, while the EDP recorded for the structure is the maximum interstorey drift (IDR_{max}), through the structure. In the part (a) of figures, the black dotted line shows IDA results for single input ground motion and the black empty dot represent the collapse capacity, the red bold line represent the median response from all records while the red filled dot represent the median collapse capacity. Part (b) shows the collapse fragility for the intact buildings, and $S_{a,MS}^C$ indicates the Mainshock spectral acceleration intensity leading to collapse. In this study, collapse has been detected considering two possible global collapse mechanism: Gravity load and Sidesway collapse, as described in §2.4.

Results of Incremental Dynamic Analyses for the American building are depicted in Fig. 3.46, where (a) clearly show the dispersion due to record-to record variability. From Fig. 3.46(a) it can be argued that for the American building the response dispersion due to RTR variability is larger than that for the Italian building (Fig. 3.47(a)) where only some spectral acceleration capacities are greater than 1.2g and the most fall into the interval 0,6-1,0g. This increased dispersion is reflected by the β value for two cases (see Fig. 3.46(b) and Fig. 3.47(b)): while for the American, the median capacity is 0.82g and the β is 0.27, for the Italian one $S_{a,MS}^C$ slightly increases to 0.85g while dispersion decreases to 0.21.
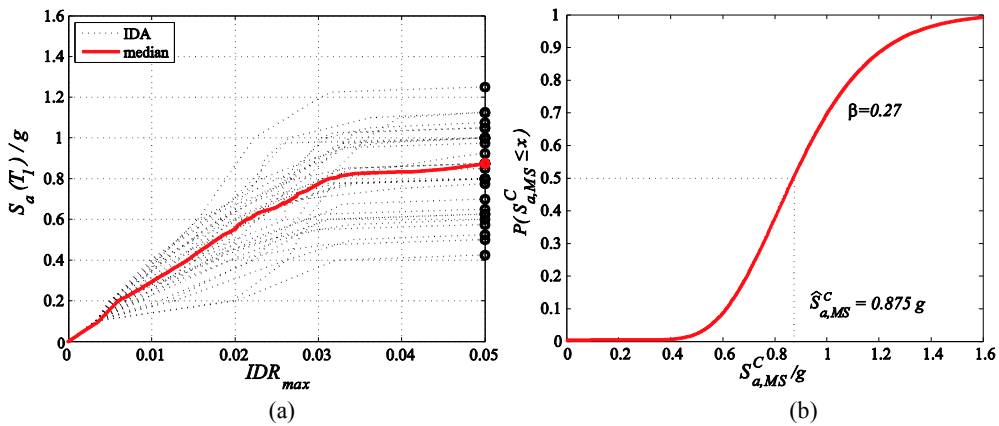
Fig. 3.46 a) Incremental dynamic analysis for intact building b) Collapse fragility for intact building (American)
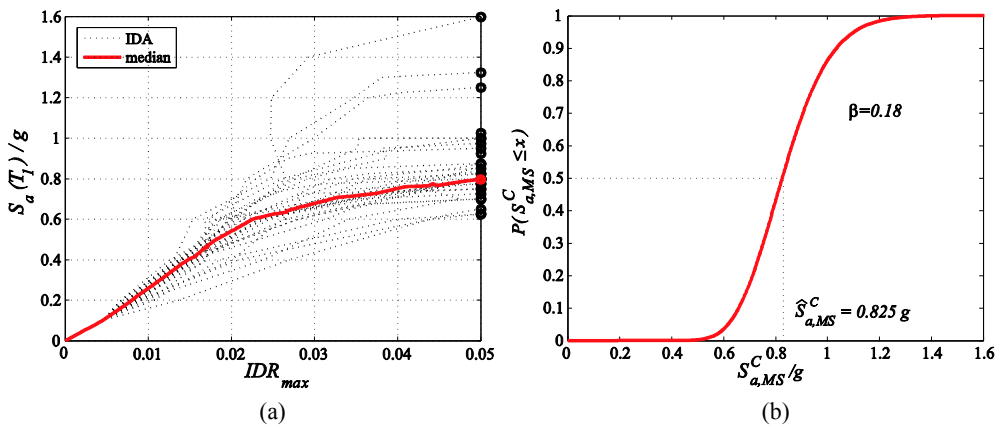
Fig. 3.47 (a) Incremental dynamic analysis for intact building (b) Collapse fragility for intact building (Italian)

It is worthy to note that in the majority of cases, as it will be highlighted in following chapter (§3.9.2), the collapse of American building is due to soft-storey collapse mechanism in first or seventh story, so the dispersion for the American building is ascribable to the variation in collapse mechanism that can lead to collapse in a different story.

Finally, it is worthy to note that, considering different joint behavior simulation models, besides to having about the same response for different intensities of the seismic action, as demonstrated in §3.7.1, the ultimate median capacity in terms of spectral acceleration is very similar, as can be noted from Fig. 3.50.
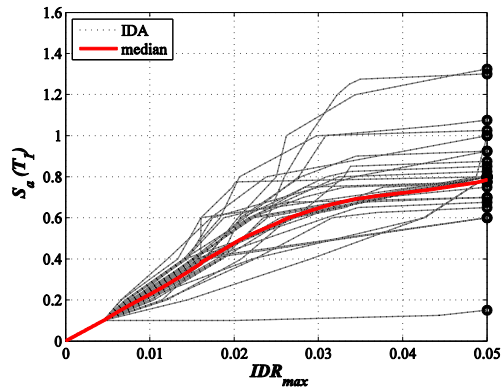
Fig. 3.48 Incremental dynamic analysis for intact building adopting the model by Hassan (2011)

3.9.2 NONLINEAR DYNAMIC COLLAPSE MECHANISM

American Case-study

Fig. 3.49 shows the various collapse mechanisms predicted by nonlinear dynamic analyses (for legend explanation see Fig. 3.24). As shown in the figure, for the 31 ground motions it is possible to identify four different failure modes, depending on the ground motion record. Note that both the static pushover analyses produce collapse mode (a). Although collapse modes can be grouped in four different types, they can be slightly different from each other depending on ground motion, for this reason in the figure these collapse modes are referred to the specific input ground motion used when performing the damage analysis. For instance, collapse mode (a) leads to Gravity Load Collapse due to axial failure of all internal columns in the first story, while other ground motions can produce the same spreading of the damage through the structure, but the collapse is due to Sidesway mechanism in first story or axial failure of only some of internal columns. In every case, independently on the collapse mechanism, collapse can occur due to Sidesway or Gravity loads. As evidenced by Fig. 3.49, in 93.5% of cases, collapse can be attributed to soft-story mechanism in first floor, but for the 6.5% of cases global mechanism occurs in the two last floors.

Collapse mode identified by static pushover analysis is the more likely, and occurs in about 61% of the dynamic analyses. This mode involves all first floor columns that experienced severe damage (shear or axial failure) and almost 50% of internal joint reached concrete cracking. Collapse mechanism (b) occurs in 29% of cases; it is quite similar to the (a) but while the extension of damage for former mechanism is concentrated in first three floors, the damage for the latter mechanism is spread through the whole frame involving the most part of internal joints and leading to concrete spalling also for upper floor columns. Collapse type (c) occurs in only 3.5% of cases and leads

to first story mechanism, but also shows an incipient collapse in the upper floor. The collapse mechanism (d) occurs in 6.5% of cases involving last two floors which columns are subjected to severe damage, while most of fifth floor columns reached rebar yielding or concrete spalling.

(a) CAP000

(b) H-E02140

(c) CHY006-W

(d) A-DEL000
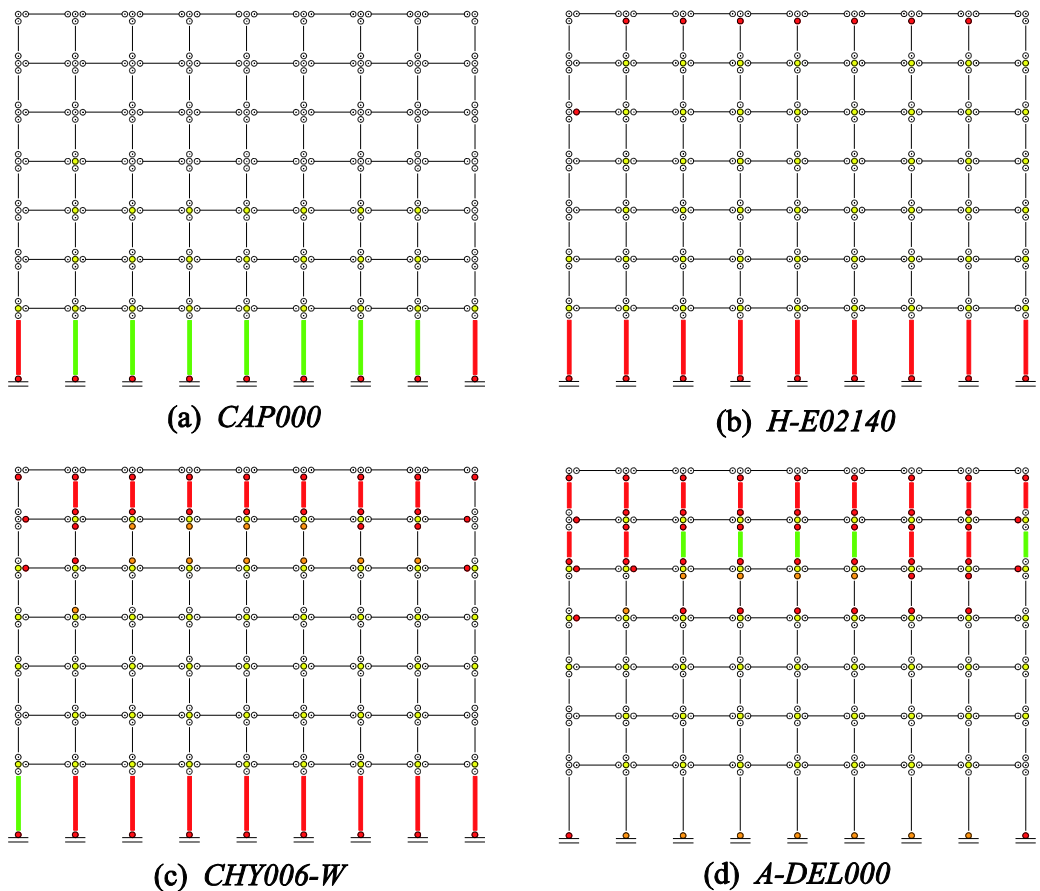
Fig. 3.49 Diagrams showing dynamic collapse modes for the American building

Italian Case-study

Fig. 3.50 shows the various collapse mechanism predicted by nonlinear analyses for the Italian case-study building. As shown in the figure, it is possible to identify six different failure modes, depending on the ground motion record. Note that the linear static analysis with inverted triangular loading pattern leads to a mechanism similar to (b), while the mass-proportional loading pattern leads to the mechanism (c). However, except than for one case, collapse mechanism does not leads to complete joint failure (i.e., reaches joint

residual capacity), despite that, Fig. 3.50 shows more significant joint demands with respect to the American building.
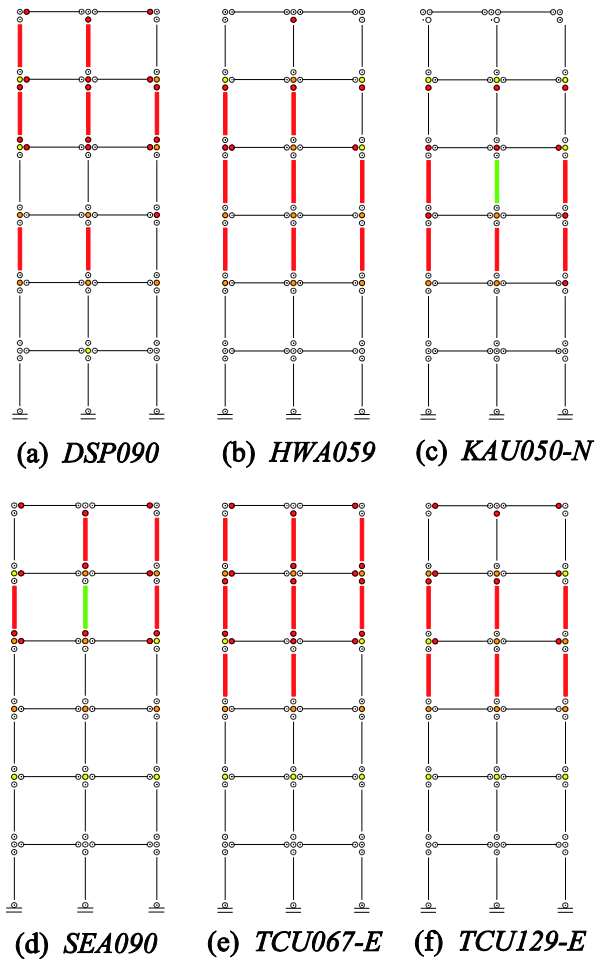
Fig. 3.50 Diagrams showing dynamic collapse modes for the Italian building

Differently from what observed in the American building, collapse mechanism can significantly differ from each other, entailing large inelastic demand in one or more storeys. Collapse mechanism (a) occurs for only 6,5% of the analyses, it involves both third and upper storeys, beams in last two storeys experienced concrete spalling and several joints experienced cracking or reached maximum resistence. Collapse mechanism (b) occurs in 13% of cases, it involves three intermediate storeys and corresponding joints. Collapse mode (c) occurs for the 6.5% of cases and involves 3rd and 4th storey with high joint inelastic demand. Mode of collapse (d) is the more likely to occur, 29% of cases. It involves last two storeys. Collapse mode (e) occurs in 3% of

cases and involves last three storeys columns and joint. Finally, collapse mode (f) is the also likely to occur developing for the 14% of cases. It involves last two storey in the collapse mechanism and produces severe joint damage in the same storeys.

3.10   SEISMIC PERFORMANCE: TR-DAMAGED BUILDINGS

This paragraph outlines the framework that has been adopted for the assessment of seismic performance of damaged building, when only the intensity of the damaging earthquake is known.

3.10.1   POST-EARTHQUAKE ASSESSMENT

To assess the post-earthquake collapse risk of structures through assembling of Mainshock-Aftershock sequences, the definition of Mainshock intensity is necessary. Two possible approaches can be followed: 1) The first requires to simulate the damage caused by damaging earthquake by scaling the mainshock intensity in order to achieve a pre-defined state of damage (e.g., the mainshock is scaled to an intensity able to cause rebar yielding in more than 50% of structure members); 2) The second is to scale the mainshock to an intensity corresponding to a given probability of exceedance in a specified period (i.e., corresponding to a specific return period).

1) When first approach is adopted, it is firstly necessary to define a set of global limit states based upon a given damage phenomenology, then, the damage state have to be simulated before to assess the mainshock-damaged capacity. In this case, two approaches may be adopted; the first require the generation of mainshock-damaged structure simulating the damage caused by a damaging earthquake; the second require generating the damaging sequence simulating the sequence mainshock-aftershock. These approaches are usually referred as: a) "Back-to-back" IDA approach (B2B-IDA) and b) Cyclic Pushover approach (CPO), respectively. Both approaches enable the simulation of the damaging earthquakes to cause the specified initial damage states, generally quantitatively related to interstorey drift of the frames. For instance, Raghunandan et al. (2012) quantified four different damage states based upon distinct physical behavior and determined corresponding drift thresholds performing a nonlinear static pushover analysis on the analytical case-study model. They also noted from results of dynamic analyses performed to reach the same damage state, that depending on the characteristics of the ground motions, the physical damage states may not occur at the same interstory drift ratios as in the pushover analysis. However, the authors observed that thresholds identified in pushover analysis are very close to the median observed in dynamic analysis results. Other authors (e.g., Abad et al. 2013) adopted drift thresholds from observational data and independent from the specific studied structure.

The B2B-IDA is capable of capture the dynamic characteristics of the damage by adopting real ground motions as mainshock to achieve a given damage state. However, this procedure is often avoided because of its complexity. Firstly, the B2B-IDA requires many efforts to set the mainshock intensity able to produce the desired damage state on the structure, in fact, due to differences in frequency content, duration and other ground motion characteristics, each ground motion have to be scaled to a different intensity before a particular damage state occurs. Furthermore, this procedure is computationally intensive due to the necessity of accounting for the effect of record-to-record variability on structural response, which requires the B2B-IDA to be performed considering every possible Mainshock-Aftershock combination (as will be better explained in §3.10).

The CPO, instead, has the main advantage of reducing the computational intensity by applying a "*hypothetical*" ground motion rather than a real one for the mainshock, because it is simulated through a reverse pushover analysis. Following this procedure it is not necessary to define the scaling factor of the mainshock because it is substituted by the CPO analysis and the computational effort is significantly reduced because the record-to-record variability of the mainshock is implicitly included in the pushover and only the aftershock has to be varied during the assessment. The CPO approach requires the assumption of a pushover load pattern and constant residual deformations. For instance Jeon et al. (2012), adopted a linear load shape and defined a specific pushover pattern consisting into gradually increasing loading up to the specific drift threshold associated with an initial damage states and decreases symmetrically until the base shear is zero.

2) When the second approach is adopted, it is only necessary to define the intensity at which scale the Mainshock performing a deaggregation analysis for the specific return period and the studied structure. This approach has the advantage that its outcomes can be used to forecast the probability of collapse and its variation applying the PBEE procedure, furthermore, performing the loss analyses considering the same return periods, the repair cost can be linked to the safety variation supplying a consistent tool to the definition of reparability limits. The results are obviously associated to the specific building and site, moreover the Mainshock intensity is not defined based on structural damage and for each return period, damage variation can be considered an aleatory variable implicitly accounted for.

3.10.2 TR-DEPENDENT AFTERSHOCK FRAGILITY FRAMEWORK

Seismic behavior of damaged buildings, and their relative seismic safety, may be suitably represented by their seismic capacity modified due to damage, the so-called REsidual Capacity (REC). Indeed, in the guidelines for seismic assessment of damaged buildings (Bazzurro et al., 2004), the building tagging is based on the likelihood that an aftershock will exceed a specific (reduced) capacity associated with each damage state

representing the quantitative measure of degradation. In Polese et al. (2013a) REC is defined as a parameter aimed at representing the building seismic capacity (up to collapse) in terms of a spectral quantity; in particular, $REC S_a$ of a building is defined as the smallest ground motion spectral acceleration (at period T_{eq}, of the Single Degree Of Freedom SDOF system equivalent to the real structure) corresponding to collapse state of the building. Considering the seismic demand and the local damage that the elements in a Multi Degree of Freedom (MDOF) system may be forced to sustain due to a mainshock earthquake, the system's capacity may be considerably reduced, as evidenced in Polese et al. (2013a).

Residual Capacity for building damaged by earthquakes of known intensity has been assessed through a dynamic procedure. Fig. 3.54 illustrates a schematic view of the framework for the dynamic computation of Residual capacity of damaged building, and the associated Performance Loss. The framework is composed of several moduli. After having identified the case-study building, first module entails its elastic and nonlinear structural modeling as well as the assessment of building dynamic properties, such as the fundamental vibration period. This first aspect has been addressed in a general way in Chapter 2 and for the specific case-studies in §3.2. Once the properties of the system are calculated, the knowledge of the geographical position of the building and the soil characteristics at the site, allows to perform a Probabilistic Seismic Hazard Analysis (§3.5) (module 2), PSHA, the results of which can be used in order to select an appropriate bin of natural ground motions to perform dynamic analyses (§3.6.1, §3.6.2). Further, PSHA allows the computation of earthquake intensities at the site with a given probability of exceedance in a time window (or representative of a given return period). In this study a bin of 31 natural accelerograms was selected to assess the capacity of the intact structure and the Residual Capacity after damage. With the selected bin of accelerograms, the so called "Back-to-back-IDA" is used to assess the capacity of building to withstand future earthquakes after damage. Conceptually, a first earthquake is applied to the undamaged structure in order to reach a specific level of damage, in this study the damage level is not known a priori because the sole damaging earthquake intensity is imposed that is representative of a given return period. Once the structure has been damaged, the IDA procedure is applied to the damaged structure in order to assess the new capacity of the building. The output of this procedure is an IDA curve and an ultimate spectral acceleration capacity of the building for the set Mainshock-Aftershock Return Period (MS-AS-TR). Note that each accelerograms of the selected bin have been used independently as Mainshock or Aftershock when assessing building's residual capacity.

This simulation must be repeated for each combination MS-AS for all considered return periods for a total of 961 simulations for 5 different return periods (4805 simulations for each case study) to properly account for record-to-record variability. The results of this framework are a set of fragility curves representing the Residual Capacity
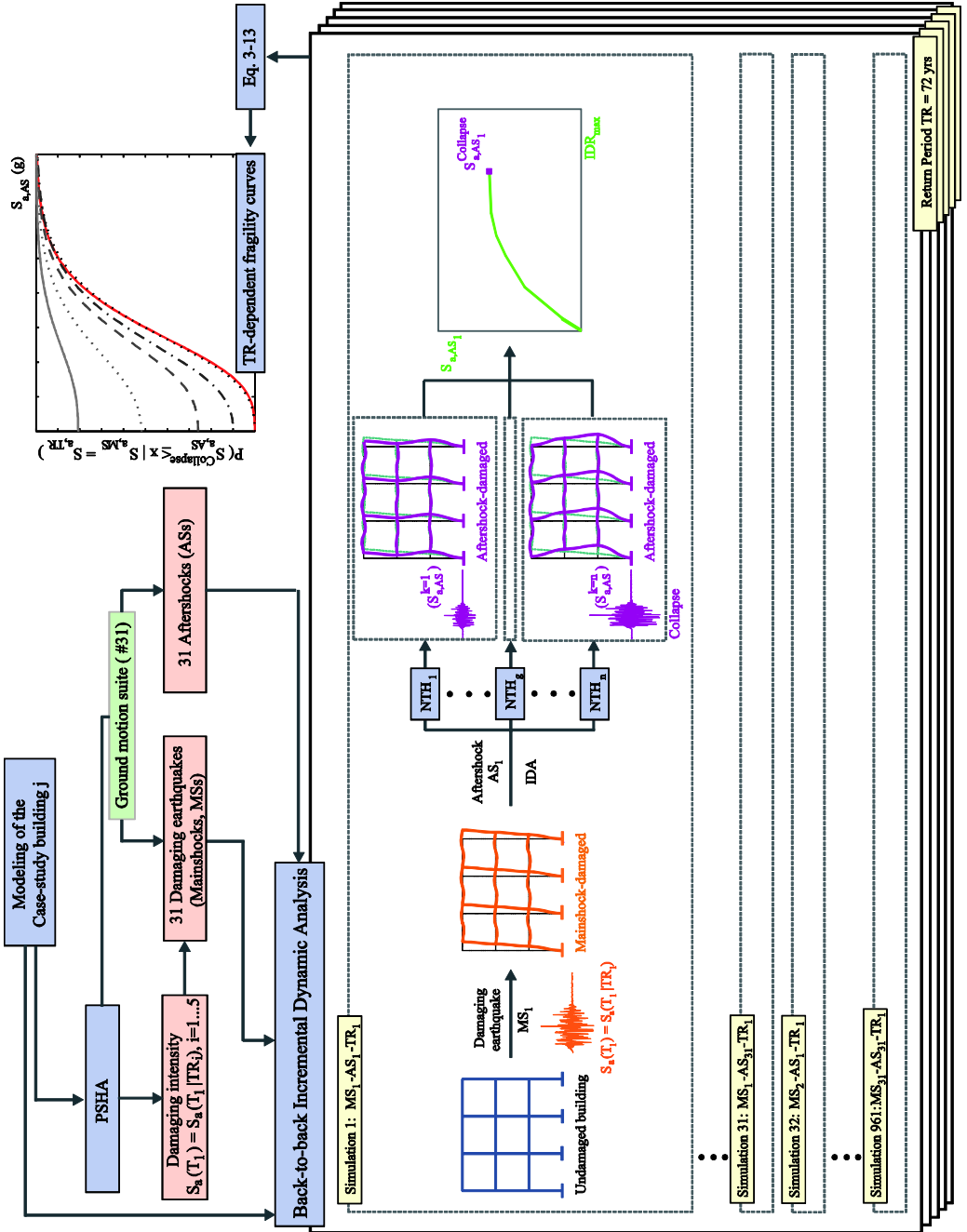
Fig. 3.51 Diagram showing Residual Capacity assessment framework

of the building conditioned on the Return Period (i.e., the intensity level of the earthquake conditioned on the site hazard), following indicated as "TR-dependent fragility curves". The simulation of the damaging earthquake and the estimation will be addressed in §3.10.3, while the mathematical formulation for TR-dependent fragility curves in 3.10.4.

3.10.3 DERIVATION OF TR-DEPENDENT AFTERSHOCK FRAGILITY CURVES

The approach here adopted to estimate the seismic capacity variation is the so called "back-to-back"-IDA (B2B-IDA). This kind of analysis requires the building of a seismic sequence in which two earthquakes are applied consecutively to the structure. The first represents the damaging earthquake, and it is scaled to be representative of a given probability of exceedance in 50 years; its intensity is fixed during the analysis for a given return period. The second earthquake is used to assess the modified capacity of the damaged building and therefore, the nonlinear time history of the Mainshock-Aftershock sequence is repeated with increasing scale factors applied to the aftershock record until the structure collapses, providing incremental dynamic analysis results for aftershocks. The aftershock response so obtained can be used to generate fragility curves conditioned on the return period of the mainshock. In order to allowing the ceasing of vibrations between two seismic sequences, an additional 10 seconds ground motion with zero acceleration has been added between Mainshock and Aftershock ground motions. The typical Mainshock-Aftershock sequence is shown in Fig. 3.52.

To account for the effect of record-to-record variability on structural response, Mainshock-Aftershock sequences have been suitably built by combining each of the 31 Mainshock ground motions with the same 31 ground motions applied as aftershock, for a total of 961 combinations Mainshock-Aftershock for each return period and studied structure.
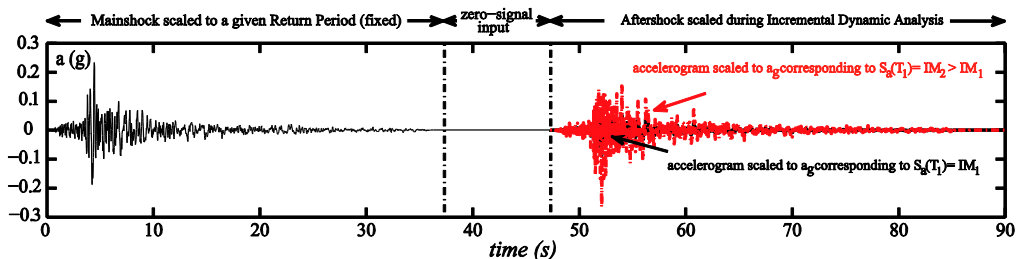
Fig. 3.52 Mainshock-Aftershock sequence

Here two definition of global collapse have been adopted (§3.2.4.1 and §3.2.4.2): Gravity load collapse (GLC) and Sidesway collapse (SSC). The capacity is defined as the smaller between these two alternative collapse capacities.

The B2B-IDAs have been carried out on the nonlinear building model in OpenSees (McKenna, 2011).

Effect of earthquake polarity

Luco et al. (2004) noted that residual drifts may strongly influence structural behavior during the aftershock. When building the Mainshock-Aftershock sequence, a factor that can significantly influence residual drifts, and consequently the building's residual capacity is the polarity of the Aftershock (i.e., the direction of the Aftershock with respect to the Mainshock), that is related to the sign of the Aftershock scaling factor (positive or negative). When the Aftershock is applied in the same direction or in the opposite direction as Mainshock, residual drifts tends to increase or reduce residual drifts. An example of polarity effect is shown in Fig. 3.53 for an SDOF system. The positive polarity leads to a displacement increment due to Aftershock, while negative polarity obtained changing Mainshock action verse produces a negative residual displacement that leads to a global displacement smaller than that produced by the Mainshock.
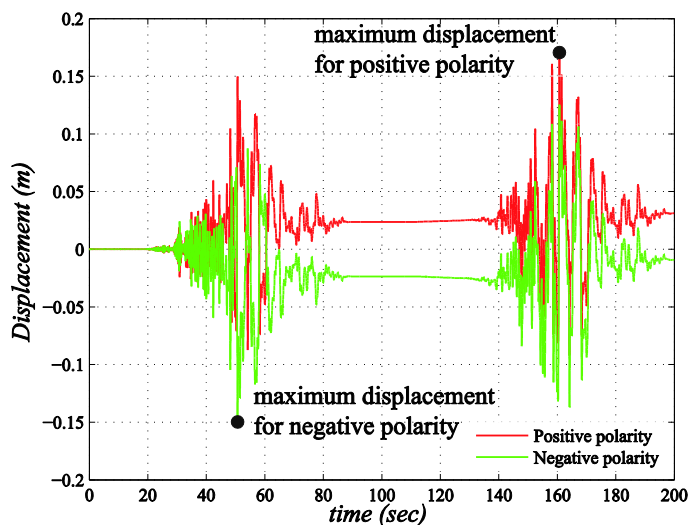
Fig. 3.53 SDOF response for different polarities

The sign of the scaling factor is related to the verse of the earthquake, which is unknown a priori. Raghunandan et al. (2012) noted that the polarity of the mainshock-aftershock ground motion sequence does not affect the residual capacity for a moderately damaged building, but it can become noticeable for the extensively damaged building. In order to minimize the structure's residual capacity, the aftershock capacity should be chosen as the minimum between positive and negative polarity. However, Raghunandan et al. (2012) and Ryu et al. (2011) concluded that it is more reasonable to select randomly

111

the aftershock sign since it is unknown a priori. Furthermore, this assumption reduces the computational time by half. For these reasons, the earthquake polarity has been neglected in this study.

Effect of Mainshocks and Aftershocks on the building's damaged capacity

It is interesting to note the effect on Incremental Dynamic Analysis (IDA) curves when fixed the damaging earthquake and its intensity. Fig. 3.54(a) shows this effect on the American building's response for a given scaled Mainshock. In particular, curves start from a given IDR_{max}, that represents the maximum response of the structure due to aftershock. Given that the first earthquake in the seismic sequence is fixed, also in terms of intensity, the maximum response due to the sole Mainshock is always the same (i.e., $IDR_{max} = 0.009$). The dispersion in *IDA* curves in Fig. 3.54(a) is about the same shown for the intact building. However, if the Aftershock is fixed and the Mainshock varies, Fig. 3.54(b), also if the intensity of the Mainshock is fixed, the damage produced in the structure is not the same because the differences in ground motion frequency content and other ground motion characteristics.

<div align="center">(a)   (b)</div>
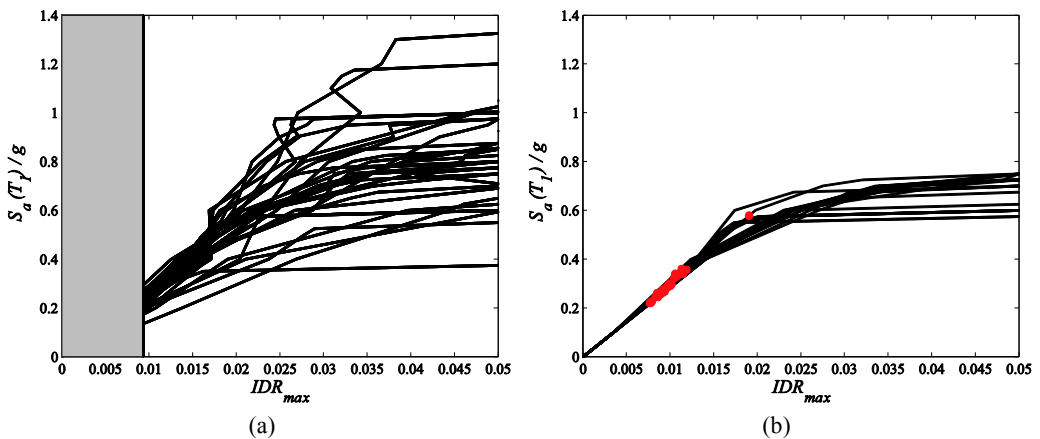
Fig. 3.54 (a) Incremental dynamic analysis for Mainshock-damaged building fixed Mainshock and different, (b) for Mainshock-damaged building fixed Afteshock and different Mainshocks.

Red dots in Fig. 3.54(a) indicates the IDR_{max} reached during the first earthquake, which can be considered an indicator of maximum demand during the Mainshock. Even if the initial damage varies, the resulting *IDA* curves are significantly less dispersed and this dispersion could almost eliminate if Mainshocks were scaled in order to reach the same IDR_{max}, or the same starting level of damage in the structure.

3.10.4 **TR-DEPENDENT AFTERSHOCK FRAGILITY FORMULATION**

Starting from the initial damage state produced by a MS corresponding to a given Return period (T_R), T_R dependent collapse fragility functions can be built. Because the structure is subject to a series of consecutive events, cumulative damage is accounted for in the estimate of the collapse probability.

Considering a seismic sequence consisted of a pair of mainshock MS and the consecutive aftershock event AS, the aftershock collapse probability conditioned on the MS intensity $S_{a,MS}$ can be calculated by considering two mutually exclusive and collectively exhaustive events (Benjamin and Cornell 1970) defined as C and NC. C accounts for cases where collapse occurs due to the mainshock and NC accounts for cases where collapse does not take place due to the mainshock (see Ebrahimian et al. 2014 and Jalayer et al. 2011a,b for more details on this type of expansion based on the Total Probability Theorem):

$$P\left(x \geq S_{a,AS}^{C} \mid S_{a,MS}\right) = P\left(x \geq S_{a,AS}^{C} \mid S_{a,MS}, NC\right) \cdot P\left(NC \mid S_{a,MS}\right) +$$
$$+ P\left(x \geq S_{a,AS}^{C} \mid S_{a,MS}, C\right) \cdot P\left(C \mid S_{a,MS}\right)$$

<div align="right">Eq. 3-15</div>

where $S_{a,MS}$ is MS spectral acceleration corresponding to a specific T_R conditioned on the site hazard, the fundamental vibration period of the intact structure (T_1), and the critical damping ratio assumed; $S_{a,AS}$ is the AS spectral intensity at T_1 and $S_{a,AS}^{C}$ is the AS spectral intensity corresponding to collapse. Assuming an equal probability of occurrence for each MS, the term $P\left(NC \mid S_{a,MS}\right)$ can be estimated as the number of NC-cases over the number of MS considered (N_{MS}), while $P\left(C \mid S_{a,MS}\right)$ can be estimated as the number of C-cases over N_{MS} and $P\left(x \geq S_{a,AS}^{C} \mid S_{a,MS}, C\right) = 1$. Hence, the AS fragility can be interpreted, for each considered structure and T_R (corresponding to $S_{a,MS}$), as the sum of the mainshock collapse fragility (last term in Eq. 3-15), and an inflating term (first term in Eq. 3-15). $P\left(x \geq S_{a,AS}^{C} \mid S_{a,MS}, NC\right) = 1$ is the collapse probability conditioned on MS intensity $S_{a,MS}$ and on NC can be expanded as:

$$P\left(x \geq S_{a,AS}^{C} \mid S_{a,MS}, NC\right) = \int_{\text{all possible } \underline{MS}} P\left(x \geq S_{a,AS}^{C} \mid \underline{MS}, S_{a,MS}, NC\right) f\left(\underline{MS} \mid S_{a,MS}, NC\right) d\underline{MS}$$

<div align="right">Eq. 3-16</div>

$$\approx \frac{1}{N} \sum_{i=1}^{N} P\left(x \geq S_{a,AS}^{C} \mid MS_i, S_{a,MS}, NC\right)$$

where $\underline{MS}$ stands for the mainshock wave-form vector; $f\left(\underline{MS} \mid S_{a,MS}, NC\right)$ is the joint probability density function for the mainshock wave-form vector given a specific value for $S_{a,AS}$ and given NC. The integral in Equation 3 is an application of the Total Probability Theorem in conditioning on all possible mainshock waveforms conditioned

on a given spectral acceleration value. It should be noted that the approximation to the integral in Equation (2) is based on the assumption that the various mainshock wave-forms have equal probability of occurrence (see Jalayer et al. 2012 for more detail on this kind of approximation).

3.10.5 RESULTS

The REC of MS-damaged building is computed in terms of S_a based on the IDA results obtained from MS-AS sequences. The results are here represented in terms of fragility curve at collapse. For the undamaged building, the collapse fragility curve is based on the IDA results performed on the intact building using the set of 31 ground motions. The collapse fragility curve for damaged building is calculated based on the AS collapse capacities obtained for each of 961 MS-AS sequences in which the MS is scaled in order to be representative of the TR of interest. Following the TR-dependent fragility assessment framework outlined in §3.10.2, the collapse fragility curves for the damaged structure conditioned on the return period of the damaging earthquake have were determined. In fact, $S_{a,MS}$ in Eq. 3-15 corresponds to the spectral acceleration at the site for a given probability of exceedance in 50 years, i.e. a specific return period for seismic action. In Fig. 3.55 the TR-dependent seismic fragility conditioned on non-collapse cases are reported.
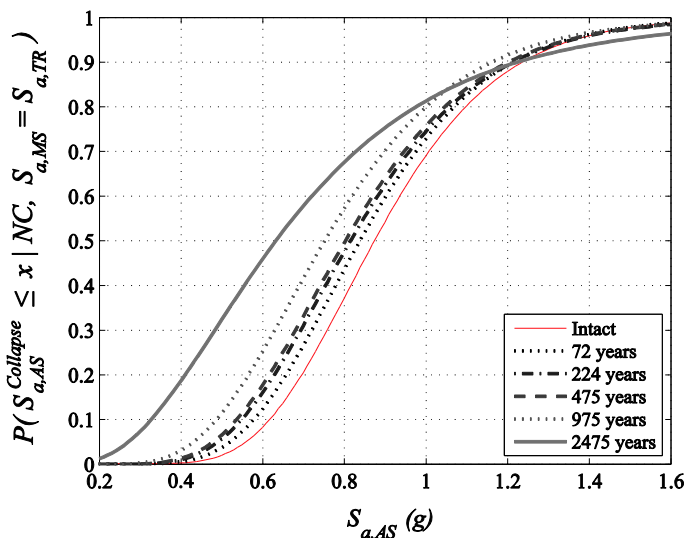
Fig. 3.55 TR-dependent fragilities for the American building conditioned on non-collapse cases

The term $P\left(S_{a,AS}^{Collapse} \leq x \mid NC, S_{a,MS} = S_{a,TR}\right)$ represents the probability of collapse for a given value of the intensity measure S_a of the Aftershock ($S_{a,AS}$) conditioned on the value

114

($S_{a,MS}$) of first damaging earthquake (MS), that corresponds to a specific return period for the studied site and to the non collapse case, i.e. collapse did not occur due to the damaging earthquake. Red curve represent the collapse fragility curve for the undamaged building.

As can be noted, increasing seismic intensities for the damaging earthquake leads to a greater probability of experiencing collapse for the same value of the aftershock intensity and curves for damaged building shift leftward. For instance, the median probability of collapse (when damaging earthquake did not lead to collapse) for the undamaged structure is S_a=0.875g but it decreases up to 0.631g when the building is damaged by a 2475 years return period earthquake that did not induce collapse as indicated in the following Table:

Return Period (yrs)	72	224	475	975	2475
median (g)	0.839	0.816	0.803	0.752	0.631
β	0.29	0.31	0.31	0.34	0.51

Table 3-15 Median and logarithmic standard deviation (β) of Residual capacity of damaged building conditioned on non-collapse for Mainshock (American case study)

According to Eq. 3-15, the TR-dependent collapse fragility can be evaluated properly accounting for collapse occurred due to the sole damaging earthquake. Fig. 3.56 illustrates the collapse fragility curves for the intact and damaged building in terms of probability of collapse conditioned on the *MS* for given *TR* as a function of *AS* spectral intensity, $S_{a,AS}(T_1)$. The red curve represents the behavior of the intact building. As the TR increases, due to the increasing building damage for MS application, the collapse fragility curve shift leftward and up. Because for increasing TR an increasing number of collapses due to MS is detected, the collapse fragility curves for higher TR have non-zero probability of collapse for $S_{a,AS} = 0$. For instance, for 475 years return period 3 ground motions over the 31 earthquake bin caused the building collapsed during the damaging earthquake, consequently the collapse fragility, independently from the Aftershock intensity, states that the probability of collapse is always greater than 3/31=9.7%

These fragility curves can be obtained by applying Eq. 3-16, considering values for fitted fragility conditioned on non-collapse cases for Mainshock reported in Table 3-15 and considering the number of Mainshocks producing collapse for different return periods ground motion intensity levels: 3, 8, 16 and 27 ground motion records over the 31 record set led to collapse for 224, 475, 975, 2475 year return period action, respectively.

Similarly, the TR-dependent fragility for the Italian building are reported in Fig. 3.57. The curves obtained for this case-study is significantly different from those obtained for the American one. Indeed, the building's capacity does not change in a substantial way up to a return period of 2475 years, for which 3 Mainshock induced

structural collapse in the structure. This is probably due to the fact that the level of damage caused by mainshock earthquakes of increasing intensity (i.e. increasing *TR*) is relatively low, with median *IDR*$_{res}$ reaching barely a value of 0.03% for T_R=975 years. Only for T_R=2475 years a significant damage is observed, leading to a sensible shift of aftershock fragility curves.
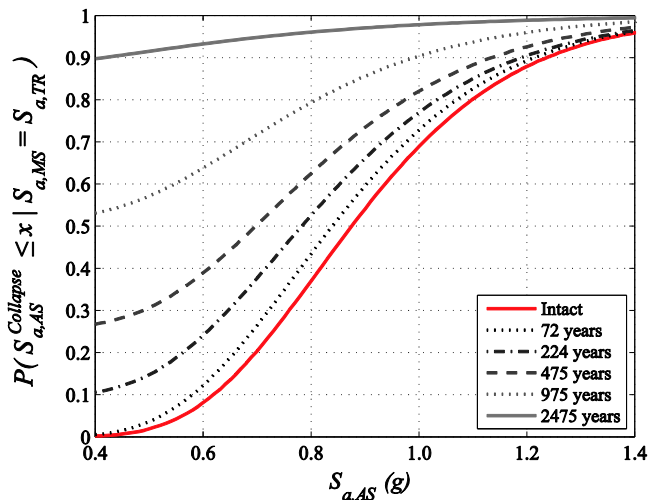
Fig. 3.56 TR-dependent fragilities for the American building

For lower return periods, second part of the Eq. 3-15 is equal to zero due to the fact that Mainshock did not induce collapse. Results for fitted fragilities conditioned on different return periods and non-collapse cases due to the sole Mainshock are reported in Table 3-16.
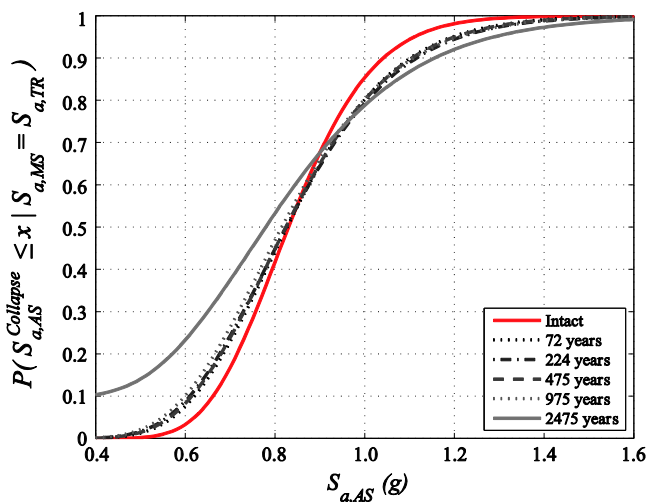
Fig. 3.57 TR-dependent fragilities for the Italian building

This effect is mainly ascribable to the strong difference in the hazard at the site.

Return Period (yrs)	72	224	475	975	2475
median (g)	0.827	0.825	0.824	0.815	0.810
β	0.22	0.23	0.23	0.24	0.29

Table 3-16 Median and logarithmic standard deviation (β) of Residual capacity of damaged building conditioned on non-collapse for Mainshock (Italian case study)

The effect of site hazard can be evidenced by considering the same earthquake acting on the two structures in their undamaged state when scaled to be representative of the same return period but conditioned on the specific hazard at the site. Fig. 3.58 and Fig. 3.59 show the damage pattern in the American (a) and the Italian (b) structure for the same earthquake and return period of ground motion, 475 and 975 years respectively, for the legend refer to Fig. 3.24.

It is possible to note that for the same return period American structure show a more extended and severe damage when compared to the Italian building. While for the 475 years return period, Fig. 3.58, the sole members reaching damage are two beam-column joints, all joints of the American building reached cracking and first storey columns reached concrete spalling deformations. Instead, for 2475 years return period, Fig. 3.59, some element of the Italian reached significant damage but the American building is prone to collapse.

(a)   (b)
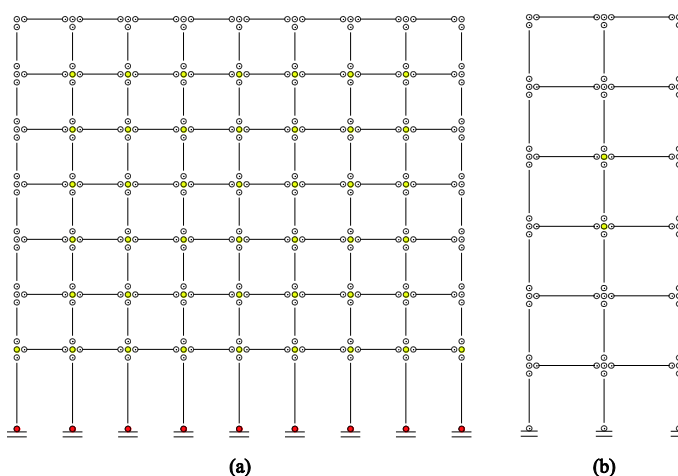
Fig. 3.58 Damage pattern for the (a) American building and the (b) Italian building for the TCU042-N earthquake ground motion scaled to the same return period of 475 years conditioned on the specific site hazard.
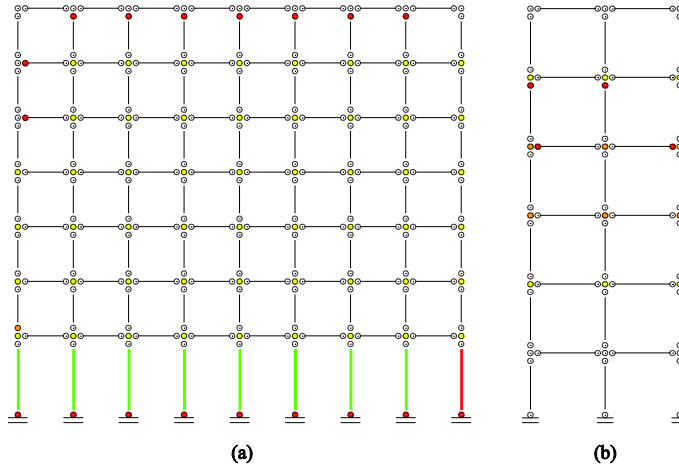
Fig. 3.59 Damage pattern for the (a) American building and the (b) Italian building for the TCU042-N earthquake ground motion scaled to the same return period of 2475 years conditioned on the specific site hazard

This difference in damage severity is mainly due to different hazard a the site, for which the spectral intensity corresponding to a return period of 2475 years is 1.06g for the American site while only 0.56g for the Italian one.

Probability of collapse in t years

A comprehensive indicator of the structural safety that involves considering both the hazard curve at the site and the collapse fragility curves is the probability of collapse over t years. Under the hypothesis that the occurrence of earthquakes in time follows a Poisson process, the probability of one collapse over t years can be computed as:

$$P_c (\text{in } t \text{ years}) = 1 - e^{-\lambda_c t} \qquad \text{Eq. 3-17}$$

with λ_c the mean annual frequency of collapse. λ_c can be calculated integrating the collapse fragility curve of the structure over the seismic hazard curve (Fig. 3.60) at the site using the relation $\lambda_c = \int_0^\infty P(C|im)|d\lambda_{IM}(im)|$ (Eads et al., 2013), where $P(C|im)$ is the probability that the structure will collapse when subjected to an earthquake with ground motion intensity level im, and λ_{IM} is the mean annual frequency of exceedance of the ground motion intensity im.
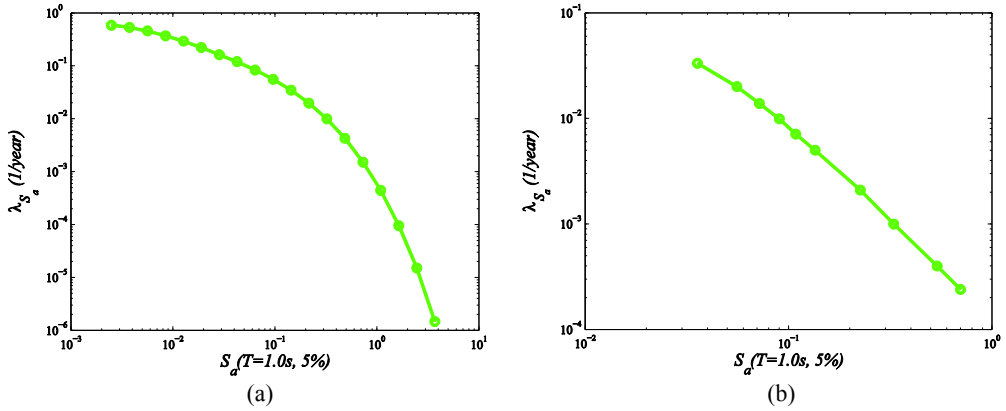
Fig. 3.60 Mean annual frequency of exceedance of S_a for a vibration period of 1 second and a system damping of 5% for (a) American, (b) Italian site.

In order to account for the possibility that the *MS* caused collapse, the Eq. 3-17 can be rewritten using the Total Probability Theorem by separating *C* and *NC* cases for a given T_R as follows:

$$P_c(\text{in } t \text{ years} \mid S_{a,MS}) = P_c(\text{in } t \text{ years} \mid S_{a,MS}, NC) \cdot P(NC \mid S_{a,MS}) + \\ + P_c(\text{in } t \text{ years} \mid S_{a,MS}, C) \cdot P(C \mid S_{a,MS})$$

Eq. 3-18

Residual Capacity

The "degraded" REC_{TR}, corresponding to each return period, is computed as the median collapse capacity from the Aftershock *IDA* analyses. Then, the corresponding PL is calculated with the following equation:

$$PL = \frac{REC_{S_{a,TR}}}{REC_{S_{a,0}}}$$

Eq. 3-19

where $REC_{Sa,TR}$ represent the spectral acceleration capacity of the damaged structure, and the $REC_{Sa,0}$ is the capacity of intact structure. Table 3-17 and Fig. 3.63 shows the relation between *PL*, *REC*, T_R and the probability of collapse in a time window of 50 years for the American case-study. Note that for T_R greater or equal than 975 years in more than 50% of cases we have collapse due to the *MS*, with a median value of *PL* corresponding to 100; obviously, in calculating collapse probability the entire fragility is taken into account, resulting in different (increasing) P_C (in 50 years) for T_R =975 (56.4%) and 2475

119

(89.6%). As expected, for increasing T_R the probability of collapse increases. The same trend is observed for PL, while the ratio REC_{TR}/REC_0 decreases.
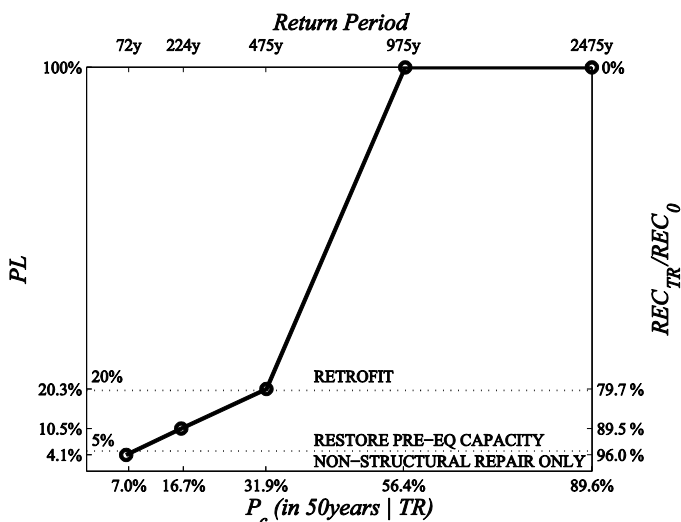
Fig. 3.61 Relations between *TR*, P_C in 50 years conditioned to *TR, PL* and REC variation for the American case-study.

The median probability of collapse in 50 years is 6.1% for the intact building while it increases to 7.0% for a 72-years-*MS*-damaged structure and up to a maximum value of 89.6% when considering a Return Period of 2475 years. In the same figure the restore and retrofit trigger values in terms of PL, as suggested in (SF, 2012), are shown, considering that for Van Nuys site $S_{a,0.3} \geq 0.4$g for any Return Period.

The relation between PL, REC, TR and the probability of collapse in a time window of 50 years for the Italian case-study are reported in Fig. 3.62 (numerical values in Table 3-18). Differently from the American building, for increasing TR the probability of collapse increases slightly, and the probability of collapse is about 0.1% for any return period but the 2475 return period for which the probability of collapse is about 10%. It is interesting to note that in this sense, the PL is more sensitive than the P_c that is strongly influenced by the site hazard. Similarly to the corresponding figure for the American case-study building, the restore trigger value in terms of PL is reported. The median probability of collapse in 50 years is 0.052% for the intact building while it increases to 0.1% for a 72-years-*MS*-damaged structure and up to a maximum value of 9.9% when considering a Return Period of 2475 years.
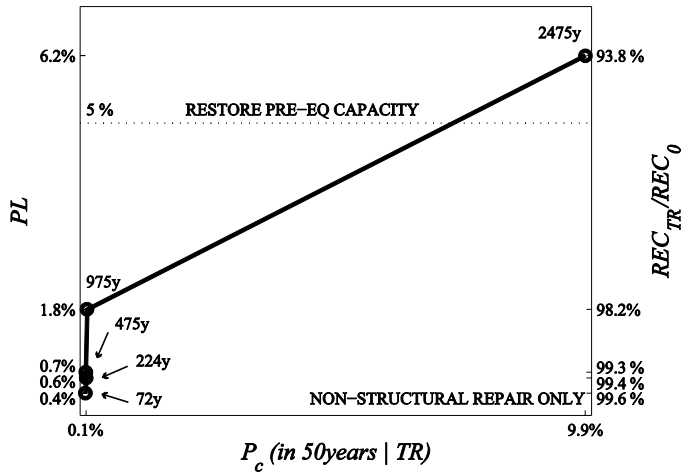
Fig. 3.62 Relations between *TR, P_C* in 50 years conditioned to *TR, PL* and *REC* variation for the Italian case-study.

		Return period (yrs)				
	undam	72	224	475	975	2475
P_c	6.09E-02	7.02E-02	1.67E-01	3.19E-01	5.64E-01	8.96E-01
PL median (%)	0	4.09	10.56	20.32	100	100
REC/REC_0 (%)	100	95.91	89.44	79.68	0	0

Table 3-17 Probability of collapse, median performance loss index (PL), Residual capacity ratio for the American building

		Return period (yrs)				
	undam	72	224	475	975	2475
P_c	5.25E-04	1.04E-03	1.20E-03	1.13E-03	1.37E-03	9.88E-02
PL median (%)	0	0.38	0.64	0.74	1.82	6.16
REC/REC_0 (%)	100	99.62	99.36	99.26	98.18	93.84

Table 3-18 Probability of collapse, median performance loss index (*PL*), Residual capacity ratio for the Italian building

It is necessary to note that the probability of collapse (P_c) is conditioned on the hazard at the site. P_c is a synthetic index that properly account for the structural capacity of the building and its dispersion (i.e., the fragility curve) and the hazard curve at the site and comes from a convolution between these two quantities. However, it is significantly sensitive to the extension of hazard curve with respect to the fragility curve. For the Italian site, the hazard curve extents only up to $S_a(T_1)$= 0.7g while the fragility curve extends up to $S_a(T_1)$= 1.4g, this means that a significant part of the fragility curve is not considered when assessing of P_c. This lacking of information can invalidate the

computation of the probability of collapse. For instance, for the American building the probability of collapse is equal to 6.09E-02 for the intact building; however, if the hazard curve only reduces in its extension, this means that information about the probability of exceedance of a given *IM* is provided only for $S_a(T_1)$ in the interval 0.04-0.7g, then the collapse probability drops to 1.53E-03 that is almost four times smaller.

PL index does not require the computation of the hazard curve, which is not always available at the site in an exhaustive way, consequently it is a simple and reliable index that is, in general, not conditioned on the hazard at the site. The conditioning of PL on site hazard in this part of the dissertation relies on the choice of a level for the intensity of the damaging earthquake conditioned on the site hazard, while the reliance of capacity on the accelerograms bin selected (i.e., ε), see Haselton et al. (2009), is canceled when the damaged capacity is normalized with respect to the capacity of the intact building in *PL*.

3.10.6 EFFECT OF INITIAL DAMAGE ON BUILDING'S RESIDUAL CAPACITY

In this study, residual capacity of damaged buildings is assessed considering as damaging earthquakes ground motions scaled to be representative of different hazard level at the site. Other authors, e.g. Luco et al. (2004), estimate the structural capacity decay starting from a given level of damage produced by earthquakes, that can be represented by the maximum transient interstorey drift ratio (IDR_{max}). This IDR_{max} threshold, representative of a given damage state, is usually calibrated based on damage observation from nonlinear static analyses. However, the goal of this study is to address structural reparability topic for two case studies through consideration about seismic safety decay and repair costs using a time-based assessment procedure, that require to consider as damaging earthquakes, ground motions of a given intensity.

Consequently, the starting damage state, or the maximum experienced IDR, cannot be known *a priori* for a given return period level. For the same return period level, the damage produced can significantly vary depending on the several ground motion characteristics (e.g., frequency content), as evidenced in **Errore. L'origine riferimento non è stata trovata.** where different Mainshocks, scaled at the same intensity, lead to different IDR_{max}.

 Another possible elaboration of the results allow to investigate on the effect of pre-fixed damage levels on aftershock fragility. Indeed, from the post elaboration of data it is possible to point out the variation of structural capacity conditioned on the damage instead of on the return period level. Here the IDR_{max} experienced during the damaging earthquake has been assumed as an indicator of damage. Fig. 3.63(a) and (b) show intact and aftershock fragilities for the two case-study buildings conditioned on the maximum IDR experienced during Mainshock. Two different level of damage due to MS have been selected, represented by 1.00% and 1.85% IDR_{max}. Note that for this post elaboration of

data, a suitable bin of Mainshock-Aftershock sequences was selected in order to consider Mainshocks leading to the selected IDR_{max} with a given tolerance (i.e. so that the mean ($\underline{IDR_{MS}}$) was corresponding to the chosen IDR_{max}).
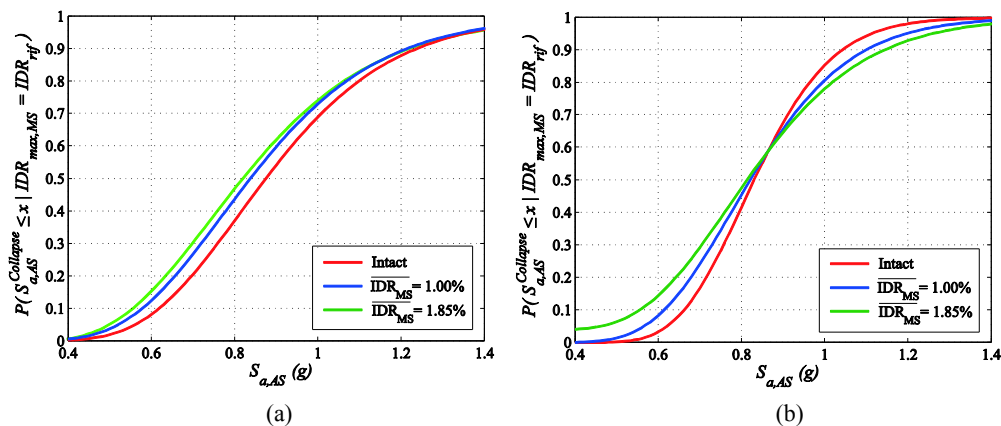
Fig. 3.63 Intact and aftershock fragilities obtained for damaging earthquakes leading to specific IDR_{max} for (a) American and (b) Italian building

Depending on the activated damage mechanism, the same initial damage level can lead to different capacity reductions, as can be observed in Fig. 3.63 (a) and (b).

It is here noted that aftershock fragilities for mainshock damaged structure, given fixed level of IDR_{max}, are obtained with a formulation dual to Eq. 3-15 and Eq. 3-16, i.e. calculating the probability of collapse varying Sa,AS conditioned on the mainshock leading to selected damage level. On the other hand, as observed in Luco et al.(2004), once the damage level due to mainshock is assigned, a greater variability of the residual seismic capacity is observed due to aftershock variability than with respect to the variation in potential mainshocks. In order to investigate on the effect of conditioning the hypothesis on the final results, the median variation of REC was also computed considering this aspect, i.e. calculating the probability of collapse varying $S_{a,AS}$ conditioned on the aftershocks. Following this second approach, for a maximum IDR experienced during Mainshock equal to 1%, capacity varies with respect to the intact one of 2.20% and of 2.86% for the American and the Italian case study, respectively, while for an IDR_{max} 1.85% the capacity varies of 6.28% and 6.66%, respectively.

Chapter 4

DIRECT ECONOMIC LOSS PREDICTION

In the previous chapters, the collapse performance of two non-ductile reinforced concrete buildings, typical of those constructed in America and Italy before '70s, has been analyzed along with their variation after experiencing damaging earthquakes. In this chapter, these results are extended to consider an additional metric of building seismic performance: economic losses. Economic losses are a measure of financial losses that may be incurred due to damage in the structure in future earthquakes. This chapter outlines the procedures that are used to calculate building performance in the assessment process. These include generation of simulated demands, determination of damage, and computation of losses in the form of repair costs. Results are presented for both intensity-based and time-based assessments, as a series of intensity-based assessments that are weighted based on frequency of occurrence.

4.1 OVERVIEW

Non-ductile RC building represent the prevalent construction type all over the world. The seismic vulnerability of such structures poses a significant threat to safety of occupants besides to entail large financial losses also for frequent earthquakes. For example, the Northridge (1994) and the Christchurch (2011) earthquakes resulted in very large economic losses that are seemed excessive especially if one considers the moderate magnitude of these events. Since the nineties, it has become increasingly clear that the protection of lives is not enough, because financial losses associated with repair, disruption to businesses and the time lost to clean up and reinstate services and activities, are important factors that need to be considered in a modern definition of seismic risk (Calvi 2014). Consequently, a need for additional performance measures has arisen in response to the need to reduce other risks posed by earthquakes.

In this sense, Performance-Based Assessment (PBA), by providing quantitative measures of building performance, support stakeholders' decisions with information, usually in probabilistic terms, about the risk of earthquake economic losses for the building, that is a means of quantifying and communicating risk. This facilitates

informed decision-making for risk management for both existing and new building during the design process. Usually, for existing building, when repair costs exceed a significant part of the replacement cost of the building, it is assumed that the structure should be demolished and reconstructed. Past studies suggest that many owners elect to replace buildings when the projected repair costs exceed about 40% of the replacement cost. However, many factors including the age of a building, occupancy, status as a historic landmark, the economic health of the surrounding neighborhood, and individual profitability affect this decision (ATC, 2012). In the same way, PBA may be used by stakeholders to the more appropriate solution that can be adopted for buildings (e.g., repair, retrofit, demolish, etc.). For instance, when considering seismic retrofit for the purpose of reducing economic losses resulting from frequent earthquakes, the retrofit design should focus on reducing nonstructural damage, either by stiffening the structural system, or by changing connections between nonstructural elements or structural and nonstructural elements. Instead, to mitigate damage to the structural system in less frequent events, one could strengthen the structural system, change its stiffness to reduce resonance with site ground motions, or both (Beck et al. 2002).

4.1.1 SEISMIC LOSS ESTIMATION METHODOLOGIES

Over last decades, various loss assessment methodologies have been proposed to provide risk assessment ranging from regional scale to specific building scale. Regional loss estimation methodology was created to assess economic losses produced over a broad geographical area, classifying buildings into generic structural types to broadly evaluate their seismic performance. For instance, HAZUS methodology and software (NIBS 2003) is one of the most widely used approaches for regional loss estimation and it estimates structural response, damage, and repair costs using generic building capacity and fragility functions that are based on the classification of a building's lateral force resisting system, height, and occupancy. This procedure has the main advantage of facilitate quick calculations of losses for large building portfolios, however since it is a generalized methods, it cannot capture unique aspects of a specific building's structural and nonstructural design. On the other hand, building-specific losses assessment methods requires performing structural analyses of a building to estimate damage to its structural and nonstructural components, and then determining the cost of repairing this damage. Damage states for each damageable component in the building is defined according on different repair actions needed to restore the component to its undamaged state. The latter method has been further developed by several researchers over the past 20 years, among these methods, the Pacific Earthquake Engineering Research (PEER) Center framework is one of the most known. PEER's loss assessment methodology incorporates probabilistic seismic hazard analysis, probability of structural collapse, correlation between various response parameters, loss disaggregation, uncertainty propagation, and many other improvements to previous approaches, establishing a more

comprehensive framework for performance assessment. For further discussion about differences, assumptions, and limitations of this method refer to Aslani and Miranda (2005).

Regional and Building-specific loss assessment leads to significant differences in losses that comes from differences in underlying procedures and assumptions. For instance, the PEER method is based on building-specific component-based damage and repair cost functions, while HAZUS uses generic building fragilities and loss functions. In addition to these differences in overall loss framework, there are several other possible sources for discrepancies between the executions of the two methods. For instance, HAZUS adopt simplified models for assessing nonlinear response of buildings, assumes a fundamental vibration period for the building, neglect the contribution of higher modes when assessing acceleration demand, estimate damage at the building-level neglecting single components contribution to losses. Ramirez et al. (2012) comparing results obtained with the use of building-specific and regional loss assessment methods for a set of buildings, found that the regional predictions are about 1.6 to 2.4 times lower than those obtained with the building-specific procedure.

In the backdrop of building-level loss assessment methods, as alternative to component-based approach, where the damageable assemblies are identified and fragility and consequence functions are assigned based on available information, Ramirez and Miranda (2009) proposed and developed a story-based loss model that combines the likely structural and non-structural inventory into a set of engineering demand parameter to decision variable functions (EDP-DV). Component and story-based loss modeling approaches differ significantly and each has its own inherent benefits and drawbacks. For instance, the component-based model allows the representation of the actual component inventory; however, experimental component fragilities are not available for any possible damageable component, often requiring the adoption of "generic fragility", e.g. in the FEMAP-58 tool (ATC, 2012). On the other hand, the story-based model relies on relative inventories based on construction estimating documents but eliminates the need to select the type and number of damageable assemblies and the so-called "double counting" (i.e., allocating repair cost to an element that must also be repaired in order to repair another). However, the latter problem can be overcome by careful formulation of a component-based model which would indeed consider the building most accurately if formulated properly.

4.1.2 PEER FRAMEWORK

At present days, the most refined PBEE procedure currently available appears to be the framework developed for the PEER PBEE methodology. In PEER's terminology, measures of seismic performance are introduced as Decision Variables, DV's. Decision variables are quantifiable measures of seismic performance that can be employed to judge seismic performance. For a realistic quantification of DV's, it is required that

various sources of uncertainty that contribute to the uncertainty corresponding to the decision variables are incorporated. In fact, the PEER methodology allows the prediction of building performance in a probabilistic format applying the total probability theorem to predict earthquake consequences in terms of the probability of incurring particular values of performance measures. In the PEER framework, DVs are often quantified in terms of monetary loss, downtime loss and life loss.

The PEER loss assessment framework (see Porter 2003, Deirlein 2004, Miranda et al. 2004, Aslani and Miranda 2005, Miranda and Taghavi 2005, Krawinkler and Miranda 2004, Aslani et al. 2004, Mitrani-Reiser and Beck 2007, Baker and Cornell 2008b, Ramirez and Miranda 2009) consists of four distinct analysis steps: hazard analysis (site definition), structural analysis, damage analysis, and decision analysis (consequences). The basic mathematical formulation of the method is expressed as a triple integral formulation as shown in Eq. 4-1:

$$\lambda(DV > dv) = \int_{im} \int_{dm} \int_{edp} P(DV > dv \mid DM = dm) \, dP(DM > dm \mid EDP = edp) \\ \left| dP(EDP > edp \mid IM = im) \right| d\lambda(IM > im) $$

Eq. 4-1

where $P[X > x \mid Y = y]$ is probability of exceedance of the variable X exceeding x, conditioned to a random variable Y assuming the value y. Conceptually, the four main variables are defined as: (IM) intensity measure, (EDP) engineering demand parameter, (DM) damage measure, and (DV) decision variable. When integrated over the full range of IM, EDP, and DM, the result is the mean annual occurrence rate of the DV (i.e., $\lambda[DV]$). When using Eq. 4-1 to estimate measures of seismic performance, damage measure is assumed to be a continuous random variable. However, measures of seismic performance such as economic losses in individual building components, that are often associated with discrete repair actions, it is more appropriate to assume that damage measures are discrete. Therefore, it was proposed that economic losses in individual components are computed from the need to apply discrete repair and replacement actions that are triggered at discrete damage states (Miranda and Aslani, 2003; Krawinkler and Miranda, 2004). PEER framework equation, for cases where damage states are assumed as discrete random variable has been modified as follows:

$$\lambda(DV > dv) = \sum_{ds} \int_{im} \int_{edp} P(DV > dv \mid DM = dm) \, \Delta P(DM > dm \mid EDP = edp) \\ \left| dP(EDP > edp \mid IM = im) \right| d\lambda(IM > im) $$

Eq. 4-2

where one of the integrals in Eq. 4-1 is replaced by a summation to account for discrete damage states and $dP(DM > dm|EDP = edp)$ is replaced by $\Delta P(DM > dm|EDP = edp)$ to incorporate the fact that damage states are considered as discrete random variables. In

the PEER PBEE methodology, see Fig. 4.1, building-specific loss is estimated through a four-step approach:

Hazard Analysis

The Hazard Analysis allows the calculation of frequency with which the intensity of a ground motion is exceeded. Usually, the main output of the of Hazard Analysis is the mean annual frequency of exceedance (i.e. $\lambda(IM)$) of the ground motion IM at the building site, considering the type and geometry of nearby faults and their distance to the site, local site conditions, etc. (Field 2005).

The IM is representative of the "strength" of an earthquake ground motion, and it is used to predict the response of a structure. Different IM can be adopted for the analyses, that can be a single parameter, IM (e.g. $S_a(T_1)$) or a vector-valued IM (Baker and Cornell, 2005).

Hazard Analysis can be performed deterministically or probabilistically. In Deterministic Seismic Hazard Analysis (DSHA), the ground motion hazard is evaluated based on a particular seismic scenario (Kramer, 1996), while in Probabilistic Seismic Hazard Analysis (PSHA), first proposed by Cornell (1968), uncertainties in size, location, and occurrence rate of earthquakes in the estimation of seismic hazard are incorporated. The outcome of a PSHA is expressed in terms of the Mean Annual Frequency (MAF) of exceedance of IM (i.e., $\lambda(IM)$) and is represented by the mean seismic hazard curve.

Structural Analysis

Once PSHA is performed and an analytical model of the building is built, a vector of engineering demand parameters (*EDPs*) is obtained through structural analysis. These EDPs are used to estimate damage in single members of structure contributing to losses, and thus, EDP vectors should include all relevant building responses that are well correlated with damage in structural, non-structural components and contents of the building. The relationships between *IM* and *EDPs* can be obtained through nonlinear time-history analyses of the building model that should include all components significantly contributing to structural strength and stiffness (i.e. structural, non-structural systems, and soil-structure interaction). The potential collapse is evaluated at this stage. The output of the Structural Analysis step is Conditional probabilistic estimate of engineering demand parameters (P[EDP|IM]) at increasing levels of ground motion intensity.

Damage Analysis

In this step, EDPs obtained from the structural analysis step are related to damage measures in single building components. Building components are usually classified into three different types: structural, non-structural, and content. For each component, a

variable, defined as the Damage Measure (DM), describes the level of damage experienced in an earthquake. DMs are defined as a function of level of damage that trigger different repairs or replacement actions of building components due to the damage induced by earthquakes. Damage analysis uses fragility functions to probabilistically describe damage to building components, defined through DMs, as a function of the engineering demand parameters, that is, (P[DM|EDP]). The main difficult of this step relies on the necessity to identify damage states in building components and then to obtain relationships between EDPs and DMs in the form of P[dm =DM | edp = EDP], i.e. the probability of being in damage state DM, given that the variable edp is equal to the value of EDP.

Loss Analysis

Through this step, the component DMs are related to DVs through probabilistic loss models, (P[DV|DM]). DVs are usually divided into three categories of losses: monetary loss, downtime loss, and life loss. Different probabilistic representation of such DVs could be used.
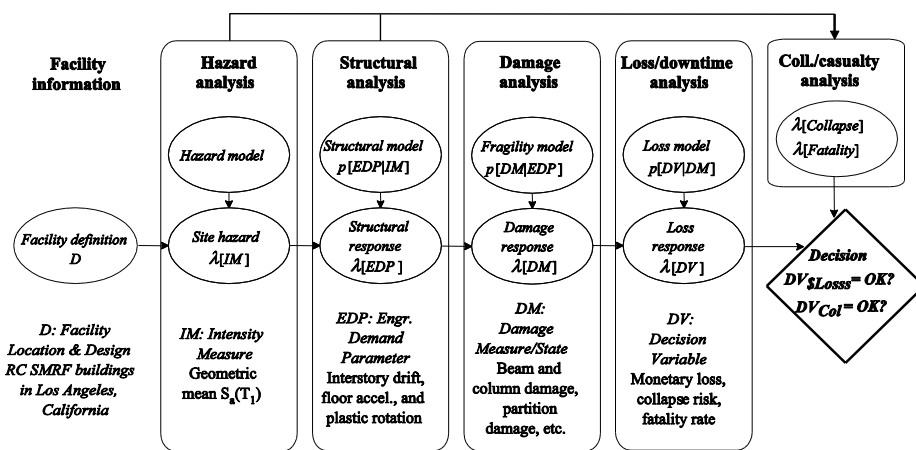
Fig. 4.1 Schematic of PBEE methodology (from Porter, 2004)

Using the aforementioned four stages, the process of executing the Performance-Based Assessment methodology can be completed. The outcome of this methodology is a probabilistic representation of *DVs*. Where the Decision Variable is often expressed in terms of loss (economic losses, downtime and fatalities). Furthermore, the ATC-58 project concluded that while some stakeholders find it more useful to work with simple measures of economic losses in order to make their decisions, others prefer more complex measures of economic losses (ATC, 2012).

In order to compute measures of seismic performance that provide information also on the dispersion of the losses, according with ATC-58 project, three probabilistic representations of DV can be calculated through PEER loss estimation methodology: 1) Probability of exceeding a certain dollar loss in a given earthquake with known intensity; 2) Probability of experiencing a dollar loss larger than a certain amount at any time during the lifetime of the building and 3) Probability of having a loss equal to or larger than a certain amount.

Finally three different types of performance assessments are possible according to FEMAP-58 (ATC 2011): 1) Intensity-based assessment, that enables development of performance functions conditioned on the occurrence of a particular ground shaking intensity; 2) Scenario-based assessment, that provides performance functions conditioned on the occurrence of a particular earthquake scenario defined by an event magnitude and distance from the building site, taking into account uncertainty in ground shaking intensity, given the defined event and 3) Time-based assessment, that produces performance functions considering all possible earthquake scenarios and the annual occurrence frequency of each scenario, taking into account occurrence uncertainty.

Although PEER loss estimation methodology is similar to other loss estimation methodologies, it mainly differs because: 1) Damage states of building components are defined based on actual repair costs; 2) It is a probability-based methodology, intending that it is presented in a probabilistic format that incorporates propagation of uncertainty in different steps of the approach and from different sources of uncertainty; 3) It properly account for the probability of collapse to monetary losses (Zareian and Krawinkler, 2006).

Since the PEER methodology requires a much higher level of expertise with respect to common engineering practice, more recently, the Applied Technology Council's Project 58 (ATC, 2012) has formalized the performance-based seismic design methodology to promote the use of building specific loss assessment in common practice developing a series of guidelines and companion tools.

4.1.3 CALCULATION OF REPAIR COSTS

During an earthquake ground motion, several components within the building may be affected by building response and, consequently, damaged. Those components can significantly contribute to the global building loss, while other components may be not affected by seismic motions at all and are treated as a loss only in the event of collapse ("rugged components"). Beck et al. (2002) showed that the building components that mostly contribute to repair cost are structural members, partitions and interior paint (i.e., non-structural components). In particular, nonstructural damage has be shown as major cost contributor even at low levels of shaking. A real-life example is for the Holiday Inn Hotel in Van Nuys, which suffered little damage in the 1971 San Fernando earthquake, and more significant damage in the 1994 earthquake. For this structure, nearly 80% of

the repair costs after the San Fernando event were associated with nonstructural damage (Trifunac et al. 1999).

Ramirez et al. (2012) showed that repair costs might significantly vary depending on building height and other architectural and structural design parameters. However, general agreement exist about the fact that nonstructural elements can be considered principal contributors to building repair cost. In fact, several authors have highlighted the importance of nonstructural damage in direct loss assessment, which is mostly derived from the fact that non-structural elements comprise a significant portion of the total construction costs of a building (Taghavi and Miranda, 2003, Miranda et al. 2004, Aslani and Miranda 2005). Damaged partitions, in particular, have been identified as a large contributor to economic losses by Mitrani-Reiser and Beck (2007) and Goulet et al. (2007). It is worthy to note that results of loss analyses strictly depends on assumptions made about building content and assumed repair costs. Since no agreement still exist, different authors obtained very different results in terms of economic losses when analyzing the same case-study building (e.g. the Van Nuys testbed).

4.2   LOSS ANALYSIS FOR CASE-STUDIES BUILDINGS

After a seismic event, a number of possible alternatives for dealing with a building damaged by an earthquake that can goes from the acceptance of the damage up to the building replacement is available. For this reason, there is the need of effective policies that can address towards reparability decisions for damaged buildings as support during the decision-making process. Despite life safety remains the most important element that can lead toward reparability decisions, effective earthquake repair policy and individual decisions require reliable estimates of future seismic performance under different aspects. From this perspective, economic losses are an alternative metric of building performance. For more rational decision making about risk management, prediction of earthquake-induced losses can be used by building owners and designer, Krawinkler and Miranda (2004). In fact, quantification and reduction of building's vulnerability to losses due to future earthquakes, may provide a financial incentive for owners of existing structures to seismically upgrade their buildings, or, after a damaging earthquake, a guidance during decision whether to repair, upgrade or demolish the damaged building. In a preventive way, if the retrofit also decreases economic losses, this provides an additional inducement for building owners to mitigate deficient structures along with considerations about the sole seismic safety, similarly, after a seismic event, costs and benefits of repairing, retrofitting or replacing these structures should be considered during the decision process.

In this section, economic losses due to seismic damage in non-ductile RC frames are assessed and compared for two case-study structures. These evaluations use loss

estimation methodologies developed by the Pacific Earthquake Engineering Research Center (see §4.1.2).

4.2.1   BUILDING-SPECIFIC LOSS METHODOLOGY

Building-specific loss estimation represents a probabilistic method that allows the prediction of economic losses that a specific structure may incur due to a given earthquake. Recent studies (e.g., Beck et al. 2002, Aslani 2005, Mitrani-Reiser 2007 and Ramirez 2009, 2012) have adopted the PEER framework for performance-based earthquake engineering to develop methods and data for building-specific loss estimation. Given the intent to examine the significance of calculated losses to policy decisions regarding older RC frame structures, this study utilizes work by Aslani (2005) and Ramirez and Miranda (2009) to assess direct economic losses, and readers are referred to these references for a more detailed discussion.

As stated in §4.1.3, economic losses may be attributed to damage to building contents, repairs of structural or non-structural elements, or business interruption. In this study the performances are expressed as probable consequences only in terms of direct earthquake-economic losses (i.e., building repair/replacement costs) resulting from building damage, while indirect losses (i.e., repair time) or human losses (i.e., deaths or serious injuries) have been neglected. Furthermore, the response analyses are performed on a 2D model that is assumed to represent the maximum response in terms of EDP (i.e., the analysis is only performed in a single direction and it is assumed that EDP in one direction assumes the same value in the orthogonal direction).

The general approach to loss estimation relies on structural analysis to calculate engineering demand parameters (EDPs) such as deformations and accelerations in the structure during an earthquake, which are used to predict to damage in structural elements, non-structural components, and building contents. The cost of providing needed repairs is determined directly from the damage state of the building's components.

4.2.2   FRAGILITY AND PERFORMANCE GROUPS

The building performance model used to assess direct economic losses due to future earthquakes is an organized collection of data used to define the building assets at risk and their exposure to seismic hazards (ATC, 2012). The data required to populate the model can be grouped into "rugged" and "damageable" components. Damageable components, can be damaged by the response of the building to earthquake shaking, while rugged components only contributes to total building cost. Total building cost is used as reference cost for leading reparability decisions.

Data for vulnerable components must include information on the types of damage these can sustain, the structural demands that cause this damage, and the consequences of the damage in terms of repair methods and repairs costs.

All vulnerable structural components, nonstructural components, and contents are categorized into fragility groups and performance groups. Fragility groups are sets of similar components having the same potential damage characteristics in terms of vulnerability and consequences, while performance groups is a subset of fragility group components that are subjected to the same earthquake demands (e.g., story drift, floor acceleration, in a particular direction, at a particular floor level) in response to earthquake shaking. For instance, a fragility group is composed by columns of the same height (that reach the same damage for the same EDP demand), while a performance group is composed by all column at the same storey (i.e. experiencing the same demand). The quantity of components and contents within a building and within each performance group can be determined from a building-specific inventory.

Individual performance groups can be designated as having either correlated or uncorrelated damage. Correlated damage means that all components within a performance group will always have the same damage state. If a performance group is designated as uncorrelated, then each component in a performance group can have a different damage state.

4.2.3 ENGINEERING DEMAND PARAMETERS

In this study, in order to incorporate both structural and non-structural elements into a comprehensive loss framework, the various types of components that are included in the inventory of a building must be assigned to engineering demand parameter (EDP) causing their damage. In particular, interstorey drift ratio (IDR) and peak floor acceleration (PFA) are the sole EDPs considered in this study. Components vulnerable to IDR are the so-called "drift-sensitive" components, while components vulnerable to acceleration are often referred as "acceleration-sensitive".

4.2.3.1 GENERATION OF ADDITIONAL EDPs
As reported in §4.1.2, the PEER methodology seeks to treat every aspect of the seismic risk of a structure in a probabilistic manner. Given that a closed form solution of the multi-level PEER integral is difficult, especially for systems as complex as real buildings, in 2004 an application of this framework was developed utilizing a modified Monte Carlo approach to implement the integration using inferred statistical distributions of building response obtained from limited suites of analyses. This application was adopted by Yang et al. (2009) and further extended in FEMA P-58 (ATC 2011) to incorporate the effects of modeling uncertainty and additional ground motion

uncertainty. To assess uncertainty and explore variability in building performance, this process would ideally involve performing a large number of structural analyses, using a large suite of input ground motions, and analytical models with properties that have been randomly varied. The generation of additional EDPs requires the assumption that EDPs are jointly lognormal. This assumption was found to be realistic for both of the EDPs here adopted (e.g., Aslani and Miranda 2005). In particular, uncertainties in building response due to record-to-record variability was here considered selecting a set of 31 natural accelerograms, while structural modeling uncertainties (e.g., concrete strength) are not explicitly modeled in the damage and repair-cost analyses for the non-collapse cases, consequently an additional uncertainty related to the sole modeling uncertainty has been considered according to FEMA P-58 (ATC 2011).

The generation of additional EDPs allows a large number of earthquake realizations. Each realization represents one possible building performance outcome in response to earthquake shaking, and each realization requires a unique set of demands to determine damage states and resulting consequences.

4.2.4 DESCRIPTION OF BUILDING COMPONENTS AND CONTENTS

When assessing economic losses due to seismic events, a more comprehensive description of both structural and non-structural damageable elements existing in the buildings. Together with the library of fragility functions in the loss estimation toolbox, these provide the needed input to evaluate earthquake-induced losses.

Economic losses are predicted for two non-ductile RC moment frames described in Chapter 3. Structural and nonstructural architectural details and building replacement costs are described below. For the American case-study architectural layouts, components and cost of new elements have been adopted from Aslani and Miranda (2005). While for the Italian case-study, for comparison purposes, similar contents and architectural layouts have been assumed with a slight modification as it will be explained below.

4.2.4.1 STRUCTURAL COMPONENTS

American case-study building

The structural system of the building is composed of perimeter moment-resisting frames and interior gravity-resisting frames (flat slabs and columns). At the second floor the slab has a thickness of 25 cm (10 in.), form the third to seventh floors it decreases to 21.25 cm (8.5 in.) and at the roof level is 20 cm (8 in.). The exterior columns are rectangular and have a constant dimensions throughout the height of the building, 50 x

35 cm (20 x 14 in.). The dimensions of the spandrel beams are almost the same for the longitudinal and transverse directions however, their dimensions decrease in the upper stories. At the second floor the longitudinal beams are 75 x 40 cm (30 x 16 in.) and the transverse ones are 75 x 35 cm (30 x 14 in.). For the third to seventh floors the height of the spandrel beams decrease from 75 cm (30 in.) to 56.25 cm (22.5 in.). The columns weak axis is perpendicular to the longitudinal direction. The interior columns have a square section of 50 x 50 cm (20 x 20 in.) at the first story, which decreases to 45 x 45cm (18 x 18 in.) in the upper stories.

Position	Slab thickness (in)	Longitudinal spandrel beams (in x in)	Transverse spandrel beams (in x in)	Exterior column sections[1] (in x in)	Interior column sections (in x in)
Ground floor	3.9	-	-		
				20x14	20x20
2nd floor	10	30x16	30x14		
				20x14	18x18
Typical floor	8.5	22.5x16	22.5x14		
				20x14	18x18
Roof floor	8	21.5x16	21.5x14		

[1]Exterior column weak axis is longitudinal direction

Table 4-1 Structural system layout for American case-study

Italian case-study building

The structural system of the building is composed of plane moment-resisting frames oriented in the transversal direction. Flooring system are composed by cast-in-place slabs having a constant thickness equal to 25 cm (10 in.), except for the roof where the thickness is equal to 30 cm (11.8 in.). Both interior and exterior columns are rectangular and have a constant dimension at the same story starting form 40 x 60 cm (16 x 23.6 in.) at the first decreasing along the height up to 30 x 40 cm (12 x 15.7 in.) at the upper story. Column weak axis is parallel to the longitudinal direction for any column. Two different types of beams define the structural layout: spandrel and flat beams. Flat beams are disposed in the sole exterior parallel frame close to the stairwell, and their dimension is the same for each floor and equal to 25 x 145 cm (9.8 x 57 in.). Remaining two longitudinal frames have 60 x 30 cm (23.6 x 11.8 in) spandrel beams of constant section for any floor. Spandrel beam of transverse frames have a section dimension that reduces along the height of the building starting form 60 x 30 cm (23.6 x 11.8 in.) up to 40 x 30 cm (15.7 x 11.8 in.) for the roof floor. Specification for structural system layout is reported in Table 4-2.

Position	Slab thickness	Longitudinal spandrel beams	Column sections
	(in)	(in x in)	(in x in)
Ground floor	10	-	
			23.6x15.7
2nd floor	10	23.6x15.7	
			19.1x15.7
3rd floor	10	21.6x13.8	
			17.7x15.7
4th floor	10	19.7x13.8	
			15.7x15.7
5th floor	10	17.7x13.8	
			15.7x13.8
6th floor	10	17.7x13.8	
			15.7x11.8
Roof floor	11.08	15.7x11.8	

Table 4-2 Structural system layout for Italian case-study

Note that for the Italian building, the sole joints of the exterior frame have been considered as vulnerable to earthquake, while, according to observation during past earthquakes, interior confined joints are assumed to be "rugged components".

4.2.4.2 NONSTRUCTURAL COMPONENTS AND ARCHITECTURAL LAYOUT

Architectural layouts as well as the number and dimension of columns, beams, joints and slab-column connections are used to populate tables of damageable assemblies needed for loss analysis. A representative layout and inventory of non-structural and structural elements characteristic of an hotel building were considered for the purpose of estimating damage and repair costs to structural members, partitions, ceilings, glazing, piping, HVAC (heating, ventilating and air conditioning) system, and other building-specific components. To be consistent with the cost analysis of both buildings, the building inventory reported in Aslani and Miranda (2005) has been adopted when analyzing performance response in terms of direct losses of the American building and a similar layout has been assumed for the Italian one. Slight modification due to dimensions of the building and construction technologies have been assumed when considering the architectural layout of the Italian building.

4.2.4.3 COSTS OF NEW ELEMENTS

The total construction cost of the American case-study building was $ 1,300,000 in 1966 dollars, as reported by John A.Blume & Associates (1973). The cost would be equivalent to $ 12,284,000 in 2014 dollars using Engineering News Records construction cost indexes (ENR, 2014). Aslani and Miranda (2009) assumed that the 17% of the

construction cost for the Van Nuys Holiday Inn was corresponding to structural components. Considering five categories of structural components and estimating the portion of construction cost for each assumed category, cost of new structural component was estimated by dividing the construction cost of a single category of structural components to the total number of components in the case study building. Cost of new structural components assumed by Aslani and Miranda (2009), has been here adopted, but actualized to costs in 2014. The total construction cost for the Italian case-study building has been assumed to be equal to $ 2,749,615. It has been calculated by summing the cost of all nonstructural components and contents, obtained by suitably scaling costs adopted for the American building (substituting cost for partitions which typology significantly differs), and the cost of the structural system estimated for the specific construction typology estimated based on regional construction cost documents for Campania (Pezziario Regione Campania 2014).

The cost for new structural components and for new elements is reported in Table 4-3 and Table 4-4, for both Italian and American building.

Component	Cost of new	
	American	Italian
Slab-column connections	8503	0
1st story columns	2542	1853
Columns in other stories	1581	2038
Interior beam-column connections	5233	5233
Exterior beam-column connections	2616	2616

Table 4-3 Cost of new damageable structural components in 2014 dollars [adapted from Aslani and Miranda, 2005]

Group Name	List of components in the group	Cost of new per story			
		American		Italian	
		First-story	Other-Storeys	First-story	Other-Storeys
Partitions	Partitions, Facade, Wall finishes, Doors, Walls	292863	444751	32631	39623
DS$_3$ Partition-like	Floor finishes, Sinks, Power outlets, Light switches	94681	97252	25136	25818
Windows group	Windows	118871	99060	36817	52745
Generic Drift-Sensitive	Vertical piping, Bath tub, F.H.C., Ducts, Elevator	268805	338086	52089	112627
Suspended Ceilings	Suspended ceiling, Horizontal piping, Vents,Plaster ceiling, Light fixtures	236753	197165	62853	52343
Acceleration-Sensitive	Fire protection system, HVAC, Heating, Cooling, Pumps, Plumbing, Elevator, Toilets	259851	210393	50354	70088

Table 4-4 Cost of new damageable structural components in 2014 dollars [adapted from Aslani and Miranda, 2005]

4.2.4.4 FRAGILITY GROUPS AND REPAIR COSTS

As reported in §4.2.2, fragility groups are sets of similar components having the same potential damage characteristics in terms of vulnerability and consequences. Fragility functions are often used to relate damage and consequences (costs). Fragility functions and repair-costs (to restore the building to an undamaged state) are usually created using experimental data, analytical investigation, expert opinion, or some combination of these. A lognormal distribution is commonly used to quantify the uncertainty in the fragilities corresponding to the various damage states for each damageable component (Porter 2000, Beck et al. 2002, Aslani and Miranda 2004). Therefore, median capacity and logarithmic standard deviation of capacity (expressed in terms of EDP value that causes a component to reach or exceed a given damage state) are used to create the fragility function. The repair cost associate to each damage state, relates the damage to consequences expressed in terms of repair cost.

Fragility functions (median and logarithmic standard deviation) and repair costs, adopted in this study are summarized in Table 4-5 to Table 4-7, where m and β represent the median and the logarithmic standard deviation, respectively, and E is the expected value of the repair cost expressed as a fraction of cost of new element.

* as defined in Pagni and Lowes (2006)

Component	Damage State	EDP	Fragility Function Parameters		Repair Cost
			m	β	E
Columns	DS1 Light Cracking	IDR (%)	0.35	0.33	0.10
	DS2 Severe Cracking		1.00	0.44	0.50
	DS3 Shear Failure		2.60	0.55	2.00
	DS4 Loss of Vertical Carrying Capacity		6.80	0.38	3.00
Beam-Column subassembly	DS1 Method of Repair 1*	IDR (%)	0.65	0.35	0.14
	DS2 Method of Repair 2		1.20	0.45	0.47
	DS3 Method of Repair 3		2.20	0.33	0.71
	DS4 Method of Repair 4		3.00	0.3	1.41
	DS5 Method of Repair 5		3.60	0.26	2.31
Slab-Column subassembly	DS1 Light Cracking	IDR (%)	0.40	0.39	0.10
	DS2 Severe Cracking		1.00	0.25	0.40
	DS3 Punching Shear Failure		4.40	0.24	1.00
	DS4 Loss of Vertical Carrying Capacity		5.40	0.16	2.75

Table 4-5 Fragility function & expected repair cost (normalized by component replacement cost) parameters for non-ductile structural components [after Ramirez and Miranda (2009)]

Component		Damage State	EDP	Fragility Function Parameters		Repair Cost
				m	β	E
Partitions (including fecade)	DS1	Visible damage and small cracks in gypsum board that can be repaired with taping, pasting and painting	IDR (%)	0.21	0.61	0.1
	DS2	Extensive crack in gypsum board that can be repaired with replacing the gypsum board, taping, pasting and painting		0.69	0.4	0.6
	DS3	Damage to panel and also frame that can be repaired with replacing gypsum board and frame, taping, pasting and painting		1.27	0.45	1.2
Partition-like	DS1		IDR (%)	1.27	0.45	1.2
Windows	DS1	Some minor damages around the frame that can be repaired with realignment of the window	IDR (%)	1.6	0.29	0.1
	DS2	Occurrence of cracking at glass panel without any fall-out of the glass that can be repaired with replacing of the glass panel		3.2	0.29	0.6
	DS3	Part of glass panel falls out of the frame. The damage state can be repaired with replacing of glass panel		3.6	0.27	1.2
Generic-Drift	DS1	Slight Damage	IDR (%)	0.55	0.6	0.03
	DS2	Moderage Damage		1	0.5	0.1
	DS3	Extensive Damage		2.2	0.4	0.6
	DS4	Complete Damage		3.5	0.35	1.2
Ceilings	DS1	Hanging wires are splayed and few panels fall down. The damage state can be repaired with fixing the hanging wires and replacing the fallen panel.	PFA (g)	0.3	0.4	0.12
	DS2	Damage to some of main runners and cross tee bars in addition to hanging wires. The damage state can be repaired with replacing the damaged parts of grid, fallen panels and damaged hanging wires.		0.65	0.5	0.36
	DS3	Ceiling grid tilts downward (near collapse). The damage state can be repaired with replacing the ceiling and panels.		1.28	0.55	1.2
Generic-Acceleration	DS1	Slight Damage	PFA (g)	0.7	0.5	0.02
	DS2	Moderage Damage		1	0.5	0.12
	DS3	Extensive Damage		2.2	0.4	0.36
	DS4	Complete Damage		3.5	0.35	1.2

Table 4-6 Fragility function & expected repair cost (normalized by component replacement cost) parameters for non-structural components [after Ramirez and Miranda (2009)]

In order to perform the loss analysis for the Italian building, a different fragility curve was assumed for Italian partition which behavior significantly differs from that of drywall partitions.

Component	Damage State		EDP	Fragility Function Parameters		Repair Cost
				m	β	E
Partitions	DS1	Minor damage	IDR (%)	0.03	0.02	0.1
	DS2	Moderate damage		0.4	0.3	0.4
	DS3	Major damage		0.8	0.4	0.8
	DS4	Complete damage		1.6	0.4	1.3

Table 4-7 Fragility function & expected repair cost (normalized by component replacement cost) parameters for Italian partitions [adapted form Colangelo (2009)]

4.2.5 RESULTS

The loss assessment procedure outlined in §4.1.2 has been used to carry out the loss simulation for the two case-study buildings. Once the response of the building has been simulated for different intensities (§3.7) corresponding to return periods ranging from 72 to 2475 years (§3.6), the loss analysis has been performed for the case-study buildings using the fragility data and costs reported in §4.2.4.4. In particular, to solve PEER equation integral (Eq. 4-1), a Monte Carlo procedure has been adopted. According to Yang et al. (2009) and FEMA P-58 (ATC 2011), the Monte Carlo approach uses inferred statistical distributions of building response obtained from limited suites of analyses to generate additional response parameters (EDP) that properly incorporate the effects of modeling uncertainty along with ground motion uncertainty (Yang et al. 2009). In this study, 500 realizations have been performed for each intensity level and building. Yang et al. (2009) indicated that stable cost estimates can be obtained with as few as 200 realizations. Fragility groups, as indicated in §4.2.4.4 were divided in subsets of group components subjected to the same earthquake demands (i.e., Performance groups, PG). For each realization and PG, a unique damage state has been determined using a uniform random generator over the interval [0,1] considering the probability of the PG experiencing each damage state at the EDP obtained from structural analysis. Once the damage state for a performance group is identified, the repair action and the associate repair cost for that performance group is obtained by multiplying cost of new elements reported in Table 4-3 and Table 4-4 by corresponding normalized repair costs in Table 4-5 to Table 4-7 by the number of elements in the PG considered. If collapse has not occurred, losses are calculated for each realization based on the damage sustained by each component and the consequence functions assigned to each performance group and by summing repair costs of each PG. If structural collapse was detected, the total repair cost is calculated using the replacement value of the building plus additional costs related to demolition and debris removal (15% of the replacement value of the building).

Ramirez and Miranda (2012) highlighted the importance in the loss estimation of the residual drifts (i.e., when residual drift exceeds a given threshold the building is considered not repairable and it can be treated as a collapse case); however, this topic has not been addressed in this study. Furthermore, it should be recognized that there may be additional costs associated with activities downtime; however, data for these additional costs are not readily available and not included in the current study.

The probability of exceeding a certain level of total repair cost accounting for both the collapse and non-collapse cases (complementary cumulative density function, CCDF) can be calculated using the total probability theorem:

$$P(C \geq x) = P(C \geq x \mid IM, NC)[1 - P(C \mid IM)] + P(C \geq x \mid IM, C)P(C \mid IM) \qquad \text{Eq. 4-3}$$

where $P(C > x \mid IM, NC)$ is the probability conditioned on IM when the structure do not collapses that the normalized repair cost exceeds x, $P(C > c \mid IM, C)$ is the probability of exceeding the normalized repair cost exceeds x given the collapse, that is actually independent from IM and equal to the replacement value of the building, and $P(C \mid IM)$ is the probability of collapse conditioned on IM.

The complementary cumulative distribution of the total repair cost, normalized with respect to the building's replacement cost (including expected demolition costs), is reported in Fig. 4.2 for the American case-study building and in Fig. 4.3 for the Italian case-study building.
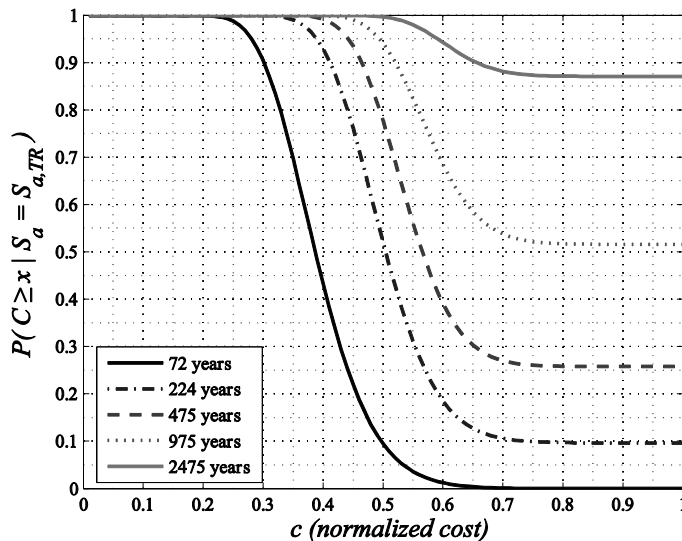
Fig. 4.2 Probability of exceeding normalized cost at five different hazard levels for the American case-study
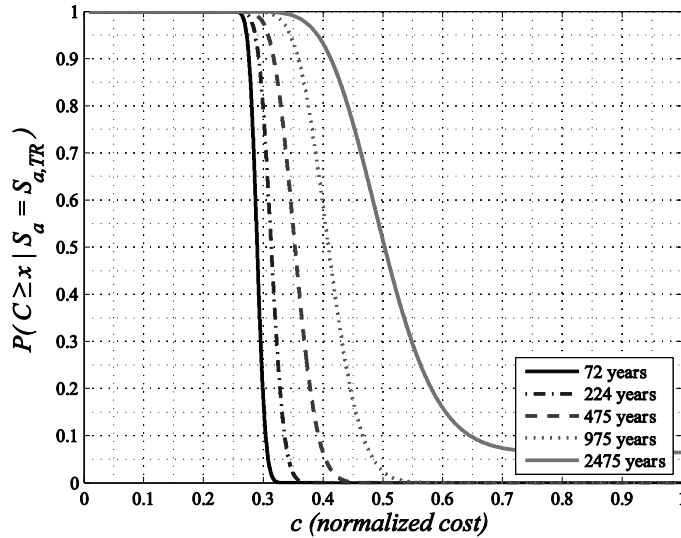
Fig. 4.3 Probability of exceeding normalized cost at five different hazard levels for the Italian case-study

With the increase of the damaging seismic action (i.e., return period), the repair cost inflates making the curve translate rightward. This effect of the seismic action, see Fig. 4.2 and Fig. 4.3, is numerically represented in Table 4-8 and Table 4-9 where median and percentiles for results are reported and in Table 4-10 and Table 4-11, where median and logarithmic standard deviation, conditioned on non-collapse, are reported for the fitted lognormal distribution for the Italian and the American building, respectively. In particular, Table 4-10 and Table 4-11 show through logarithmic dispersion of data that along with an increase of median normalized repair cost, also an increase of results dispersion occurs.

Furthermore, similarly to results from computation of residual building's capacity conditioned on the mainshock intensity, the total normalized repair cost conditioned on the return period of the damaging action at the site is strongly influenced by occurred collapse cases. This effect is particularly evident for the American case-study building depicted in Fig. 4.2, where with the increasing of the seismic action the second part of the Eq. 4-3 produces the major contribution to the repair cost making the curve translate upward.

As it can be evidenced from analysis of Fig. 4.2 and Fig. 4.3, the probability of exceeding a normalized total repair cost of 20-25% is equal to the 100% for both building and any level of the damaging action. This high cost is due to the contribution of nonstructural components and contents, which result damaged since a return period for seismic action of 72 years. In fact, Fig. 4.4 and Fig. 4.5 (b) to (f) show the contribution to total repair cost of different fragility groups considered in this study for return period ranging from 72 to 2475 years as a function of the realization number. These results are conditioned on non-collapse during strong motion. For both building is evident that the

143

nonstructural components and building's contents play an important role in the definition of repair costs. Since the return period of 72 years, the contribution of suspended ceilings and General acceleration-sensitive components result damaged, while for higher return periods the contribution of structural components take influence in the definition of repair costs. For instance, for the Italian building, Fig. 4.5(b) shows that sole contributors to cost are suspended ceilings and General acceleration-sensitive components, while a slight contribution is due to the repair cost for partitions, and other structural and nonstructural component do not exhibit significant damage. For increasing damaging actions, Fig. 4.5(d), the contribution of suspended ceilings and General acceleration-sensitive components cannot further increase, while the repair cost of columns and partitions play an important role. When the expected action at the site is the most, Fig. 4.5(f), for some realizations, the repair cost of partitions do not increase because the maximum damage has been reached for the 975 years intensity, while the contribution of column's repair cost is very high.

Although for the same return period, the level of seismic actions is almost twice that for the Italian site, and a direct comparison cannot be done, it is interesting to note that the contribution of repair cost of columns for American building is not negligible since lower return periods, Fig. 4.4. In addition, partition contribution to cost results very high since a return period of 72 years, Fig. 4.4 (b), and results to be the major contributor to repair costs for any return period.

	c (normalized repair cost)				
Return Period	72	224	475	975	2475
16th percentile (%)	46.9	62.7	100.0	100.0	100.0
median (%)	38.3	50.7	56.9	100.0	100.0
84th percentile (%)	31.0	42.6	47.9	54.1	100.0

Table 4-8 Percentile values for normalized repair cost of the American building conditioned on the return period level

	c (normalized repair cost)				
Return Period	72	224	475	975	2475
16th percentile (%)	30.2	33.1	38.6	45.3	60.3
median (%)	29.0	31.4	35.5	40.8	50.5
84th percentile (%)	27.9	29.7	32.6	36.7	43.2

Table 4-9 Percentile values for normalized repair cost of the Italian building conditioned on the return period level

Return Period (yrs)	72	224	475	975	2475
median	0.39	0.49	0.53	0.58	0.61
β	0.19	0.15	0.12	0.12	0.10

Table 4-10 Median and logarithmic standard deviation (*β*) of the lognormal fitted fragilities for the normalized repair cost (c) of the American building conditioned on the return period level and for non-collapse cases.
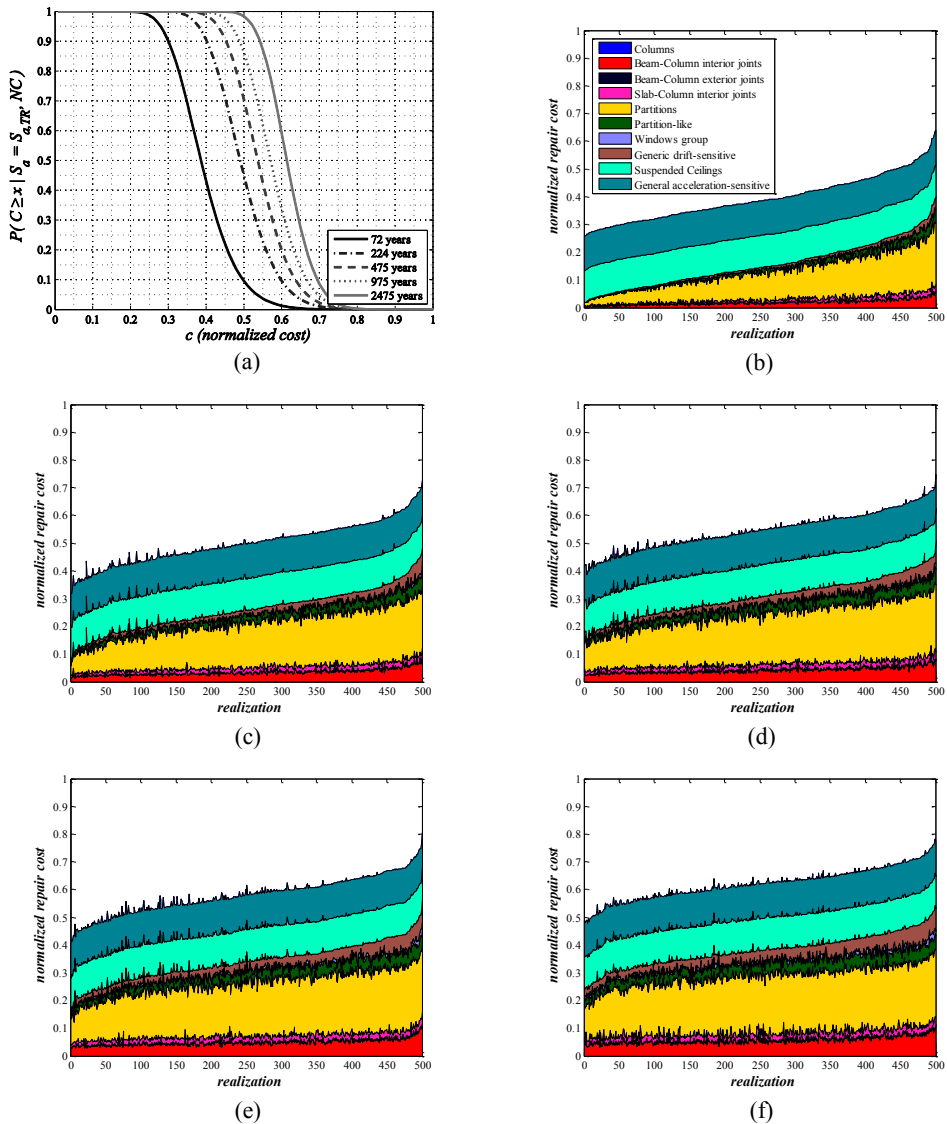
Fig. 4.4 American case-study: (a)Probability of exceeding normalized cost at five different hazard levels conditioned on Non-collapse cases; component contribution to normalized repair cost for (b) 72 years, (c) 224 years, (d) 475 years, (e) 975 years, (f) 2475 years return period.

Return Period (yrs)	72	224	475	975	2475
median	0.29	0.31	0.35	0.41	0.49
β	0.04	0.06	0.08	0.11	0.14

Table 4-11 Median and logarithmic standard deviation (β) of the lognormal fitted fragilities for the normalized repair cost (c) of the Italian building conditioned on the return period level and for non-collapse cases.

(a)

(b)

(c)

(d)

(e)

(f)
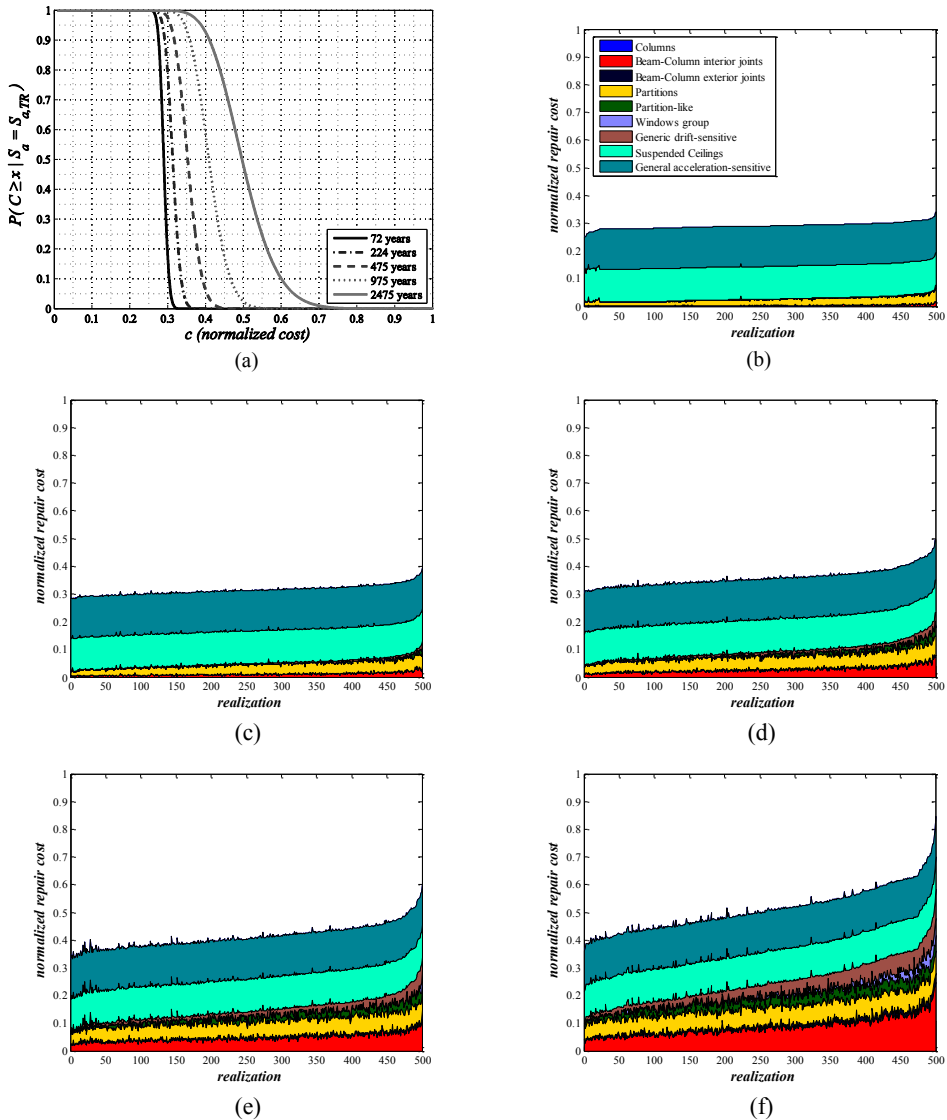
Fig. 4.5 Italian case-study: (a)Probability of exceeding normalized cost at five different hazard levels conditioned on Non-collapse cases; component contribution to normalized repair cost for (b) 72 years, (c) 224 years, (d) 475 years, (e) 975 years, (f) 2475 years return period

Expected Annual Loss

An additional metric for performance-based assessment can be carried out once the expected value of the loss conditioned in the intensity level has been computed: the expected annual loss (EAL). EAL, which can be expressed in dollars, is an effective way of communicating the seismic vulnerability of constructed facilities to owners and insurers.

The EAL can be obtained by integrating the total-cost curve with the site-specific hazard curve, and represents the economic loss that occurs on average every year in the building to repair earthquake damage, considering the frequency and severity of possible future earthquakes. EAL is computed by integrating the mean loss conditioned on ground motion intensity, *E(DV|IM)*, that is, the vulnerability function, over all possible values of the ground motion intensity as follows (e.g., Aslani and Miranda 2004):

$$EAL = \int_{im} E[DV|IM] |d\lambda(IM)| \qquad \text{Eq. 4-4}$$

where *E[DV|IM]* is the expected value of the decision variable conditioned on *IM* and *dλ(IM)* is the derivative of the seismic hazard curve (Fig. 3.60) evaluated performing the PSHA at the site as a function of a ground motion intensity measure, IM. Here the DV is the normalized repair cost.

The expected repair cost for a given IM, accounting for both the collapse and non-collapse cases, can be calculated using the total probability theorem:

$$E(DV|IM) = E(DV|IM,NC)[1 - P(C|IM)] + E(DV|IM,C)P(C|IM) \qquad \text{Eq. 4-5}$$

where *E(DV|IM,NC)* is the expected repair cost of the system conditioned on *IM* when the structure does not collapse, *E(DV|IM, C)* is the expected repair cost of the system when the structure collapses, *P(C|IM)* is the probability that structure collapses for a given IM.

Liel and Deierlein (2008) examined eight different non-ductile 1967 RC frames, ranging from two to twelve stories and with space or perimeter MRF, finding that EAL values can range from 1.6 % to 5.2 % with an average of 2.5 % of replacement cost suggesting that a possible "non-ductile" range of EAL could be 1.5–3.0 % (Calvi, 2014).

The American case-study building, the Van Nuys Holiday Inn, has been extensively studied by several authors which prediction of EAL significantly varies depending on assumption associated to fragility functions, building contents, and construction and replacement cost. For instance, Porter et al. (2004), estimated a replacement cost of 7 $M in 2001 USD and a EAL expressed as a function of replacement cost of 0.77%, Krawinkler (2005) estimated a replacement cost of 9 $M in 2002 USD and a EAL equal to 2.2%, finally Aslani and Miranda (2004) assumed a replacement cost 9 $M in 2003 USD calculating an EAL equal to 1.57%.

For this study, the EAL is equal to 2.89%, this result is quite different from the 1.57% computed by Aslani and Miranda (2005) from which cost of new components was adopted. This difference is due to different damage fragilities and consequence functions as well as structural model, selected earthquake bin and collapse definition adopted in this study.

For the Italian building the EAL is equal to 0.74%. This value is significantly smaller due to the lower hazard at the site. Furthermore, as highlighted above, this is influenced by limited hazard curve data.

4.2.6   RELATIONS PERFORMANCE LOSS – ECONOMIC LOSS

Performance Loss (PL) is a measure of variation of building seismic capacity from intact to damaged state and also implicitly account for the seismic safety variation after damage. Nowadays, other performance objectives are coming significant for owners and risk managers: providing that safety requirements are met, the question that arises is how much does it cost repair and if it is more convenient to retrofit before earthquakes making the system more resilient and significantly reducing future direct and indirect costs for society. Consequently, repair costs represent a different metric that should properly accounted for during the decision-making process given they can significantly influence choices of owners and risk managers.

Fig. 4.6 and Fig. 4.7 show the relationship between the median PL and the earthquake-induced repair cost for the American and the Italian building, respectively. The continuous black bold line is referred to the median repair cost while dotted lines represent the 16th and 84th percentiles. On the same figures the two PL thresholds as indicated in the San Francisco building code (SF, 2012) of 5% and 20% are reported (only 5% for the Italian PL-c curve). In particular, Fig. 4.6 shows that also for lower PL (corresponding to lower return periods) the repair cost is not negligible. While for higher PL the slope of the curve reduces. This effect can be explained considering the particular nature of repair cost (direct losses), in fact, the sources of repair costs are structural components, nonstructural components, and building contents. These damageable quantities were further divided in drift-sensitive and acceleration-sensitive (mainly building contents). The latter quantities result to be severely damaged also for lower return periods driving to huge repair costs also for a 72 years return period. When the return period increases along with PL, then the increased repair costs are only due to drift-sensitive components and collapses, consequently, repair costs increase with a lower velocity for equal PL increments.
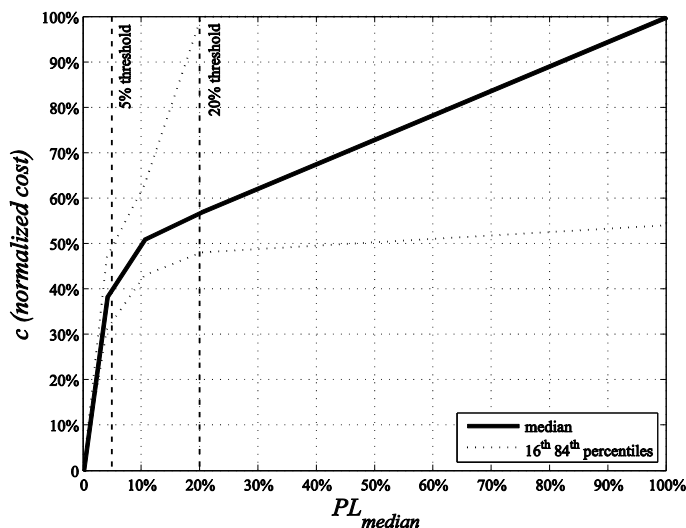
Fig. 4.6 Relationship between median Performance Loss (PL) and normalized cost (c) for the American case-study

The same trend is visible for both buildings, although for the Italian building the maximum PL is equal to 6.16%. For higher PL, the percentile curves show an increment in repair costs dispersion, note that for the American building, when PL is equal to 32%, then, the normalized median repair cost is equal to 57%, while the 16th percentile is equal to 100%. This is due to the number of collapses occurred for the 975 years return period that significantly contribute to global repair costs making them significantly high.
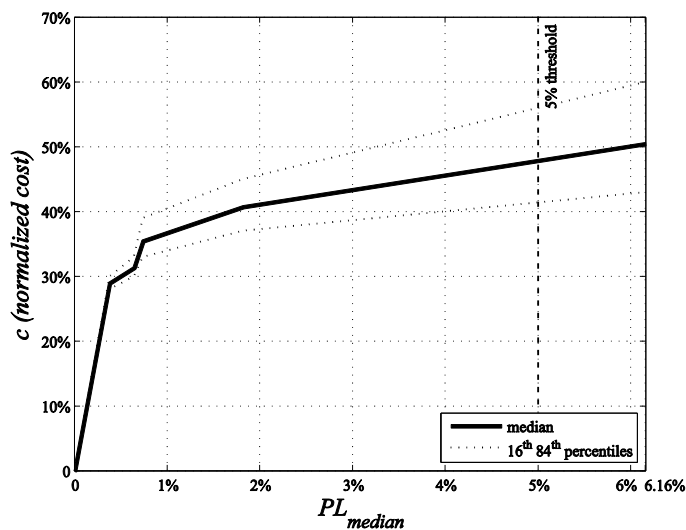
Fig. 4.7 Relationship between median Performance Loss (PL) and normalized cost (c) for the Italian case-study

For the Italian building instead, except that for the 2475 years return period, no collapses occurred; for this reason the dispersion remain within acceptable levels.

PL in this study is conditioned on the site hazard, consequently, for the Italian building PL does not exceed the value of 6.2%; however, it is possible to note that for similar PL both of buildings show similar median normalized repair costs (c): for a PL of 5% c is equal to 40% for the American building while it increases to 48% for the Italian one.

Given that for the sole American case study building the PL-c curve is completely developed, it is interesting to report PL values and corresponding median normalized repair costs, Table 4-12.

PL_{median} (%)	c_{median}(%)
5	40
10	50
20	57
25	60
30	62
50	72

Table 4-12 Median Performance Loss (PL_{median}) and median normalized repair cost (c_{median})

Table 4-12 shows that for two PL thresholds, repair and retrofit respectively, suggested in the San Francisco Building Code (SF, 2012), the median repair costs correspond to 40% and 57% of building's replacement value, respectively.

Another interesting relationship is shown in Fig. 4.8, where Initial performance (IP) and PL are plotted together, as median values. The IP represents the building's capacity in terms of spectral acceleration normalized with respect to the design spectral acceleration for the site. The building's capacity cannot be estimated considering the system-level collapse mechanisms adopted in this study but a component-based collapse approach similar to that proposed in ASCE-SEI 41 (ASCE 2007). In this section, the capacity has been assessed considering the *IDA* curve for the intact building and determining the $S_{a,median}$ corresponding to a prefixed IDR_{max}. This IDR_{max} corresponds to the maximum interstorey drift ratio estimated on the pushover curve for which the first element reaches its ultimate conditions. It is interesting to note that while the American building is non-conforming to seismic provision, having a median capacity that is about 0.75 times the required resistance, the Italian building has a capacity that is almost 2.2 times the capacity required by seismic provisions.
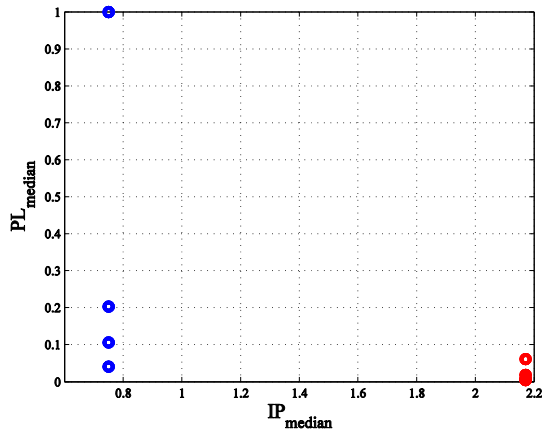
Fig. 4.8 Relation between *PL* and *IP*, for the American (blue markers) and the Italian (red) buildings.

Finally, another comparison can be proposed for the American building, that is between the *PL-c* relationship observable in Fig. 4.6 and a *PL-c* relationship proposed in Polese et al. (2015). This relationship, reported in Fig. 4.9, has been obtained considering a simplified mechanism-based approach that doesn't account for brittle failures, and observed repair costs after L'Aquila earthquake (2009). The relation between PL and c proposed in Polese et al. (2015) for equal PL, leads to lower repair costs, however two methods adopted to carry out these relationship are completely different and based upon different basic hypothesis, and further investigations are required to completely understand the real trend of PL-c curves.
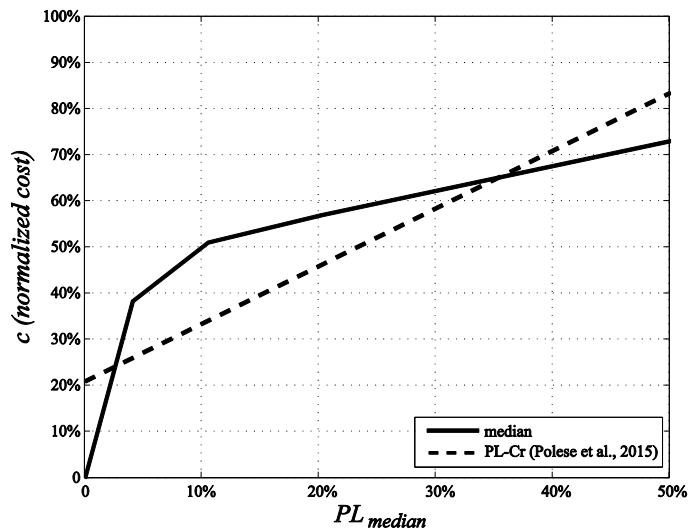
Fig. 4.9 Relation between PL and c, median values, for the American building and the PL-c$_r$ relationship proposed in Polese et al. (2015).

Chapter 5

SIMPLIFIED PROCEDURE FOR ESTIMATION OF RESIDUAL CAPACITY

This chapter address the computation of building's safety decay due to earthquake damage with a simplified approach. The method adopted here is based on the assessment of structural capacity through pushover analyses performed on both the intact structure and in its damaged state through suitable modification of plastic hinge to account for damage. Firstly existing formulations for modifying the moment-rotation plastic hinges of damaged RC columns as a function of damage are analyzed, and then experimental based formulations for modifying the moment-rotation plastic hinges of RC columns that have entered the plastic range are proposed, introducing suitable expressions of modification factors for stiffness, strength and displacement capacity as a function of the rotational ductility demand for typical Mediterranean elements. Those expressions may be used in order to assess the performance loss of a building that has been damaged by an earthquake. Next, applying the simplified methodology with proposed modification factors, damage dependent behavior is estimated for varying levels of initial seismic (damaging) intensity for two case-study building. Finally, the simplified procedure is validated by comparing results of the simplified method with NTH by subsequent application of suitably scaled pairs of accelerograms.

5.1 MOTIVATION

Seismic behavior of damaged buildings, and their relative seismic safety, may be suitably represented by their seismic capacity modified due to damage, the so-called REsidual Capacity (*REC*). In Chapter 3 a probabilistic framework to assess building's residual capacity with a Nonlinear-Time-History-based approach was proposed. Ideally, NTH analyses, that predicts the forces and cumulative deformation (damage) demands in every element of the structural system, would be the best solution for capturing building's seismic performance. In fact, the use of structural models with appropriate stiffness/strength deterioration mechanisms would allow the simulation of response taking into account the cyclic accumulation of damage. The method results to be the

more realistic when simulating the actual behavior of existing buildings allowing to account also for brittle failure of both column and joint as well as introducing two possible system-level collapse (Gravity Load and Sidesway collapse). Despite the advantages connected to the use of this method, it requires advanced knowledge regarding refined simulation methods, dynamic analysis, statistics, as well as remarkable computational efforts. Furthermore, it is hardly suitable for practical design/assessment by engineering professionals. In addition, in order to overcome the sensitivity of dynamic response to the characteristics of the input motions (RTR variability), a suite of representative accelerograms has to be carefully selected, greatly increasing the computational effort.

For the above reasons, it can be preferred to rely on simplified procedure for the assessment of the behavior of damaged buildings. Pushover Analysis (PA) represent an optimal compromise between the need to investigate building's nonlinear behavior and to perform a relatively simple static analysis, applicable for design/assessment purposes by practitioners. Indeed, under the limitation of applying it mainly to building structures oscillating predominantly in a single (fundamental) mode, standard PA allows a sound evaluation of damage progression for increasing levels of seismic demand and investigation of damage distribution within the MDOF systems (Polese et al., 2008).

As explained in Polese et al. (2013a), *REC* may be evaluated based on PA obtained for the structure in different (initial) damage state configurations, where the behavior of the damaged building is simulated with modification of plastic hinges for damaged elements. According to this methodology, if the structural system is represented with a lumped plasticity model, damaged building's behavior may be simulated with a suitable modification of plastic hinges for damaged elements, see Fig. 5.1. Such a modification is based on stiffness, strength and residual displacement reduction factors, λ_k, λ_Q and *RD*, respectively, accounting for the achieved damage states on the structural elements. Based on the type of elements, and observed behavior (e.g. pure flexural, flexure-shear, sliding shear etc.), and considering the damage severity, suitable factors to be applied for modification of plastic hinges in the damaged models may be considered.
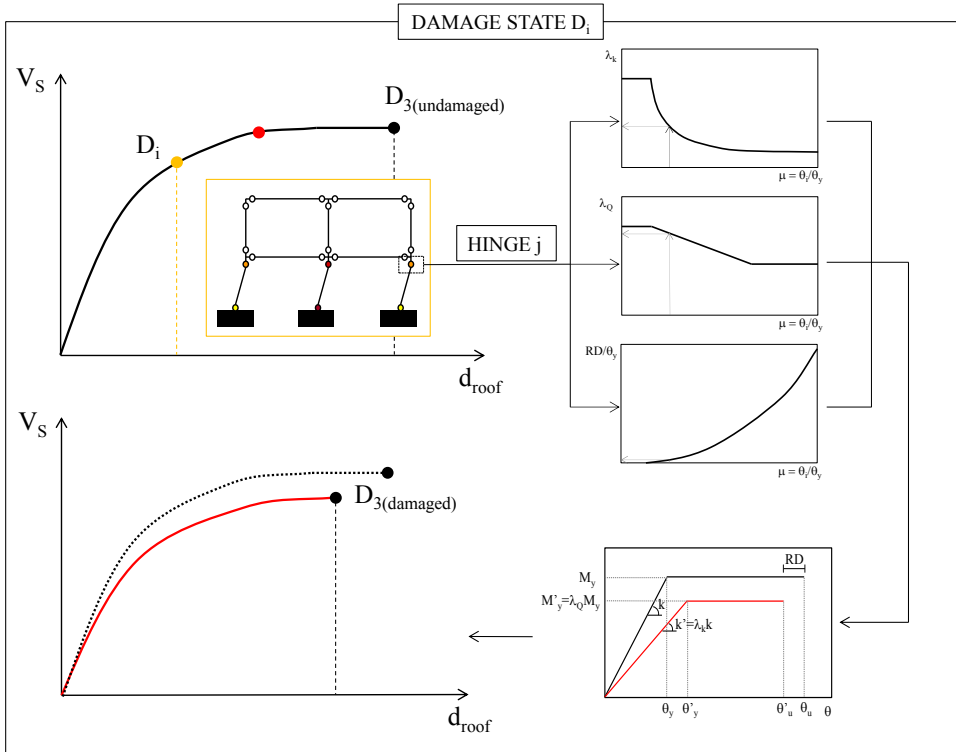
Fig. 5.1 Example application of the plastic hinges modification factors for analytical assessment of post-earthquake behavior (adapted from Polese et al., 2013a).

5.2 EXISTING MODIFICATION FACTORS

In FEMA 307 (1998) values of λ and RD are proposed for various element typologies and behavioral modes; these values are based on experimental calibration and/or on theoretical derivation.

Japanese guidelines for the assessment of buildings capacity in the post-earthquake (Nakano et al., 2004; JBDPA, 2001) suggest a method which takes into account the variation of a seismic capacity index depending on observed damage severity. In these guidelines, the building occupancy assessment depends on the variation of index I_s in the pre-earthquake and post-earthquake stage; I_s is proportional to the product of a strength index C (i.e. base shear) and a ductility index F, representative of the building deformation capacity. In particular, in order to assess post-earthquake condition, a residual capacity percentage index, R, is defined as follows:

$$R = \frac{I_{S,D}}{I_S} \cdot 100 \ (\%)$$

where $I_{s,D}$ is the seismic index on the damaged structure. $I_{s,D}$ can be computed on the basis of a capacity reduction factor, λ, depending on the structural elements hysteretic dissipation capacity in the pre and post-earthquake stage (defined in Fig. 5.2).

Japanese Guidelines suggest different η values, calibrated on experimental tests (Maeda et al.,2004), depending on damage severity level for different element typologies (brittle or ductile columns, walls etc). However, the authors recognize that a wider range of experimental tests are necessary to better calibrate the member residual capacity. The Japanese approach, based on the factor η, is conceptually similar to that reported in FEMA 306 (1998), based on suitable modification of plastic hinges for damaged elements, λ and RD. The values of η (or λ, RD) are mainly representative of reinforced concrete (RC) members such as walls or strong piers that can be typically found in Japanese (or North American) buildings.
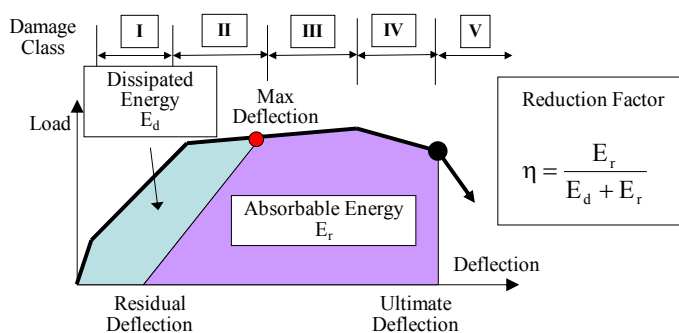
Fig. 5.2 Capacity reduction factor η (after Nakano et al., 2004).

5.3 A PROPOSAL FOR PLASTIC HINGES MODIFICATION FACTORS FOR DAMAGED RC COLUMNS

Starting from the approach proposed in FEMA 306 (1998), guidelines for seismic assessment of damaged buildings were proposed in Bazzurro et al. (2004) and a detailed application of the procedure, which relies on the execution of pushover analyses of the buildings in various damage states, may be found in Maffei et al. (2006) for some steel buildings. However, there are not explicit indications for suitable modification factors to be applied to RC members of buildings in Mediterranean regions, where reinforcement detailing and confinement of columns are usually inadequate (Bal et al. 2008; Verderame et al. 2010). The few indications that may be found for RC columns cannot be indiscriminately used for RC members typical of Mediterranean regions, because their mechanical properties, the type of reinforcement (smooth or deformed bars) and the relative percentage as well as type of detailing, may differ significantly from those of

North America or Japan. Therefore, there is a need for proper calibration of damage–dependent modification factors for plastic hinges of damaged columns representative of existing elements with design characteristics non-conforming to present-day seismic provisions.

This paper presents the methodology and results of such a calibration, performed on 36 cyclic tests on non-conforming columns (23 RC columns reinforced with deformed bars and 13 with smooth ones) extracted from available databases. In particular, modification factors for plastic hinges in flexure are considered, while it is hypothesized that shear failures, due to local shear effects in the elements, and unconfined joint failures are prevented. Indeed, due to the difficulty of capturing axial-load and/or shear failures with simple nonlinear models, the element's shear behavior and joint modeling are often neglected in nonlinear analyses (Dolšek 2010), especially if the latter are oriented to rapid assessment of building vulnerability within a risk analysis framework.

The proposed modification factors are calibrated considering the sole monotonic envelope of column response, while the cyclic degrading due to fatigue effects are neglected; recent studies propose to account for this degrading effect with a proper simulation of the hysteretic behavior (Cuevas and Pampanin, 2014).

In the next section, the database adopted for the study and test selection criteria are presented, while the third section introduces the main parameters extracted from experimental tests. Then, the following sections explain how these parameters are elaborated in order to derive suitable modification factors for stiffness, strength and displacement capacity, respectively.

5.3.1 EXPERIMENTAL DATABASE

In many European countries a very large percentage of RC buildings are 40 years old, or even older; since only in the 1970's early applications of deformed bars appeared, it can be argued that a high percentage of RC buildings have elements reinforced with smooth bars (Fabbrocino, 2005).

Hence, the experimental calibration of damage modification factors proposed in this paper is performed for nonconforming columns reinforced with either deformed or smooth bars.

The database used in this study for elements with deformed bars is mainly constituted by the tests available on the Pacific Earthquake Engineering Research Center's Structural Performance Database (PEER, Berry et al.). The latter includes the results of 416 tests under axial load and uniaxial bending provided by monotonic or cyclic horizontal actions. The selected tests were chosen considering mainly the geometry and reinforcement details, to be representative of existing members in Mediterranean region and with low normalized axial load. In particular, the experimental tests to be used for the calibration of modification factors have been selected based on the following criteria: i) tests performed under cyclic actions; ii) tests on columns with square or rectangular

cross sections; iii) tests on columns under a constant normalized axial load, $\nu < 0.5$ ($\nu = N/(A_c f_{cm})$, with N the axial load, A_c the concrete gross area, and f_{cm} the mean cylindrical concrete strength); iv) tests on columns characterized by poor confinement "nonconforming" to present day seismic codes (i.e. elements with hoops spacing, s, higher than $d/3$, with d effective cross section depth according to ASCE/SEI 41-06 (2007) provisions); v) tests governed by flexural or combined flexure-shear collapse mode (i.e. *condition i* or *ii* according to ASCE/SEI 41-06, 2007).

For columns with transverse reinforcement having 135° hooks, pure flexural failure (*condition i*) is reached if $V_p/(V_n/k) \leq 0.6$, where V_p is the shear demand on the column, V_n is the nominal shear strength, and k is a modifier based on ductility demand; flexure-shear failure (*condition ii*) if $0.6 \leq V_p/(V_n/k) \leq 1.0$; shear failure if $V_p/(V_n/k) \geq 1.0$ (*condition iii*). Further, *condition i* is limited to columns with a transverse reinforcement ratio $A_v/b_w s$ (with A_v cross sectional area of transverse reinforcement, b_w cross-sectional width and s transverse reinforcement spacing) greater than or equal to 0.002 and a spacing to depth ratio less than 0.5. In the case of columns with 90-degree hooks transverse reinforcement, *condition i* is adjusted to *condition ii*.

Based on these selection criteria, a database of 20 tests, extracted from the original PEER database, is obtained (Atalay, 1975; Nosho, 1996; Matamoros, 1999; Lynn, 1996); this selection was enriched with the results of 3 experimental cyclic tests performed at University of Naples Federico II (Di Ludovico et al., 2009), that are all considered as representative for old-type columns since specifically designed for this purpose. Hence a final database of 23 cyclic tests was used for calibration of modification factors for non-conforming RC columns reinforced with deformed bars.

The database for RC elements with smooth bars consists of 13 tests on square or rectangular RC columns specifically designed to be representative of nonconforming elements designed for pure flexure failure (Di Ludovico, 2009, 2012; Verderame et al., 2008a, 2008b; Acun, 2010).

Table 5-1 synthesizes the main parameters characterizing the 23 tests selected for elements with deformed bars, while Table 5-2 refers to 13 tests on elements with smooth bars; the parameters listed in Table 5-1 (or Table 5-2) are explained in more detail in the next section.

It has to be noted that, although some of the tests are characterized by high concrete compressive strength, they have been still included in the database since it has been verified that this parameter does not influence significantly the scatter of modification factors. Furthermore, the selected tests with $\nu=0$ (two out of 23 tests) may be considered as representative for columns with very low axial load that during an earthquake may be unloaded due to reversal cyclic actions; indeed the longitudinal reinforcement of those tests is symmetric, as typical of columns.

		(Atalay & Penzien, 1975)		(Nosho et al. 1996)	(Matamoros et al., 1999)												(Di Ludovico et al., 2009)			(Lynn et al., 1996)				
Reference																									
Specimen		*No.10*	*No.12*	*No.1*	*C10-05N*	*C10-05S*	*C10-10N*	*C10-10S*	*C10-20N*	*C10-20S*	*C5-00N*	*C5-00S*	*C5-20N*	*C5-20S*	*C5-40N*	*C5-40S*	*R300D_c*	*R500d_c*	*S300d_c*	*2CLH18*	*2CMH18*	*3CMD12*	*2SLH18*	*2SMD12*
Label		*AP10*	*AP12*	*Nosho*	*M1*	*M2*	*M3*	*M4*	*M5*	*M6*	*M7*	*M8*	*M9*	*M10*	*M11*	*M12*	*R300D_c*	*R500d_c*	*S300d_c*	*2CLH18*	*2CMH18*	*3CMD12*	*2SLH18*	*3SMD12*
b	[mm]	305	305	279.4	203	203	203	203	203	203	203	203	203	203	203	203	500	300	300	457.2	457.2	457.2	457.2	457.2
h	[mm]	305	305	279.4	203	203	203	203	203	203	203	203	203	203	203	203	300	500	300	457.2	457.2	457.2	457.2	457.2
L_s	[mm]	1676	1676	2134	610	610	610	610	610	610	610	610	610	610	610	610	1500	1500	1500	1473	1473	1473	1473	1473
ρ_t	[%]	0.37	0.37	0.1	0.92	0.92	0.92	0.9	0.92	0.9	0.92	0.9	0.92	0.9	0.92	0.9	0.13	0.22	0.22	0.26	0.26	0.26	0.26	0.26
ρ_l	[%]	1.63	1.63	1.02	1.93	1.93	1.93	1.93	1.93	1.93	1.93	1.93	1.93	1.93	1.93	1.93	0.9	0.57	1	1	1	1	1	1
v		0.27	0.27	0.34	0.05	0.05	0.1	0.1	0.21	0.21	0	0	0.14	0.14	0.36	0.36	0.12	0.1	0.18	0.22	0.32	0.4	0.22	0.4
s/h		0.47	0.47	0.9	0.45	0.45	0.41	0.42	0.41	0.43	0.4	0.41	0.45	0.46	0.41	0.42	0.54	0.31	0.54	1	1	0.67	1	0.67
f_{cm}	[Mpa]	32.4	31.8	40.6	69.6	69.6	67.8	67.8	65.5	65.5	37.9	37.9	48.3	48.3	38.1	38.1	18.85	18.85	18.85	33.1	25.5	27.6	33.1	25.5
f_{yl}	[Mpa]	363	363	407	586.1	586.1	572.3	573.3	572.3	573.3	572.3	573.3	586.1	587.1	572.3	573.3	520	520	520	331	331	331	331	331
f_{yt}	[Mpa]	392	373	351	406.8	406.8	513.7	513.7	513.7	514.7	513.7	514.7	406.8	407.8	513.7	514.7	520	520	520	368	368	368	368	368
F^+_{max}	[kN]	90.2	93.5	69.7	73.2	70.8	103.7	100.9	123.7	118.3	59.2	58.3	79.2	76	97	96.5	91.5	144.8	61.4	250.4	320.3	371	245.4	390.8
F^-_{max}	[kN]	-90.2	-91.4	-58.1	-69.3	-69.2	-99.7	-100	-118	-121	-57.4	-56.5	-77.9	-78	-94.3	-91.8	-98.8	-145	-72.5	-245	320.5	-372	-247	-368
θ^+_{Fmax}	[%]	1.62	1.92	1.48	2.07	1.94	2.82	2.79	2.82	3.12	3.06	3.08	2.8	2.77	2.82	2.82	2.18	1.96	3.05	1.92	1.01	0.81	1.09	1.58
θ^-_{Fmax}	[%]	-1.82	-1.71	-1.36	-2.12	-2.05	-2.99	-2.92	-3.03	-3.03	-3.11	-2.92	-1.9	-1.93	-2.97	-2.92	-2.08	-0.96	-2.25	-2.08	-0.96	-0.87	-0.9	-0.92
θ^+_y	[%]	1.11	1.22	0.82	1.9	1.83	1.65	1.65	2.33	2.21	2.21	2.25	2.2	1.65	2.25	2.09	1.26	0.8	1.58	0.86	0.82	1.06	0.83	0.95
θ^-_y	[%]	-1.19	-1.09	-0.92	-2	-1.86	-1.42	-1.41	-1.88	-2.14	-2.04	-2.29	-1.53	-1.91	-2.67	-2.65	-1.03	-0.67	-1.14	-0.96	-0.96	-1.03	-0.65	-0.78
θ^+_u	[%]	2.85	2.82	1.67	6.84	7.28	7.87	7.93	7.11	7.38	6.69	6.69	5.48	5.46	5.61	5.33	5.47	3.65	5.47	2.59	-	1.95	-	1.68
θ^-_u	[%]	-2.95	-2.91	-1.62	-7.3	-7.07	-8.2	-8.36	-7	-7.34	-6.95	-6.84	-6	-5.49	-5.21	-5.07	-3.87	-3.68	-3.87	-	-	-1.68	-3.19	-
k^{th}_y	[kNmm^{-1}]	4.91	4.88	3.27	7.28	7.62	12.03	12.1	11.28	10.1	6.03	5.8	8.68	8.8	8.61	8.84	5.55	12.96	3.37	32.44	59.27	57.63	32.44	59.28
$k_{p\text{-}p,y}$	[kNmm^{-1}]	4.34	4.37	2.99	5.94	6.15	9.97	9.92	8.86	8.53	4.37	4.06	6.62	6.84	6.34	6.48	4.61	9.98	2.72	16.78	22.57	27.14	20.49	26.18

Table 5-1 Geometrical and mechanical parameters for selected tests on RC columns reinforced with deformed bars.

		(Di Ludovico et al., 2009, 2012)			(Verderame et al., 2008b)						(Acun & Sucuoglu, 2010)			
Specimen		R300P_c	R500P_c	S300P_c	C-270A1	C-270A2	C-270B1	C-540A1	C-540B1	C-540B2	1P2	2P3	3P3_N04	4P4
Label		R300P_c	R500P_c	S300P_c	270A1	270A2	270B1	540A1	540B1	540B2	1P3	2P4	3P3	4P5
b	[mm]	500	300	300	300	300	300	300	300	300	350	350	350	350
h	[mm]	300	500	300	300	300	300	300	300	300	350	350	350	350
L_s	[mm]	1500	1500	1500	1570	1570	1570	1570	1570	1570	1800	1801	1802	1803
ρ_t	[%]	0.13	0.22	0.22	0.34	0.34	0.34	0.34	0.34	0.34	0.26	0.26	0.26	0.26
ρ_l	[%]	0.9	0.57	1	0.75	0.75	0.75	0.75	0.75	0.75	1	1	1	1
ν		0.098	0.11	0.176	0.12	0.12	0.12	0.24	0.24	0.24	0.21	0.2	0.4	0.2
s/d		0.536	0.313	0.536	0.357	0.357	0.357	0.357	0.357	0.357	0.5	0.5	0.5	0.5
f_{cm}	[Mpa]	18.9	18.9	18.9	25	25	25	25	25	25	13.5	12.2	13.1	12.4
f_{yl}	[Mpa]	330	330	330	355	355	355	355	355	355	315	315	315	315
f_{yt}	[Mpa]	330	330	330	355	355	355	355	355	355	368	368	368	368
F^+_{max}	[kN]	67.74	119.52	52.25	42.96	43	39.9	64.97	61.07	64.68	56.68	53.52	60.15	53.51
F^-_{max}	[kN]	-66.76	-117.67	-54.08	-41.48	-44.14	-40.67	-60.99	-61.75	-64.57	-57.9	-53.6	-61.7	-54.8
θ^+_{Fmax}	[%]	2.15	1.9	2.14	1.19	1.46	1.04	1.82	1.75	1.25	3.21	2.39	2.03	3.42
θ^-_{Fmax}	[%]	-3.02	-2.1	-2.27	-1.81	-2.63	-1.59	-1.78	-1.63	-1.34	-2.93	-3.16	-1.92	-3.42
θ^+_y	[%]	1.22	0.69	1.32	0.48	0.45	0.68	0.64	0.64	0.55	0.92	1.2	0.88	1.1
θ^-_y	[%]	-1.23	-0.65	-1.14	-0.58	-0.5	-0.68	-0.74	-0.63	-0.61	-0.9	-1.63	-0.36	-1.18
θ^+_u	[%]	6.23	5.27	5.49	4.89	4.65	5.8	3.34	3.57	2.62	-	-	2.51	-
θ^-_u	[%]	-7.28	-5.4	-6.38	-4.89	-5.35	-5.54	-4.46	-3.62	-3.04	-	-	2.53	-
k^{th}_y	[kNmm^{-1}]	5.74	16.71	4.23	10.68	11.71	8.19	10.76	11.66	12.78	5.7	5.48	8.07	5.52
$k_{p-p.y}$	[kNmm^{-1}]	4.98	14	3.73	8.99	9.93	7.06	9.72	10.67	11.67	3.16	1.97	4.81	2.44

Table 5-2 Geometrical and mechanical parameters for selected tests on RC columns reinforced with smooth bars.

5.3.2 PLASTIC HINGE MODIFICATION FACTORS

In order to perform pushover analyses for RC frame buildings, with adoption of a lumped plasticity model, element flexural behaviour has to be properly characterized with a moment rotation relation. Different approaches exist for the definition of the moment-rotation relationship of plastic hinges (Dolšek, 2010). In this work, the moment rotation of plastic hinges is idealized with a bilinear curve, as suggested in ASCE-SEI41-06 (ASCE, 2007); however, the formulations for damage dependent modification factors could be theoretically derived also for other kind of hinge idealizations.

The bilinear moment-rotation plastic hinge is described by yielding (M_y and θ_y) and ultimate (M_u and θ_u) moment and rotation. The moments M_y and M_u can be determined by moment-curvature analyses for the element's end sections, while yielding and ultimate rotations are derived from the ASCE-SEI41-06 (ASCE, 2007) approach, with updated limit values as suggested in ACI 369R-11 (2011). In particular, yielding rotation θ_y is calculated for a reduced effective stiffness, EI_{eff}, with respect to that of the un-cracked gross section (see Eq. 5-9 to follow), while ultimate rotation θ_u is obtained by summing a plastic rotation a to the yielding one.

As suggested in FEMA 306 (1998), the plastic hinges of damaged elements may be modified with a suitable variation of stiffness, strength and residual drifts modification factors. Fig. 5.3 shows the definition of modified relative stiffness ($K'=\lambda_k K$), strength ($M_y'=\lambda_Q M_y$) and plastic rotation capacity ($a'= a-a_d = a-(\theta'_y-\theta_y)-RD = a-[\theta_y(\lambda_Q/\lambda_k-1)-RD]$, with λ stiffness or strength modification factors and RD residual drift of the element.
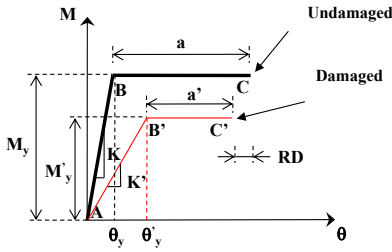
	stiffness	strength	Plastic rotation
intact	K	M_y	a
damaged	K'=λ_KK	My'=λ_QM$_y$	a'=a-a$_d$

Fig. 5.3 Modeling criteria for the damaged plastic hinges (adapted after FEMA 306, 1998).

5.3.2.1 EXPERIMENTAL PARAMETERS

In order to establish plastic hinge modification factors owing to damaging, the best approach would be to perform laboratory testing with two identical test specimens for each element, specifically designed for that purpose FEMA 306 (1998). The first should be tested to represent the element in its post-event condition subjected to performance earthquake, the second to represent the same element in its pre-event condition subjected to the damaging earthquake. The stiffness, strength and residual drift modification factors, λ_k, λ_Q and RD, would be derived from the different response between these two specimens. However, to the authors knowledge none of the existing tests performed on RC columns were designed with the scope of comparing previously damaged components to undamaged ones. As suggested in FEMA 307 (1998) a valid alternative could be to infer the modification factors from individual cyclic-static tests, by examining the change in force-displacement response from cycle to cycle. In particular, initial cycles can be considered representative of the behavior of intact elements, whereas subsequent cycles for the damaged component.

In this work, based on the force-displacement relationship of the selected cyclic tests, the latter approach has been used to calibrate stiffness, strength and residual drift modification factors.

The procedure to analyse the test results and the main parameters retrieved from experimental tests to derive modification factors are presented in the following and summarized in Table 5-1 and Table 5-2. To determine the column flexural capacity, the effective horizontal force, $F_{eff.}$, applied on the column has been calculated for each test as:

$$F_{eff} = \frac{M_{base}}{L_S} = \frac{F \cdot L_S + N \cdot \Delta}{L_S}$$

Eq. 5-2

where M_{base} is the column base bending moment, F is the lateral applied load, N is the applied axial load, and Δ is the lateral column displacement. The column chord rotation has been assumed equal to drift: $\theta = \Delta/L_S$.

The envelope curve has been obtained for each experimental cyclic test according to the approach proposed in Elwood et al. (2007) (i.e. by connecting the first cycle peak point for each loading step, see Fig. 5.4(a)). On the envelope curve the following parameters have been selected:

- F^+_{max}, F^-_{max}: maximum force attained in the test with respect to both positive and negative loading actions;

- θ^+_{Fmax}, θ^-_{Fmax}: rotation corresponding to F^+_{max}., F^-_{max}, see Fig. 5.4 (a);

- θ^+_y, θ^-_y: positive and negative yield rotation, defined according to experimental practice proposed by Elwood and Eberhard (2009). The procedure requires the use of envelope curve. First it is necessary to determine the line passing through the intersection point between envelope curve and the horizontal line through F_y (force at which the tension reinforcement yields or the maximum concrete strain reaches a value of 0,002) and the origin; then the intersection between this line and the horizontal one through $F_{0,004}$ (force at which the strain of 0,004 is reached in the concrete) gives the yield, see Fig. 5.4 (b);

- θ^+_u, θ^-_u: ultimate rotation with respect to both positive and negative loading actions, defined as the rotation at failure condition, set at 20% drop of the maximum lateral load (Fardis and Biskinis, 2003), $0.8F^+_{max}$ (or $0.8F^-_{max}$), see Fig. 5.4 (a).

In order to assess the cyclic degradation, both peak drift, θ_i and residual drift, RD_i, were evaluated for each cycle with respect to positive and negative load actions (see Fig. 5.4 (c)); RD values for each cycle were determined as the drift for which F_{eff} is equal to zero. The column experimental stiffness at each cycle, k_{p-p}, was defined as the slope of the straight line joining positive and negative peak displacement (Fig. 5.4(d)); this experimental peak to peak stiffness has been computed at each cycle according to Eq. 5-3:

$$k_{p-p} = \frac{F_i^+ + \left|F_i^-\right|}{\theta_i^+ + \left|\theta_i^-\right|}$$

Eq. 5-3
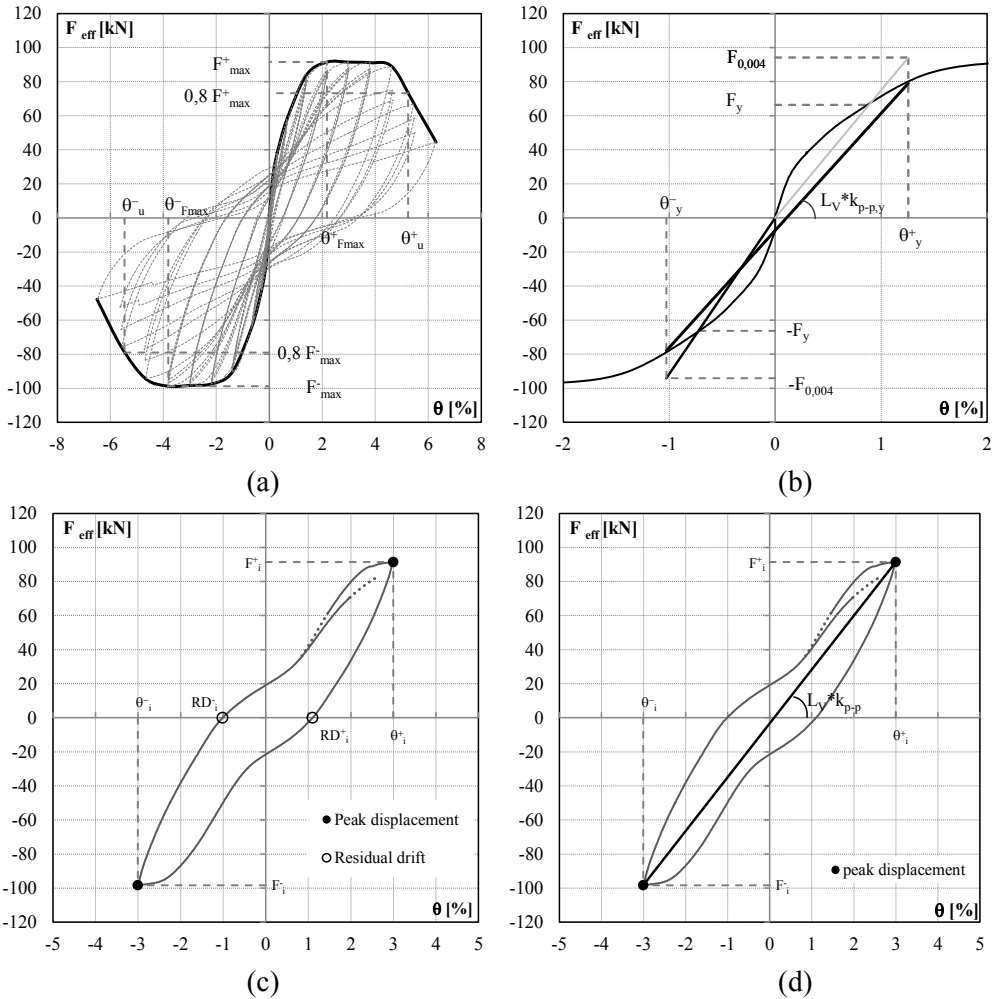
Fig. 5.4 Experimental force-drift envelope curve (a); experimental yield rotation, θ_y, and yielding stiffness, $k_{p-p,y}$ (b); peak drift, θ_i and residual drift, RD_i, at i^{th}-cycle (c); peak to peak stiffness, k_{p-p} at i^{th}-cycle (d).

5.3.2.2 STIFFNESS MODIFICATION FACTOR

In order to compute the stiffness degradation on the damaged members, a proper stiffness modification factor has been introduced, λ'_k. It has been defined as the ratio between the peak to peak experimental stiffness, k_{p-p}, and the experimental yield stiffness, $k_{(p-p),y}$, computed as the slope (in the F_{eff}-Δ reference system) of the line joining the positive and negative points, on the envelope curve, corresponding to θ^+_y and θ_y (see Fig. 5.4(b)).

$$\lambda'_k = \frac{k_{p-p}}{k_{(p-p),y}}$$

Eq. 5-4

163

The experimental stiffness has been normalized with respect to $k_{(p-p),y}$ to compare the experimental data resulting from columns with different geometrical and mechanical properties. The experimental values of λ'_k as a function of the ratio θ/θ_y are reported in Fig. 5.5(a) for deformed and in Fig. 5.5(b) for smooth bars. The parameter θ/θ_y has been adopted in order to correlate the stiffness degradation to the ductility level attained by the column after the damage. Note that drift demand has been computed at each drift level as the average peak positive and negative drift, $(\theta_i^+ + |\theta_i^-|)/2$, while θ_y has been conservatively assumed as the (absolute value of the) minimum yield rotation experienced in positive and negative load actions. Further, these assumptions are based on the peak to peak stiffness definition which leads to a single stiffness value for every load cycle. The experimental points are characterized by a low variability and they show a hyperbolic trend. In the regression formula to follow they have been considered up to an experimental drift equal to the ultimate one (according to the definition of ultimate rotation given above); however, in order to represent the plots in the same scale not all the experimental points are shown. It can be noted that member's stiffness decreases quite steeply with ductility demand.
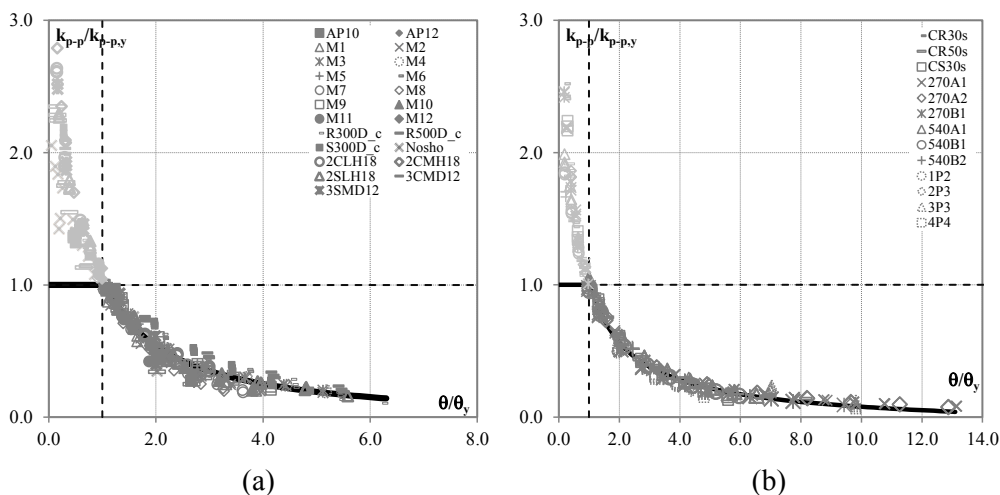
Fig. 5.5. Experimental $k_{p-p}/k_{(p-p),y}$ - θ/θ_y points; the continuous line represents experimental points best fitting for (a) elements with deformed bars; (b) elements with smooth bars.

Looking for example at $k_{p-p}/k_{(p-p),y}$ for a ductility demand of 2, it lowers to approximately 53% in the case of elements reinforced with deformed bars, and to 56% for elements with smooth bars; for a ductility demand of 4, $k_{p-p}/k_{(p-p),y}$ lowers to 25% in the first case and to 28% in the second case. As can be noted by comparison between Fig. 5.5 (a, b), experimental results highlight that rotational capacity of columns with smooth bars is rather large, even higher than the capacity of similar columns reinforced

with deformed bars. This is due to the increase in deformability caused by the fixed-end rotation mechanism, particularly exalted when bond capacities are low (Verderame et al., 2010).

The ratio $k_{p-p}/k_{(p-p),y}$ assumes values higher than 1.1 for θ/θ_y lower than 1.1 since they represent column initial stiffness; however, the meaningful points are those for θ/θ_y greater than 1.1 which represent the stiffness degradation in the post-elastic stage. Indeed, the experimental range for θ/θ_y greater than 1 indicate the stiffness decrease once the yielding drift has been exceeded due to a seismic event; it is assumed that in the pre-yielding state the damage influence on the member stiffness is negligible. According to this assumption, the following simple expressions can be used to predict the stiffness degradation:

Eq. 5-5 and Eq. 5-6 refer to elements reinforced with deformed bars:

$$\lambda'_k = 1.0 \qquad\qquad \text{for } \theta/\theta_y \leq 1.1 \qquad\qquad \text{Eq. 5-5}$$

$$\lambda'_k = 1 - \left[1.07 - 1.15 \cdot \left(\theta/\theta_y\right)^{-0.92}\right] \qquad\qquad \text{for } 1.1 < \theta/\theta_y \leq \theta_u/\theta_y \qquad\qquad \text{Eq. 5-6}$$

and Eq. 5-7 and Eq. 5-8 refer to elements reinforced with smooth bars:

$$\lambda'_k = 1.0 \qquad\qquad \text{for } \theta/\theta_y \leq 1.1 \qquad\qquad \text{Eq. 5-7}$$

$$\lambda'_k = 1 - \left[1.12 - 1.17 \cdot \left(\theta/\theta_y\right)^{-0.77}\right] \qquad\qquad \text{for } 1.1 < \theta/\theta_y \leq \theta_u/\theta_y \qquad\qquad \text{Eq. 5-8}$$

The theoretical best fitting of experimental values is depicted with a continuous line in Fig. 5.5(a, b), respectively for elements reinforced with deformed or smooth bars. The expressions Eq. 5-5 and Eq. 5-6 for elements reinforced with deformed bars, or Eq. 5-7 and Eq. 5-8 for those with smooth bars, allow to compute the stiffness degradation, i.e. to estimate λ'_k, as a function of the attained drift level by means of an interpolating function rather than by using discrete values depending on damaging as suggested in FEMA 307 (1998). The coefficient of determination R^2 obtained with the proposed regression formulas is 0.92 and 0.98 for Eq. 5-6 and Eq. 5-8, respectively.

For comparison purposes also the suggested λ'_k values for element type RC2A in FEMA 307 (1998) (weaker pier with ductile/flexural behaviour) are shown in Fig. 5.6. In particular, only comparison with experimental based modification factor for elements with deformed bars is proposed since the RC2 elements are with deformed bars. Based on experimental calibration, FEMA 307 (1998) suggests λ'_k=0.8 for displacement (experimental) ductility lower or equal than 3, λ'_k=0.6 for displacement ductility = 4-6, while λ'_k =0.5 for displacement ductility in the range 3-10.
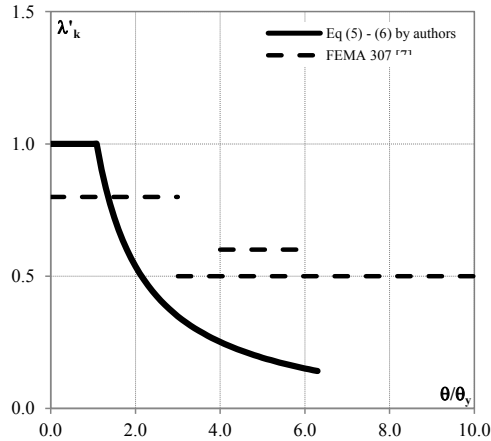
Fig. 5.6 Comparison between λ_k proposed by authors in Eq. 5-5, Eq. 5-6 and FEMA 307 (1998).

As it can be seen, the values for RC2A are significantly higher with respect to the ones proposed here. This may be understandable considering that the reinforced concrete elements considered in FEMA 307 (1998) are typical of RC wall buildings, where vertical elements are in most of the cases walls (or strong piers); indeed, the λ_k values suggested for RC2A for all the ductility ranges are the same to the one of RC1A element type/behaviour defined in FEMA 306, 1998, (walls or stronger piers), whose behaviour and damage pattern are very different from ordinary columns.

It has to be observed that the proposed formulations for stiffness modification factors (as well as those for strength and residual displacement, discussed in the following paragraphs) are expressed as a function of the sole ductility demand and they do not allow to properly introduce the effects of cyclic deterioration or the loading history. Nevertheless, they are intended to be used as auxiliary tools for the assessment, via pushover analyses, of the behaviour of damaged buildings. Pushover, being a nonlinear static analysis, does not allow to evaluate the cyclic demand for the structural elements, while cinematic ductility at the element and global scale is a parameter that can be straightforwardly determined. On the other hand, pushover is recognised to be an optimal compromise between the need to investigate a building's nonlinear behaviour and to perform a relatively simple, yet accurate, static analysis (Krawinkler and Seneviratna, 1998), applicable for design/assessment purposes by practitioners (CEN 2004, 2005). Indeed, there exist some proposals (Fajfar, 1992; Sucuoğlu and Erberik, 2004; Cosenza et al., 2009) for including cumulative damage in the spectral assessment of Single Degree Of Freedom (SDOF) systems (that may be considered as representative of equivalent SDOF system of the real Multi Degree of Freedom structure in a CSM method).

Considering the above formulations (Eq. 5-5 and Eq. 5-6 or Eq. 5-7 and Eq. 5-8), λ'_k may be derived for members on which it is possible to compute the drift level attained due to the seismic event. For example, the value of θ, locally attained in RC

166

columns, can be computed based on a theoretical analysis (e.g. non linear pushover analysis) in correspondence of a given global damage state. Indeed, for a given structural roof displacement induced by the seismic event, it is possible to determine on each member of the structural model the relevant chord rotation. However, the use of the above given expressions depends on the knowledge of the experimental yield rotation, θ_y, provided by a proper experimental test on the column prototype. Therefore, in order to provide a suitable tool to be used for the theoretical assessment of the residual building capacity through pushover analyses on the structure in different damage state configurations, it is necessary to normalize k_{p-p} and θ values with respect to theoretical yielding stiffness and rotation, k^{th}_{eff} and θ^h_y, rather than experimental ones, $k_{(p-p),y}$ and θ_y.

Theoretical yield rotation, θ^h_y, and stiffness, k^{th}_{eff}, can be computed, according to elastic theory, with Eq. 5-9 and Eq. 5-10 to follow:

$$\theta^{th}_y = \frac{M_P L_S}{3EI_{eff}}$$

Eq. 5-9

where M_P is the theoretical bending moment corresponding to bar yielding, L_s is the shear span and EI_{eff} is the effective member stiffness computed according to the expressions reported in Di Ludovico et al. (2012), ($EI_{eff} = 0.3EI_g$ for $0<\nu\leq0.1$; $EI_{eff} = 0.7EI_g$ for $\nu>0.5$; and EI_{eff} obtained using a linear interpolation in the range $0.1<\nu\leq0.5$; with E=concrete modulus and I_g=moment of inertia of gross column cross-section).

$$k^{th}_{eff} = \frac{3EI_{eff}}{L_S}$$

Eq. 5-10

The experimental points trend obtained by using θ^h_y and k^{th}_{eff} to normalize drift and stiffness is reported in Fig. 5.7(a, b) for deformed and smooth bars, respectively. The points scattering is very low and the trend is similar to that presented in Fig. 5.5(a, b). Since theoretical yield rotations are typically conservative with respect to the experimental ones, the experimental points are shifted to higher values of theoretical ductility demand (θ/θ^h_y), with respect to θ/θ_y computed based on experimental θ_y. Based on the trend reported in Fig. 5.7(a, b), it is possible to determine the theoretical expressions which provide a best fitting of experimental data (see continuous line in Figure). The fitting analysis is performed considering the same number of points as used in deriving Eq. 5-5 and Eq. 5-6 or Eq. 5-7 and Eq. 5-8. In particular, the stiffness degradation modification factor $\lambda_k = k_{p-p}/k^{th}_{eff}$ can be calculated as a function of θ/θ^h_y with:
Eq. 5-11 and Eq. 5-12 that refer to elements reinforced with deformed bars:

$$\lambda'_k = 1.0 \qquad\qquad \text{for } \theta/\theta_y^{th} \leq 1.0 \qquad\qquad \text{Eq. 5-11}$$

$$\lambda_k = 1 - \left[1.01 - 0.96 \cdot \left(\theta/\theta_y\right)^{-1.10}\right] \qquad\qquad \text{for } 1.0 < \theta/\theta_y^{th} \leq \theta_u/\theta_y^{th} \qquad\qquad \text{Eq. 5-12}$$

or Eq. 5-13 and Eq. 5-14 that refer to elements reinforced with smooth bars:

$$\lambda'_k = 1.0 \qquad\qquad \text{for } \theta/\theta_y^{th} \leq 0.9 \qquad\qquad \text{Eq. 5-13}$$

$$\lambda_k = 1 - \left[1.07 - 0.98 \cdot \left(\theta/\theta_y\right)^{-0.80}\right] \qquad\qquad \text{for } 0.9 < \theta/\theta_y^{th} \leq \theta_u/\theta_y^{th} \qquad\qquad \text{Eq. 5-14}$$

The R^2 obtained with the proposed regression formulas is 0.96 and 0.98 for Eq. 5-12 and Eq. 5-14, respectively.
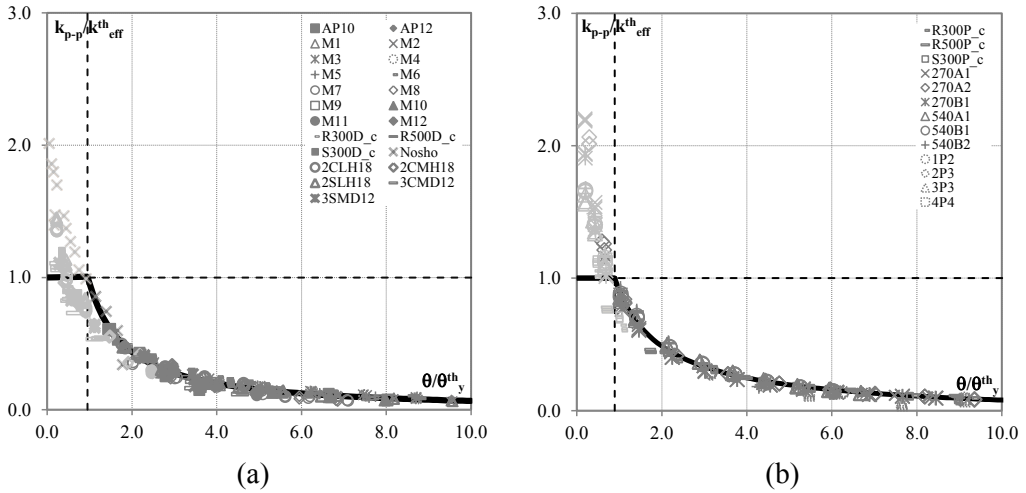
Fig. 5.7 Theoretical k_{p-p}/k^{th}_{eff} - θ/θ_y^{th} points; the continuous line represents experimental points best fitting for (a) elements with deformed bars; (b) elements with smooth bars.

5.3.2.3 STRENGTH MODIFICATION FACTOR

The strength modification factor is a measure of the member strength degradation after damage. In order to compute such factor, the experimental peak forces, F_i, have been determined for each test at different drift levels; these values have been normalized with respect to the maximum force for each test, $F_{max.}$, in order to make comparable the different test results. Both positive and negative peak and maximum forces have been determined and the relevant ratio $|F_i|/|F_{max}|$ has been computed. The strength degradation is then determined as a function of the ratio $|\theta_i|/\theta_y$. in the case of strength each peak corresponds to a single rotation and thus positive and negative values have

been considered. Hence, the strength degradation modification factor, λ'_Q, has been defined as:

$$\lambda'_Q = \frac{|F_i|}{|F_{\max}|}$$

Eq. 5-15

The experimental points have a very similar trend up to $|\theta_i|/\theta_y = 1$, while a significant scattering may be observed for high values of $|\theta_i|/\theta_y$ (see Fig. 5.8); this can be explained considering that the experimental strength degradation may be significantly different for positive and negative horizontal load actions (i.e. the envelope cyclic experimental curves are often not symmetrical due to the damage initiation in one direction); further, number and yield strength of columns longitudinal bars could significant influence the strength drop after the maximum force has been experienced.
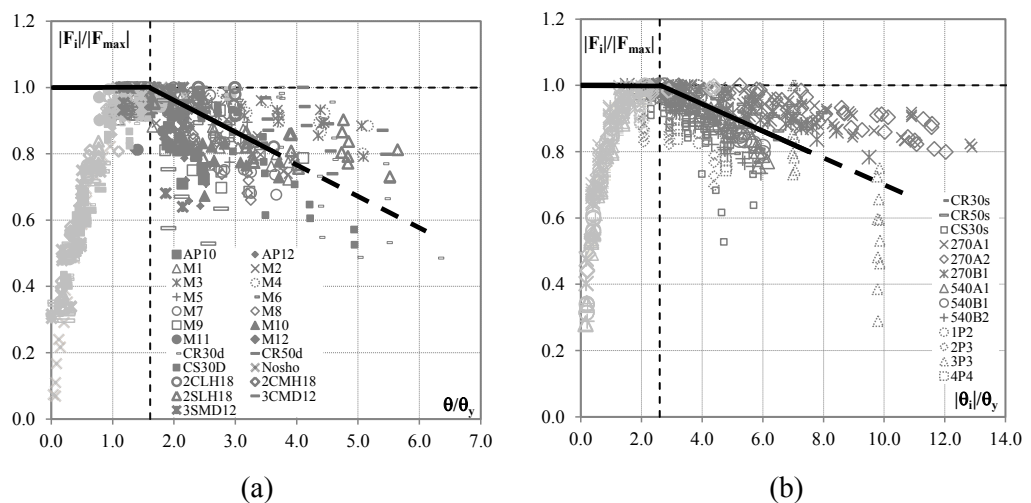
Fig. 5.8 Experimental $|F_i|/F_{max}$ - $|\theta_i|/\theta_y$ points and fitting curves for: (a) elements with deformed bars; (b) elements with smooth bars

The strength degradation starts when the maximum lateral force is experienced; this value is typically attained for $|\theta_i|/\theta_y$ ratio greater than 1 and, considering the experimental database, for a mean value of $(|\theta_i|/\theta_y)_{mean} = 1.6$ for elements with deformed bars and $(|\theta_i|/\theta_y)_{mean} = 3.1$ for those with smooth bars. The strength degradation is in any case limited by the attainment of θ_u (that is set at the 20% drop of F_{max}). Therefore, a simplified linear trend has been assumed between the points A=$((|\theta_i|/\theta_y)_{mean}, 1)$ and B=$((\theta_u/\theta_y)_{mean}, 0.8)$.

Eq. 5-16 and Eq. 5-17 apply for elements reinforced with deformed bars:

$$\lambda'_Q = 1.0 \qquad\qquad \text{for } \theta/\theta_y \leq 1.6$$

Eq. 5-16

169

$$\lambda'_Q = 1.0 - 0.10 \cdot \left(|\theta| / \theta_y - 1.6 \right) \qquad \text{for } 1.6 < \theta / \theta_y \leq \theta_u / \theta_y \qquad \text{Eq. 5-17}$$

or Eq. 5-18 and Eq. 5-19 that refer to elements reinforced with smooth bars:

$$\lambda'_Q = 1.0 \qquad \text{for } \theta / \theta_y \leq 3.1 \qquad \text{Eq. 5-18}$$

$$\lambda'_Q = 1.0 - 0.05 \cdot \left(|\theta| / \theta_y - 3.1 \right) \qquad \text{for } 3.1 < \theta / \theta_y \leq \theta_u / \theta_y \qquad \text{Eq. 5-19}$$

Similarly to what has been done for the stiffness modification factor, also strength modification proposed in FEMA 307 (1998) for RC2A elements and behaviour type are plotted in Fig. 5.9, (relative to elements with deformed bars), with $\lambda'_Q = 1$ for displacement (experimental) ductility lower or equal than 3 or $= 4$-6, while $\lambda'_Q = 0.8$ for displacement ductility in the range 3-10.
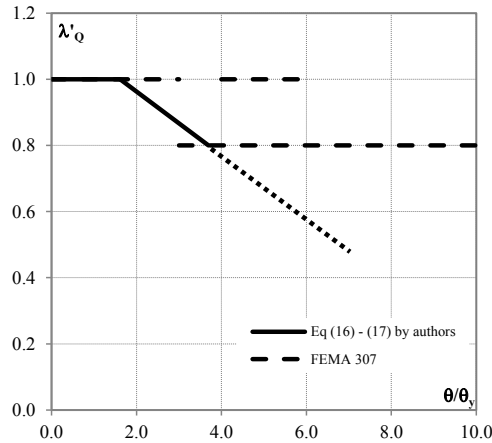
Fig. 5.9 Comparison between λ_Q proposed by authors in Eq. 5-16, Eq. 5-17 and FEMA 307 (1998).

Also in this case it may be observed that the λ'_Q factors, being referred to an element that behaves more like a wall than to an ordinary column, are significantly higher with respect to the ones extracted from the considered columns database.

To overcome the difficulties related to the computation of θ_y as well as of the experimental maximum lateral force which can be sustained by the column, the force degradation trends have been also computed by using the theoretical parameters F_p and θ^h_y representing the maximum theoretical force and yield rotation respectively. In particular, F_p can be computed as M_p/L_S while Eq. 5-9 has been used for θ^h_y. By using these parameters to normalize the maximum force and the member drift, the trend reported Fig. 5.10 (a) for elements reinforced with deformed bars and in Fig. 5.10 (b) for those with smooth bars are obtained. Comparing the trends of strength degradation in (a,

b), it can e noted that reinforced columns reinforced with smooth bars show a more gradual strength decreasing branch with respect to columns reinforced with deformed bars. The linear trends based on the experimental data shown in Fig. 5.10(a, b) is obtained with the same criteria explained above for the derivation of λ'_Q.

Eq. 5-20 and Eq. 5-21 apply for elements reinforced with deformed bars:

$$\lambda_Q = 1.0 \qquad\qquad \text{for } \theta/\theta_y^{th} \leq 3.9 \qquad\qquad \text{Eq. 5-20}$$

$$\lambda_Q = 1.0 - 0.05 \cdot \left(\theta/\theta_y^{th} - 3.9\right) \qquad\qquad \text{for } 3.9 < \theta/\theta_y^{th} \leq \theta_u/\theta_y^{th} \qquad\qquad \text{Eq. 5-21}$$

while Eq. 5-22 and Eq. 5-23 for those with smooth bars:

$$\lambda_Q = 1.0 \qquad\qquad \text{for } \theta/\theta_y^{th} \leq 4.0 \qquad\qquad \text{Eq. 5-22}$$

$$\lambda_Q = 1.0 - 0.03 \cdot \left(|\theta|/\theta_y^{th} - 4.0\right) \qquad\qquad \text{for } 4.0 < \theta/\theta_y^{th} \leq \theta_u/\theta_y^{th} \qquad\qquad \text{Eq. 5-23}$$

(a)   (b)
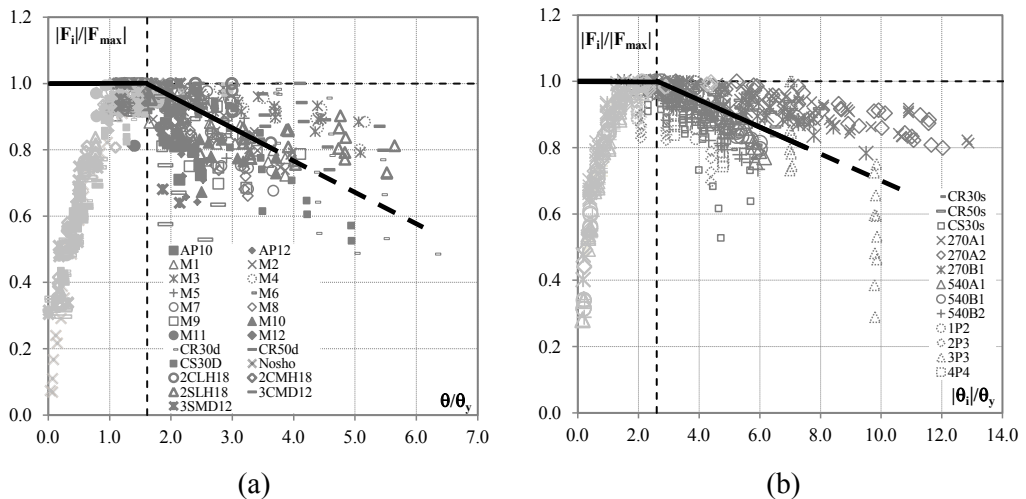
Fig. 5.10 Experimental $|F_i|/F_P$ - $|\theta_i|/\theta_y$ points and fitting curves for: (a) elements with deformed bars; (b) elements with smooth bars.

5.3.2.4 RESIDUAL DRIFT MODIFICATION FACTOR

The residual drift, *RD,* is here defined as the plastic rotation measured on the column for an external lateral load equal to zero. This assumption tends to overestimate the *RD* values with respect to the ones that could be expected in reality. In fact, the specimen in a displacement controlled static testing is not actually released at the end of the test, hence the kinetic and elastic recovery forces, that would contribute to lower the residual drift (and even more in a real MDOF structure, where the column is usually embedded), are disregarded. Acknowledging its limitations, we adopt the above definition for *RD,*

that is simple to be determined and still has the advantage of being on the safe side for performance evaluations.

With a similar approach to that illustrated above for the member stiffness and strength, RD has been initially normalized with respect to the yield rotation and its trend studied as a function of θ/θ_y. In particular, RD an θ are obtained as average values recorded for positive and negative external load actions. The experimental points (not shown for brevity reason) show that an ascending pseudo-parabolic trend of RD versus the yield rotation is attained for increasing values of θ/θ_y ratios. This confirms that RD/θ_y increases for actions overcoming the member elastic threshold and are clearly negligible for $\theta/\theta_y < 1.3$. Thus interpolating equations are derived for $\theta/\theta_y > 1.3$, while a fixed null value of RD is assigned for lower drift demands.

Eq. 5-24 and Eq. 5-25 apply for elements reinforced with deformed bars:

$$RD/\theta_y = 0.0 \qquad\qquad\qquad \text{for } \theta/\theta_y \leq 1.3 \qquad \text{Eq. 5-24}$$

$$RD/\theta_y = -0.005\left(\theta/\theta_y - 1.3\right)^2 + 0.63\left(\theta/\theta_y - 1.3\right) \qquad \text{for } 1.3 \leq \theta/\theta_y \leq \theta_u/\theta_y \qquad \text{Eq. 5-25}$$

While Eq. 5-24 and Eq. 5-26 for those with smooth bars:

$$RD/\theta_y = 0.006\left(\theta/\theta_y - 1.3\right)^2 + 0.26\left(\theta/\theta_y - 1.3\right) \qquad \text{for } \theta/\theta_y^{th} \leq 4.0 \qquad \text{Eq. 5-26}$$

With the above formulations the plastic hinge for a column with deformed bars that has attained a ductility demand of $\mu = \theta/\theta_y = 2$ would be characterised by a residual drift RD approximately equal to $0.44\,\theta_y$ while if it had smooth bars RD would be approximately 17% of θ_y. For increasing ductility levels ($\mu = 4$-6) the RD/θ_y ratio slowly increases to 1.65 and 2.84 in the first case (deformed bars) and to 0.64 and 1.06 for the second one (smooth bars). The coefficient of determination R^2 obtained with the proposed regression formulas is 0.72 and 0.58 for Eq. 5-25 and Eq. 5-26, respectively.

As for stiffness and strength also in this case it is possible to normalize both RD and θ with respect to θ^h_y rather than θ_y; in this way it is possible to provide a proper modification factor of member plastic hinge in the pushover analysis according to theoretical provisions. The experimental points trend obtained in such a case is shown in Fig. 5.11(a) for columns reinforced with deformed bars and in Fig. 5.11 (b) for those with smooth bars. The interpolating best fitting curve are represented as continuous lines in the same figures. Note that since θ^h_y is typically lower than that recorded in the experiments, the range of variation of ratio θ/θ^h_y is significantly wider than that related to θ/θ_y. By comparison of Fig. 5.11 (a, b), it can be noted that residual drifts versus yield drift ratio in elements with smooth bars are generally lower with respect to those with deformed bars. This is probably due to the poor bond between smooth bars and

172

surrounding concrete; indeed, for the tests on specimens with smooth bars, a significant closure of the hysteretic cycle both in the final stage of the unloading branch and in the initial stage of the reloading phase (*pinching effect*) could be observed. On the other hand, on columns reinforced by using deformed bars, the pinching effect started to be significant only after a large number of cycles due to the degradation of bond (Di Ludovico et al., 2009).

The best fitting curve analytical expressions are given in Eq. 5-27 and Eq. 5-28 for elements with deformed bars:

$$RD/\theta_y^{th} = 0.0 \qquad\qquad\qquad\qquad\text{for } \theta/\theta_y^{th} \le 2.9 \qquad\qquad \text{Eq. 5-27}$$

$$RD/\theta_y^{th} = 0.05\left(\theta/\theta_y^{th} - 2.9\right)^2 + 0.40\left(\theta/\theta_y^{th} - 2.9\right) \qquad \text{for } 2.9 < \theta/\theta_y^{th} \le \theta_u^{th}/\theta_y^{th} \qquad \text{Eq. 5-28}$$

while Eq. 5-29 and Eq. 5-30 for those with smooth bars:

$$RD/\theta_y^{th} = 0.0 \qquad\qquad\qquad\qquad\text{for } \theta/\theta_y^{th} \le 2.0 \qquad\qquad \text{Eq. 5-29}$$

$$RD/\theta_y^{th} = 0.007\left(\theta/\theta_y^{th} - 2.0\right)^2 + 0.30\left(\theta/\theta_y^{th} - 2.0\right) \qquad \text{for } 2.0 < \theta/\theta_y^{th} \le \theta_u^{th}/\theta_y^{th} \qquad \text{Eq. 5-30}$$
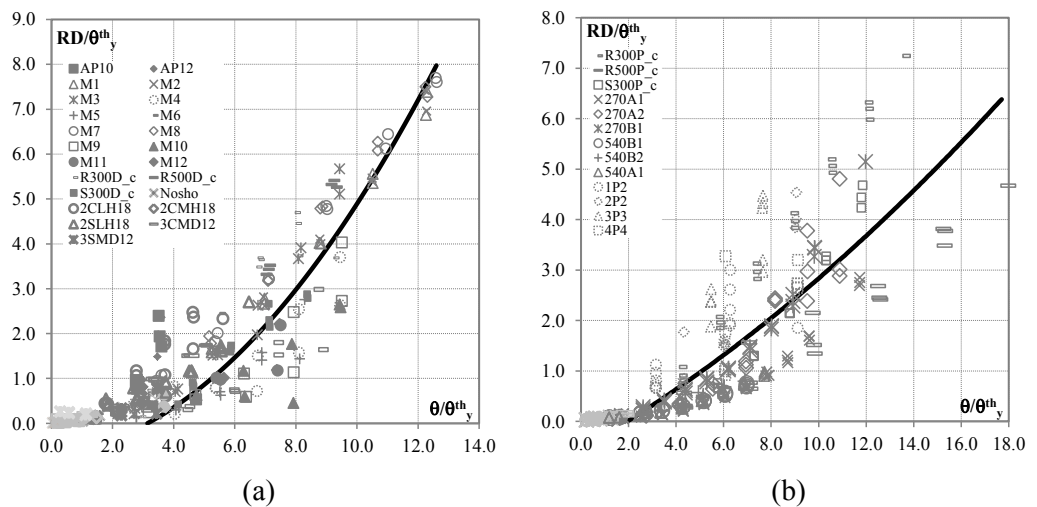
Fig. 5.11 Experimental RD/θ_y-θ/θ_y^h points and fitting curves for: (a) elements with deformed bars; (b) elements with smooth bars.

The R^2 obtained with the proposed regression formulas is 0.80 and 0.67 for Eq. 5-28 and Eq. 5-30 respectively. However, the proposed formulations have the advantage of allowing an easy derivation of the needed parameters, and can be adopted for estimation

of reduced rotational capacity starting from theoretical modeling of a building seismic behaviour. Thus for each column cross section, once the θ^h_y has been computed, it possible to easily determine RD for a given drift demand. In this way the plastic hinge can be modified by simply reducing the plastic deformation capacity (see notation in Fig. 5.3).

5.4   OVERVIEW OF THE SIMPLIFIED METHOD

The formulations proposed in §5.3 may be applied for the assessment of seismic performance of damaged buildings if the damage state is evaluated analytically with nonlinear static analysis (i.e. if the ductility demand for the elements is retrieved from pushover based on a lumped plasticity model). In fact, the plastic hinges modification factors are expressed as function of maximum ductility demand for each element; the latter is a parameter that can be straightforwardly determined based on analytical simulation of building nonlinear seismic response to an earthquake, e.g. via Capacity Spectrum Method, CSM, (Fajfar, 1999, Polese et al., 2008) after pushover analysis. In Polese et al. (2013a), a first application of the modification factors proposed in this paper is presented, with the assessment of residual capacity for an existing RC building in L'Aquila region. In particular, the building initial performance (for a main-shock) is analyzed with pushover analysis determining a global displacement demand (e.g. at the roof level); the latter corresponds to local ductility demand for the elements that have entered the plastic range. In order to determine the potential seismic behaviour for a future earthquake (in case the structure is not repaired after the main-shock) the "damaged" building model is analyzed, where the nonlinear model is obtained by suitable modification of the hinges for those elements that have entered the plastic range; this way a modified pushover is obtained, that allows to assess the residual capacity of the damaged building (see Fig. 5.1). Further details for the procedure to determine building's residual capacity may be found in Polese et al. (2013a).

5.5   GROUND ACCELERATION REDISUAL CAPACITY

In Polese et al. (2013a) REC is defined as a parameter aimed at representing the building seismic capacity (up to collapse) in terms of a spectral quantity; in particular, REC_{Sa} of a building is defined as the smallest ground motion spectral acceleration (at period T_{eq}, of the Single Degree Of Freedom SDOF system equivalent to the real structure) corresponding to collapse state of the building. Considering the seismic demand and the local damage that the elements in a Multi Degree of Freedom (MDOF) system may be forced to sustain due to a mainshock earthquake, the system's capacity may be considerably reduced, as evidenced in Polese et al. (2013a). Because of the convenience of direct estimation of peak ground acceleration, a_g, as a damaging intensity parameter,

174

the residual capacity is evaluated also in terms of a_g: given the spectral shape, REC_{ag} is the minimum anchoring peak ground acceleration such as to determine building collapse and corresponds to REC_{Sa} scaled by the spectral amplification factor for T_{eq}. By way of example, with reference to an EC8 spectral shape (CEN, 2004) and considering a system with $T_C<T_{eq}<T_D$, the following relation applies:

$$REC_{ag} = \frac{REC_{Sa}}{(S \cdot \eta \cdot 2.5)} \cdot \left(\frac{T_{eq}}{T_C} \right)$$
<div align="right">Eq. 5-31</div>

5.6 VALIDATION OF THE SIMPLIFIED PROCEDURE

The applicability of PA has been evaluated in several previous studies (Fajfar and Gašperšič, 1996; Mwafy and Elnashai, 2001; Krawinkler and Seneviratna, 1998; Tso and Moghadam, 1998; Lawson et al., 1994; Antoniou et al., 2002). The first studies followed the approach of comparing the results of PA with those of NTH only at certain loading levels, e.g. design level, or at equal top displacement (roof displacement from pushover equal to the maximum dynamic roof displacement). For example, in (Tso and Moghadam, 1998; Lawson et al., 1994) a set of 10 and 7 ground motions, respectively, were selected so to be compatible with given spectral shapes, and comparison of PA results with those of NTH analyses were performed, for a single scaling of those ground motions, in terms of displacements (or deflection profiles), inter-storey drifts and plastic hinge rotations. More recently, (Mwafy and Elnashai, 2001; Antoniou et al., 2002) presented more exhaustive comparisons, developing complete pushover-like load–displacement curves from incremental dynamic analysis up to collapse for different structural configurations. They compared the pushover curves obtained for different lateral load distributions with the dynamic envelops (maximum absolute drifts and base shear) obtained for increasing levels of ground motion intensity.

Despite the availability of several validation examples for PA, the usability of pushover analysis for the assessment of the behavior of damaged buildings (Polese et al., 2013a) has not been verified yet, and the study presented in this paper aims at contributing in the evaluation of this issue.

5.6.1 DESCRIPTION OF BUILDINGS AND MODELING ASSUMPTIONS

The comparison of PA with NTH analysis is performed with reference to two bare Reinforced Concrete Frames (RCF), of 4 and 8 storeys respectively (see Fig. 5.12), that have been designed to be representative of existing under-designed buildings in the Mediterranean area. In particular, the RCF were designed with a simulated design procedure as suggested in (Verderame et al., 2010) and in the first seismicity class with reference to old seismic codes (R.D.L. no. 2229/1939) in force in the beginning of age

'60s, not applying principles of capacity design or proper reinforcement detailing and based on allowable stress method. The structure of the RCFs, that represent the perimeter frames of buildings with planar dimensions of 18m x10m, is formed by two bays of 5 m length, while the inter-storey height is of 3 m. As explained in (Polese et al., 2013a), the simulated design is performed with allowable stresses for concrete of σ_c = 6 MPa for columns and 7.5 MPa for beams, while the allowable stress for steel, that considering the design period is assumed to be a smooth type Aq50 (R.D.L. no. 2229/1939), is σ_s = 180 MPa (Verderame et al., 2012).

The columns dimensions are represented in Fig. 5.12. For what concern the beams, their dimension for the 4 storey RCF vary from 30x60 at the first two storeys to 30x50 at the upper ones, while for 8 storey building the beams at the first three storeys have section 35x65, 30x60 at fifth and sixth storeys, and 30x50 at the upper ones.
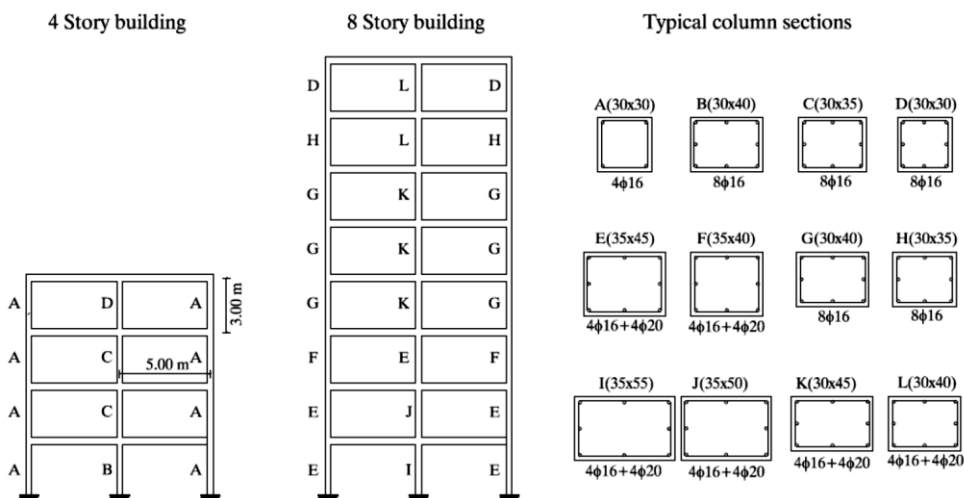
Fig. 5.12 Model geometry and typical columns section and reinforcement.

5.6.1.1 MODELING ISSUES FOR PUSHOVER ANALYSIS

Structural modeling, numerical analyses and post-processing of damage data, including the 3D graphic visualization of the deformed shape, are performed through the "PBEE toolbox" (Dolšek, 2010), which allows rapid generation of simple nonlinear models and the analysis of RC frames combining MATLAB® with OpenSees (McKenna, 2011). The toolbox was suitably modified in order to allow definition of bilinear plastic hinges according to ASCE-SEI/41 (ASCE, 2007) and in order to allow the plastic hinge modification for the analyses of damaged buildings, as described later.

A lumped plasticity model was adopted for the two-dimensional MDOF Reinforced Concrete Frame buildings. The model is very simplified, not including geometric nonlinearity (i.e. P-Δ effects). In addition, although brittle shear failures in columns or beams may be expected in existing under-designed buildings (Verderame et al., 2009;

Polese et al. 2011) and brittle behavior of beam-columns joints (Pagni and Lowes, 2006) is an additional vulnerability factor, these aspects are not considered in this study. Indeed, the main aim of this study is to test the capability of PA to capture, after suitable modification of flexural type plastic hinges, the post-seismic behavior of a damaged building. Therefore, in order to avoid introducing further complexity in the model the sole flexural behavior is explicitly investigated.

For RCF buildings, element flexural behavior is conveniently characterized by a bilinear moment–rotation relationship in the plastic hinges of the beams and columns, described by means of two characteristic points, i.e. the yielding (M_y and θ_y) and ultimate (M_y and θ_u) moment and rotation. The moment M_y can be determined by moment–curvature analyses for the element's extreme sections. In particular, a mean concrete strength of f_c =26.7 MPa and a steel yield stress of f_y=370 MPa are assumed. The latter corresponds to mean yielding value for smooth type steel Aq50 (R.D.L. no. 2229/1939) that, considering a hypothesized construction age of 1960, was one of the most used type of steel. Yielding and ultimate rotations are derived from the ASCE-SEI41 (ASCE, 2007) approach, with updated limit values as suggested in ACI 369R-11 (2011). In particular, yielding rotation θ_y is calculated accounting for a reduced effective stiffness, EI_{eff}, with respect to that of the un-cracked gross section (Elwood and Eberhard, 2009), while ultimate rotation θ_{CP} is obtained by summing a plastic rotation a to the yielding one, depending on section characteristics, see Fig. 5.13.
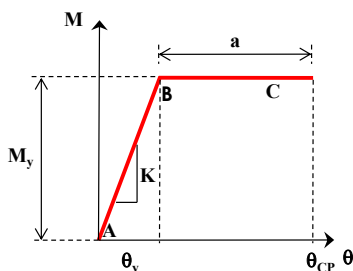
Fig. 5.13 Moment-rotation relationship for plastic hinges

As noted in (Ibarra and Krawinkler, 2005), the frame members in Opensees are modeled as an elastic element connected in series with rotational springs at either end, and the stiffness of these components must be modified so that the equivalent stiffness of this assembly is equivalent to the stiffness of the actual frame member. Following the approach proposed in (Ibarra and Krawinkler, 2005), the rotational springs are made "n" times stiffer than the rotational stiffness of the elastic element in order to avoid numerical problems. To ensure the equivalent stiffness of the assembly is equal to the stiffness of the actual frame member, the stiffness of the elastic element must be "(n+1)/n" times greater than the stiffness of the actual frame member, see Fig. 5.14.
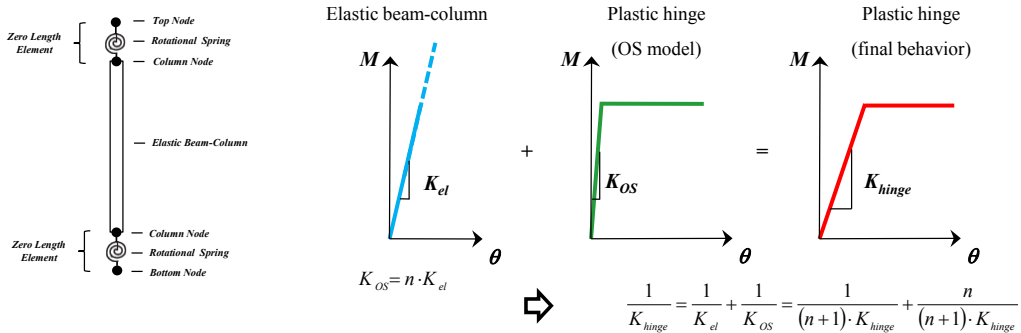
Fig. 5.14 Accounting for serial stiffness of elastic beam-column element and plastic rotational hinge.

5.6.1.2 MODIFICATION OF PLASTIC HINGES FOR DAMAGED ELEMENTS IN PA

For Nonlinear Time History analyses, the seismic behavior of intact buildings may be studied by performing nonlinear static Pushover Analyses (PA). In the same manner, the seismic behavior of damaged buildings may be studied with PA performed on a suitably modified nonlinear model that conveniently account for damage. In fact, given the local damage level in each of the structural elements caused by a hypothetical main-shock, the moment-rotation relationships describing the plastic hinges of the elements that have entered the plastic range are modified as suggested in (Polese et al., 2013a, Di Ludovico et al., 2013), and a new PA for the structure in its damaged state may be performed.

The flowchart in Fig. 5.15, illustrates the basic steps needed to determine the variation in building behavior from the intact to the different damage states.

In particular, each global damage level for the structure corresponds to a local distribution of damage for the structural elements, that may be represented by the local ductility demand for the plastic hinges that have entered the plastic range, see Fig. 5.15. Based on the local ductility demand for the elements, the relative plastic hinges are modified applying a suitable variation in the relative stiffness ($K'=\lambda_k K$), strength ($M_y'=\lambda_Q M_y$) and plastic rotation capacity ($a'= a-a_d = a-(\theta'_y - \theta_y) -RD = a-(\theta_y(\lambda_Q/\lambda_k -1)-RD$), with λ stiffness or strength modification factors and RD residual drift of the element The PBEE toolbox has been conveniently modified in order to allow, after computation of the elements ductility demand for the generic step of PA analysis, the modification of plastic hinges with the formulations proposed in §5.3.2.

Nonlinear static analysis of the modified damaged models yields pushover curves that, depending on the number of elements involved in the damaged mechanism and on their damage level, may differ significantly with respect to the original ones.

178
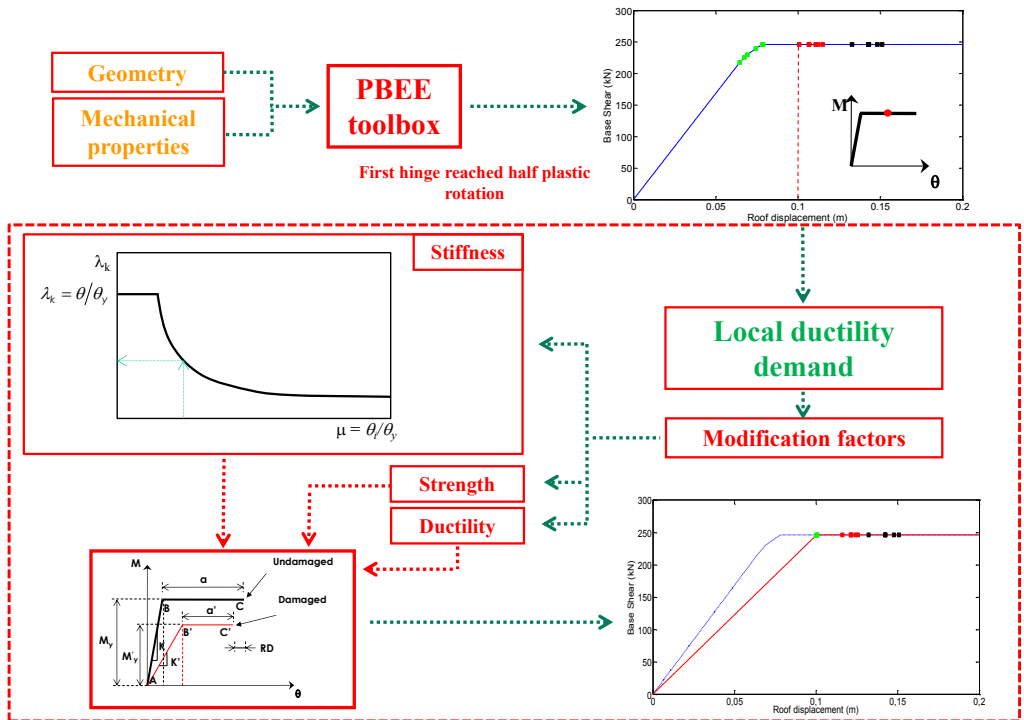
Fig. 5.15 Assessment framework

5.6.1.3 MODELING ISSUES FOR DYNAMIC ANALYSIS

The plastic hinges for beam-column elements are modeled with pinching4 material (Lowes et al., 2004) in Opensees (McKenna, 2011), that allows to simulate their degrading hysteresis behavior with damage progression. Degradation due to damage is assumed to be a function of displacement history and energy accumulation.

Bilinear backbone has been adopted in order to be consistent with the bilinear model adopted in static PA, furthermore, a slight hardening (0.1% of the Young's modulus) has been considered in plastic phase in order to avoid convergence problems.

For NTH analyses, 5% critical damping was assigned (Charney, 2008); mass proportional damping was assumed. During the analysis, local P-delta effects were not included.

5.6.2 PUSHOVER ANALYSIS FOR INTACT AND DAMAGED BUILDINGS

In order to describe the progression of damage due to a hypothetical mainshock, four global damage states (Polese et al., 2013a) were assumed as reference for the assessment for the case-study buildings:

179

D_0 (no damage) in this state the building is still in its intact, or pre-mainshock, condition.

D_1 (limited damage) corresponds to the onset of non-linear behavior, it is assumed as the Yield Displacement on the Idealized (*YDI*) bilinear pushover curve.

D_2 (moderate damage) corresponds to the first attainment of the 50% of the Collapse Prevention (*CP*) limit state for an element (Polese et al., 2013a);

D_3 (collapse) corresponding to the first attainment of the Collapse Prevention limit state (*CP*), that is conventional collapse.

5.6.2.1 ANALYSIS OF THE INTACT STRUCTURE

Pushover analysis for the 'intact' building was performed applying two different horizontal force distributions (proportional to the main vibration mode MO and proportional to masses MA), as required by modern seismic codes (e.g., CEN 2005). The resulting pushover curves are shown as gray dashed line in Fig. 5.16(a), and (b), respectively, referring to 4 and 8 storey RCF under MA forces , and in Fig. 5.16(c) and (d) referring to 4 and 8 storey RCF under MO forces, respectively.
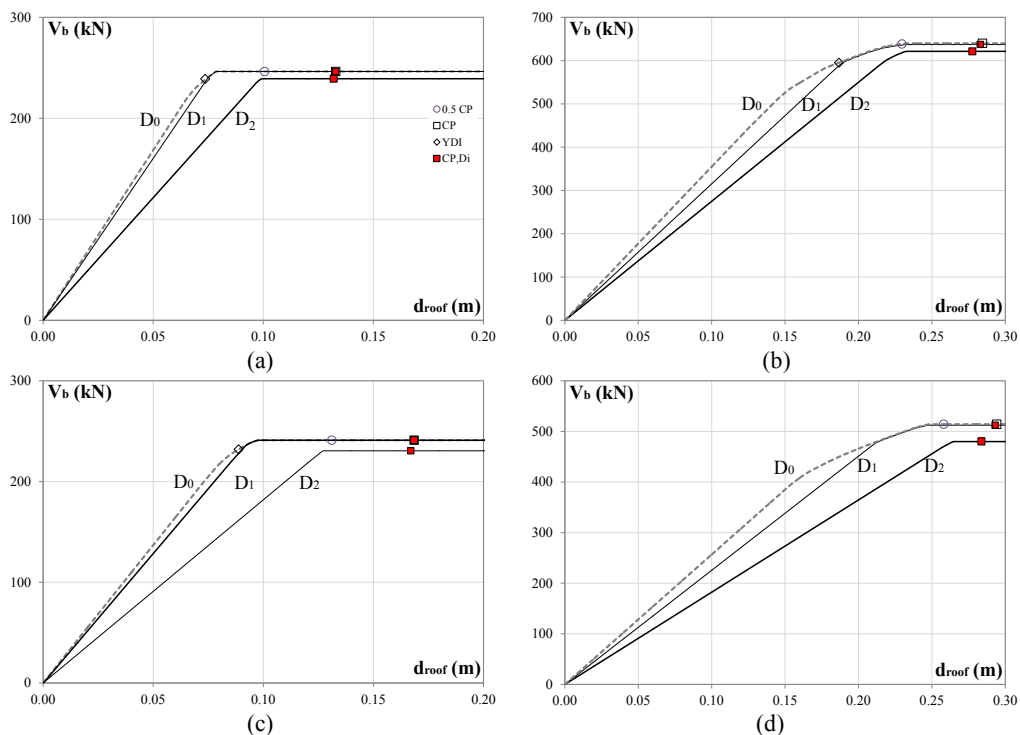
Fig. 5.16 Pushover curves for the 4 and 8 RCFs obtained under MA and MO horizontal forces distribution and for intact (D_0), and D_1 or D_2 damaged states. (a, c) 4 storey MA or MO; (b, d) 8 storey MA or MO

5.6.2.2 ANALYSIS OF THE DAMAGED STRUCTURE

We study the behavior of the two RCFs for the damage states D_1 and D_2. For each of the global damage states a separate analysis of the 'damaged' structure is performed. Each pushover analysis performed for the "intact" structure is stopped in the deformed configuration at D_k (for $k = 1, 2$) and the plastic hinge state (ductility demand) is recorded. Next, the plastic hinges of the elements that have entered the plastic range are modified as a function of their ductility demand. Fig. 5.16 shows the pushover curves obtained for each of the considered damaged models. The grey dashed line represent the pushover curves for the intact structure, indicated as D_0, together with the points corresponding to D_1 and D_2; the black thin line represents the Pushover curve obtained for a structure that has attained damage state D_1 and the black bold line for the damage state D_2. On each of the curves corresponding to the analysis of the damaged building the points corresponding to the first attainment of the (reduced) CP for an element are also shown as small red squares.

The building residual capacity for the intact and damaged states was computed applying the IN2 method (Dolsek and Fajfar, 2004) on the equivalent SDOF obtained based on the relative PA, as explained in (Polese et al., 2013a). Table 5.3 and Table 5.4 summarize the results in terms of REC_{Sa} and REC_{ag}, together with the representative parameters of the equivalent SDOF, obtained after bi-linearization of the capacity curve, T_{eq}, C_b, and μ_{cap}, for the 4 storey and 8 storey building respectively.

ID	Damage	T_{eq} [s]	μ_{cap}	C_b [g]	REC_{Sa} [g]	REC_{ag} [g]	PL
MA	D_0	1.42	1.81	0.15	0.26	0.26	0%
	D_1	1.45	1.73	0.15	0.25	0.26	1%
	D_2	1.67	1.34	0.14	0.19	0.19	26%
MO	D_0	1.24	1.89	0.17	0.33	0.27	0%
	D_1	1.47	1.79	0.17	0.31	0.26	2%
	D_2	1.52	1.31	0.17	0.22	0.24	11%

Table 5.3 Representative parameters of the equivalent SDOF system for the structure in different configurations (intact and damaged) and *REC* in terms of spectral acceleration and anchoring (peak) ground acceleration, for the 4 storey building

ID	Damage	T_{eq} [s]	μ_{cap}	C_b [g]	REC_{Sa} [g]	REC_{ag} [g]	PL
MA	D_0	1.98	1.52	0.19	0.29	0.53	0%
	D_1	2.07	1.39	0.19	0.27	0.52	2%
	D_2	2.21	1.23	0.19	0.23	0.50	5%
MO	D_0	1.68	1.41	0.21	0.30	0.39	0%
	D_1	1.77	1.28	0.27	0.27	0.39	1%
	D_2	1.88	1.15	0.24	0.24	0.38	3%

Table 5.4. Representative parameters of the equivalent SDOF system for the structure in different configurations (intact and damaged) and *REC* in terms of spectral acceleration and anchoring (peak) ground acceleration, for the 8 storey building

It is here noted that, in order to allow appropriate comparison with NTH, the spectrum assumed to determine REC_{ag} from REC_{Sa} is the mean spectrum built from the accelerograms in NTH (see § 5.6.3.1). The mean spectrum is close to Eurocode 8 (CEN 2004), soil type B, spectral shape.

Further important information that may be inferred by Table 5.3 Table 5.4 is the *PL* for each of the damaged configurations. *PL*, which represents a measure of the loss of lateral capacity, is defined as:

$$PL = 1 - \frac{REC_{ag,k}}{REC_{ag,0}}$$
Eq. 5-32

where $REC_{ag,k}$ is residual capacity in terms of peak ground acceleration of the structure in the D_k damage configuration and $REC_{ag,0}$ for the intact structure.

5.6.3 DYNAMIC ANALYSIS FOR INTACT AND DAMAGED BUILDINGS

We want to check if the PA, performed on a suitably modified building model accounting for damage experienced during an earthquake, is able to capture the effective variation of building *REC* and the relative *PL*.

To this end, the REC_{ag} obtained with the methodology described above, relying on modified building model for two considered damage states, namely D_1 and D_2, is compared to the REC_{ag} that can be obtained via NTH.

Similarly to the approach adopted in Rahunandan (2004), in order to study the behavior of the MDOF system after the attainment of the same damage level D_i, as considered for the PA assessment, multiple earthquake sequences are built through suitable scaling of selected accelerograms. In particular, each nonlinear time history analysis is performed applying sequences of two suitably scaled earthquakes. The first one has to be scaled at the intensity able to "damage" the MDOF system to the same damage level considered on the initial pushover (D_1 or D_2). In order to find this damaging intensity, Incremental Dynamic Analysis (IDA) (Vamvatsikos and Cornell, 2002), with the aid of PBEE toolbox (Dolsek, 2010), is performed and the intensities determining the attainment of D_1 and D_2 and D_3 on the initially intact structures, $a_{g,D1}$, $a_{g,D2}$ and $a_{g,D3}$ are retrieved. In particular, $a_{g,D3}$ and $a_{g,D2}$ correspond to the first attainment on IDA curve of CP and CP/2 rotation for a structural element, and $a_{g,D1}$ corresponds to the identification on IDA curve of the maximum Interstorey Drift Ratio (IDR_{max}) corresponding to the YDI evaluated with PA analysis. $a_{g,D3}$ is, by definition, the REC_{ag} for the intact structure computed based on NTH for a single earthquake.

The second earthquake (applied after the first one scaled at $a_{g,Di}$) is the sole one that is successively scaled, performing IDA analysis on a structure that has already attained a given damage state (see Fig. 5.17). This way the $REC_{ag,i}$, varied with respect to the initial one determined on the intact structure, may be determined as the a_g (to which the

second accelerogram has to be scaled) corresponding to building collapse (D_3 state, as defined above).

The PBEE has been modified in order to allow scaling only second record in the sequence, while the first record one is scaled to a fixed IM, namely $a_{g,D1}$ or $a_{g,D2}$, that corresponds to the reaching of a given damage state. A time gap of 20 seconds between first earthquake and second earthquake is added between multiple earthquake events (see Fig. 5.17).
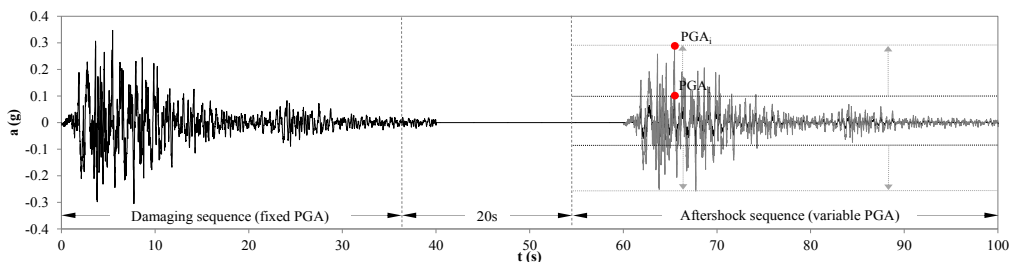
Fig. 5.17 Example seismic sequence.

After the excitation of the first record, the vibration of structure will cease gradually due to damping, so that when the second earthquakes arrives it may be considered as a new one; on the other hand, the structural elements and plastic hinges had been previously damaged by the first record and this shall be properly accounted for by application of the earthquakes in such a "continuous" sequence.

Dynamic analysis of the sequence is repeated with increasing scale factors applied to the second records in the series until the structure collapses, providing incremental dynamic analysis results for structures having attained a given damage level due to the first earthquake.

For what concerns the NTH evaluation, a set of 8 representative ground motions (16 accelerograms, considering the x and y directions of the recorded signals) is selected in order to be compatible with EC 8 spectrum for Soil Type B (stiff soil) (CEN 2004). To account for the effect of record-to-record variability on structural response, IDA is repeated for each of 16 ground motions in the set.

By combining each of the 16 "damaging" ground motions with the same 16 ground motions applied as subsequent earthquakes, a set of 256 record sequences are created for each damage state and structure model.

5.6.3.1 INPUT GROUND MOTIONS
A set of 8 couples of response spectrum compatible natural accelerograms has been used to perform Incremental dynamic analyses (see Table 5.5). Different combinations of first record-second record have been performed in order to simulate damaging earthquake and a subsequent variation in residual capacity in a more realistic way. These records

are earthquakes with M_w between 5.4 and 6.9 and sites with epicentral distance 2.9 to 72.0 km. The unscaled records have peak ground accelerations from 0.11 to 0.40 g.

Single earthquakes were selected from *European Strong-Motion Database (*Ambraseys et al, 2002), according to the following criteria: a) magnitude of event equal to or greater than 4.0; b) available information about the soil condition, which correspond to Soil Type B (CEN 2004); c) seismic sequences having peak ground acceleration (a_g) of the mainshock horizontal component greater than 100 cm/s^2; d) significant duration smaller than 35 s; e) Cosenza and Manfredi Index smaller than 12 (Cosenza and Manfredi, 2009; Trifunac and Brady, 1975). Under these criteria, 8 seismic earthquakes with two orthogonal horizontal components were selected for this investigation. Table 5.5 lists the selected earthquakes and significant seismological parameters.

Earthquake Name	Station	Code	M_w	a_g (g)	I_D	Signif. duration (s)	Epicentral distance (km)
Montenegro 15/4/1979	Ulcinj-Hotel Olimpic, NS	197x	6.9	0.29	10.6	20.9	24
Montenegro 15/4/1979	Ulcinj-Hotel Olimpic, EW	197y	6.9	0.24	7.2	21.7	24
Montenegro 15/4/1979	Bar-Skupstina Opstine, NS	199x	6.9	0.38	8.4	17.9	16
Montenegro 15/4/1979	Bar-Skupstina Opstine, EW	199y	6.9	0.36	10.4	15.7	16
Kalamata 13/9/1986	Kalamata-Prefecture, N265	413x	5.9	0.21	5.4	5.5	5.9
Kalamata 13/9/1986	Kalamata-Prefecture, N355	413y	5.9	0.30	5.8	7.1	5.9
Kalamata 13/9/1986	Kalamata-OTE Build., N80E	414x	5.9	0.24	4.6	5.1	2.9
Kalamata 13/9/1986	Kalamata-OTE Build., N10W	414y	5.9	0.27	7.4	6.3	2.9
Umbria-Marche - 06/10/97	Colfiorito, NS	622x	5.5	0.12	5.2	8.4	5.5
Umbria-Marche - 06/10/97	Colfiorito, EW	622y	5.5	0.11	6.7	7.2	5.5
Filippias 16/06/90	Vasiliki town-Hall, NS	1981x	5.5	0.14	8.7	12.0	59
Filippias 16/06/90	Vasiliki town-Hall, EW	1981y	5.5	0.12	10.2	12.0	59
Mt. Hengill 04/06/98	Thorlakshofn, NS	5081x	5.4	0.20	9.3	10.9	21
Mt. Hengil 04/06/98	Thorlakshofn, EW	5081y	5.4	0.37	8.3	10.9	21
Kozani 13/05/95	Katerini-Agric. Institute, NS	6101x	6.5	0.40	9.2	32.2	72
Kozani 13/05/95	Katerini-Agric. Institute, SW	6101y	6.5	0.34	10.4	32.2	72

Table 5.5 Accelerograms used in the study

Fig. 5.18 shows the elastic 5% damped spectra for the selected earthquakes as well as their mean acceleration spectrum. The mean spectrum is quite similar and even higher for periods around 1.0 to 2.5s as EC 8 spectrum for Soil Type B (CEN 2004).
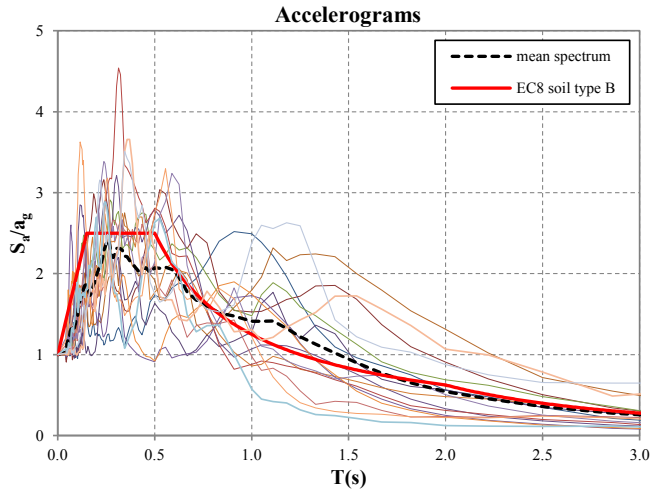
Fig. 5.18 Acceleration spectra for accelerograms recorded on stiff soil.

5.6.3.2 DAMAGING SEQUENCE

As explained §5.6.3.1, for each record initially applied on the structure the intensity measure (in terms of a_g) corresponding to the attainment of damage level D_i is estimated via IDA.
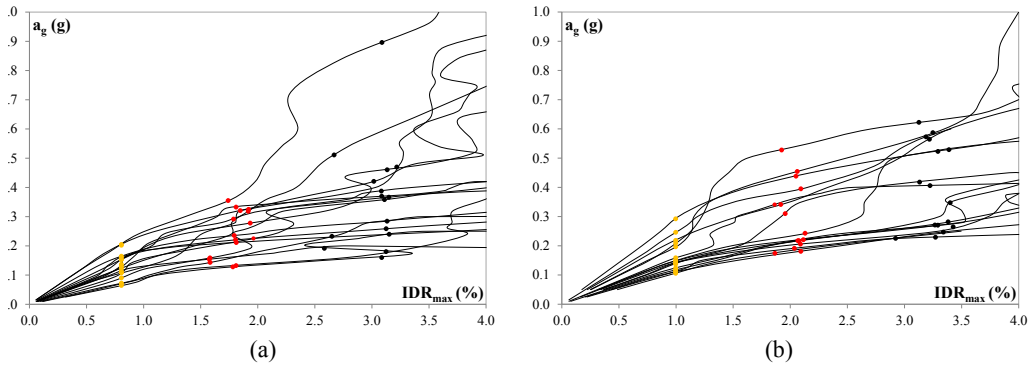
Fig. 5.19 IDA curves for 'intact' buildings subjected to each mainshock. (a) 4 storey, (b) 8 storey building.

In Fig. 5.19 the IDA results for the 4-storey intact building are shown, where x-axis represents the Maximum experienced Interstorey Drift Ratio (IDR_{max}) and the y-axis the peak ground acceleration (a_g). The dot points marked on each IDA curve, that is, CP (black), 0.5CP (red) and that corresponding to the yield displacement of the idealized pushover curve (orange), represent the attainment of global damage states D_3, D_2, and D_1 that will be considered for further analysis of the 'damaged' structure, respectively. Due to differences in frequency content, duration and other ground motion characteristics, each ground motion have to be scaled to a different intensity before a particular damage level occurs.

185
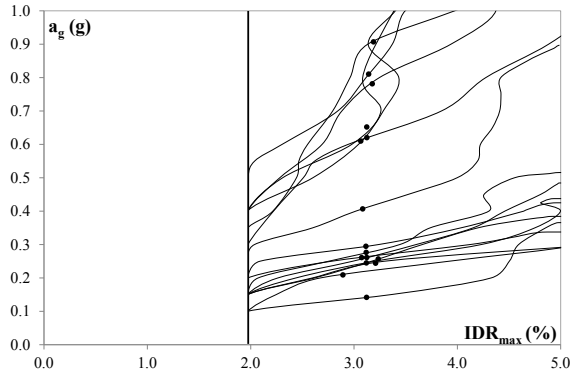
Fig. 5.20 IDA curves for 4 storey building in D_2, subjected to record 197x

Once the $a_{g,D1}$ (or $a_{g,D2}$) is found for each damaging earthquake (first record), the (first record-second record) sequence may be built; the first record is scaled to $a_{g,D1}$ (or $a_{g,D2}$) while the second record has to be scaled in order to perform IDA on D_1 or (D_2) damaged structure. The results for the 4 storey RCF obtained from those IDA sequences are shown in Fig. 5.20 that refers to the record 197x as (first record) damaging earthquake, scaled to $a_{g,D2} = 0.22$. Each point on those curves represent IDR_{max} (maximum interstorey drift ratio) that is attained in correspondence of each intensity level a_g (of the second ground motion in the sequence). Black dots in Figure represent the MDOF response when $D_3|D_2$ damage state is obtained.

Results are shown for 4-storey building that has reached damage state D_2 due to the first record. The black bold line indicates the threshold after which the interstorey drifts undergone during the second record are greater than those experienced during the first record. Indeed, when applying the earthquake sequence, the IDR_{max} that is registered in each analysis will be always the IDR_{max} corresponding to the first earthquake until the second earthquake has an IM such as to let the maximum inter-storey drift increase. The Figure shows significant scatter in the intensity levels at which a particular damage state occurs for different records after the same damaging (first) record.

5.6.4   COMPARISON OF PA AND NTH RESULTS

In this paragraph a comparison between PA and NTH results for the two considered MDOF RCFs is performed. In particular, with the aim of assessing the ability of PA to evaluate the behavior of damaged buildings, we make reference to systems that have attained varying damage levels due to hypothetical main-shocks.

First comparison is performed in terms of the IDR_{max}. Initially, the IDR_{max} distribution along the height for buildings in the undamaged state are compared. In particular, making reference to increasing levels of earthquake demand, i.e. such as to determine the attainment of D_2 or D_3 damage states on the RCFs, the IDR_{max} shapes

obtained through pushover analyses with MA or MO forces distribution (indicated as PA-MA and PA-MO, respectively), are compared with the median values (and 16th and 84th fractiles) obtained with the NTH approach.
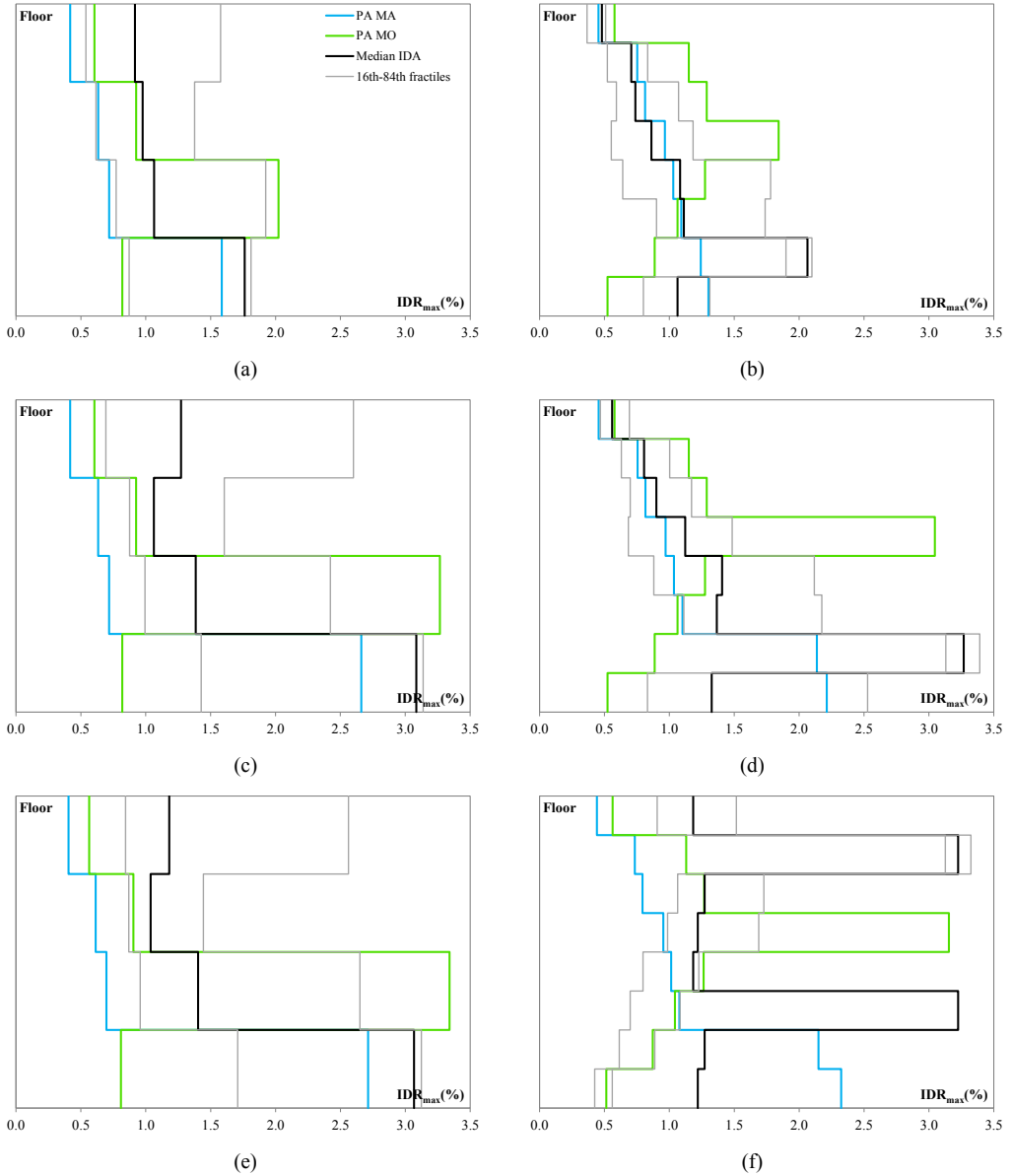
Fig. 5.21 IDR$_{max}$ for 4 storey (a, c, e) and 8 storey building (b, d, f), for 'intact' building with respect to D$_2$ (a, b) and D$_3$ (c, d), and for D$_2$ damaged structure with respect to D$_3$, i.e. IDR$_{max}$ shape at D$_3$|D$_2$ (e, f), respectively.

Fig. 5.21 (a, c) shows the diagrams obtained for the initially intact 4 storey RCF at D_2 and at D_3, respectively. It may be noted, that PA satisfactorily captures the median IDR_{max} shape and value that is obtained through NTH approach; indeed, the plastic mechanism type does not change relevantly for increasing levels of seismic intensity and the MA forces distribution in this case better simulates earthquake response.

Fig. 5.21(b, d) shows similar diagrams for the 8 storey initially undamaged RCF. Although the storey where maximum IDR_{max} is not suitably identified with PA approach, its value compared with median results obtained with NTH approach is satisfactorily captured by the PA-MO.

Fig. 5.21 (e, f), referring to 4 and 8 RCFs respectively, show the IDR_{max} distribution along the height at $D_3|D_2$, i.e. derived for systems that had initially sustained D_2 damage state due to the first earthquakes and that arrive at D_3 for the second earthquake (or are are pushed to D_3 damage state after modification of the MDOF model for PA analysis).

With reference to the 4 storey RCF (Fig. 5.21(e)), it can be seen the maximum inter-storey drifts obtained via PA-MA, and the relative distribution, satisfactorily represent the results that may be obtained via NTH analysis approach. Considering the 8 storey RCF (Fig. 5.21(f)), it is, again, noted that the maximum inter-storey drifts value is captured with reasonable approximation with PA-MO, while the storey where the concentration of damage occurs is the 5th, differently from NTH analysis evidencing a most probable formation of soft storey at level 7. Such discrepancy could be possibly reduced using an adaptive pushover approach.

Second comparison is performed in terms of the REC_{ag}. Fig. 5.22 (a, b, c, d) shows the comparison in terms of $REC_{ag,i}$ for the two considered MDOF systems and two considered damage level. More in detail, Fig. 5.22 (a) refers to the 4 storey RCF, displaying the $REC_{ag,1}$ for the D_1 damaged system. The single $REC_{ag,1}$ values corresponding to each first record (damaging earthquakes) are represented by a number of points aligned along vertical lines (identified by the same ID). Each group of points with the same ID represent the $REC_{ag,1}$ obtained varying the second record in the relative ID sequence (i.e. the sequence with ID record as the first damaging earthquake).

For each group of first record-second record sequence, the median of $REC_{ag,1}$ is represented by black square, while the horizontal continuous line in figure represents the median obtained as the median of those medians. For comparison, the median value of $REC_{ag,1}$ obtained with PA considering the MO and MA distribution is represented as horizontal dashed line in Figure. Fig. 5.22(b), (c) and (d) show similar results with respect to $REC_{ag,1}$ for the 8 storey RCF, for $REC_{ag,2}$ for the 4 storey RCF and for $REC_{ag,2}$ for the 8 storey RCF.

Observing the Fig. 5.22(a) relatively good agreement between the results in terms of $REC_{ag,i}$ obtained with PA, performed on suitably modified model for D_i damaged structure , and those obtained through the consecutive records sequences, suitably scaled as described in §5.6.3.2, is noted. Table 5.6 resumes the median $REC_{ag,i}$ that are obtained

on the intact structures ($REC_{ag,0}$), as well as those obtained for the structures that had been damaged to D_1 or D_2 damage states ($REC_{ag,1}$ or $REC_{ag,2}$), for both PA and NTH based analyses.
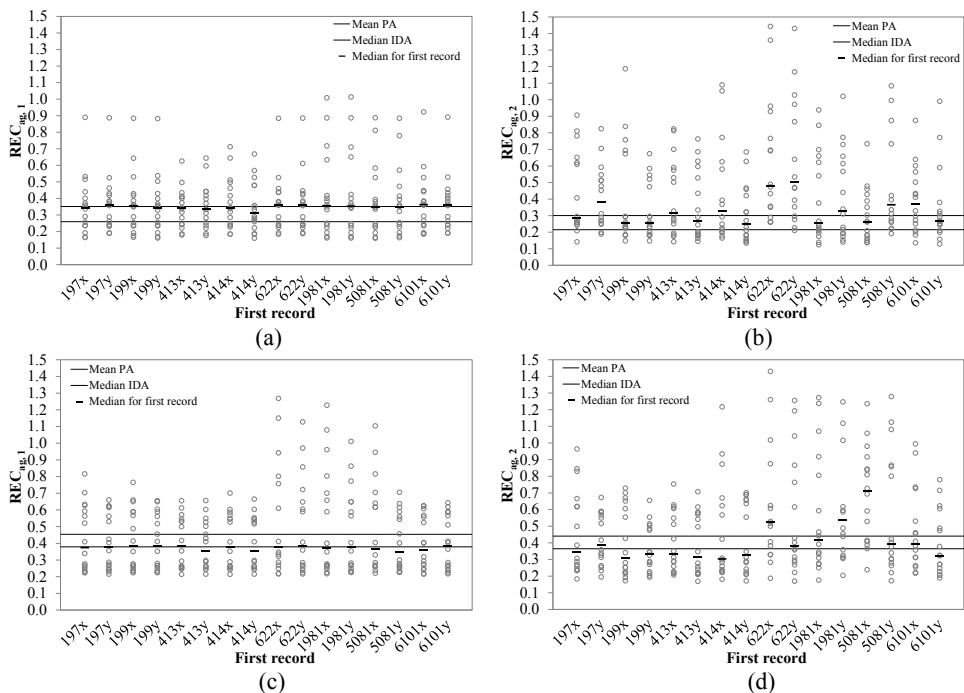
Fig. 5.22 Comparison between PA and NTH computations of $REC_{ag,i}$ for 4 storey (a, c) and 8 storey (b, d) buildings, in damage states D_1 and D_2 respectively.

It has to be noted that it may (rarely) happen that, for the single first record-second record sequences, the REC_{ag} computed after the entire sequence is larger than the REC_{ag} computed for the sole first record. This may happen because of different polarity (i.e direction) of the second earthquake with respect to the first one; indeed if earthquakes have different polarity the second record may beneficially act in reducing residual displacements attained after the first one. It has been shown (Rahunandan et al., 2004) that the polarity of second record with respect to first one may impact the post-earthquake fragilities for extensively damaged buildings. This issue was not investigated in the present study and has to be properly taken into account in future works.

It is interesting to observe that median Performance Loss (Eq. 5-31) that may be expected considering the results of NTH based analyses, i.e. referring to the ratio of the median $REC_{ag,i}$ versus the median $REC_{ag,0}$, is quite close to the median PL that is computed with pushover based approach. In fact, a PL equal to 3.0% or 17.1% is obtained for 4 storey RCF with NTH based analyses for the D_1 or D_2 damaged structures, while PL equal to 1.4% or 18.5% for the same cases is obtained via pushover based

analyses. For the 8 storey RCF, a *PL* of 1.2% or 4.1% is obtained for PA. Analyzing the D_1 or D_2 damaged structures with the NTH approach a slightly negative *PL* is found in the former case, probably due to the polarity issue evidenced before, while a *PL* equal to 3.1% is obtained for the latter case. However, in absolute terms those median *PL* values retrieved with NTH analysis approach are very close to the PA based results.

	4 storey			8 storey		
	$REC_{ag,0}$	$REC_{ag,1}$	$REC_{ag,2}$	$REC_{ag,0}$	$REC_{ag,1}$	$REC_{ag,2}$
NTH (median (g))	0.36	0.35	0.30	0.38	0.38	0.37
PA (median (g))	0.26	0.26	0.22	0.46	0.45	0.44

Table 5.6 Comparison between PA and NTH analysis at damage state D_i

Chapter 6

CONCLUSIONS AND FUTURE WORKS

6.1 CONCLUSIONS

Non-ductile reinforced concrete frame structures represent a large portion of the existing building stock all over the world; the lacking of important reinforcement details on such constructions render them vulnerable and a significant source of hazard to life in future earthquakes as well as a of economic losses during moderate to severe seismic ground motions. Ideally, effective risk mitigation may be obtained with structural retrofit or by building demolition and replacement. However, economic and social constraints impair abrupt application of those solutions, requiring the study of alternative policies to encourage owners of more vulnerable structures to undertake risk assessment and mitigation. One important aspect in debate on risk mitigation is the treatment of buildings damaged by earthquakes and their possible reparability; different solutions may be adopted in order to make cities safer and more resilient to earthquakes, for instance by strengthening those buildings that have been shown by an earthquake to have inadequate seismic resistance.

Building reparability strongly depends on the expected future performance of damaged building and the required repair costs. After earthquakes, the exhaustive assessment of the costs requires detailed on site surveys to establish the damage level, amount of needed interventions to restore the building in all its structural and nonstructural components and the computation of related costs. On the other hand, analytical prediction of damage level due to earthquakes could help significantly to forecast expected costs; also, applying performance-based earthquake engineering methods can contribute significantly to this scope and further allow the sound evaluation of safety variation due to damage, in addition to costs.

The main objective of this research is to explore and test different methods and tools for the assessment of buildings reparability taking into account both the expected safety variation and costs.

In particular, two main level of analyses for the assessment of damaged buildings are explored, namely detailed analysis based on non-linear time-histories, that is finalized to accurate estimation of expected safety variation for mainshocks

corresponding to increasing return period and related repair costs, and pushover based ones, that allows simplified, practice oriented, assessment of variation of the residual capacity and performance loss due to assigned earthquakes.

Accordingly, the thesis is organized in two main parts, describing the models, analyses and results of the two different approaches.

In the first part of this dissertation, a framework for the development of analytical TR-dependent fragility curves is described in order to produce a quantitative evaluation tool for the evaluation of increased vulnerability to collapse conditioned on the return period TR of the damaging earthquake. TR-dependent fragility curves express the probability that capacity of damaged building is equal or smaller than given value conditioned on the return period of the damaging earthquake.

Fragility curves for damaged buildings were developed through a computationally intensive IDA approach to properly account for record-to-record variability. The framework requires several steps including a) the building of a realistic analytical model of structure properly accounting for likely brittle failure of members, consistent system-level collapse definition, b) ground motion suite assembling and probabilistic seismic hazard analysis to define intensity of damaging earthquakes, c) execution of mainshock-aftershock analyses (the so-called back to back incremental dynamic analysis) for a large number of earthquake sequences, d) assessment of earthquake-induced repair costs. The peculiarity of this framework consists in the definition of damaging earthquake as a function of hazard at the site in order to allow a "time-based" assessment possibly accounting for earthquake scenarios with different probabilities of occurrence. Additionally, TR-dependent fragility curves were obtained by modifying classical fragility functions in order to account for possible collapses due to damaging earthquakes.

This framework is demonstrated through two existing non-ductile reinforced concrete (RC) structures with moment-resisting frame, and the response of the building is simulated with a detailed 2D nonlinear multi-degree-of freedom (MDOF) model.

The two studied frames are representative of design and construction practices typical of America and Italy before 1970s. Based on original drawings, building information and analytical modeling techniques of components, high-fidelity frame models accounting for both geometric and material nonlinearities are created in OpenSees (McKenna, 2011).

The analytical model properly account for cumulative damage due to multiple earthquakes through hysteretic rules, damage progress, as well as both shear and axial failure in structural members. In order to account for shear and axial failure, the model proposed by Elwood (2004), that properly account for columns failing in shear after flexural yielding (typical for existing non-ductile columns), was implemented. For beam-column joints two different existing joint shear stress-strain models for the case study buildings, reflecting different construction detailing, are adopted. Two system-

level collapse criteria, namely Gravity Load and Sidesway collapse, have been considered in this study. The former, recently introduced in numerical analyses by Baradaran Shoraka (2013), is introduced considering that collapse of non-ductile buildings could be controlled by the loss of support for gravity loads prior to the complete development of a sidesway collapse mechanism.

Once the analytical models of RC frames for the two case-study buildings were generated, the behavior of intact structures was properly assessed. The initial performance for these analytical frame models was evaluated through both pushover and nonlinear time-history analyses. Pushover analysis was used to study structural deficiencies in the structural behavior by evidencing the structural damage pattern for increasing loads, and then the global damage leading to collapse was properly described. Concerning the dynamic analysis, the probabilistic seismic hazard analysis was carried out for the studied sites, and then a bin of ground motions was selected to estimate the structural response to different return periods of the seismic action, evidencing the probable response of the studied structures. Later, the structural capacity of the intact buildings was estimated and the nonlinear dynamic collapse mechanism evidenced. The post-earthquake behavior of structures was assessed building TR-dependent fragility curves for different return periods of the damaging action in order to investigate the influence of the intensity level (conditioned on site hazard) for the damaging earthquake on residual building capacity. Finally, the PEER framework was adopted for a reliable assessment of repair costs, and relationships between the probability of collapse, performance loss, and costs were investigated.

One interesting aspect that was investigated is the influence of different beam-column joint analytical models. In fact, adopting different joint model for the Italian building, results from pushover analysis show that the model by Jeon et al. (2015) leads to an increased initial stiffness when compared to that when the structure adopts stress-strain relationship by Hassan (2011). The adoption of the analytical model by Jeon et al. (2015) significantly increase the drift demand for the linear load pattern and for both linear and uniform load patterns it also reduces the maximum shear force due to the spread of the damage into joints. The analytical frame model that account for joints and column brittle behavior is the most vulnerable with respect to model that does not consider joint contribution, because it has a sudden drop of lateral load resistance in pushover analysis. However, it is observed that concentrated inelastic action in joints delays the inelastic shear response in columns when compared to the model that account for the sole column brittle failure.

Concerning the collapse mechanism, it is observed that both buildings show inadequate details that lead to concentration of plastic demand in a limited portion of building due to the triggering of brittle member failures. In particular, for the American one, the plastic demand is concentrated in first two storeys leading to a soft-storey

mechanism, however for some ground motions the particular waveform can lead the damage to be concentrated in upper storeys. For the Italian, the damage is more spread through the structure; the contribution of beam-column joints is not negligible delaying the occurring of system-level collapse and allowing the development of a more dissipative collapse mechanism that involves several storeys.

Results carried out from the analysis of the intact building show that as a function of earthquake ground motion waveform, the collapse mechanism can lead to significantly different collapse mechanism that differ for number and level of damage of involved elements.

The results of TR-fragility curves show that the REsidual Capacity REC of a MS-damaged building may be significantly smaller (PL higher) than the REC of an intact building depending on the site hazard. For the American case, when subjected to a MS with a TR of 72 years the building capacity is only slightly affected. For increasing TR, the PL increases very fast up to the 100% for MS corresponding to TR=975 years. For TR=975 years or larger, the number of collapse cases due to MS becomes greater than the non-collapse cases, and the median capacity becomes zero. Concerning the performance loss for the Italian building, different results were carried out. It have to be noted that the performance loss of building in this study is conditioned on the hazard of the specific building site. The American site shows a hazard significantly greater than that obtained for the Italian site leading to a very different earthquake intensity level for a same reference return period. For the same return period of the damaging earthquake, mainshock-induced damage is variable due to frequency content and other ground motion characteristics leading to a dispersion of initial damage from which the reduction of building's capacity is influenced. However, dispersion in damaged capacity is greater when the aftershock adopted for estimate building's capacity vary with respect to the case in which the Mainshock (damaging earthquake) vary and the Aftershock is the same. Performance loss index has been demonstrated to be a reliable and simple parameter to estimate the level of damage in structures. On the other hand, the probability of collapse can be sometimes of difficult computation depending on allowable data. In general, the Performance Loss is a mean index that do not depend on the site hazard unless the damaging earthquake is conditioned on the site hazard.

Repair costs, along with PL, represent a useful indicator able to lead through decision-making process. Main contributors to repair costs are represented by both nonstructural components and building's content for non-collapse cases. When the level of seismic action increases, also the number of collapses increases and the repair cost for non-collapses is significantly higher. For the studied cases, lower values of PL corresponds to high costs; however, over a specific PL threshold, equal increment of PL repair costs corresponds to lower increment of repair costs. This is mainly because acceleration-sensitive, that are some of main contributors to repair costs, are severely damaged since lower values of earthquake intensities adopted in this study; for

increasing intensities, only drift-sensitive components and collapses can lead to an increment of repair costs, and these quantities increase slowly with the increasing of seismic demand

The second part of this dissertation aims at contributing in the evaluation of the usability of a pushover-based analysis method for the assessment of damaged buildings' behavior. In fact, Polese et al. (2013b) demonstrated that Performance Loss of RC frames can be assessed by comparing the capacity of the intact structure assessed through standard pushover analysis with the pushover performed on the damaged structure. In this method, the plastic hinge relationship are suitably modified applying correction factors in order to simulate the damage state in RC members that have entered the plastic range after an earthquake.

In order to allow for concrete application of the procedure presented in Polese et al. (2013b), suitable modification factors of moment-rotation plastic hinges depending on damage state were calibrated. Tests on non-conforming columns typical of existing buildings in Mediterranean regions were selected. In particular, a database of 23 cyclic tests on flexure or flexure-shear controlled square/rectangular RC columns reinforced with deformed bars and of 13 cyclic tests for columns with smooth bars was assembled. The experimental outcomes in terms of lateral load versus drift were elaborated in order to calibrate modification factors for plastic moment rotation hinges. Based on experimental trends suitable formulations for stiffness, strength and residual drift modification factors have been proposed as a function of member rotational ductility demand.

The further step for demonstrating the efficiency of Pushover analysis PA to capture the variation of buildings Residual Capacity REC after they have sustained varying damage levels due to hypothetical main-shock, was to check by comparison of the PA results with those of Nonlinear Time-History analysis NTH. Two case study Reinforced Concrete Frames (RCF) were considered, namely a 4 storey and an 8 storey RCFs that were designed in 1st seismicity class according to old seismic codes in force in Italy in the early '60s. The results suggest that, although by applying a pushover based procedure for the assessment of damaged buildings the results will be inevitably affected by a certain degree of approximation with respect to nonlinear time history analyses executed on a set of seismic sequences, such approximation does not vary significantly with respect to the one that is obtained with standard PA applied to intact structures.

6.2 FUTURE WORKS

The study presented in this dissertation should be further extended through additional research:

Application of PEER framework for Italian case-study has highlighted that reliable data for the estimation of direct losses are still lacking. Fragility curves proposed for typical American structural and nonstructural members cannot be improperly and indiscriminately extended to typical Italian components. Fragility functions could be created starting from experimental data, analytical studies or expert opinion, while consequence function suitably established based on expert opinion or elaboration of data from past earthquake by associating observed damage and repair costs.

In this dissertation variability of repair costs for the single components has not been addressed. Further studies will have to take into account variability of costs as a function of different repair techniques (that for severe damages should include retrofit costs) and the variation in the extension of damage, as well as cost discount for large quantities.

The present study has adopted a two-dimensional model for the assessment of building performances, assuming same building's response in two orthogonal directions to carry out repair costs. The modeling of three-dimensional effects, including torsional motions and irregularities, as well as the presence of infill walls should be incorporated in the finite element models and their contribution to structural performance should be addressed to reliably assess building performances.

TR-dependent fragilities have been determined for two sole case-study buildings. The framework could be extended to different building classes suitably selecting representative buildings for each class, including different building age of construction and height classes, in order to dispose of a set of aftershock fragility curves for the most common building categories.

It has been demonstrated that PL is a useful index able to indicate the variation of building performance after damage. The establishment of PL thresholds that trigger a specific intervention on a damaged building cannot exclude consideration about repair costs associated with a damaging ground motion and of possible retrofit costs. Further studies are required to assess these thresholds conduced on a large building inventory, in order to suggest a comprehensive and uniformly applicable post-earthquake repair framework, that includes economic loss estimate coupled with variation of post-earthquake seismic safety.

The validation of Pushover Analyses PA with Nonlinear Time Histories NTH was carried out for only two case study frame buildings. Moreover, a number of assumptions were applied and further studies will have to further address these issue.

Hinge modification factors have been calibrated taking into account the sole flexural response of members, while simplified pushover-based assessment tools should properly take into account also the variation of capacity connected to brittle failures of members as well as the effect of fatigue on material degradation. Furthermore, modification factors for other structural member (e.g., beam-column joints) should be obtained.

REFERENCES

Abad, J., Ulrich, T., Réveillere, A., & Gehl, P. (2013). Development of damage state-dependent fragility functions for a MDOF structure through dynamic analyses with successive un-scaled time-histories. In *Vienna Congress on Recent Advances in Earthquake Engineering and Structural Dynamics 2013 (VEESD 2013*.

Abrahamson N. and Silva W. (1997). Empirical response spectral attenuation relations for shallow crustal earthquakes." *Seismological Research Letters,* 68 (1), 94 -127.

ACI 318-63 (1963). Building Code Requirements for Reinforced Concrete. American Concrete Institute, Detroit, MI.

ACI 369R-11 (2011). Guide for Seismic Rehabilitation of Existing Concrete Frame Buildings and Commentary. Reported by ACI committee 369, American Concrete Institute. ISBN: 978-0-87031-419-3.

Acun B. and Sucuoglu, H. (2010). Performance of Flexure Controlled Concrete Columns under Severe Displacement Cycles, ACI Structural Journal; 107(3): 364-371.

Alath, S., and Kunnath, S. (1995). Modeling Inelastic Shear Deformation in RC Beam-Column Joints. *Proceedings of the 10th Engineering Mechanics Conference*, Boulder, CO, 822-825.

Alire, D, (2002). Seismic Evaluation of Existing Unconfined Reinforced Concrete Beam-Column Joints*,* Masters Thesis, Seattle, WA: University of Washington: Department of Civil and Environmental Engineering.

Altoontash, A. (2004). Simulation and damage models for performance assessment of reinforced concrete beam-column joints, Ph.D. Thesis, Department of Civil and Environmental Engineering, Stanford University, CA.

Ambraseys, N. (1985). Intensity-attenuation and magnitude-intensity relationships for northwest European earthquakes. *Earthquake engineering & structural dynamics*, *13*(6), 733-778.

Ambraseys, N., Smit, P., Sigbjornsson, R., Suhadolc, P., and. Margaris, B. (2002). Internet-site for european strong-motion data, European Commission, Research-Directorate General, Environment and Climate Programme.

Anderson, M., Lehman, D., and Stanton, J. (2008). A cyclic shear stress-strain model for joints without transverse reinforcemen+B8t. Engineering Structures 30, 941-954

Antoniou, S., Rovithakis, A., Pinho, R. (2002). Development and verification of a fully adaptive pushover procedure, *12th European Conference on Earthquake Engineering*, paper # 822, London.

ASCE (2000). Prestandard and commentary for the seismic rehabilitation of buildings, FEMA-356, Federal Emergency Management Agency, Washington DC.

ASCE (2003). Seismic Evaluation of Existing Buildings, ASCE/SEI 31-03, American Society of Civil Engineers, Reston, Virginia.

ASCE (2005). Minimum design loads for buildings and other structures. ASCE/SEI 7-05 including Supplement No.1, Reston, VA.

ASCE (2007). Seismic Rehabilitation of Existing Buildings, ASCE-SEI 41–06 American Society of Civil Engineers, Reston, Virginia.

Aschheim, M. and Moehle, J.P. (1992). Shear strength and deformability of RC bridge columns subjected to inelastic displacements, UCB/EERC 92/04, University of California, Berkeley, CA.

Aslani H, Miranda E, (2004). Component-level and system-level sensitivity study for earthquake loss estimation. Proceedings of the Thirteenth World Conference on Earthquake Engineering, Vancouver, BC, Canada.

Aslani H, Miranda E. (2005). Probabilistic Earthquake Loss Estimation and Loss Disaggregation in Building. Technical Report No. 157, John A. Blume Center Earthquake Engineering Center, Stanford, CA

Atalay, M.B., Penzien, J. (1975). The Seismic Behavior of Critical Regions of Reinforced Concrete Components as Influenced by Moment, Shear and Axial Force, Report No. EERC 75-19, *University of California, Berkeley*, December, 226 pages.

ATC (1996). Seismic evaluation and retrofit of concrete buildings, Report No. ATC-40, California Seismic Safety Commission (SSC 96- 01), Sacramento, CA.

ATC (2009). Quantification of Building Seismic Performance Factors, FEMA P-695 Report, prepared by the Applied Technology Council for the Federal Emergency Management Agency, Washington, D.C.

ATC (2010). ATC 52-4, Here Today—Here Tomorrow. The Road to Earthquake Resilience in San Francisco, Post-Earthquake Repair and Retrofit Requirements, Applied Technology Council, Prepared for the Department Of Building Inspection (DBI) City And County Of San Francisco under the Community Action Plan for Seismic Safety (CAPSS) Project.

ATC (2012). *FEMA P-58* Next-generation Seismic Performance Assessment for Buildings, Volume 1 – Methodology, Federal Emergency Management Agency, Washington, D.C.

Attaalla, S.A. (2004). General analytical model for normal shear stress of type 2 normal and high strength concrete beam-column joints, ACI Structural Journal, Vol. 101, No. 1, pp. 65–75.

Aycardi, L.E., Mander, J., and Reinhorn, A. (1994). Seismic resistance of reinforced concrete frame structures designed only for gravity loads: experimental performance of subassemblages. *ACI Structural Journal*, 91 (5), pp. 552-563.

Baggio, C., Bernardini, A., Colozza, R., Di Pasquale, G., Dolce, M., Goretti, A., Martinelli, A., Orsini, G., Papa, F., Zuccaro, G., Pinto, A. V., and Taucer, F. (2007). Field Manual for post-earthquake damage and safety assessment and short term countermeasures AeDES , EUR 22868 EN - 2007. *Joint Research Center*, Ispra, Italy.

Baker J. W., Cornell C. A., 2005. Vector-valued ground motion intensity measure consisting of spectral acceleration and epsilon. *Earthquake Engineering & Structural Dynamics*, 34(10), 1193-1217.

Baker, J.W., and Cornell, C.A. (2006a). Spectral shape, epsilon and record selection. *Earthquake Engineering & Structural Dynamics*, *35*(9), 1077-1095.

Baker, J.W., and Cornell, C.A. (2006b). Correlation of response spectra values for multi-component ground motions. *Bulletin of Seismological Society of America*, 96, 215-227,

Baker, J.W., and Cornell, C.A. (2008a). Vector-Valued Intensity Measures Incorporating Spectral Shape for Prediction of Structural Response. *Journal of Earthquake Engineering*, 12(4), 534- 554.

Baker, J.W., and Cornell, C.A. (2008b). Uncertainty Propagation in Probabilistic Seismic Loss Estimation, Structural Safety; 30(3):236–252.

Baker, J.W. (2011). The conditional mean spectrum: A tool for ground motion selection. ASCE *Journal of Structural Engineering*, Vol. 137, No. 3.

Baker, J.W. (2014). Efficient analytical fragility function fitting using dynamic structural analysis. Earthquake Spectra, (in press).

Bakir, P.G., and Boduroglu, H.M. (2002). A new design equation for predicting the joint shear strength of monotonically loaded exterior beam-column joints, Engineering Structures, No. 24, pp. 1105-1117

Bal, İ. E., Crowley, H., Pinho, R., Gülay, G. (2008). Detailed assessment of structural characteristics of Turkish RC building stock for loss assessment models. *Soil Dynamics and Earthquake Engineering*; 28: 914-932.

Bao Y. and Kunnath S. K. (2010). Simplified progressive collapse simulation of RC frame-wall structures. *Engineering Structures* 32, 3153-3162 to conduct system-level progressive collapse

Baradaran Shoraka, M , Elwood, K. J. (2013). Mechanical Model for Non Ductile Reinforced Concrete Columns. Journal of Earthquake Engineering Vol. 17, Iss. 7.

Barin, B., and J. A. Pincheira (2002). Influence of Modeling Parameters and Assumptions on the Seismic Response of an Existing RC Building. Madison, WI: University of Wisconsin-Madison: Department of Civil and Environmental Engineering.

Bazan, M. L. (2008). Response of reinforced concrete elements and structures following loss of load bearing elements. *Civil Engineering Dissertations*, 5.

Bazzurro, P., and Cornell, C.A. (1994). Seismic hazard analysis of nonlinear structures. I: Methodology. Journal of Structural Engineering, 120(11), 3320-3344.

Bazzurro, P., and Cornell, C.A. (1999). Disaggregation of Seismic Hazard. Bulletin of the Seismological Society of America, 89(2), 501-520.

Bazzurro, P., Cornell, C. A., Menun, C. A. and Motahari, M. (2004). Guidelines for seismic assessment of damaged buildings. *Proceedings of the 13th World Conference on Earthquake Engineering*. Vancouver B.C., Canada. Paper No. 1708.

Beck JL, Porter KA, Shaikhutdinov R, Au SK, Mizukoshi K, Miyamura M, Ishida H, Moroi T, Tsukada Y, Masuda M. (2002). Impact of seismic risk on lifetime property values. *Report CKIV-03, Consortium of Universities for Research in Earthquake Engineering*, Richmond, CA.

Benjamin, Jack R. and Cornell, C. Allin (1970). Probability, statistics and decision for civil engineers, McGraw-Hill.

Berry, M., Parrish, M., and Eberhard, M. (2004). PEER structural performance database user's manual, Pacific Earthquake Engineering Research Center, University of California, Berkeley, CA.

Biddah, A., and Ghobarah, P. (1999). Modelling of Shear Deformation and Bond Slip in Reinforced Concrete Joints.*Structural Engineering and Mechanics* 7(4), 413-432.

Birely, A., Lowes, L., and Lehman, D. (2011). A model for the practical nonlinear analysis of reinforced-concrete frames including joint flexibility. *Engineering Structures 34*, 455-465.

Bommer, J.J., Scott, S.G., and Sarma, S.K. (2000). Hazard-consistent earthquake scenarios, *Soil Dynamics and Earthquake Engineering*, Vol. 19, pp. 219-231.

Burak, B. (2010). Analytical Verification of a Simplified Reinforced Concrete Joint Model, Proceedings of the 9th U.S. National and 10th Canadian Conference on Earthquake Engineering, Toronto, Ontario, Canada, July 25-29.

Calvi, G. M., Pinho, R., Magenes, G., Bommer, J. J., Restrepo-Vélez, L. F., and Crowley, H. (2006). Development of seismic vulnerability assessment methodologies over the past 30 years. ISET journal of Earthquake Technology, 43(3), 75–104.

Calvi, G. M., Sullivan, T. J., & Welch, D. P. (2014). A Seismic Performance Classification Framework to Provide Increased Seismic Resilience. In*Perspectives on European Earthquake Engineering and Seismology* (pp. 361-400). Springer International Publishing.

Campbell, K. W., & Bozorgnia, Y. (2008). Empirical ground motion model for shallow crustal earthquakes in active tectonic environments developed for the NGA project. In *Proceedings of fourteenth world conference on earthquake engineering.*

CCSF (2010). San Francisco Building Code, The City and County of San Francisco American Legal Publishing Co., Walnut Creek, California.

Celik, OC. (2007). Probabilistic Assessment of Non-Ductile Reinforced Concrete Frames Susceptible to Mid-America Ground Motions, PhD Dissertation, School of Civil and Environmental Engineering, Georgia Institute of Technology.

Celik, O. C., and Ellingwood, B. R. (2008). Modeling beam-column joints in fragility assessment of gravity load designed reinforced concrete frames.*Journal of Earthquake Engineering*, *12*(3), 357-381.

Charney, F.A. (2008). Unintended consequences of modeling damping in structures, Journal of Structural Engineering, 134(4), 581–592, April 1.

Chiou, B., Darragh, R., Gregor, N., and Silva, W. (2008). NGA Project strongmotion database, *Earthquake Spectra*, Vol. 24, No. 1, pp. 23-44.

Ciampi, V., Eligehausen, R., Bertero, V., and Popov, E. (1981), "Analytical Model for Deformed Bar Bond under Generalized Excitations." *Proceedings of the IABSE Colloquium on Advanced Mechanics of Reinforced Concrete,* Delft, Netherlands

Colangelo, F. (2009). Nonstructural damage of infilled RC frames designed to eurocode. *Atti del XIII Convegno L'Ingegneria Sismica in Italia ANIDIS*.

CEN (2005). Eurocode8 . Design of structures for earthquake resistance. Part 1. General rules, seismic actions and rules for buildings, Brussels.

CEN (2004): Eurocode8. Design of structures for earthquake resistance. Part 3. Assessment and retrofitting of buildings, Brussels.

Convertito, V., and A. Herrero (2004). Influence of focal mechanism in probabilistic seismic hazard analysis, *Bulletin of the Seismological Society of America,* 94, 2124-2136.

Cordova, P. P., Deierlein, G. G., Mehanny, S. S. F., and Cornell, C. A. "Development of a Two-Parameter Seismic Intensity Measure and Probabilistic Assessment Procedure." *The Second U.S.-Japan Workshop on Performance-Based Earthquake Engineering Methodology for Reinforced Concrete Building Structures*, Sapporo, Hokkaido, 187-206.

Cornell CA, 1968. Engineering seismic risk analysis. *Bulletin of the Seismological Society of America*, 58, 1583-1606.

Cosenza, E., Manfredi, G. (2000). Damage indices and damage measures, *Progress in Structural Engineering and Materials,* 2(1) 50–59.

Cosenza E, Manfredi G, Verderame GM (2006) "*A fibre model for push-over analysis of underdesigned reinforced concrete frames*", Computers & structures, 84(13): 904-916.

Cosenza, E., Manfredi, G., Polese, M. (2009). A simplified method to include cumulative damage in the seismic response of SDOF systems, *Journal of Engineering Mechanics*, ASCE, 135(10), 1081-1088.

CS.LL.PP, DM 14 gennaio, (2008). Norme Tecniche per le Costruzioni, *Gazzetta Ufficiale della Repubblica Italiana*, 29 (in Italian).

D. Spallarossa, and S. Barani. Disaggregazione della pericolosità sismica in termini di M-R-ε. Progetto DPC-INGV S1, Deliverable D14, http://esse1.mi.ingv.it/d14.html, 2007.

Dandoulaki, M., Panoutsopoulou, M., and Ioannides, K. (1998). An overview of post-earthquake building inspection practices in Greece and the introduction of a rapid building usability evaluation procedure after the 1996 Konitsa earthquake, *Proceedings of the 11th European Conference on Earthquake Engineering*, Balkema, Rotterdam.

de Souza R.M. (2000). Force-based finite element for large displacement inelastic analysis of frames. PhD thesis, University of California, Berkeley, United States – California.

DeBock , Kim K. Y., Liel A. B. (2013). A Scenario Case Study to Evaluate Methods of Seismic Loss Assessment for Communities of Buildings   D. ICOSSAR 11th International Conference on Structural Safety & Reliability June 16-20, 2013 Columbia University New York, NY.

Deierlein, G.G. 2004. Overview of a Framework Methodology for Earthquake Performance Assessment. Performance- Based Seismic Design: Concepts and Implementation, Bled, Slovenia, PEER 2004/05, 15–26.

Di Ludovico, M., Verderame, G.M., Prota, A., Manfredi, G., Cosenza, E. (2009). Experimental investigation on non-conforming full scale RC columns, *ANIDIS 2009 Conference, Bologna, Italy.*

Di Ludovico, M., Verderame, G., Prota, A., Manfredi, G., and Cosenza, E. (2012). Experimental Behavior of Non-Conforming RC Columns with Plain Bars under Biaxial Bending, ASCE- Journal of Structural Engineering , doi; 10.1061/(ASCE)ST.1943-541X.0000703.

Di Ludovico M, Polese M, Gaetani d'Aragona M, Prota A, Manfredi G (2013). Modeling of damaged RC columns in nonlinear static analyses: a proposal for plastic hinges modification factors. Engineering Structures, 51, 99–112, 2013.

Di Pasquale, E., Ju, J. W., Askar, A., & Çakmak, A. S. (1990). Relation between global damage indices and local stiffness degradation. Journal of Structural Engineering, 116(5), 1440-1456.

DoD. (2005). Unified Facilities Criteria: Design of Buildings to Resist Progressive Collapse, *UFC 4-023-03*. US Department of Defense Washington DC.

Dolšek, M. (2010). Development of computing environment for the seismic performance assessment of reinforced concrete frames by using simplified nonlinear models. *Bulletin of Earthquake Engineering*, 8(6), 1309-329.

Dolsek, M., Fajfar, P. (2004). IN2- A simple alternative for IDA, 13th World Conference on Earthquake Engineering, Paper No. 3353, Vancouver, B.C., Canada.

Eads, L., Miranda, E., Krawinkler, H., and Lignos, D. G. (2013). "An efficient method for estimating the collapse risk of structures in seismic regions." Earthquake Engineering & Structural Dynamics, 42(1), 25–41

Ebrahimian, H, Jalayer, F, Asprone, D, Lombardi, AM, Marzocchi, W, Prota, A, Manfredi, G. A (2014). Performance-based Framework for Adaptive Seismic Aftershock Risk Assessment. Earthquake Engineering and Structural Dynamics, Volume 43, Issue 14, pages 2179–2197, November.

EERI (1994). Northridge Earthquake January 17, 1994 Preliminary Reconnaissance Report. Oakland, CA: Ed. J.F. Hall, 1994.

El-Attar, A. G., White, R. N., & Gergely, P. (1997). Behavior of gravity load design reinforced concrete buildings subjected to earthquakes. *ACI Structural Journal*, *94*(2).

Elwood, K. J. (2002). *Shake table tests and analytical studies on the gravity load collapse of reinforced concrete frames* (Doctoral dissertation, University of California, Berkeley).

Elwood, K.J. and Moehle, J.P. (2003) *Shake table tests and analytical studies on the gravity load collapse of reinforced concrete frames*, PEER Report 2005/13, Pacific Earthquake Engineering Research Center, University of California, Berkeley, CA.

Elwood, K. J. (2004). *Modelling Failures in Existing Reinforced Concrete Columns*. Canadian Journal of Civil Engineering: 846-859.

Elwood, K.J. and Moehle, J.P. (2005) *Drift capacity of reinforced concrete columns with light transverse reinforcement*, Earthquake Spectra, Vol. 12, No. 1, pp. 71–89

Elwood, K.J., Matamoros, A., Wallace, J.W., Lehman, D.E., Heintz, J.A., Mitchell, A., Moore, M.A., Valley, M.T., Lowes, L. Comartin, C., and Moehle, J.P. (2007). Update of ASCE/SEI 41 Concrete Provisions, *Earthquake Spectra*, August; 23(3): 493-523

Elwood, K.J. and Eberhard, M., (2008). Effective stiffness of reinforced concrete columns. American Concrete Institute.

Elwood, K.J. and Moehle, J.P. (2008). Dynamic collapse analysis for a reinforced concrete frame sustaining shear and axial failures, Earthquake Engineering and Structural Dynamics; 37(7):991–1012.

Elwood, K.J. and Eberhard, M.O. (2009). Effective Stiffness of Reinforced Concrete Columns, *ACI Structural Journal*, American Concrete Institute, July; 106(4): 476-484.

Engindeniz, M. (2008). "*Repair and Strengthening of Pre-1970 Reinforced Concrete Corner Beam-Column Joints Using CFRP Composites*", PhD Thesis, Civil and Environmental Engineering Department, Georgia Institute of Technology, August.

Fabbrocino, G., Verderame, G.M., Manfredi, G. (2005). Experimental behavior of anchored smooth rebars in old type reinforced concrete buildings. *Engineering Structures*, August; 27(10): 1575-1585.

Fajfar, P. (1992). Equivalent ductility factors taking into account low cycle fatigue. *Earthquake Eng. Struct. Dyn.*; 21: 837–848.

Fajfar, P., Gašperšič, P. (1996).The N2 method for the seismic damage analysis of RC buildings. *Earthquake Engineering and Structural Dynamics*, 25, 31–46.

Fajfar P. (1999). Capacity spectrum method based on inelastic demand spectra. *Earthquake Engineering and Structural Dynamics,* August; 28: 979-93

Fardis, M.N., Biskinis, D.E. (2003). Deformation capacity of r.c. members, as controlled by flexure or shear. In: Performance based engineering for earthquake resistant reinforced concrete structures: A Volume Honoring Shunsuke Otani, Kabeyasawa T, Shiohara H, editors. *University of Tokyo*; p. 511.

Favata M., Izzuddin B.A., Karayannis, C.G., *Modeling Exterior Beam-Column Joints for Seismic Analysis of RC Frame Structures*, Earthquake Engineering and Structural Dynamics, 37:1527-1548, 2008.

FEMA 306 (1998) Evaluation of Earthquake Damaged Concrete and Masonry Wall Buildings – Basic procedures manual. Federal Emergency Management Agency. Washington D.C.

FEMA 308 (1998) Repair of earthquake damaged concrete and masonry wall buildings. Federal Emergency Management Agency. Washington D.C.

FEMA P-440A (2009). The Effects of Strength and Stiffness Degradation on Seismic Response, Technical Report FEMA, Washington, D.C

FEMA P-695 (2009). Quantification of Building Seismic Performance Factors, Technical Report FEMA, Washington, D.C.

Field EH. 2005. Probabilistic seismic hazard analysis (PSHA): A primer. http://www.relm.org/tutorial_materials/ PSHA_Primer_v2.pdf.

Filippou, F., Popov, E., and Bertero, V. (1983). Modeling of R/C Joints under Cyclic Excitations. *Journal of Structural Engineering* 109(11), 2666-2684.

Goulet, C. A., Haselton, C. B., Mitrani-Reiser, J., Beck, J. L., Deierlein, G. G., Porter, K. A., & Stewart, J. P. (2007). Evaluation of the seismic performance of a code-conforming reinforced-concrete frame building—from seismic hazard to collapse safety and economic losses. *Earthquake Engineering & Structural Dynamics*, *36*(13), 1973-1997.

Goulet, C. A., Watson-Lamprey, J., Baker, J. W., Haselton, C. B., & Luco, N. (2008). Assessment of ground motion selection and modification (GMSM) methods for non-linear dynamic analyses of structures. *Geotechnical Earthquake Engineering and Soil Dynamics IV*, 1-10.

Grierson, D.E., Safi, M., Xu, L. and Liu, Y. (2005a). Simplified Methods for Progressive-Collapse Analysis of Buildings. *Proceedings - 2005 Structures Congress and the 2005 Forensic Engineering Symposium - Metropolis and Beyond*. New York, NY, USA, ASCE 2279-2286.

Grierson, D.E., Xu, L. and Liu, Y. (2005b). Progressive-Failure Analysis of Buildings Subjected to Abnormal Loading. *Computer-Aided Civil and Infrastructure Engineering* 20(3): 155-171.

GSA. (2003). Progressive Collapse Analysis and Design Guidelines for NewFederal Office Buildings and Major Modernization Projects. US General Service Administration Washington DC.

Hakuto S, Park R, Tanaka H. (2000). Seismic load tests on interior and exterior beam–column joints with substandard reinforcing details, *ACI Structural Journal*; 97(1):11–25.

Haselton C. B. (2006). Assessing seismic collapse safety of modern reinforced concrete frame buildings. Ph.D. dissertation, Department of Civil and Environmental Engineering, Stanford University, United States.

Haselton, C. B., & Baker, J. W. (2006, April). Ground motion intensity measures for collapse capacity prediction: Choice of optimal spectral period and effect of spectral shape. In *8th National Conference on Earthquake Engineering* (pp. 18-22).

Haselton, C. B., & Deierlein, G. G. (2008). Assessing Seismic Collapse Safety of Modern Reinforced Concrete Moment-Frame Buildings. *University of California, Berkeley*.

Haselton, C. B., Liel, A. B., Taylor Lange, S., and Deierlein, G. G. (2008). Beam-Column Element Model Calibrated for Predicting Flexural Response Leading to Global Collapse of RC Frame Buildings. *Pacific Earthquake Engineering Research Cente*r, Berkeley, CA.

Haselton, C. B., Baker, J. W., Liel, A. B., & Deierlein, G. G. (2009). Accounting for ground-motion spectral shape characteristics in structural collapse assessment through an adjustment for epsilon. *Journal of Structural Engineering*, *137*(3), 332-34

Hassan, W. M., Park, S., Lopez, R.R., Mosalam, K. M., and Moehle, J. P. (2010). Seismic Response of Older-Type Reinforced Concrete Corner Joints, Proceedings of the 9th U.S. National and 10th Canadian Conference on Earthquake Engineering, Toronto, Ontario, Canada, July 25-29.

Hassan WM. (2011). *Analytical and experimental assessment of seismic vulnerability of beam–column joints without transverse reinforcement in concrete buildings*. Ph.D. thesis, Department of Civil and Environmental Engineering, University of California, Berkeley, CA; 2011.

Hassan, W. M., & Moehle, J. P. (2012). A Cyclic Nonlinear Macro Model for Numerical Simulation of Beam-Column Joints in Existing Concrete Buildings. In*Proceedings of the 15 th World Conference of Earthquake Engineering*.

Hoffman GW, Kunnath SK, Mander JB, Reinhorn AM. Gravity-load designed reinforced concrete buildings: Seismic evaluation strategies for improved seismic resistance. National Center of Earthquake Engineering Research, State University of New York at Buffalo, NY, Technical Report NCEER-92-0016; 1992.

Holmes, W. T. (1994). Policies and Standards for Reoccupancy Repair of Earthquake-Damaged Buildings. Earthquake Spectra, February, 10(1): 197-208.

Holmes WT, Luco N, Turner F, (2014) Application of the Recommendations of the Canterbury Earthquakes Royal Commission to the Design, Construction, and Evaluation of Buildings and Seismic Risk Mitigation Policies in the United States, Earthquake Spectra; 30(1):427–450

Hwang, S. and Lee, H. (1999). Analytical model for predicting shear strengths of exterior reinforced concrete beam-column joints for seismic resistance, ACI Structural Journal, Vol. 96, No. 5, pp. 846–857. 320

Hwang, S. and Lee, H. (2000). Analytical model for predicting shear strengths of interior reinforced concrete beam-column joints for seismic resistance, ACI Structural Journal, Vol. 97, No. 1, pp. 35–44.

Ibarra, L. F., and Krawinkler, H. (2005). Global collapse of frame structures under seismic excitations. John A. Blume Earthquake Engineering Center, Stanford, CA, 324.

Iervolino I, Maddaloni G, Cosenza E, (2008). Eurocode 8 compliant real record sets for seismic analysis of structures. Journal of Earthquake Engineering;12(1):54–90.

Iervolino I, Maddaloni G, Cosenza E. (2009). A note on selection of time-histories for seismic analysis of bridges in Eurocode 8. Journal of Earthquake Engineering 2009;13(8):1125–52.

Iervolino I, Galasso C, Cosenza E. (2010). REXEL: computer aided record selection for code-based seismic structural analysis. Bulletin of Earthquake Engineering;8:339–62.

Islam, M.S., (1996a). "Analysis of the response of an instrumented 7-story non-ductile concrete frame building damaged during the Northridge Earthquake," *Proceedings of 1996 Annual Meeting of Los Angeles Tall Buildings Structural Council,* Los Angeles, CA, May.

Islam, M.S., (1996b). "Holiday Inn," *1994 Northridge Earthquake Buildings Case Study Project, Proposition 122: Product 3.2,* Seismic Safety Commission, Sacramento CA, 189-233.

Islam, M. S., Gupta, M., and Kunnath, S. (1998). Critical review of the state-of-the-art analytical tools and acceptance criterion in light of observed response of an instrumented nonductile concrete frame building, *Proceedings of 6th U.S. National Conference on Earthquake Engineering, Seattle, WA, May 31–June 4, 1998*, Earthquake Engineering Research Institute, Oakland, CA.

Jalayer F. and Cornell C. A. (2009). Alternative non-linear demand estimation methods for probability-based seismic assessments. *Earthquake Engineering and Structural Dynamics* 38, 951-972.

Jalayer F., Asprone D., Prota A., Manfredi G, (2011a). A decision support system for post-earthquake reliability assessment of structures subjected to after-shocks: an application to L'Aquila earthquake, 2009, Bulletin of Earthquake Engineering, 9 (4) , pp. 997-1014.

Jalayer F., Asprone D., Prota A., Manfredi G. (2011b). Multi-Hazard Upgrade Decision-Making for Critical Infrastructure based on Life Cycle Cost Criteria, Earthquake Engineering and Structural Dynamics, 40 (10) , pp. 1163-1179.

Jayaram, N., and Baker, J. W. (2010). Ground-motion selection for PEER Transportation Systems Research Program, in Proceedings, 7th CUEE and 5th ICEE Joint Conference, Tokyo, Japan.

Jayaram, N., Lin, T., and Baker, J. W. (2011). "A computationally efficient ground-motion selection algorithm for matching a target response spectrum mean and variance." Earthquake Spectra, 27(3), 797-815

Jalayer, F., Beck, J.L., Zareian, F. (2012). Intensity Measures of Ground Shaking Based on Information Theory, Journal of Engineering Mechanics, 138 (3) , pp. 307-316.

JBDPA (1977). *The Japan Building Disaster Prevention Association*. Guideline for Post-earthquake Damage Evaluation and Rehabilitation, revised in 1990 and 2001 (in Japanese).

Jennings, P.C. (1971). *Engineering Features of the San Fernando Earthquake of February 9, 1971,* Report EERL 71–02, California Institute of Technology, Pasadena, CA.

Jeon, J. S., DesRoches, R., Brilakis, I., & Lowes, L. N. (2012). Aftershock fragility curves for damaged non-ductile reinforced concrete buildings. In*Proceedings of the 15 th World Conference on Earthquake Engineering*.

Jeon, J. S. (2013). Aftershock vulnerability assessment of damaged reinforced concrete buildings in California. PhD Dissertation.

Jeon, J. S., Lowes, L. N., DesRoches, R., & Brilakis, I. (2015). Fragility curves for non-ductile reinforced concrete frames that exhibit different component response mechanisms. *Engineering Structures*, *85*, 127-143.

Joint ACI-ASCE Committee 352. (2002). Recommendations for design of beam–column connections in monolithic reinforced concrete structures *(ACI 352R-02)*. Farmington Hills, MI, American Concrete Institute.

Kaewkulchai, G., & Williamson, E. B. (2004). Beam element formulation and solution procedure for dynamic progressive collapse analysis. *Computers & Structures*, *82*(7), 639-651.

Kaewkulchai, G. and Williamson, E.B. (2006). Modeling the Impact of Failed Members for Progressive Collapse Analysis of Frame Structures. *ASCE Journal of Performance of Constructed Facilities* 20(4): 375-383.

Kaku T, Asakusa H. (1991). *Bond and anchorage of bars in reinforced concrete beam–column joints. Design of Beam–Column Joints for Seismic Resistance (ACI SP-123)*, Detroit, MI, American Concrete Institute; p. 401–23.

Katsanos, E. I. (2010). Selection of earthquake ground motion records: A state-of-the-art review from a structural engineering perspective, Soil Dynamics and Earthquake Engineering 30, 157–169.

Kim, H. (2006*)*. Progressive Collapse Behavior of Reinforced Concrete Structures with Deficient Details*, PhD Thesis, The University of Texas at Austin, USA.

Kim H., Kim J. and An D. (2009). Development of integrated system for progressive collapse analysis of building structures considering dynamic effects. *Advances in Engineering Software* 40, 1-8.

Kim, J. and LaFave, J.M. (2009). Joint shear behavior of reinforced concrete beamcolumn connections subjected to seismic lateral loading, Report No. NSEL–020, Department of Civil and Environmental Engineering, University of Illinois at Urbana-Champaign, IL.

Kramer, S. L. (1996). Geotechnical Earthquake Engineering, Prentice Hall.

Krawinkler, H., Seneviratna, G.D.P.K. (1998). Pros and cons of a pushover analysis of seismic performance evaluation. *Engineering Structures*, 20(4-6), 452–64.

Krawinkler, H., and Miranda, E. (2004) "Performance-based earthquake engineering", "Earthquake Engineering: From Engineering Seismology to Performance-Based Engineering." Chapter 9, pp. 9-1 to 9-59.

Krawinkler, H. (2005). Van Nuys Hotel Building Testbed Report: Exercising SeismicPerformance Assessment*, PEER 2005/11, University of California, Berkeley, Oct. 2005.*

Kunnath, S.K., Hoffmann, G., Reinhorn, A.M., and Mander, J.B. (1995). Gravity-load-designed reinforced concrete buildings -- part I: seismic evaluation of existing construction, *ACI Structural Journal*, 92 (3).

Kurama, Y. C., Pessiki, S. P., Sause, R., & Wu, S. (1994). Seismic behavior of non-ductile concrete frame structures. In *Structures Congress XII* (pp. 1496-1501). ASCE.

LaFave JM, Shin M (2005). Discussion of 'Modeling reinforced-concrete beam-column joints subjected to cyclic loading, by Lowes LN, Altoontash A, *Journal of Structural Engineering* (ASCE) 131(6): 992–993.

Lawson, R.S., Vance, V., Krawinkler, H. (1994). Nonlinear static push-over analysis — why, when, and how? In: *Proceedings 5th US NCEE*, vol. 1. IL, USA: Chicago; 283–92.

LeBorgne, M.R. (2012) *Modeling the post shear failure behavior of reinforced concrete columns*, Ph.D. Thesis, The University of Texas at Austin, Austin, TX.

LeBorgne MR, Ghannoum W.(2014). Analytical element for simulating lateral-strength degradation in reinforced concrete columns and other frame members, ASCE Journal of Structural Engineering 2014; 140(7):04014038, 1–12.

Lee, D.H. and Elnashai, A.S. (2001) *Seismic analysis of RC bridge columns with flexureshear interaction*, ASCE Journal of Structural Engineering, Vol. 127, No. 5, pp. 546–553.

Leon, R.T. (1989). Interior joints with variable anchorage lengths. ASCE J Struct Eng;115(9):2261–75.

Li, Y.R., and Jirsa, J.O. (1998). Nonlinear analyses of an instrumented structure damaged in the 1994 Northridge Earthquake," *Earthquake Spectra*, 14 (2), 245-264.

Liel, A. B., Deierlein, G.G. (2008). Assessing the Collapse Risk of California's Existing Reinforced Concrete Frame Structures: Metrics for Seismic Safety Decisions, Blume Earthquake Engineering Center, No. 166, Stanford University.

Liel, A.B. (2011). Communication with professional engineers J. Heintz (of the Applied Technology Council, Redwood City), J. Maffei and W. Holmes (of Rutherford and Chekene Engineers, San Francisco), and E. Reis (of Certus Consulting, Oakland).

Lowes, L. N., and . Moehle, J.P. (1999). Evaluation and Retrofit of Beam-Column T-Joints in Older Reinforced Concrete Bridge Structures. *ACI Structural Journal*: 519-532.

Lowes, L. N., Mitra, N., & Altoontash, A. (2003). A beam-column joint model for simulating the earthquake response of reinforced concrete frames. Pacific Earthquake Engineering Research Center, College of Engineering, University of California.

Lowes, L.N., and Altoontash, A. (2003). Modeling Reinforced-Concrete Beam-Column Joints Subjected to Cyclic Loading, ASCE Journal of Structural Engineering, V. 129, No. 12, pp. 1686-1697

Lowes, L.N., Nilanjan, M., Altoontash, A. (2004). A beam-column joint model for simulating the earthquake response of reinforced concrete frames, PEER Report 2003/10, Pacific Earthquake Engineering Research Center, University of California, Berkeley, February.

Luco, N., Bazzurro, P. and Cornell, C. A. (2004). Dynamic versus static computation of the residual capacity of a mainshock-damaged building to withstand an aftershock. *13th World Conference on Earthquake Engineering*. Paper No. 2405

Lynn, A. C.; Moehle, J. P.; Mahin, S. A. and Holmes, W. T. (1996). Seismic Evaluation of Existing Reinforced Concrete Columns, Earthquake Spectra; 21(4): 715-739.

Maeda, M., Nakano, Y., Lee, K.S. (2004). Post-Earthquake Damage Evaluation for R/C Buildings Based on Residual Seismic Capacity, *13th World Conference on Earthquake Engineering*, Vancouver, B.C., Canada. Paper No. 1179.

Maffei J, Telleen K, Mohr D, Holmes W (2006). Test Applications of Advanced Seismic Assessment Guidelines, PEER Report 2005/09, Pacific Earthquake Engineering Research Center. University of California, Berkeley.

Marini, A., and Spacone, E. (2006). Analysis of Reinforced Concrete Elements Including Shear Effects. *ACI Structural Journal*: 645-655.

Matamoros, A.B. (1999). Study of Drift Limits for High-Strength Concrete Columns, *Department of Civil Engineering*, University of Illinois at Urbana-Champaign, Urbana, Illinois, Oct.

McGuire, R. K. (1995). "Probabilistic Seismic Hazard Analysis and Design Earthquakes: Closing the Loop." Bulletin of the Seismological Society of America, 85(5), 1275-1284.

McGuire, R. K. (2004). Seismic hazard and risk analysis. Report MNO-10. Oakland, CA, UA: Earthquake Engineering Research Institute Publication.

McKenna, F. (2011). OpenSees: a framework for earthquake engineering simulation. *Computing in Science & Engineering*, *13*(4), 58-66.

Meletti, C., and V. Montaldo (2007). Stime di pericolosità sismica per diverse probabilità di superamento in 50 anni: valori di ag, *Progetto DPC-INGV S1, Deliverable D2*. [http://esse1.mi.ingv.it/d2.html] (in Italian).

Meletti, C., F. Galadini, G. Valensise, M. Stucchi, R. Basili, S. Barba, G. Vannucci, and E. Boschi (2008). A seismic source zone model for the seismic hazard assessment of the Italian territory, *Tectonophysics* 450, 85–108.

Miranda, E., and Aslani, H. (2003). Probabilistic response assessment for building-specific loss estimation. Report No. *PEER 2003/03*, Pacific Earthquake Engineering Research Center, Richmond, CA. 49 pages.

Miranda E, Aslani H, Taghavi S. (2004). Assessment of seismic performance in terms of economic losses. Proceedings, International Workshop on Performance-Based Seismic Design: Concepts and Implementation, Bled, Slovenia, 2004; 149–160.

Miranda E, Taghavi S. (2005). Approximate Floor Acceleration Demands in Multistory Buildings I: Formulation. Journal of Structural Engineering; 131(2):203–211

Mitra, N. and Lowes, L.N. (2007). *E*valuation, calibration, verification of a reinforced concrete beam-column joint model, ASCE Journal of Structural Engineering, Vol. 133, No. 1, pp. 105–120.

Mitrani-Reiser, J. (2007). An Ounce of Prevention: Probabilistic Loss Estimation for Performance Based Earthquake Engineering, Doctoral Dissertation, California Institute of Technology.

Mitrani-Reiser J, Beck JL. (2007). Incorporating Losses Due to Repair Costs, Downtime and Fatalities in Probabilistic-Based Earthquake Engineering. Proceedings, Computational Methods in Structural Dynamics and Earthquake Engineering, Crete, Greece. 2007

Moehle, J. P., and Mahin, S.A. (1991). Observations on the Behavior of Reinforced Concrete Buildings during Earthquakes, Earthquake-Resistant Concrete Structures—Inelastic Response and Design, SP-127, S. K. Ghosh, ed., American Concrete Institute, Farmington Hills, Mich, pp. 67-89.

Mosier, W. G. (2000). Seismic Assessment of Reinforced Concrete Beam-Column Joints. Master Thesis, Seattle, WA: University of Washington: Department of Civil and Environmental Engineering.

Mwafy, A.M., Elnashai, A.S. (2001). Static pushover versus dynamic collapse analysis of RC buildings. *Engineering Structures*, 23, 407–424.

Naeim, F. and Lew, M. (1995). "On the use of design spectrum compatible time histories," *Earthquake Spectra*, Vol. 11, No. 1, pp. 111-127.

Naeim, F., Alimoradi, A., and Pezeshk, S. (2004). Selection and scaling of ground motion time histories for structural design using genetic algorithms, Earthquake Spectra 20, 413–426.

Nakano, Y., Maeda, M., Kuramoto, H., Murakami, M. (2004). Guideline for post-earthquake damage evaluation and rehabilitation of RC buildings in Japan, *13th World Conference on Earthquake Engineering*, Vancouver, B.C., Canada. Paper No. 124.

Neuenhofer, A., & Filippou, F. C. (1997). Evaluation of nonlinear frame finite-element models. *Journal of Structural Engineering*, *123*(7), 958-966.

NIBS (2003). Earthquake loss estimation methodology, HAZUS-MH MR3:Technical manual. Report prepared for the Federal Emergency Management Agency: Washington D.C.

NIST GCR 10-917-7 (ATC-76-5), (2010). *Program Plan for the Development of Collapse Assessment and Mitigation Strategies for Existing Reinforced Concrete Buildings*. National Institute of Standards and Technology (NIST).

NNT (2008), Ministerial Decree D.M. 14.01.2008 "New Technical Standards for Construction" (In Italian).

Nosho, K., Stanton, J., MacRae, G. (1996). Retrofit of Rectangular Reinforced Concrete Columns using Tonen Forca Tow Sheet Carbon Fiber Wrapping" Report No. SGEM 96-2, *Department of Civil Engineering*, University of Washington, Seattle, Washington, July.

Nuclear Regulatory Commission. Identification and characterization of seismic curves and determination of safe shutdown earthquake ground motion. Regulatory guide 1.165, www.nrc.gov/reading-rm/doc-collections/reg-guides/power-reactors/active/01-165/ (accessed 8/17/2005), 1997.

OPCM 3790 (2009). Ordinance of the President of Counsel of Ministry "Urgent intervention to deal with seismic events occurred in the Abruzzo region on April 6, 2009 and other urgent civil protection provisions" (In Italian)

Otani, S. and Sozen, M.A. (1972). Behavior of multistory reinforced concrete frames during earthquakes, Structural Research Series No. 392, University of Illinois at Urbana-Champaign, IL.

Pagni, C.A., Lowes, L.N. (2006). Fragility Functions for older reinforced concrete beam-column joints, *Earthquake Spectra*, 22 (1), 215–238.

Pampanin, S., et al. (2002). Modeling of Shear Hinge Mechanism in Poorly Detailed R.C. Beam Column Joints, 12th European Conference on Earthquake Engineering, London.

Pampanin, S., Magenes, G., and Carr, A. (2003), Modeling of Shear Hinge Mechanism in Poorly Detailed RC Beam-Column Joints. *FIB Symposium, Concrete Structures in Seismic Regions*, Athens, Greece

Pantelides, C.,Hansen, J.,Nadauld, J., Reaveley, L. (2002). Assessment of Reinforced Concrete Building Exterior Joints With Substandard Details, Technical Report PEER 2002-18, Pacific Earthquake Engineering Research Center (PEER), University of California, Berkeley, CA, May.

Park, R. (1997). A static force-based procedure for the seismic assessment of existing reinforced concrete moment resisting frames. B*ulletin of the New Zealand National Society for Earthquake Engineering*, 30(3), 213-226.

Park, S. and Mosalam, K.M. (2009), Shear Strength Models of Exterior Beam-Column Joints without Transverse Reinforcement. *Report No. Peer-2009/106*, Berkeley, CA.

Park, S. and Mosalam, K.M. (2012a). Analytical model for predicting shear strength of unreinforced exterior beam-column joints, ACI Structural Journal, Vol. 109, No. 2, pp. 149–160.

Park, S. and Mosalam, K.M.(2012b). Parameters for shear strength prediction of exterior beam–column joints without transverse reinforcement. Engineering Structures, 36, 198–209.

Park, S. and Mosalam, K.M. (2013). Experimental investigation of nonductile RC corner beam-column joints with floor slabs, ASCE Journal of Structural Engineering, Vol. 139, No. 1, pp. 1–14.

Park, S. and Mosalam, K.M. (2013b). Simulation of reinforced concrete frames with nonductile beam-column joints, Earthquake Spectra, Vol. 29, No. 1, pp. 233–257.

Parker, D.E., and Bullman, P.J.M. (1997). Shear Strength within Reinforced Concrete Beam- Column Joints, The Structural Engineer, V. 75, No. 4, pp. 53-57.

Paspuleti, C. (2002). Seismic Analysis of an Older Reinforced Concrete Frame Structure. Masters Thesis, Seattle, WA: University of Washington: Department of Civil and Environmental Engineering, 2002.

PEER Testbed Website. URL: http://www.peertestbeds.net/

PEER. Pacific Earthquake Engineering Research Center: Structural Performance Database, University of California, Berkeley, Available at http://nisee.berkeley.edu/spd/.

Pezziario Regione Campania (2014). http://www.lavoripubblici.regione.campania.it/joomla/index.php?option=com_content&view=article&id=455&Itemid=131

Pincheira, J. A., and Jirsa, J.O. (1992). Seismic Strengthening of Reinforced Concrete Frames Using Post-Tensioned Bracing Systems. Phil M. Furguson Structural Engineering Lab Report N. 92-3, University of Texas at Austin, Austin, TX.

Pincheira, J. A., Dotwiala, F. S., and D'Souza J.T. (1999). Seismic Analysis of Older Reinforced Concrete Columns. Earthquake Spectra: 245-272.

Polese M., Verderame G.M., Mariniello C., Iervolino I., Manfredi G. (2008). Vulnerability curves for gravity load designed RC buildings in Naples – Italy, Journal of Earthquake Engineering, 12 (S2), 234-245, ISSN 1363-2469.

Polese, M., Di Ludovico, M., Prota A., Manfredi G. (2010). Damage dependent vulnerability curves for existing buildings", Earthquake Engineering and Structural Dynamics, DOI:10.1002/eqe.2249

Polese, M., Verderame, G.M., Manfredi, G. (2011). Static vulnerability of existing R.C. buildings in Italy: a case study, *Structural Engineering and Mechanics*, Techno-Press, 39 (4), 599-620.

Polese M., Di Ludovico M., Prota A., Manfredi G., (2013a). Damage-dependent vulnerability curves for existing buildings, *Earthquake Engineering and Structural Dynamics*, 42 (6), 853-870, DOI: 10.1002/eqe.2249.

Polese, M., Marcolini, M., Prota, A., Zuccaro, G. (2013b). Mechanism based assessment of damaged building's residual capacity. *Computational Methods in Structural Dynamics and Earthquake Engineering, Compdyn 2013*, Paper No. 1524, Kos, Greece.

Polese, M., Marcolini, M., Zuccaro, G., & Cacace, F. (2014). Mechanism based assessment of damage-dependent fragility curves for RC building classes. *Bulletin of earthquake Engineering*, 1-23.

Porter KA. (2000). Assembly-based vulnerability of buildings and its uses in seismic performance evaluation and riskmanagement decision-making. Ph.D. Dissertation, Stanford University, Stanford, CA. ProQuest Co.: Ann Arbor, MI.

Porter KA (2003). An overview of PEER's performance-based earthquake engineering methodology. Proceedings, Ninth International Conference on Applications of Statistics and Probability in Civil Engineering, San Francisco, California. 2003.

Porter, K.A., Kennedy, R., and Bachman, R. (2007). Creating Fragility Functions for Performance-Based Earthquake Engineering. Earthquake Spectra, 23(2), 471–489.

Priestley, M.J.N. (1997). Displacement-Based Seismic Assessment of Reinforced Concrete Buildings, Journal of Earthquake Engineering, V. 1, No. 1, 1997, pp. 157-192.

Pujol, S., Ramirez, J.A., and Sozen, M.A. (1999). Drift capacity of reinforced concrete columns subjected to cyclic shear reversals. Seismic Response of Concrete Bridges, SP-187, American Concrete Institute, Farmington Hills, MI, pp. 255–274.

R.D.L. no. 2229/1939. Regulations for the execution of simple and reinforced concrete constructions [in Italian].

Raghunandan, M., Liel, A. B., Ryu, H., Luco, N., & Uma, S. R. (2012). Aftershock fragility curves and tagging assessments for a mainshock-damaged building. *Proceedings of the 15th WCEE, Lisboa, Portugal Paper*, (1708), 24-28

Raghunandan, M., Liel, A. B., & Luco, N. (2014). Aftershock collapse vulnerability assessment of reinforced concrete frame structures. *Earthquake Engineering & Structural Dynamics*.

Ramirez, C. M., & Miranda, E. (2009). Building-specific loss estimation methods & tools for simplified performance-based earthquake engineering, Doctoral dissertation, Stanford University.

Ramirez, C. M., & Miranda, E. (2012). Significance of residual drifts in building earthquake loss estimation. *Earthquake Engineering & Structural Dynamics*, *41*(11), 1477-1493.

Ramirez, C. M., Liel, A. B., Mitrani-Reiser, J., Haselton, C. B., Spear, A. D., Steiner, J., ... & Miranda, E. (2012). Expected earthquake damage and repair costs in reinforced concrete frame buildings. *Earthquake Engineering & Structural Dynamics*, *41*(11), 1455-1475.

Reiter, L., 1990, *Earthquake Hazard Analysis: Issues and insights*, Columbia University Press, New York.

Réveillère, A., Gehl, P., Seyedi, D., & Modaressi, H. (2012). Development of seismic fragility curves for damaged reinforced concrete structures. In*Proceedings of the 15 th World Conference on Earthquake Engineering*.

Ryu, H., Luco, N., Uma, S. R., & Liel, A. B. (2011). Developing fragilities for mainshock-damaged structures through incremental dynamic analysis. In *Ninth Pacific Conference on Earthquake Engineering, Auckland, New Zealand*.

S.C. Harmsen, 2001. Mean and Modal e in the Deaggregation of Probabilistic Ground Motion. *Bull. Seism. Soc. Am.*, 91(6), 1537-1552.

San Diego Municipal Code, SDMC (2004). Unreinforced Masonry (URM) Program http://www.sandiego.gov/development-services/industry/information/codesregreq/index.shtml

San Francisco, City of (SF), (2012). Post-earthquake repair and Retrofit Requirements, Administrative Bulletins, AB-099, Department of Building Inspection, San Francisco, CA

Santucci de Magistris F, d'Onofrio A, Penna A, Puglia R, Silvestri F (2014). Lessons learned from two case histories of seismic microzonation in Italy, Natural Hazards, DOI 10.1007/s11069-014-1281-6

Sarsam, K.F., and Phipps, M.E. (1985). The Shear Design of In-situ Reinforced Beam-Column Joints Subjected to Monotonic Loading, Magazine of Concrete Research, V. 37, No. 130, pp. 16-28.

Sasani, M. and Kropelnicki, J. (2007). Progressive Collapse Analysis of an RC Structure, *International Journal of The Structural Design of Tall and Special Buildings,* 17:1, 757-771.

Scholl, R.E., Kustu, O., Perry, C.L., and Zanetti, J.M. (1982). Seismic Damage Assessment for High-Rise Buildings, Report URS/JAB 8020, URS/John A. Blume & Associates, Engineers, San Francisco, CA.

Seismic Safety Commission, SSC 2006-04, (2006). Status of the Unreinforced Masonry Building Law.   State of California, Seismic Safety Commission.

Sezen, H. (2002). Seismic behavior and modeling of reinforced concrete building columns, Ph.D. Thesis, Department of Civil and Environmental Engineering, University of California at Berkeley, CA.

Sezen, H. and Moehle J.P. (2003). Bond-slip behavior of reinforced concrete members, Proceedings of Fib Symposium on Concrete Structures in Seismic Regions, Athens, Greece.

Sezen, H. and Chowdhury, T. (2009). Hysteretic model for the lateral behavior of reinforced concrete columns including shear deformation, ASCE Journal of Structural Engineering, Vol. 135, No. 2, pp. 139–146.

Sharma, A., Eligehausen, R., and Reddy, G. (2011). A new model to simulate joint shear behavior of poorly detailed beam-column connection in RC structures under seismic loads, Part I: Exterior joints." *Engineering Structures* 33, 1034-1051

Shin, M. and LaFave, J.M. (2004). Modeling of cyclic joint shear deformation contributions in RC beam-column connections to overall frame behavior, Structural Engineering and Mechanics, Vol. 18, No. 5, pp. 645–669.

Shiohara, H. (2004). Quadruple flexural resistance in R/C beam-column joints, 13th world Conference on Earthquake Engineering, Paper No. 491, Vancouver, Canada.

Shome, N., Cornell, C. A., Bazzurro, P., and Carballo, J. E. (1998). Earthquakes, records and nonlinear responses. Earthquake Spectra, 14(3), 469–500.

Somerville, P.G. and Thio, H.K. (2011). "Development of ground motion time histories for seismic design," *Proceedings of the Ninth Pacific Conference on Earthquake Engineering: Building an Earthquake-Resilient Society*, 14-16 April, 2011, Auckland, New Zealand.

Spacone, E., Filippou, F.C., and Taucer, F.F. (1996). Fibre beam-column model for nonlinear analysis of R/C frames: Part I Formulation, Earthquake Engineering and Structural Dynamics, Vol. 25, No. 7, pp. 711–725.

Stevens N.J., Uzumeri, S.M., and Collins, M.P. (1991). "*Reinforced-Concrete Subjected to Reverse-Cyclic Shear – Experiment and Constitutive Model.*" ACI Structural Journal, Vol. 88, No. 2, pp.135-146.

Sucuoğlu, H., Erberik, A. (2004). Energy-based hysteresis and damage models for deteriorating systems. *Earthquake Eng. Struct. Dyn.*; 33: 69–88.

Taghavi S, Miranda E. (2003). Response of Nonstructural Building Elements. PEER 2003/05. Berkeley, CA: Pacific Earthquake Engineering Research Center.

Talaat, M. Mosalam, K.M. (2007). Modeling Progressive Collapse in Reinforced Concrete Buildings Using Direct Element Removal, *International Journal of Earthquake Engineering and Structural Dynamics,* 38:3, 609-634.

Theiss, A.G. (2005). Modeling the Earthquake Response of Older Reinforced Concrete Beam-Column Building Joints, M.Sc. Thesis, University of Washington.

Tinsley, J.C., and Fumal, T.E. (1985). Mapping quaternary sedimentary deposits for areal variations in shaking response, *Evaluating Earthquake Hazards in the Los Angeles Region—An Earth-Science Perspective, U*.S. Geological Survey Professional Paper 1360, U.S. Government Printing Office, Washington DC, pp. 101-126.

Trifunac, M.D., and Brady, A.G. (1975). A study on the duration of strong earthquake ground motion. Bulletin of the Seismological Society of America, 65, 581-626.

Trifunac, M.D., Ivanovic, S.S. and Todorovska, M.I. (1999). Instrumented 7-Storey Reinforced Concrete Building in Van Nuys, California: Description of the

Damage from the 1994 Northridge Earthquake and Strong Motion Data, Report CE 99-02, University of Southern California Department of Civil Engineering, Los Angeles, CA

Tsai, K.C., Loh, C.H., Lin, K.C., and Chen, C.H. (2000) *Cyclic load tests of 0.7 scale 2-story RC frames retrofitted with steel jackets*, National Center for Research on Earthquake Engineering, Taiwan.

Tso, W.K., Moghadam, A.S. (1998). Pushover procedure for seismic analysis of buildings. *Progress in Structural Engineering and Materials*, 1(3), 337–44.

Tsonos AG (2007). Cyclic load behaviour of reinforced concrete beam–column subassemblages of modern structures, *ACI Structural Journal*; 104(4):468–78.

Uma, S. R., Ryu, H., Luco, N., Liel, A. B., & Raghunandan, M. (2011). Comparison of main-shock and aftershock fragility curves developed for New Zealand and US buildings. In *Proceedings of the ninth pacific conference on earthquake engineering structure building and Earthquake-Resilient Society, Auckland, New Zealand* (pp. 14-16).

Vamvatsikos, D., & Cornell, C. A. (2002). Incremental dynamic analysis.*Earthquake Engineering & Structural Dynamics*, *31*(3), 491-514.

Vamvatsikos, D., & Cornell, C. A. (2004). Applied incremental dynamic analysis. *Earthquake Spectra*, *20*(2), 523-553.

Vamvatsikos, D., and Cornell, C. A. (2005). Developing efficient scalar and vector intensity measures for IDA capacity estimation by incorporating elastic spectral shape information. *Earthquake Engineering & Structural Dynamics*, 34(13), 1573-1600.

Vecchio, F.J. and Collins, M.P. (1986). The modified compression field theory for reinforced concrete elements subjected to shear, ACI Structural Journal, Vol. 83, No. 2, pp. 219–231.

Verderame, G.M., Fabbrocino, G., Manfredi, G. (2008a). Seismic response of r.c. columns with smooth reinforcement, Part I: monotonic tests, *Engineering Structures,*; 30(9): 2277-88.

Verderame, G.M., Fabbrocino, G., Manfredi, G. (2008b). Seismic response of r.c. columns with smooth reinforcement, Part II: cyclic tests, *Engineering Structures*; 30(9): 2289-2300.

Verderame, G.M., Polese, M., Cosenza, E. (2009). Vulnerability of existing R.C. buildings under gravity loads: A simplified approach for non-sway structures, *Engineering Structures,* 31 (9), 2141-2151.

Verderame, G.M., Ricci, P., Manfredi, G., Cosenza, E. (2010a). Ultimate chord rotation of RC columns with smooth bars: some considerations about EC8 prescriptions, *Bulletin of Earthquake Engineering*, June; 8:1351-1373.

Verderame, G.M., Polese, M., Mariniello, C., Manfredi, G. (2010b). A simulated design procedure for the assessment of seismic capacity of existing reinforced concrete buildings, *Advances in Engineering Software*, 41 (2), 323-335.

Verderame, G.M., Ricci, P., Esposito, M., Manfredi, G. (2012). STIL v1.0 – Software per la caratterizzazione delle proprietà meccaniche degli acciai da c.a. tra il 1950 e il 2000. ReLUIS. http://www.reluis.it/ (in Italian).

Vollum, R.L. and Newman J.B. (1999). Strut and Tie Models for the Analysis/Design of External Beam-Column Joints, Magazine of Concrete Research, Vol. 51, No. 6, pp. 415-425.

Walker, S.G. (2001). Seismic Performance of Existing RC Beam–Column Joints, M.Sc. Thesis, University of Washington.

Watanabe, F. and Ichinose, T. (1992) *Strength and ductility of RC members subjected to combined bending and shear*, Concrete Shear in Earthquake, Elsevier Applied Science, New York, pp. 429–438.

Wong, H.F. (2005). *S*hear Strength and Seismic Performance of Non-Seismically Designed Reinforced Concrete Beam-Column Joints, PhD Dissertation, Department of Civil Engineering, The Hong Kong University of Science and Technology, August.

Yang, T. Y., Moehle, J., Stojadinovic, B., & Der Kiureghian, A. (2009). Seismic performance evaluation of facilities: methodology and implementation. *Journal of Structural Engineering*, *135*(10), 1146-1154.

Youngs, R., Power, M., Wang, G., Makdisi, F., & Chin, C. C. (2007, September). Design ground motion library (DGML)–Tool for selecting time history records for specific engineering applications. In *SMIP07 Seminar on Utilization of Strong-Motion Data* (pp. 109-110). Sacramento, CA: California Geological Survey

Youssef, M. and Ghobarah, A. (2001). Modelling of RC beam-column joints and structural walls, Journal of Earthquake Engineering, Vol. 5, No. 1, pp. 93–111.

Zareian, F., & Krawinkler, H. (2006). Simplified performance-based earthquake engineering, Doctoral dissertation, Stanford University.